HAL
open science

# Molecular study of the mechanisms of action of CDK4 and CDK6 inhibitors

Su-Jung Kim

## To cite this version:

Su-Jung Kim. Molecular study of the mechanisms of action of CDK4 and CDK6 inhibitors. Cellular Biology. Université Paris Cité, 2021. English. NNT : 2021UNIP7240 . tel-04010306

**HAL Id: tel-04010306**

**https://theses.hal.science/tel-04010306v1**

Submitted on 1 Mar 2023

**HAL** is a multi-disciplinary open access archive for the deposit and dissemination of scientific research documents, whether they are published or not. The documents may come from teaching and research institutions in France or abroad, or from public or private research centers.

L'archive ouverte pluridisciplinaire **HAL**, est destinée au dépôt et à la diffusion de documents scientifiques de niveau recherche, publiés ou non, émanant des établissements d'enseignement et de recherche français ou étrangers, des laboratoires publics ou privés.

Université de Paris
**Ecole doctorale Bio Sorbonne Paris Cité ED562**
***Institut Jacques-Monod, Equipe Pathologies de la réplication de l'ADN***

# Molecular study of the mechanisms of action of CDK4 and CDK6 inhibitors

Par Su-Jung KIM

Thèse de doctorat de Biologie cellulaire et moléculaire

Dirigée par Jean-Charles CADORET et par Fabien FAUCHEREAU

Présentée et soutenue publiquement le 24 Juin 2021

Devant un jury composé de :

*Sophie VRIZ, Professeur, Université de Paris, Présidente*
*Yea-Lih LIN, DR, Université de Montpellier, Rapportrice*
*Etienne SCHWOB, DR, Université de Montpellier, Rapporteur*
*Kathrine MARHEINEKE, CR-HDR, Université Paris Saclay, Examinatrice*
*Benoit MIOTTO, CR-HDR, Université de Paris, Examinateur*
*Pierre ROGER, DR, Université Libre de Bruxelle, Examinateur*
*Stéphane KOUNDRIOUKOFF, Maître de conférences, Sorbonne Université Campus Pierre et Marie Curie, Membre invité*
*Jean-Charles CADORET, Maître de conférences-HDR, Université de Paris, Directeur de thèse*
*Fabien FAUCHEREAU, Maître de conférences-HDR, Université de Paris, Co-directeur de thèse*

Except where otherwise noted, this is work licensed under
https://creativecommons.org/licenses/by-nc-nd/3.0/fr/

**Titre: Etude moléculaire des mécanismes d'action des inhibiteurs de CDK4 et CDK6**

Résumé: Les inhibiteurs de CDK4/6 sont des médicaments anticancéreux prometteurs. Récemment, la Food and Drug Administration (FDA) a approuvé trois inhibiteurs de CDK4/6 (palbociclib, ribociclib et abemaciclib) pour les traitements du cancer du sein avancé ou métastatique négatif aux récepteurs hormonaux (HR) et positif au récepteur 2 du facteur de croissance épidermique humain (HER2). La fonction de CDK4/6 dans la transition G1/S du cycle cellulaire repose sur la phosphorylation de leurs substrats. En effet, la phosphorylation de leur substrat majeur, pRb, modifie l'expression de gènes impliqués dans la progression du cycle cellulaire et la réplication de l'ADN. Ma thèse vise à comprendre les actions des inhibiteurs de CDK4/6 sous trois aspects.

Tout d'abord, j'ai étudié les effets anti-prolifératifs des inhibiteurs de CDK4/6 par rapport à la présence de pRb dans les carcinomes adrénocorticaux (ACC). J'ai validé que la réponse aux inhibiteurs de CDK4/6 dépend de la présence de pRb. En effet, les inhibiteurs de CDK4/6 induisent efficacement la sénescence cellulaire dans une lignée d'ACC exprimant pRb (SW-13). En revanche, la réponse est différente pour une lignée déficiente pour pRb (NCI-H295R) puisqu'elle est résistante à ces traitements. Dans un deuxième temps, je me suis concentrée sur les actions du palbociclib sur la dynamique de la réplication de l'ADN dans un contexte pRb négatif. En utilisant deux lignées cellulaires déficientes en pRb (MDA-MB-468 et NCI-H295R), j'ai démontré comment le palbociclib empêche l'initiation de la réplication de l'ADN. Enfin, je participe à une étude en cours au laboratoire qui propose que l'abemaciclib, en combinaison avec des inhibiteurs de l'autophagie, induit des effets synergiques sur la viabilité cellulaire de cellules déficientes en pRb. Cette perte de viabilité est la conséquence de l'apoptose induite par la combinaison de ces molécules. C'est la première fois que nous montrons que ce genre de combinaison a un effet dans un contexte pRb négatif et peut laisser présager de nouvelles voies thérapeutiques.

Cette étude fournira des connaissances approfondies et significatives sur les actions des inhibiteurs de CDK4/6 et contribuera au développement d'un traitement personnalisé pour les cancers.

Mots clefs: Inhibiteurs de CDK4/6, Réplication de l'ADN, Autophagie, Cancer, Cibles thérapeutiques

**Title: Molecular study of the mechanisms of action of CDK4 and CDK6 inhibitors**

Abstract: CDK4 and CDK6 (CDK4/6) inhibitors are promising anticancer drugs. Recently, the Food and Drug Administration (FDA) approved three CDK4/6 inhibitors (palbociclib, ribociclib and abemaciclib) for treatments of hormone receptor (HR)-positive, human epidermal growth factor receptor 2 (HER2)- negative advanced or metastatic breast cancer. CDK4/6 play an important role in the G1/S transition of the cell cycle. This function relies on the phosphorylation of their substrates, including the retinoblastoma protein (pRb) which is a main mediator for the expression of genes involved in the progression of cell cycle and DNA replication.

My thesis aims to understand the actions of CDK4/6 inhibitors in three projects. Using two cellular models established from adrenocortical carcinomas (ACC), namely SW-13 and NCI-H295R, I validated that response to CDK4/6 inhibitors depends on the presence of pRb. Actually, CDK4/6 inhibitors effectively induce cell senescence in the pRb proficient ACC cell line SW-13 but not in pRb deficient NCI-H295R. Then, I focused on the actions of palbociclib on DNA replication dynamics in a pRb negative context. Using two pRb deficient cell lines (MDA-MB-468 and NCI-H295R), I showed how palbociclib interferes with the initiation of DNA replication. Finally, an ongoing study proposes the use of abemaciclib in combination with autophagy inhibitors. These co-treatments with two drugs induced synergistic effects on cell viability through the induction of apoptosis.

In summary, during my PhD thesis I studied the actions of three CDK4/6 inhibitors (ribociclib, palbociclib and abemaciclib) in different contexts (positive or negative pRb) on DNA replication and autophagy. This study provides meaningful understanding on the actions of CDK4/6 inhibitors and contributes to the development of a personalized treatment for cancers.

Keywords: CDK4/6 inhibitors, DNA replication, Autophagy, Cancer, Therapeutic targets

**Résumé en français**

Au cours de ma thèse, je me suis intéressée aux inhibiteurs de CDK 4/6 (Cyclin Dépendant kinase 4 et 6) qui sont des médicaments anticancéreux prometteurs. Ces molécules font partie de la troisième génération d'inhibiteurs de CDK qui est développée pour être plus puissante et spécifique envers les protéines CDK4 et CDK6. Récemment, la « Food and Drug Administration (FDA) » américaine a approuvé trois inhibiteurs de CDK4/6 (palbociclib, ribociclib et abemaciclib) pour les traitements du cancer du sein avancé ou métastatique, négatif aux récepteurs hormonaux (HR) et positif au récepteur 2 du facteur de croissance épidermique humain (HER2). Les protéines CDK4 et CDK6 jouent un rôle primordial dans la progression du cycle cellulaire. En effet, la fonction de CDK4/6 dans la transition G1/S du cycle cellulaire repose sur la phosphorylation de leurs substrats. En effet, la phosphorylation de leur substrat majeur pRb, modifie l'expression de gènes impliqués dans la progression du cycle cellulaire et la réplication de l'ADN. Ma thèse vise à comprendre les actions des inhibiteurs de CDK4/6 sous trois aspects.

<u>I. Identification des inhibiteurs de CDK4/6 comme des médicaments candidats pour le traitement des carcinomes adrénocorticaux.</u>

Cette étude se compose de deux parties, dont l'une est l'analyse *in silico* des données transcriptomiques de la base de données The Cancer Genome Atlas (TCGA). Nous nous sommes concentrés sur 136 gènes impliqués dans la transition G1/S et la réplication de l'ADN en utilisant les données RNAseq de patients souffrant de carcinomes adrénocorticaux (ACC). Premièrement, nous avons constaté que le regroupement hiérarchique basé sur les niveaux d'ARNm déterminait 4 groupes de gènes. La plupart des gènes des clusters 3 et 4 sont corrélés à l'expression de MKI67, un marqueur classique du taux de prolifération cellulaire. Le cluster 1 est inversement corrélé à ce marqueur de prolifération. Ensuite, parmi le reste des gènes, qui n'ont montré aucune corrélation significative avec l'expression de MKI67, nous avons identifié CDK6 dont la surexpression est fortement associée à des rechutes et décès précoces.

Sur la base de ces résultats, nous avons cherché, dans une deuxième partie, à évaluer les effets des inhibiteurs de CDK4/6 (palbociclib et ribociclib) sur des lignées cellulaires de carcinome adrénocortical, une lignée cellulaire pRb positive nommée SW-13 et une lignée cellulaire déficiente en pRb nommée NCI-H295R. Les inhibiteurs de CDK4/6 ajoutés en dose

croissante diminuent efficacement la viabilité cellulaire et induisent l'arrêt du cycle cellulaire en phase G1 à faible dose (1µM) dans les cellules SW-13. Ceci est accompagné d'un niveau réduit de pRb phosphorylé. Pour mieux distinguer si l'arrêt du cycle cellulaire est transitoire ou permanent, nous avons étudié plusieurs caractéristiques de la sénescence, notamment l'activité de la β-galactosidase, les changements de granularité et de taille cellulaire, la présence de vésicules et l'irréversibilité de l'arrêt du cycle cellulaire. Les cellules traitées avec 1 ou 5µM de ribociclib présentent la plupart de ces caractéristiques. Une certaine proportion de cellules va redémarrer leur cycle cellulaire après élimination du traitement, illustrant ainsi la réversibilité du cycle cellulaire. Cependant, le palbociclib induit un arrêt irréversible appelé sénescence à 5µM, suggérant la présence d'« off-targets ».

Contrairement aux cellules SW-13, les cellules déficientes en pRb NCI-H295R présentent une résistance aux inhibiteurs de CDK4/6. Nous avons observé que la viabilité cellulaire n'est pas affectée jusqu'à 5µM d'inhibiteurs. Pourtant, le palbociclib diminue la viabilité cellulaire à 10 µM ou plus, contrairement au ribociclib. Nous avons en outre démontré que le palbociclib utilisé à forte dose induit l'apoptose dans les cellules NCI-H295R. Cela confirme que le palbociclib a des effets plus prononcés sur les cellules que le ribociclib. Nos résultats proposent les inhibiteurs de CDK4/6 comme nouveau traitement des carcinomes adrénocorticaux qui sont des cancers agressifs et qui n'ont pour l'instant que des options de traitement limitées.

Le premier chapitre décrit les effets anti-prolifératifs de CDK4/6 par rapport à la présence de pRb dans l'ACC. L'analyse des données transcriptomiques nous a permis d'identifier différents sous-groupes d'ACC avec un groupe dans lequel CDK6 est révélé comme biomarqueur. Ensuite, nous avons validé que les inhibiteurs de CDK4/6 induisent efficacement la sénescence cellulaire dans une lignée cellulaire ACC contenant pRb (SW-13) mais pas dans une lignée cellulaire déficiente en pRb (NCI-H295R). Au cours de ce projet, nous avons mis en évidence certaines preuves montrant que le palbociclib induit une réduction de la viabilité des cellules déficientes en pRb couplée à des cycles cellulaires aberrants. Ces observations nous conduisent à caractériser les actions du palbociclib dans un contexte pRb négatif. Cette étude est publiée dans le journal «Aging » (Hadjadj *et al.*, 2017)

II.A Palbociclib et la réplication de l'ADN

Dans le deuxième chapitre, nous avons particulièrement étudié les effets du palbociclib sur la dynamique de réplication de l'ADN à l'aide de deux lignées cellulaires déficientes en pRb (MDA-MB-468 et NCI-H295R). L'originalité de ce travail est que nous avons étudié le palbociclib dans un contexte pRb négatif. Comme pRb est un substrat majeur pour CDK4/6 dans la transition G1/S du cycle cellulaire, son absence est largement considérée comme un marqueur de résistance. Cependant, nous avons observé de manière surprenante une progression aberrante du cycle cellulaire accompagnée d'une synthèse d'ADN diminuée dans les lignées cellulaires déficientes en pRb (MDA-MB-468 et NCI-H295R) et traitées avec du palbociclib. Cette découverte indique que le palbociclib peut avoir des impacts sur la réplication de l'ADN même en l'absence de pRb.

Pour décrypter les mécanismes d'action du palbociclib, j'ai mis en œuvre deux méthodes puissantes dédiées à l'analyse du processus de réplication de l'ADN à savoir, l'analyse du programme temporel de la réplication (voir II.B) et le peignage moléculaire de l'ADN. L'analyse du programme temporel nous permet de visualiser comment le palbociclib perturbe la réplication de l'ADN à l'échelle du génome entier. Le peignage moléculaire nous apporte une compréhension approfondie de la progression des fourches répliquées et de l'efficacité des origines au niveau moléculaire. En utilisant les deux méthodes susmentionnées, nous avons démontré comment le palbociclib perturbe la réplication de l'ADN et altère particulièrement l'étape d'initiation dans deux lignées cellulaires déficientes en pRb. De plus, en analysant les protéines liées à la chromatine, nous avons montré que le palbociclib diminue la quantité des protéines constituant le complexe de Pré-initiation (Pré-IC), induisant des défauts dans l'activation des origines. Nous avons constaté que le palbociclib altère l'étape d'initiation des origines de la réplication en régulant à la baisse l'expression des gènes codant pour les protéines du pré-IC.

En conclusion, cet article démontre l'existence de nouveaux mécanismes d'action du palbociclib dans la réplication de l'ADN d'une manière indépendante de pRb. Ces découvertes pourraient offrir de nouvelles possibilités d'utilisation du palbociclib comme traitement anticancéreux pour cibler les cancers déficients en pRb caractérisés par l'instabilité de leur génome. Le palbociclib pourrait exacerber cette instabilité en rendant les cellules plus

vulnérables au stress réplicatif. Dans ce contexte, le palbociclib a le potentiel d'être associé à d'autres molécules thérapeutiques ciblant la réplication de l'ADN.
Cette étude est en cours d'écriture.

II.B Analyse efficace, rapide et facile à utiliser du programme temporel de la réplication de l'ADN avec la suite START-R

La réplication de l'ADN est régulée par un programme spatio-temporel bien conservé permettant une activation contrôlée des origines de réplication. L'analyse de ce programme nous permet de comprendre comment les cellules organisent le déroulé de la réplication pour chaque région du génome tout au long de la phase S du cycle cellulaire. Cette analyse donne aussi un aperçu de l'efficacité de l'activation des origines et des mouvements de fourche à l'échelle du génome du début à la fin de la phase S. De plus, en comparant deux conditions, cela permet d'évaluer les impacts d'un médicament ou d'une modification génétique comme sources de stress réplicatif. Ainsi, la confrontation des résultats d'analyse du programme temporel de la réplication avec d'autres données disponibles telles que la cartographie des origines de réplication, le transcriptome ou la prédiction des structures secondaires de l'ADN nous permet d'identifier les caractéristiques moléculaires des régions altérées lors d'un stress réplicatif.

Dans cet article, nous montrons des méthodes rapides et faciles à utiliser pour analyser le programme temporel de la réplication. Tout d'abord, l'étape d'immunoprécipitation a été automatisée à l'aide du robot IP-Star® rendant les étapes expérimentales plus rapides et plus précises. Deuxièmement, nous avons développé la suite START-R, qui est dédiée à l'analyse des résultats de programme temporel de la réplication de l'ADN. Ce logiciel fournit des outils robustes que tout biologiste peut utiliser. L'analyseur START-R propose différents paramètres et outils statistiques simples d'utilisation. L'outil de visionnage START-R permet la visualisation des profils de programme temporel de la réplication à l'échelle du génome entier et distingue les régions de changements du programme temporel de la réplication en comparant deux conditions différentes. Notre méthode a été validée avec des données de microarray et de Repli-Seq et convient aux données de différentes espèces telles que la drosophile, le poisson zèbre, la souris et les cellules humaines.

Cet article propose un pipeline complet pour étudier efficacement et facilement le programme temporel de la réplication. Nous confirmons que notre méthode est aussi précise que le Repli-Seq tout en consommant moins de temps et d'argent. Enfin, la suite START-R rend la manipulation d'énormes quantités de données plus accessibles aux biologistes.
Cette étude est publiée dans le journal 'NAR Genomics and Bioinformatics' (Hadjadj *et al.*, 2020).

III. Amélioration des effets de l'abemaciclib en association avec des inhibiteurs de l'autophagie

Enfin, le troisième volet de mon projet montre les effets de l'abemaciclib en association avec d'autres médicaments qui inhibent l'autophagie sur des lignées cellulaires déficientes en pRb. L'objectif de cette étude est de parvenir à des traitements plus efficaces contre le cancer en utilisant des doses plus faibles de médicaments grâce à une stratégie de combinaison. Le co-traitement avec l'abemaciclib et la chloroquine montre des effets synergiques sur la viabilité cellulaire des deux lignées cellulaires déficientes en pRb que nous avons particulièrement étudiées (MDA-MB-468 et NCI-H295R). Cela indique que l'action de l'abemaciclib n'est pas médiée par la présence de pRb. Nous avons également démontré que cette combinaison induit la mort cellulaire par apoptose à faibles doses de chaque médicament. Les résultats pourraient promouvoir l'utilisation de l'abemaciclib en association avec la chloroquine pour le traitement du cancer.
Cette étude est soumise pour publication.

En résumé, au cours de ma thèse, j'ai étudié chacun des trois inhibiteurs de CDK4/6 (ribociclib, palbociclib et abemaciclib) dans différents contextes (pRb positif ou négatif) pour différents aspects de leurs actions (réplication de l'ADN, autophagie). Cette étude fournira des connaissances approfondies et significatives sur les actions des inhibiteurs de CDK4/6 et contribuera au développement d'un traitement personnalisé pour les cancers.

# Remerciements

Je tiens d'abord à remercier Yea-Lih Lin et Etienne Schwob d'avoir consacré du temps pour lire et évaluer ma thèse en tant que rapporteurs ; ainsi que Sophie Vriz, Kathrine Marheineke, Benoit Miotto et Pierre Roger d'avoir accepté d'être examinateurs.

Je remercie tous ceux qui m'ont aidée dans la conception et la réalisation de ma thèse et particulièrement les membres de notre équipe « Pathologies de la réplication de l'ADN ».

Fabien Fauchereau, merci de m'avoir accueillie dans ce laboratoire. Grâce à ton encadrement, j'ai pu développer rigoureusement ma façon de travailler en tant que scientifique. Jean-Charles Cadoret, merci de m'avoir donné des challenges tout au long de ma thèse qui m'ont permis d'acquérir les compétences nécessaires pour devenir scientifique. Giuseppe Baldacci, merci pour votre encouragement et vos conseils à la fois justes et chaleureux. Tout cela était très bénéfique. Chrystelle Maric, merci d'avoir toujours voulu m'aider en me répétant la phrase « Ne t'inquiètes pas Su-Ji, ça va le faire ! ». Djihad Hadjadj, Pauline Clément, Eva Guérin, Lina-Marie Briu, merci à vous. J'ai passé de bons moments avec chacun de vous. Je me suis bien amusée au labo durant ma thèse grâce à vous.

Je voudrais également remercier les membres de mon comité de thèse, Vanessa Ribes et Stéphane Koundrioukoff. Merci beaucoup d'avoir pris le temps lors de ces comités et de m'avoir toujours donné de bons conseils dans la volonté que ma thèse se passe pour le mieux.

Je remercie tous les membres de l'équipe « 4Rs : Replication, Repair, Recombination and ROS » à l'institut Gustave Roussy où j'ai effectué une collaboration. Merci de m'avoir toujours bien accueillie. Encore merci à Stéphane Koundrioukoff pour votre aide technique et scientifique.

Ma thèse a pu être réalisée grâce aux financements : Ligue contre le cancer, EUR G.E.N.E et Labex Who Am I?.

Enfin, Merci à ma famille et mes amis. Je vous aime fort.

# Table of contents

REMERCIEMENTS ..... 9

INTRODUCTION ..... 12

I. CELL CYCLE AND CELL CYCLE INHIBITORS ..... 12

I.A CELL CYCLE REGULATION ..... 12
I.A.1 G1 PHASE AND CDK4/6 REGULATION ..... 13
I.A.2 CDK2 REGULATION IN THE G1/S TRANSITION ..... 14
I.A.3 S PHASE AND CDK1/2-CYCLIN A ..... 15
I.B CHEMICAL CDK INHIBITORS ..... 18
I.B.1 FIRST CDK INHIBITORS ..... 18
I.B.2 THE THIRD GENERATION OF CDK INHIBITORS: CDK4/6 SELECTIVE INHIBITORS ..... 18
I.B.3 CDK4/6 INHIBITORS BEYOND THE PRB PATHWAY ..... 24

II. DNA REPLICATION AND CANCER ..... 27

II.A DNA REPLICATION ..... 27
II.A.1 ORIGIN LICENSING ..... 27
II.A.2 ORIGIN FIRING ..... 30
II.A.3 ELONGATION ..... 31
II.A.4 TERMINATION ..... 32
II.B REPLICATION STRESS AND CANCER ..... 33
II.B.1 NATURAL SOURCES OF REPLICATION STRESS ..... 33
II.B.2 ONCOGENE INDUCED REPLICATION STRESS ..... 35
II.C S-PHASE CHECKPOINT AND CELLULAR RESPONSES ..... 37
II.D CONSEQUENCE OF REPLICATION STRESS ..... 39

PROJECTS OF THESIS ..... 41

RESULTS ..... 42

I. A HYPOTHESIS DRIVEN APPROACH IDENTIFIES CDK4/6 INHIBITORS AS CANDIDATE DRUGS FOR TREATMENTS OF ADRENOCORTICAL CARCINOMAS ..... 42

I.A SUMMARY ..... 42
I.B ARTICLE ..... 43

II. PALBOCICLIB AND DNA REPLICATION ..... 66

II.A PALBOCICLIB INTERFERES WITH ORIGIN FIRING IN A PRB INDEPENDENT MANNER ..... 66
II.A.1 SUMMARY ..... 66

II.A.2 ARTICLE (IN PREPARATION) ..... 68
II.A.3 ANNEXES ..... 99
**II.B EFFICIENT, QUICK AND EASY-TO-USE DNA REPLICATION TIMING ANALYSIS WITH START-R SUITE ..... 104**
II.B.1 SUMMARY ..... 104
II.B.2 ARTICLE ..... 105

**III. IMPROVEMENT OF ABEMACICLIB EFFECTS IN COMBINATION WITH AUTOPHAGY INHIBITORS ..... 129**

**III.A ARTICLE (ON-GOING) ..... 129**

**CONCLUSION ..... 134**

**DISCUSSION AND PERSPECTIVES ..... 135**

**REFERENCES ..... 143**

# INTRODUCTION

## I. Cell cycle and cell cycle inhibitors

### I.A Cell cycle regulation

The cell cycle is a process that allows a cell to duplicate the whole material and divide into two identical daughter cells. This consists of 4 phases G1 (Gap1), S (Synthesis), G2 (Gap2) and M (Mitosis) comprising two major events: DNA replication and segregation of the replicated DNA. Each step is controlled by numerous proteins and contributes to faithfully duplicate the DNA content and to distribute identical genetic material to two daughter cells (Figure 1). The main actors that regulate cell cycle progression are Cyclin-Dependent Kinases (CDKs), and the fine-tuning of which is essential for an accurate control of the cell cycle. The activation of CDKs is mainly regulated by their regulatory subunits, namely Cyclins D, E, A and B (Table1). In each phase, the abundance of Cyclins fluctuates along with the progression of the cell cycle, triggering the activation of their CDK partners. Besides, inhibitory proteins, called CDK inhibitors (CKI) are responsible for blocking the activity of CDKs. Two families of CKI have been discovered, namely the INK4 and Cip/Kip protein families (Table2).

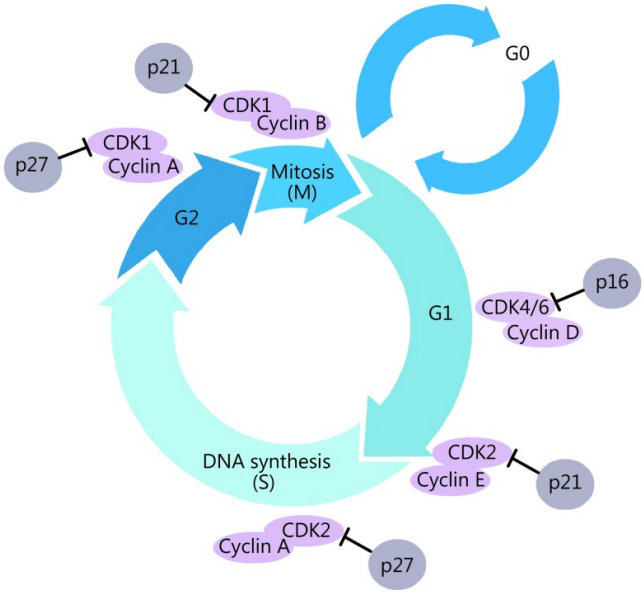


**Figure 1.** A schematic view of the cell cycle. The cell cycle progression is regulated by cyclin-dependent kinases (CDKs), their regulatory partner proteins cyclins, and CDK inhibitors. (Figure from Jingwen, Yaochen and Guojun, 2017)

| CDKS | Cyclin | Cell cycle |
|---|---|---|
| CDK4 | Cyclin D1/2/3 | G1 phase |
| CDK6 | Cyclin D1/2/3 | G1 phase |
| CDK2 | Cyclin E | G1/S phase transition |
| CDK2 | Cyclin A | S phase |
| CDK1 | Cyclin A | G2/M phase transition |
| CDK1 | Cyclin B | Mitosis |
| CDK, cyclin-dependent kinases; G1, pre-DNA synthesis; S, DNA synthesis; G2, pre-division | | |

**Table 1.** CDKs/cyclins activities during the cell cycle (Table from Jingwen, Yaochen and Guojun, 2017)

| **CKI family** | **Function** | **Family members** | |
|---|---|---|---|
| INK4 family | Inactivationof $G_1$ CDK(CDK4, CDK6) | p15 | (INK4b) |
| | | p16 | (INK4a) |
| | | p18 | (INK4c) |
| | | p19 | (INK4d) |
| Cip/Kip family | Inactivation of$G_1$ cyclin-CDKcomplexes andcyclin B-CDK1 | p21 | (Waf1, Cip1) |
| | | p27 | (Cip2) |
| | | p57 | (Kip2) |

**Table 2.** Cyclin dependent kinases inhibitors (CKI) bind to CDK alone or to the CDK-Cyclin complexes and regulate CDK activities. (Table from Vermeulen, Van Bockstaele and Berneman, 2003)

## I.A.1 G1 phase and CDK4/6 regulation

During early G1 phase, synthesis of D-type cyclins (D1, D2, D3) is stimulated by mitogenic stimuli such as extracellular growth factors EGF (epidermal growth factor) and IGF (Insulin-like growth factor). Abundant Cyclin D then associates with either CDK4 or CDK6 (CDK4/6) to form an active CDK4/6-Cyclin D complex (Figure 2.A and 2.B). In fact, CDK4/6

activation is achieved in multiple steps. After the formation of the CDK-Cyclin D complex, the CDK activating kinase (CAK) Cdk7 in complex with Cyclin H and Mat1 fully activates CDK4/6 through the phosphorylation of a conserved Threonine residue located in the active site (as known as T-loop) of CDK4 and CDK6 (Gu, Rosenblatt and Morgan, 1992). Active CDK4/6 then phosphorylate proteins of the pRb-family, namely pRb, p107 and p130 that sequester the transcription factors of the E2F family. Phosphorylated pRb releases the transcription factors E2F1, E2F2 and E2F3 that activate the expression of their respective target genes such as *ORC1, CDC6, CCNA* (Cyclin A) and *CCNE* (Cyclin E) that are involved in cell cycle progression and DNA synthesis (Bracken *et al.*, 2004; Ohtani *et al.*, 1996). P107 and p130 of the pRb family share the function of gene repression in association with E2F4 and E2F5 inhibitory transcription factors (Dyson, 1998).

However, CDK4/6 complexes may also be regulated by their inhibitors, the CKI. The p16 protein inhibitor of the INK4 family can as well bind to both monomeric CDK4/6 and CDK4/6-Cyclin complexes. P16 prevents the activation of monomeric CDK4/6 by blocking their binding to Cyclin D. Actually, p16 is also able to bind CDK4/6-Cyclin D complexes and to inhibit their kinase function by interfering with the accessibility of ATP to the CDK4/6 ATP binding pocket (Jeffrey, Tong and Pavletich, 2000). In contrast to p16, the Cip/Kip family proteins that include p21 and p27 have been found to bind the active forms of CDK4 or CDK6 in complexes with Cyclin D (Cheng, 1999).

## I.A.2 CDK2 regulation in the G1/S transition.

In the early G1-phase, the CIP/KIP family inhibitors p21 and p27 inhibit the catalytic activity of CDK2 by their binding. This maintains the repression of E2F target genes mediated by hypo-phosphorylation of pRb. During the G1/S transition, the activation of CDK2 is mainly coordinated through its association with Cyclin E and by subsequent dephosphorylation/phosphorylation. CDK2 activation relies on the phosphorylation of Threonine 160 by CDK Activating Kinase (CAK) activity. Then, the full activation is achieved by phosphatases CDC25A and CDC25B which are up-regulated at the G1/S transition. These phosphatases dephosphorylate CDK2 on T14 and Y15 residues localized in the inhibitory cleft (Hoffmann, Draetta and Karsenti, 1994; Gu, Rosenblatt and Morgan, 1992), leading to a conformational change that opens the substrate binding site (Bártová *et al.*, 2004). Hence, this active CDK2/CyclinE complex induces the hyperphosphorylation of pRb

that in turn will activate the expression of the E2F target genes involved in DNA replication (Figure 2.C; Bertoli, Skotheim and Bruin, 2015).

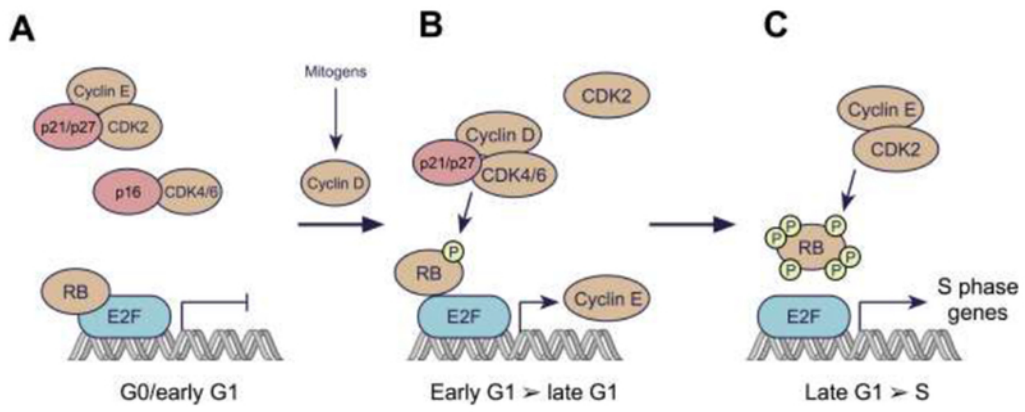


**Figure 2.** The classical model for regulation of the G1/S transition by cyclins and CDKs. (Figure from Goel *et al.*, 2018)

## I.A.3 S phase and CDK1/2-Cyclin A

The increasing level of Cyclin A that will be associated either with CDK2 or CDK1 promotes the S-phase progression. Thus, Robert Fisher's group demonstrated coordination in time for the binding of Cyclin A with the S-phase CDKs. Although CDK1 and CDK2 share common steps for their activation (phosphorylation in their T-loop active site by CAK and binding with Cyclin), they are activated by distinct mechanisms (Figure 3). According to this model, CDK2 takes advantage in the early S phase of its competition with CDK1 for the binding to Cyclin A with whom it forms a stable active complex. It is only when a large part of available CDK2 is associated with Cyclin A in mid-late S phase that Cyclin A begins to bind to CDK1. Then, the full activation of CDK1 requires more complex steps including dephosphorylations on Tyr15 and Thr14 residues by CDC25.

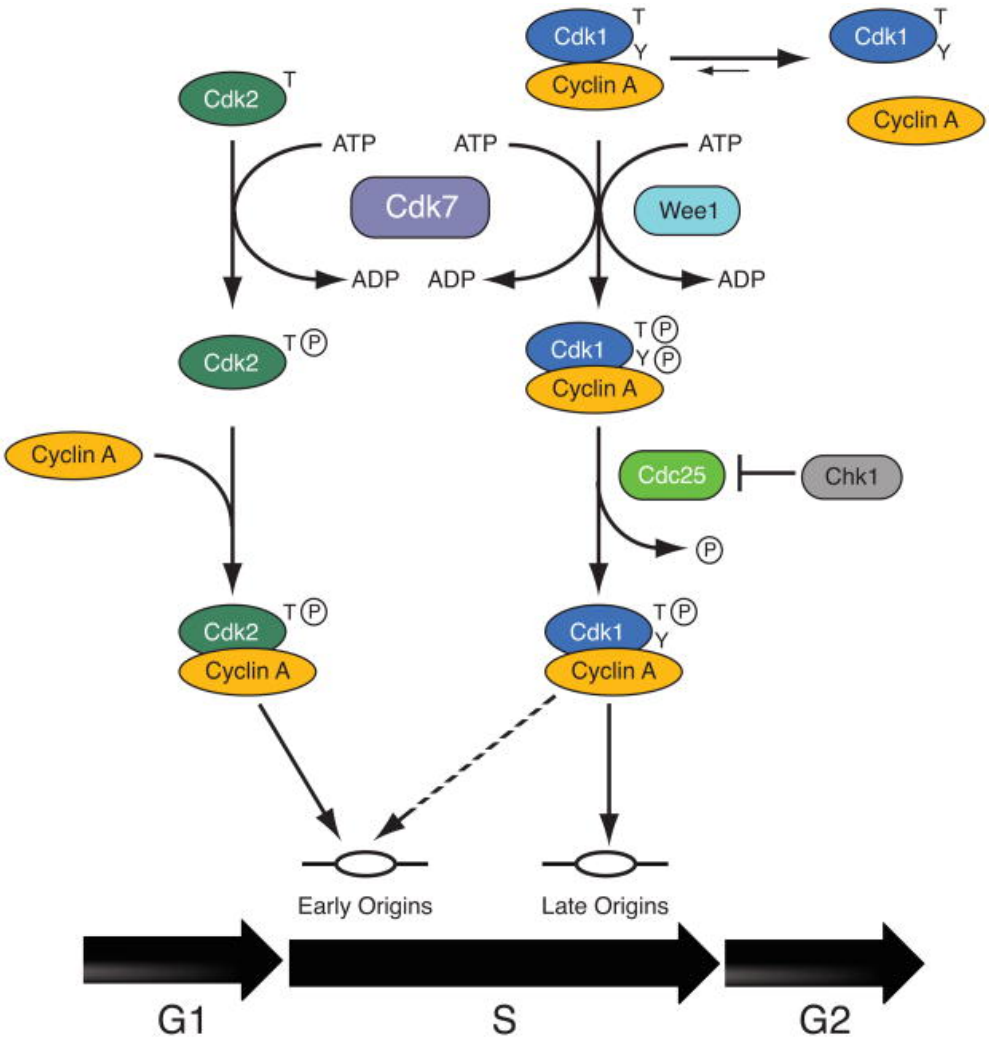


**Figure 3.** Sequential activation of CDK2 and CDK1.
The activation of CDK2 requires the phosphorylation in T-loop before its binding to Cyclin A. The monomer CDK2 could be recognized by CAK and then bind to Cyclin A to form a stable complex. In contrast, CDK1 bound to Cyclin A remains unstable before the phosphorylation by CAK in Thr161. By the fact, CDK2 acts in the early and mid S-phase and CDK1 takes over in late S-phase.
(Figure from Merrick and Fisher, 2010).

Thus, S-phase CDK1/2-Cyclin A complexes are involved in the regulation of DNA replication through two different processes (Coverley, Laman and Laskey, 2002). First, it promotes the initiation of DNA replication and the synthesis of deoxynucleotides during elongation. Secondly, it inhibits the assembly of new pre-RCs (Pre-replication complex) on chromatin to prevent origin relicensing (See more in the chapter Introduction II.A).

## I.A.4 CDK1 in the G2/M phase

CDK1 also plays a pivotal role in the G2- to M-phase transition through its association with either A-type or B-type Cyclin (Enserink and Kolodner, 2010). These complexes ensure a proper chromosome condensation and segregation before the cell division. During the G2-phase, the CDK1/Cyclin A complex phosphorylates the Bora protein required for Aurora A-dependent Polo like kinase 1 (Plk1) activation (Figure 4). The activated Plk1 then phosphorylates Cdc25 which in turn activates the CDK1-CyclinB complex ensuring the entry into mitosis (Gheghiani *et al.*, 2017; Vigneron *et al.*, 2018).

After DNA damage, the G2/M checkpoint is activated to prevent cells harboring irreversible defects from entering into M-phase. Thus, ATM and ATR pathways are activated together with their downstream associated kinases (CHK1 and CHK2) in a context of DNA double strand breaks (DSB) during the G2-phase (Gong *et al.*, 2017; Löbrich and Jeggo, 2007). CHK1 and CHK2 inhibit CDC25 phosphatase, which leads to CDK1 inhibition and prevents mitotic entry (Timofeev *et al.*, 2010).

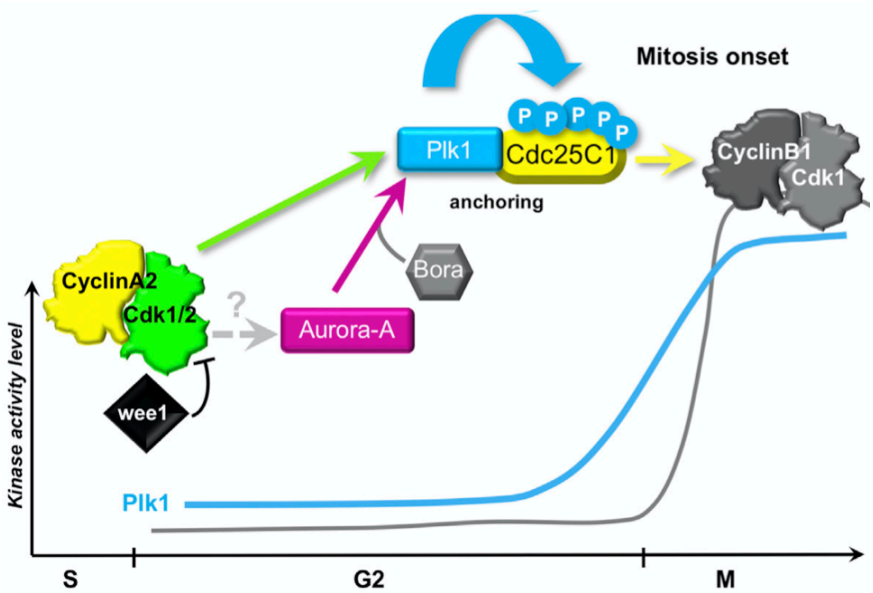


**Figure 4.** Regulation of CDK1 in mitotic entry (Figure from Gheghiani *et al.*, 2017).

Well-controlled progression of the cell cycle is essential to maintain cell integrity. Considering that aberrant cell cycle activity is one of the characteristics of cancer development, targeting the cell cycle has been considered as an attractive option in the field of cancer therapy.

## I.B Chemical CDK inhibitors

### I.B.1 First CDK inhibitors

Based on numerous studies demonstrating involvements of CDK in cancer development, several CDK inhibitors have been developed for cancer treatments. First generations of CDK inhibitors are referred to as 'Pan-CDK' inhibitors because they bind to CDKs with relatively low specificity (Figure 5; Asghar *et al.*, 2015). One of the most studied CDK inhibitors of the first-generation is Flavopiridol developed by Sanofi-Aventis. This molecule has been shown to inhibit *in vitro* CDK1, CDK2, CDK4, CDK6 CDK7 and CDK9. The study of the crystal structure of the CDK2 and flavopiridol complex showed that the aromatic portion of flavopiridol binds particularly to the ATP-binding pocket of CDK2 (De Azevedo *et al.*, 1996). In preclinical studies, flavopiridol was shown to induce either cell cycle arrests in G1/S or G2/M phases or apoptosis. This evidence prompted scientists to drive massive investigations in more than 60 clinical trials since 1988. However, flavopiridol failed to enter phase III-trial due to low level of clinical activity in several solid tumor types.

The second generation of CDK inhibitors was designed with the aim of increasing their specificities for distinct CDKs. Among these, the Dinaciclib developed by Merck has shown more specificity toward CDK1, CDK2, CDK5 and CDK9 than toward CDK4, CDK6 and CDK7. Many studies have demonstrated that Dinaciclib blocks cell cycle progression in several cancer cell lines and reduces tumor development in mouse models. However, Dinaciclib showed no benefit for patients in Phase II clinical trials (Jingwen, Yaochen and Guojun, 2017).

### I.B.2 The third generation of CDK inhibitors: CDK4/6 selective inhibitors

Many evidences have proven that the selectivity of inhibitory action is a key element for more efficacy and less toxicity of a given molecule when used as a cancer treatment. In this context, the third generation of CDK inhibitors is developed to be more potent and specific toward CDK4 and CDK6 proteins. Three CDK4/6 inhibitors are now approved by the FDA (Food

and Drug Administration): Palbociclib (PD-0332991, IBRANCE, Pfizer), Ribociclib (LEE011, KISQALI, Novartis) and Abemaciclib (LY-2835219, VERSENIO, Lilly) (Figure 5).

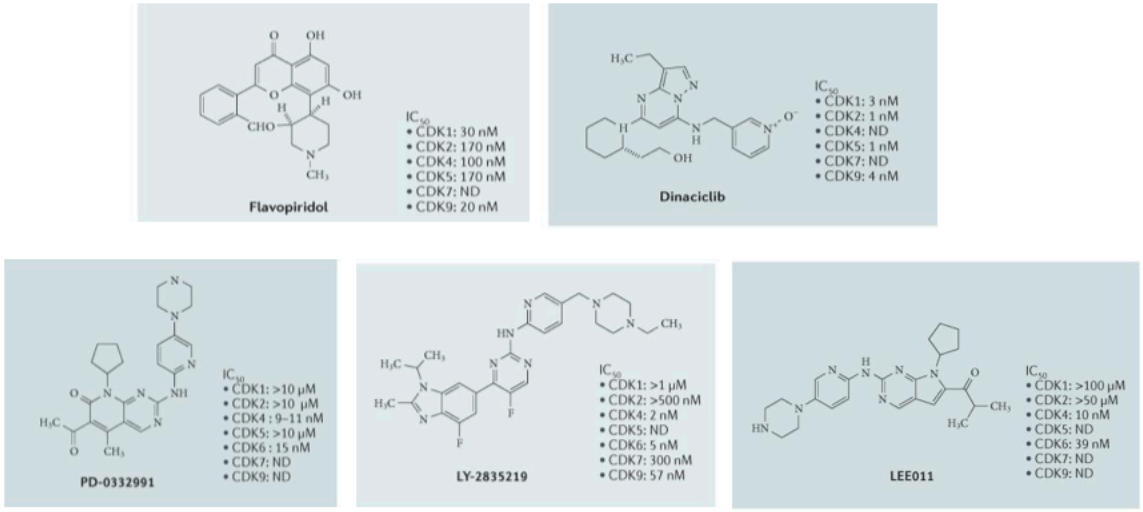


**Figure 5.** The chemical structures of CDK inhibitors.
The published half-maximal inhibitory concentration (IC50) values against selected CDK complexes are shown. ND, not determined (Figure from Asghar *et al.*, 2015)

*I.B.2.a Structural mechanism of inhibition*

The high specificity of these CDK4/6 inhibitors may be illustrated with their IC50 in the nanomolar range exclusively for CDK4 and CDK6 (Chen *et al.*, 2016). X-ray co-crystal structures of CDK6 with each inhibitor were undertaken to explain this specificity at the atomic level (Figure 6). Structural analysis of the CDK6/inhibitor complex reveals that these small inhibiting molecules bind to the ATP-pocket of CDK6, thus inducing a change in the protein conformation from an active to an inactive form. The authors also found that the interaction of the inhibitor with His100 and Thr107 residues near the hinge region of CDK4/6 proteins is responsible for the specificity of the inhibitors, since these residues are only found in CDK4 and CDK6.

In addition, recent studies have revealed that the CDK4/6 activation status influences the affinity of CDK4/6 inhibitors. For instance, the phosphorylation of Thr 172 residue on CDK4 by CAK is necessary for the binding of inhibitors. Also, when bound with p27, CDK4/6 cannot be targeted by CDK4/6 inhibitors (Guiley *et al.*, 2019; Raspé *et al.*, 2017).

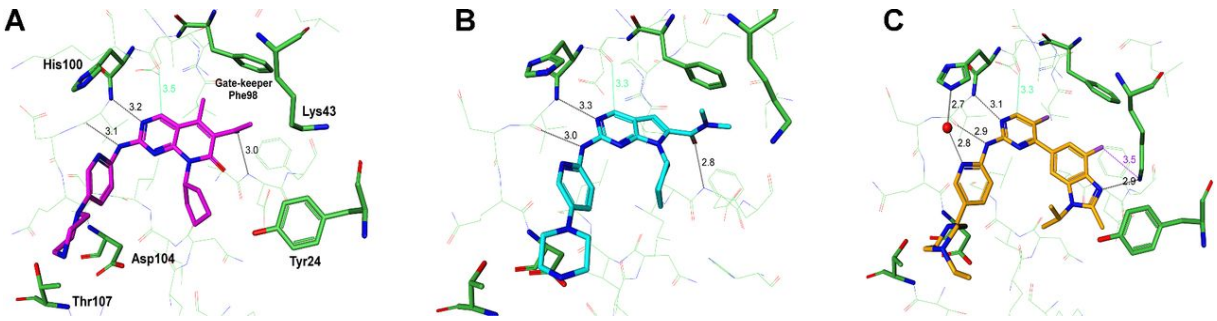


**Figure 6.** Binding modes for third-generation drugs. CDK6 co-crystal structures for: palbociclib (A), ribociclib (B), and abemaciclib (C). Hydrogen bonds are depicted as dotted lines, and key active site residues are named (Figure from Chen *et al.*, 2016)

*I.B.2.b Principal molecular mode of action in cell lines*

Over the past decade, many independent groups have investigated the effects of CDK4/6 inhibitors, unraveling their principal mechanisms of action. The main target of CDK4/6 is the tumor suppressor pRb. Binding of these inhibitors to the ATP-pocket of CDK4/6 hampers the phosphorylation activity of these kinases, which maintains pRb in a hypo-phosphorylated state in particular at the Ser780 residue. Thus, the hypo-phosphorylated pRb sequesters E2F family transcription factors and represses the transcription level of many genes involved in the cell cycle progression and the DNA replication process (Figure 7; Bracken *et al.*, 2004; Sánchez-Martínez *et al.*, 2015) Many studies including ours (See the chapter Result I.A) have described how the inhibitors induce transient (quiescence) or permanent (senescence) cell cycle arrest in G1-phase by monitoring several non-exclusive features for senescence including flat cell morphology, positive staining for senescence-associated β-galactosidase, DNA damage and reversibility after withdraw of drug.

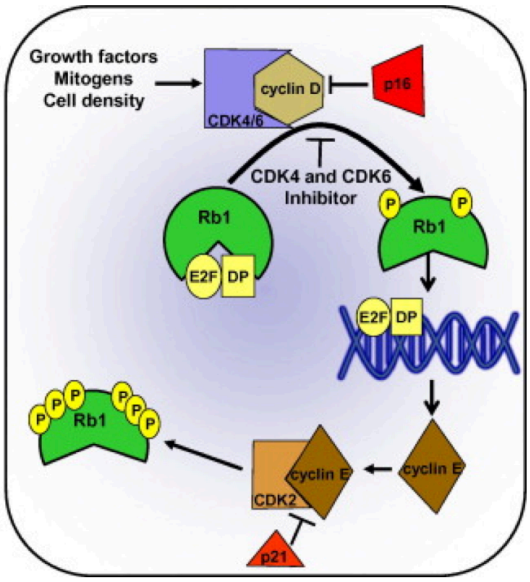


**Figure 7.** CDK4/6 inhibitors and pRb pathway (Figure from Sánchez-Martínez *et al.*, 2015)

The inhibition of CDK4/6 also hampers the phosphorylation of the pRb-like proteins p107 and p130 and maintain "Dimerization partners, Rb-like, E2F and Multi-vulval class B (DREAM)" complex (Figure 8; Engeland, 2018). When p107 and p130 are hypo-phosphorylated, they promote the formation of DREAM complexes that function as transcriptional repressors. Many of the downstream genes regulated by DREAM are related to the progression of the cell cycle, notably to important genes for the G2/M transition and mitosis.

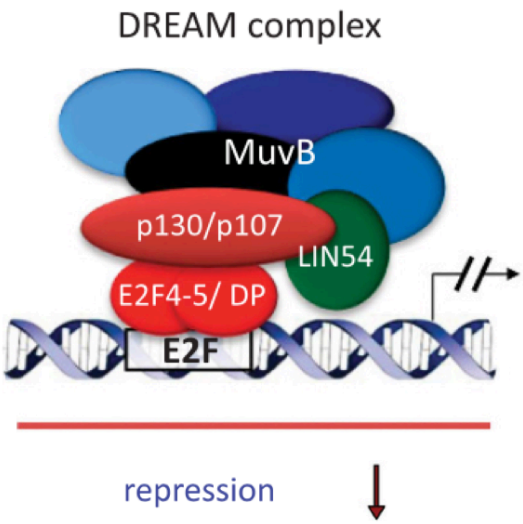


**Figure 8.** DREAM complex binds E2F to repress the expression of target genes (Figure from Engeland, 2018).

It has been shown that palbociclib effectively leads to dephosphorylation of p107 and p130 in several cancer cell lines, contributing to cell cycle arrest along with pRb (Dayana B Rivadeneira *et al*., 2010). Erik S Knudsen's group revealed that an acute loss of pRb in pRb proficient hepatoma cell lines triggers the accumulation of p107 that compensates the response upon CDK4/6 inhibition. However, the authors found that p107 and p130 are not affected in pRb-deficient hepatoma cell line (Hep3B) exhibiting resistance to CDK4/6 inhibition, implying that the proliferation in pRb negative cancer cells is not dependent on CDK4/6 activity.

*I.B.2.c Predictive biomarkers*

In an effort to refine the response to CDK4/6 inhibitors, many studies have investigated the resistance and adaptation shown upon treatment with CDK4/6 inhibitors. Most cases are related to an alteration of the pRb pathway. For example, a group has shown that the effect of palbociclib in hepatocellular carcinoma (HCC) cell lines are dependent on the presence of pRb (Bollard *et al.*, 2016). They tested the effects of 1μM of palbociclib on the proliferation of 15 liver cancer cell lines and observed that 14 out of 15 were sensitive to palbociclib. Hep3B cells were the exception and displayed an absence of pRb. Furthermore, the authors generated palbociclib-resistant cell lines by long exposure of cells with increasing doses of the inhibitor. They showed that pRb protein level was completely lost or reduced, indicating that the loss of pRb function would be a signature for the resistance to palbociclib. Another predictive feature for resistance is the overexpression of Cyclin E. Thus, palbociclib resistant MCF-7 cells (from a breast cancer cell line) were obtained by chronic exposure to 1μM of palbociclib during 3 to 4 months. Resistant cells showed a higher expression of Cyclin E1 protein that was due to the amplification of the *CCNE1* gene (Garcia-murillas *et al.*, 2017). These cells failed to reduce the phosphorylation level of pRb and bypassed the G1/S checkpoint. These findings underlie that alterations in the expression of genes like *CCNE1* and *RB1* are now largely considered as common biomarkers to predict resistance to CDK4/6 inhibitors.

*I.B.2.d Clinical trials and therapeutic uses*

On the basis of the numerous preclinical studies that supported anti-proliferative effects of CDK4/6 inhibitors, these inhibitors have been investigated for several clinical trials. Among these, phase III studies have demonstrated improvement in median PFS (progression free survival) for patients treated with CDK4/6 inhibitors in combination with endocrine therapies in advanced and metastatic breast cancer (Table 3; Spring *et al.*, 2019). (Note that PFS means the length of time during and after the treatment of a disease, such as cancer, that a patient lives with the disease but without any worsening as defined by the National Cancer Institute) As a consequence, these three inhibitors are FDA-approved for the treatment of hormone receptor-positive (HR+) metastatic breast cancers in combination with endocrine therapies such as non-steroidal aromatase inhibitor or fulvestrant (oestrogen receptor antagonist). Regarding toxicity or adverse effects, hematologic toxicities were reported but could be managed by a decrease in the inhibitors dose. Other non-hematologic toxicities such as fatigue, nausea, diarrhea, decreased appetite, and infections are considered to have a mild impact on the therapy efficacy (Sobhani *et al.*, 2019). To date, based on these encouraging results, more ongoing clinical trials have been conducted for treatments of other breast cancer subtypes (HER2 positive or triple negative) by CDK4/6 inhibitors either alone or in combination with other therapies (Chen *et al.*, 2019). However, as mentioned above, resistance to inhibitors that mainly involves the pRb pathway has been observed in preclinical studies. Consistent with these findings, an alteration of the pRb pathway was observed in patients in PALOMA-3 study by the analysis of the circulating tumor DNA (Chen *et al.*, 2019; Spring *et al.*, 2019). Understanding the molecular mechanisms of resistance is thus an essential key to reduce failure of treatments.

Phase III studies of CDK 4/6 inhibitors in breast cancer

| Study | CDK 4/6 Inhibitor | Study Population | Line of Therapy | Sample Size | Median PFS (months) vs. Placebo |
|---|---|---|---|---|---|
| *Trials in combination with NSAIs* | | | | | |
| PALOMA-2 [17] | Palbociclib | Postmenopausal women with HR+/ HER2- ABC and no prior systemic treatment for ABC; (neo)adjuvant ET permitted if disease-free interval > 12 months from therapy completion | 1st line | 666 | 24.8 vs. 14.5 (HR 0.58; *P*< . 001) |
| MONALEESA-2 [16] | Ribociclib | | 1st line | 668 | 25.3 vs. 16.0 (HR 0.57; *P*< . 001) |
| MONARCH 3 [18] | Abemaciclib | | 1st line | 493 | NR vs. 14.7 (HR 0.54; *P*< .001) |
| *Trials in combination with fulvestrant* | | | | | |
| MONALEESA-3 [21] | Ribociclib | Postmenopausal women and men with HR+/HER2- ABC, 0–1 line of ET for ABC ** | 1st and 2nd line | 726 | 20.5 vs. 12.8 (HR 0.60; *P*< . 001) |
| MONARCH 2 [22] | Abemaciclib | Women with HR+/HER2- ABC that had progressed during prior ET, any menopausal status, ≤ 1 ET, no prior CT for advanced disease *** | 2nd line | 669 | 16.4 vs. 9.3 (HR 0.55; *P*< .001) |
| PALOMA-3 [19,20] | Palbociclib | Women with HR+/HER2- ABC that relapsed or progressed during ET, any menopausal status, ≤ 1 line of CT for advanced disease * | 2nd line and plus | 521 | 9.5 vs. (HR 0.46; *P*< .001) |
| *Trials in combination with tamoxifen or NSAI + Goserelin* | | | | | |
| MONALEESA-7 [23] | Ribociclib | Pre/perimenopausal women with HR+/HER2- ABC, no prior ET for advanced disease, ≤ 1 line of CT for advanced disease | 1st line | 672 | 23.8 vs. 13.0 (HR 0.55; *P*< . 001) |

Palbociclib dose was 125 mg daily orally and ribociclib dose was 600 mg daily orally on a 3 week on, 1week off schedule in all studies. Abemaciclib final dose was 150 mg orally twice a day continuously. Abbreviations: NSAI, non-steroidal aromatase inhibitor; ABC, advanced breast cancer; ET, endocrine therapy; CT, chemotherapy; NR, not reached; PFS, progression-free survival; HR, hazard ratio.

**Table 3**. Phase III studies of CDK4/6 inhibitors in breast cancers (Figure from Spring *et al.*, 2019)

## I.B.3 CDK4/6 inhibitors beyond the pRb pathway

Given that pRb is considered as a biomarker for the response to CDK4/6 inhibitors, many studies have focused on their antitumoral effects in pRb proficient cells. Actually, due to their narrow specificity for CDK4 and CDK6, these inhibitors are highly dependent on the presence of pRb. However, these three inhibitors have their own specificity with different spectra of affinity to other proteins referred to as “off-target”. Indeed, ribociclib is the most specific drug targeting CDK4 and CDK6 as compared to palbociclib and abemaciclib which also target other kinases with relatively low affinity. Palbociclib has been shown to target among others casein kinase 2 and PIK3R4 (Phosphoinositide-3-Kinase Regulatory Subunit 4) which regulate autophagy (Natalia J. Sumi). Unlike ribociclib and palbociclib, abemaciclib

shows toxicity at doses lower than 1μM in pRb deficient cell lines, implying a larger spectrum of off-targets (Knudsen *et al.*, 2017). Consistent with the finding, a multi-omic study revealed that abemaciclib also targets other kinases including CDK1 and CDK2 (Hafner *et al.*, 2019).

Some studies showed that CDK4/6 inhibitors may have "non-canonical" mechanisms of actions on CDKs. Pierre Roger's group has shown that palbociclib efficiently inhibits the activity of CDK4/6 but paradoxically stabilizes CyclinD3 bound to CDK4/6 (Paternot *et al.*, 2014). Strikingly, this complex has been found to be devoid of p21 and p27 kinase inhibitors. This CDK6/CyclinD3 complex could be activated after the elimination of palbociclib by inducing cell cycle entry even in absence of any mitogenic stimulation. Moreover, a recent study has revealed the crystal structure of trimeric p21/p27-CDK4-CylinD complexes and discovered different mechanisms of action of palbociclib in relation to different allosteric forms of these enzymes (Figure 9; Guiley *et al.*, 2019). Indeed, phosphorylated p27 complexes with CDK4/CyclinD1 are activated to promote its kinase activity. This trimeric complex has been shown to be insensitive to palbociclib. Surprisingly, palbociclib preferentially binds to monomeric CDK4/6 in breast cancer cell lines, which prevents the binding of p21 to the CDK4/6-CyclinD complexes. As a consequence, this free p21 was shown to inhibit CDK2 instead. This reveals that the CDK4/6 inhibitors have indirect effect on CDK2 by a non-canonical pathway of p21.

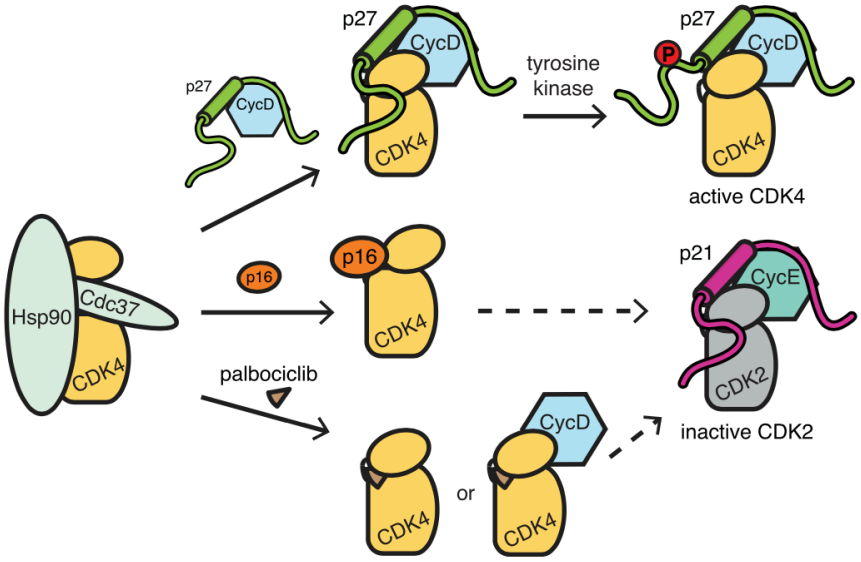


**Figure 9.** Model for understanding how palbociclib contributes to the formation of inactive CDK2. (Figure from Guiley *et al.*, 2019)

Finally, many evidences illustrate that CDK4/6 inhibitors impact cellular metabolism. For instance, it has been reported that CDK4/6 inhibitors induce autophagy in several cancer cell lines. In this context, autophagy inhibitors such as chloroquine and Spautin-1 have been combined with CDK4/6 inhibitors and have been shown to have synergistic effects in breast and gastric cancer cell lines (Valenzuela *et al.*, 2017; Vijayaraghavan *et al.*, 2017). All these findings strongly suggest that the mechanisms of action of CDK4/6 inhibitors are not as simple as expected but seem more sophisticated.

# II. DNA replication and cancer

## II.A DNA Replication

DNA replication is a highly regulated molecular process that ensures the duplication of the genetic material with accuracy and fidelity. This process comprises several steps that occur through G1- and S- phases of the cell cycle: origin licensing, origin activation, duplication of DNA and termination (Figure 10). In metazoans, thousands of origins are licensed in G1-phase and a subset of them will be activated in S-phase to initiate the synthesis of DNA by applying the replication timing program defined during the Timing Decision Point (TDP) at the very beginning of the G1-phase.

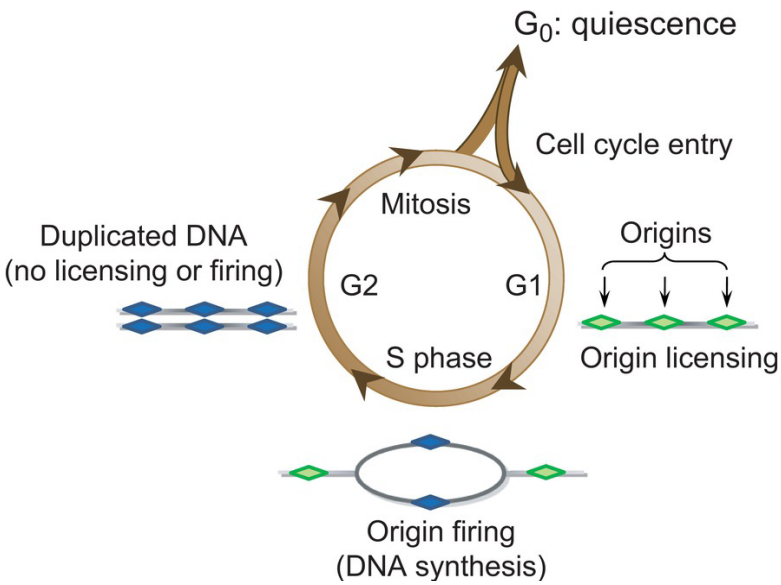


**Figure 10.** Cell cycle and DNA replication (Figure from Nevis *at al*.,2015).

## II.A.1 Origin licensing

### *II.A.1.a Loading of the Origin Replication Complex*

At the molecular level, during the G1-phase, CDKs signaling pathway drives cells to prepare the DNA synthesis through the origin licensing step, named Origin Decision Point (ODP). The very first step of DNA replication initiation occurs with the loading on chromatin of the origin recognition complex (ORC) composed of 6 protein subunits (ORC 1-6) (Kara *et al.*,

2015). This complex binds to chromatin in an ATP-dependent manner and then recruits two essential origin licensing factors, namely Cdc6 and Cdt1. It is of note that the level of Cdt1 is regulated through its sequestration by Geminin (Ballabeni *et al.*, 2013; Fujita, 2006). Furthermore, Geminin maintains the levels of Cdt1 by preventing its degradation in mitosis, thus contributing to prepare the pre-RC formation in G1-phase (Ballabeni *et al.*, 2013).

*II.A.1.b Assembly of the Pre-RC*

During the early G1-phase, the cell cycle regulatory E3 ubiquitin ligase anaphase promoting complex/cyclosome (APC/C) targets Geminin for proteasome degradation, releasing Cdt1. Then, the chromatin-bound ORC/Cdc6 complex and Cdt1 are essential to recruit the Minichromosome Maintenance (MCM) Complex required for the assembly of pre-replication complex (Pre-RC) (Figure 11.A; Randell *et al.*, 2006). MCM complexes are then loaded as head-to-head double hetero-hexamers (composed of the 6 subunits MCM2-7) and function as replicative helicases that will unwind DNA into two directions once activated (Evrin *et al.*, 2009).

The Pre-RC assembly is not sufficient to decide where and at what time replication will initiate. Therefore, the initiation is regulated by a precise spatial and temporal program during the G1-phase set up at the TDP and ODP at a whole genome scale (Figure 11.B and C; Gilbert, 2009; Marchal, Sima and Gilbert, 2019).

*II.A.1.c Spatial and Temporal regulation of DNA replication*

After the formation of the pre-RCs, the TDP occurs in early G1-phase. Replication timing is tightly linked to the re-positioning of the chromosomes in nuclear architecture, by which early replicating domains and late replicating domains are distinguished (Gilbert, 2010). Indeed, two distinct compartments of chromatin have been distinguished by comparison of 'replication foci' in early S phase and late S phase. These two compartments are indicative of early replication and late replication domains which are located in interior regions of the nucleus and in the regions at the nuclear periphery and around the nucleolus, respectively (Figure 11.C).

Hence, after the TDP, the ODP determines which origins will be activated. Initially, this concept was well established in a model using isolated nuclei from Chinese hamster ovary cells and Xenopus egg cytosol (Wu and Gilbert, 1996). The authors demonstrated that DNA

replication in the Dihydrofolatereductase (DHFR) locus initiates at specific origin sites when nuclei are isolated in late-G1, but at random sites when nuclei are isolated in early-G1. The findings identified a distinct G1 step that specifies the replication origins. This spatial and temporal organization of replication guarantees cells the availability of limiting factors such as nucleotides and required proteins at different times in order to ensure a complete duplication of DNA.

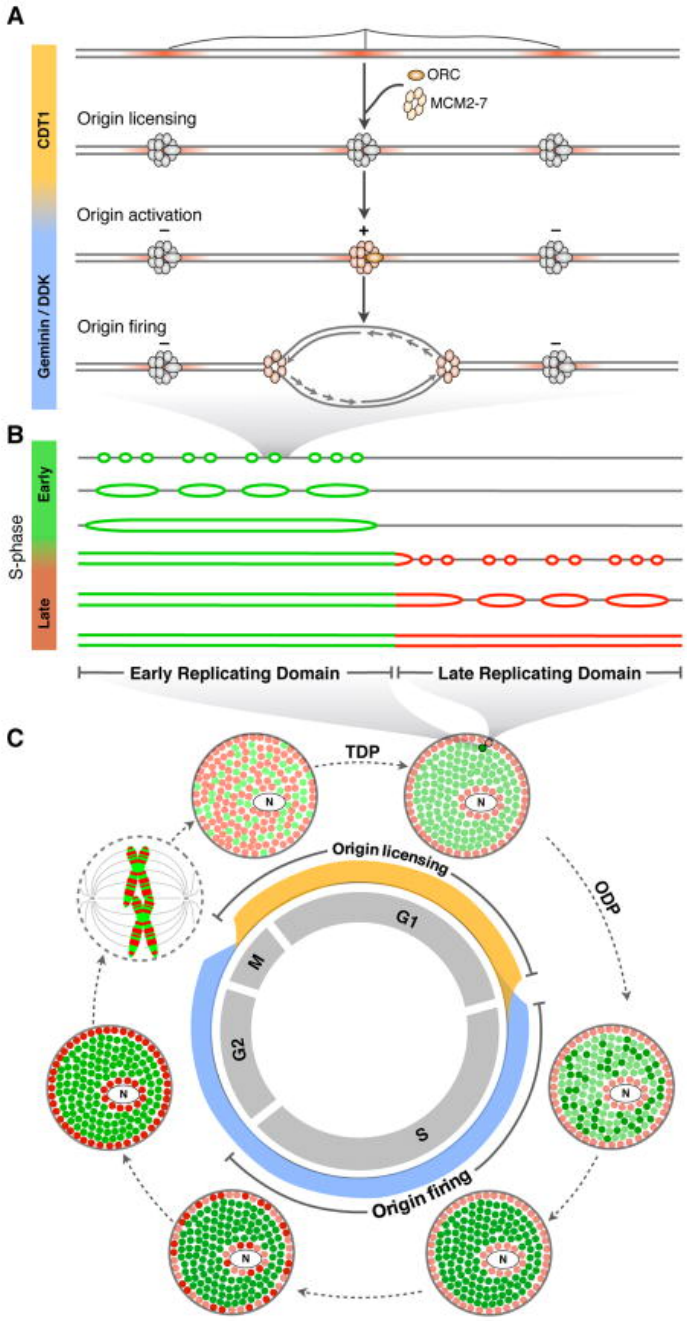


**Figure 11.** The distinct scales of DNA replication regulation in eukaryotes. A) Replication origin regulation at the molecular level B) DNA replication regulation at the replication domain scale. C) DNA replication at the nuclear scale and its regulation during the cell cycle. (Figure from Rivera-Mulia and Gilbert, 2016)

## II.A.2 Origin firing

Once the Pre-RC is assembled, licensed origins are ready to be activated throughout the S-phase (Figure 12.a). To activate replication origins, the Pre-RC needs to be converted to a Pre-Initiation Complex (Pre-IC) through multiple steps (Figure 12.b). The key elements that coordinate the transition between Pre-RC and Pre-IC are Dbf4 dependent kinase (DDK) and S-phase CDKs. DDK complex consists of the protein serine/threonine kinase Cell Division Cycle 7 protein (CDC7) and its catalytic subunit DBF4. The regulation of *DBF4* gene expression depends on the cell cycle progression (Jiang *et al.*, 1999). Indeed, *DBF4* gene expression has been shown to be upregulated in the G1-phase, which in turn elicits the functional activity of CDC7. High activity of DDK and S-phase CDK is required for the initiation of replication. They collaborate to phosphorylate MCM components, which promotes the recruitment of helicase activators, Cell division cycle 45 (CDC45) and Go-Ichi-Ni-San complex (GINS) on chromatin. This leads to the formation of a functional helicase: the Cdc45-MCM-GINS (CMG) complex (Sheu and Stillman, 2010). It is also of note that CDK and DDK play pivotal roles in activating other replicative factors necessary for the CMG assembly such as Treslin, TOPBP1, RecQL4 and MCM10 (Figure 12.b; Im *et al.*, 2009). CDK2 will then phosphorylate Treslin, facilitating its binding with TopBP1. Indeed, Treslin and TOPBP1 have been demonstrated to interact with CDC45 and to be required for its recruitment to chromatin. In addition, CDK2 phosphorylates RecQ4 which is required for the activation of the CMG complex together with Mcm10 (Tanaka and Araki, 2013).

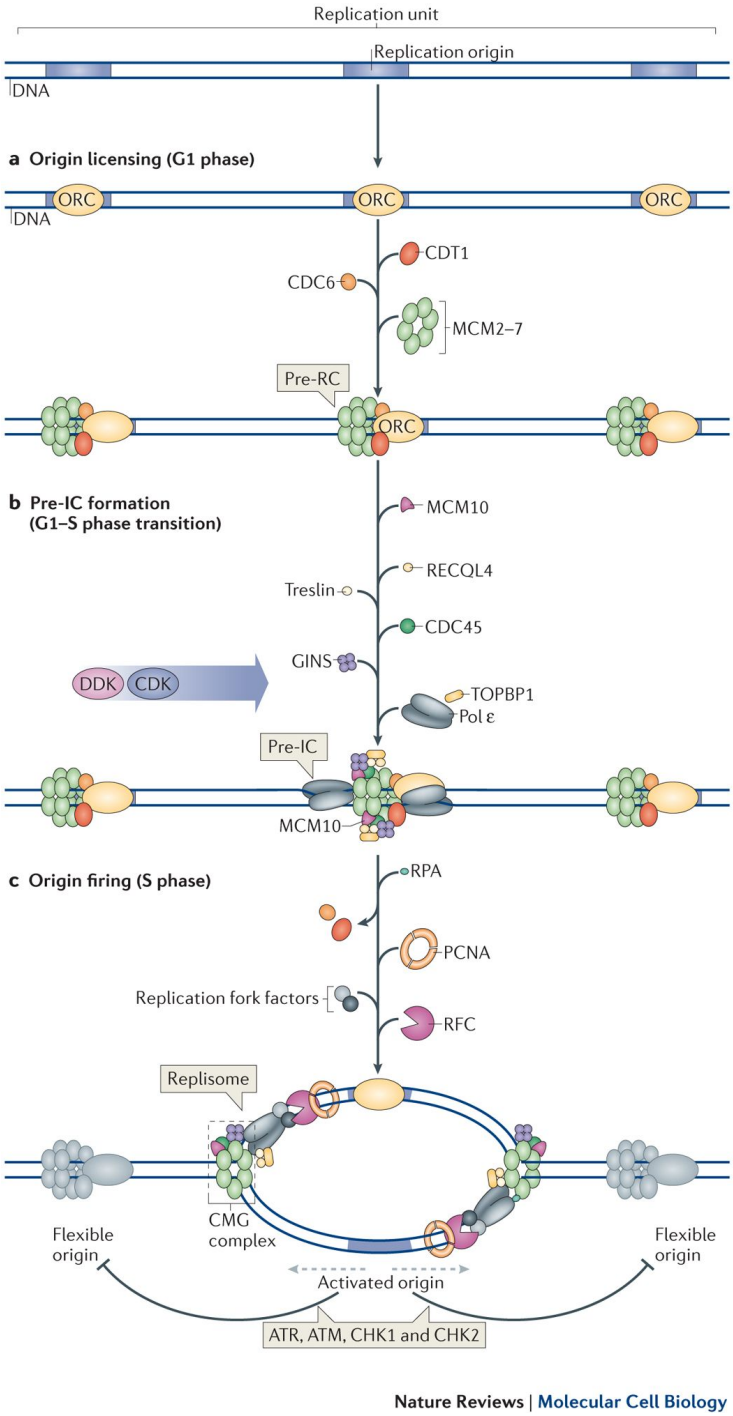


**Figure 12.** Formation and activation of DNA replication origins (Figure from Fragkos *et al.*, 2015)

## II.A.3 Elongation

To start DNA synthesis, a replicative machinery referred to as the replisome is required to be assembled. In addition to the CMG complex, DNA polymerases, replication factor C (RFC), proliferating cell nuclear antigen (PCNA), replication protein A (RPA) and other factors are needed to be loaded onto chromatin (Figure 12.c).

As a functional helicase, the CMG complex unwinds double strand DNA. Indeed, as the helicase progresses, single strand DNA (ssDNA) is formed and stabilized by RPA binding, thus protecting the gap between DNA polymerases and the helicase. The elongation of DNA replication then relies on the activity of three replicative DNA polymerases, α, δ, ε (in the direction 5'-3' on the DNA strands). DNA Polymerase α-primase complex is essential for the initiation of the elongation on both the leading and lagging strands. This complex consists of 4 subunits including p48 for the RNA primase activity and p180 for the polymerase activity. Primase synthesizes a short stretch of RNA on ssDNA to provide a primer for Polα which initiates the synthesis of DNA. Then, RFC recruits PCNA and helps switch from Polα to Polε on the leading strand. Polε extends bulk DNA with a high fidelity through its 3′-5' exonuclease activity which allows the proofreading of its own errors. On the lagging strand, Polα initiates and Polδ takes over the DNA synthesis forming the Okazaki fragment. To complete DNA synthesis, maturation of the Okazaki fragment is required (Stodola and Burgers, 2016). When Polδ reaches to the end of each downstream Okazaki fragment, it carries out the strand displacement synthesis. Then, Flap Endonuclease 1 (FEN1) and DNA ligase I allow to remove the RNA primer and ligate the gaps between two Okazaki fragments (Dewar and Walter, 2017).

## II.A.4 Termination

The termination of DNA replication occurs when two replication forks converge, ensuring the completion of DNA synthesis. This process includes the convergence of the forks, the decatenation for the resolution of topological stress and the disassembly of the replisomes (Dewar and Walter, 2017). First, two replication forks encounter without detectable pausing or stalling, but bypass each other, remaining the formation of positive DNA supercoils. In order to resolve this topological stress, DNA topoisomerases are involved in the elimination of catenanes, which is called decatenation. Finally, the replisomes dissociate from the chromatin. This step requires CMG disassembly by ubiquitination. E3 ubiquitin ligase Cullin Ring Ligase 2 with Lrr1 ($CRL2^{Lrr1}$) ubiquitin Mcm7, which recruits the p97/VCP segregase, an AAA–ATPase that in turn releases CMG complexes from chromatin (Dewar *et al.*, 2017).

Accurate DNA replication determines the integrity of the genome. In the next chapter, we will see how defects in the DNA replication process threaten genomic instability and contribute to the development of cancer.

## II.B Replication stress and cancer

Classically, Replicative stress (RS) is defined as slowing down, stalling or collapsing of replication forks (Gaillard, García-Muse and Aguilera, 2015). This phenomenon is characterized by the uncoupling of the helicase and the DNA polymerase, forming a large gap of ssDNA between the two machineries. Then, ssDNA is coated with RPA and triggers S-phase DNA checkpoint through ATM/ATR pathways (Figure 13).

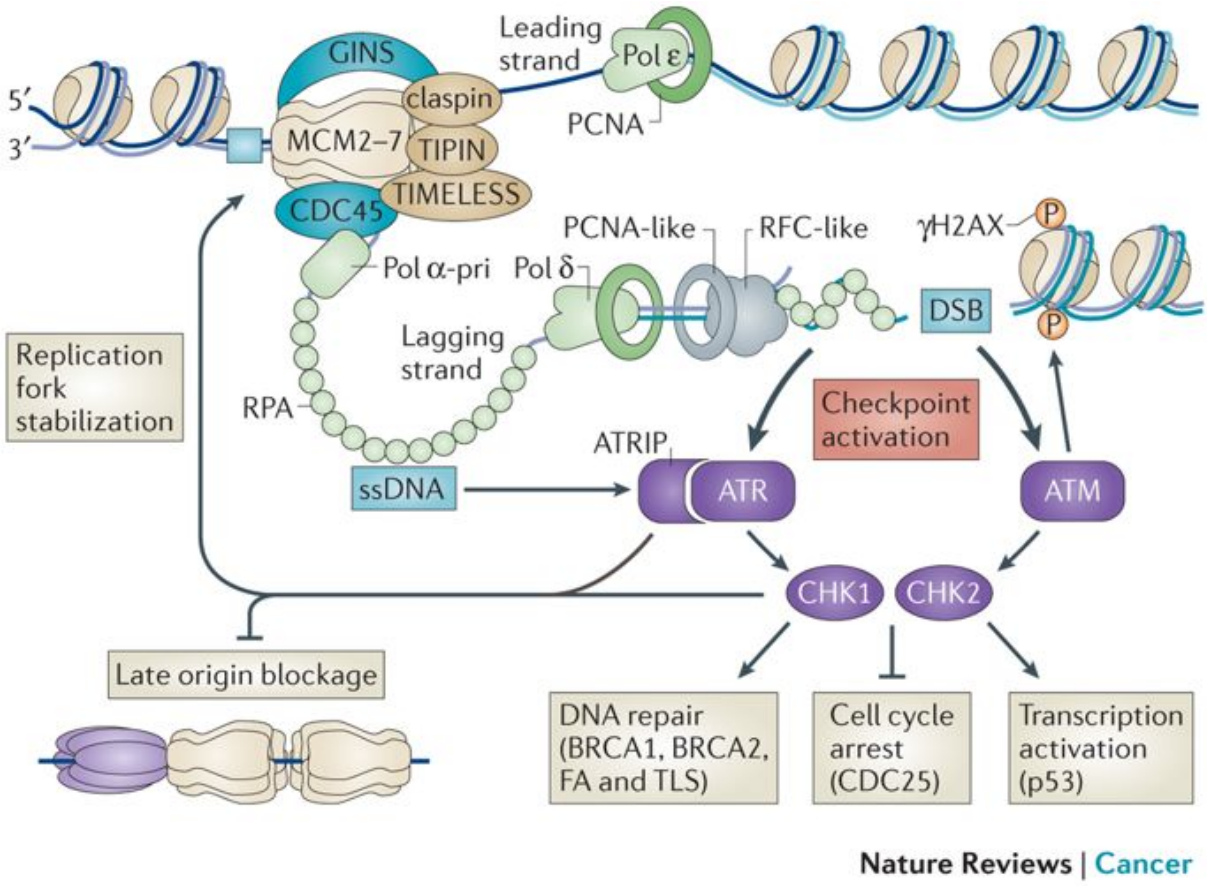


**Figure 13.** Replication impairment activates the checkpoint. (Figure from Gaillard, García-Muse and Aguilera, 2015)

### II.B.1 Natural sources of replication stress

During the elongation process, replication forks encounter natural barriers that may be sources of replicative stress. These barriers represent DNA secondary structures such as hairpins, G-quadruplexes (G4), R-loops or altered DNA topology induced by torsional stress,

and also ssDNA or DSBs (Figure 14.a; Gaillard, García-Muse and Aguilera, 2015). In order to complete DNA replication, the cells have to manage these obstacles through several strategies including the ones based on the ability of DNA helicases to unwind double stranded DNA. Among them, Werner syndrome ATP-dependent helicase (WRN) is a member of the RecQ family of helicases that possesses a 3'->5' exonuclease activity. It has been demonstrated that WRN is necessary to restart stalled forks, and that it efficiently unwinds G4. Actually, defects in WRN have been shown to induce replication stress (Mohaghegh, 2001). Mutations affecting WRN activity are the cause of Werner syndrome and are associated with a high risk of cancer development (Mukherjee *et al.*, 2018).

In addition, several trans-acting factors can also have impacts on the progression of replication forks. Since Deoxynucleotide triphosphates (dNTPs) are critical replicative factors, their shortage could also slow down the progression of replication forks. A reduced chromatin accessibility due to its local condensation, to tightly DNA-bound proteins or to active RNA polymerases are also factors that may impede the progression of replicative forks during elongation (Figure 14.b).

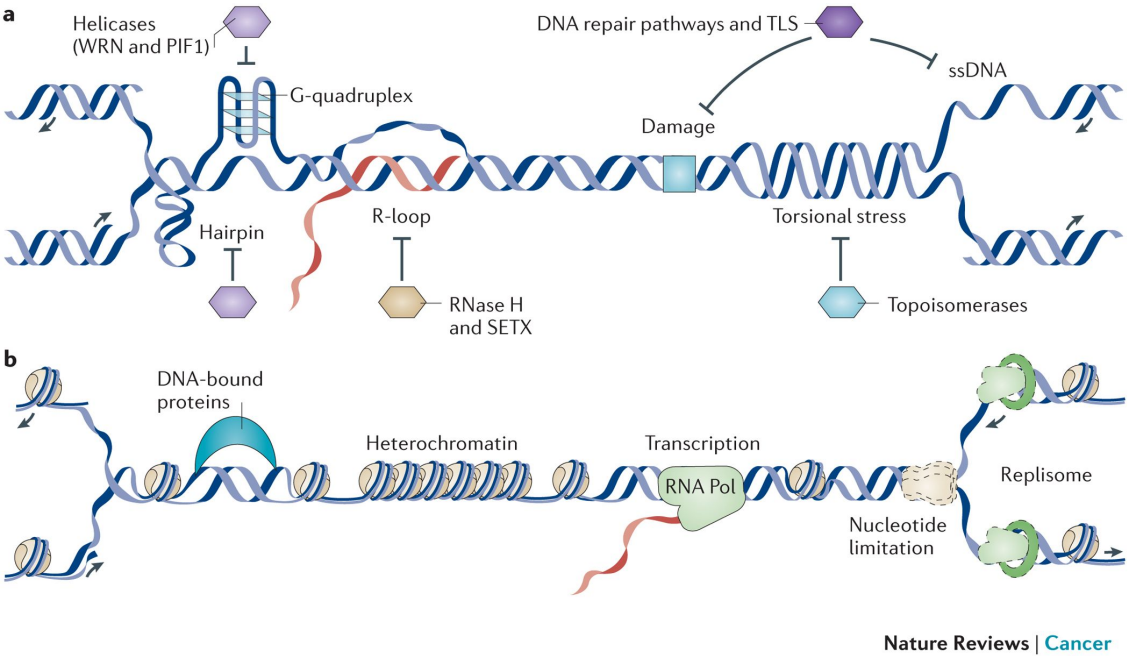


**Figure 14.** Impaired replication fork progression. a) Secondary DNA structures and b) Trans factors or conditions impairing replication fork progression (Figure from Gaillard, García-Muse and Aguilera, 2015)

## II.B.2 Oncogene induced replication stress

Defects in the initiation of DNA replication are sources of replication stress. Activation of oncogenes can cause aberrations in origin licensing and firing steps through different mechanisms (Petropoulos *et al.*, 2019). This includes either inefficient origin licensing or origin firing, or unscheduled replication initiation such as re-replication or premature origin activation (figure 15). Those defects in the initiation of DNA replication may generate replication stress and threaten the stability of the genome, thus contributing to tumorigenesis.

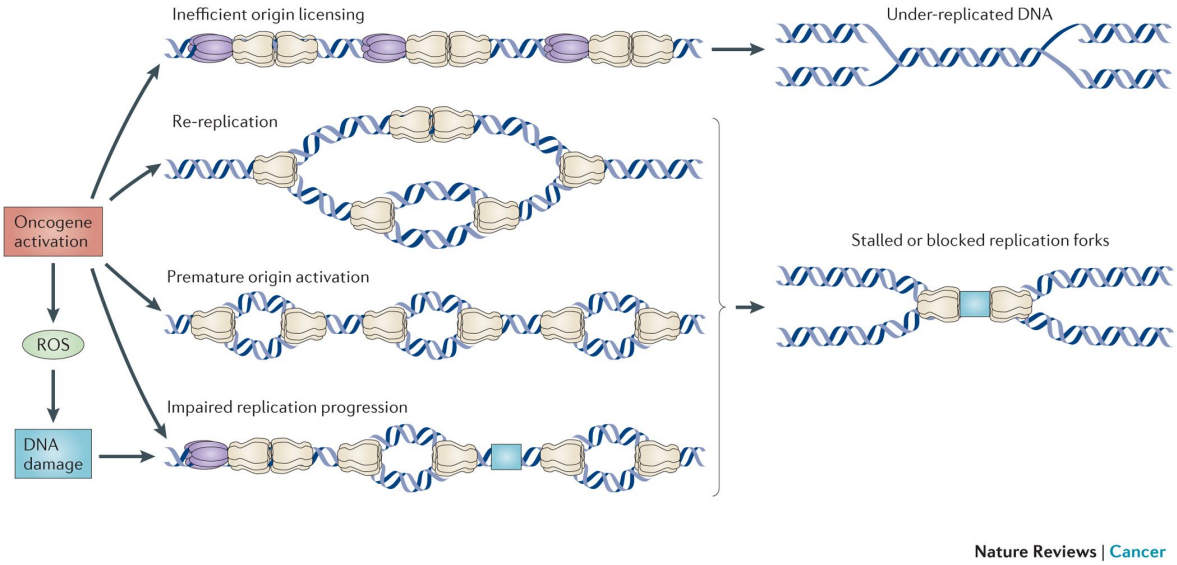


**Figure 15.** Oncogene-induced replication stress. (Figure from Gaillard, García-Muse and Aguilera, 2015)

*Perturbation in the number of activated origins*

Thousands of origins are licensed in human cells to ensure a complete and timely controlled DNA replication, even though many of them remain dormant in an unperturbed S phase. Actually, these dormant origins are only fired as a backup system in presence of replicative stress (Mcintosh *et al.*, 2012; Courtot, Hoffmann and Bergoglio, 2018). An efficient origin licensing and firing is obviously critical to maintain the integrity of the genome. In this context, a reduced number of licensed origins or an insufficient number of activated origins could be a threat to a successful and on time replication process. Armelle Lengronne and Etienne Schwob demonstrated the role of the yeast CDK inhibitor Sic1 in promoting origin licensing in late G1-phase. The lack of Sic1 triggers the initiation of DNA replication with a reduced number of origins and an extension of S-phase, resulting in the instability of the genome (Lengronne and Schwob, 2002). Similarly, in human cells an overexpression of

Cyclin E in late mitosis and early G1 prevents the loading of MCMs on chromatin and interferes with the assembly of Pre-RCs, which leads to a reduced number of licensed origins. In addition, the shortening of the G1-phase is an underlying mechanism by which cells prematurely enter in the S-phase (Ekholm-Reed *et al.*, 2004; Ahuja *et al.*, 2016). A reduced number of active origins can generate replication stress, as in this condition replicative forks would have to overcome longer distances. This could increase the probability of the forks to encounter barriers that would induce their stalling. This, in turn, would activate the S-phase checkpoint in the cells, resulting in a decrease in the firing of dormant origins. Hence, some defects in origin activation may cause uncompleted DNA replication called under-replication (figure 15; Gaillard, García-Muse and Aguilera, 2015)

In contrast, ectopic or premature origin firing may also induce replication stress. This can lead to a lack of necessary replication factors that may induce a slowdown of forks. It has also been shown that a greater number of activated origins increases the chances for the replisome to encounter the transcription machinery, which will cause collisions of the two machineries and potential impediments to the replication fork progression (Macheret and Halazonetis, 2018).

*Re-replication*

The DNA Replication is a precisely regulated process prone to occur with a 'once and only once' rule in a single cell cycle (Machida, Hamlin and Dutta, 2005). Another source of replication stress is the re-replication phenomenon, which occurs when pre-RCs are re-loaded on chromatin, indicating a re-licensing of the origins. This unscheduled replication contributes to form a multi-fork structure with a higher risk of fork collision (Figure 15). Through this increase in the number of replication forks, re-replication may also result in a deficit of replication factors that cause fork stalling or slowing down. As a result, re-replication prompts DNA breaks and partial aneuploidy after the segregation of chromosomes (Neelsen *et al.*, 2013). As mentioned above, Cdt1 plays a key role in the formation of pre-RCs, and its degradation avoids the re-replication process to prevent new origin licensing in S-phase. An overexpression of Cdt1 has been shown to cause re-replication with an accumulation of cells in G2/M phase and the appearance of a subpopulation of cells whose DNA content is greater than 4C (Hall *et al.*, 2008).

*Reactive Oxygen Species*

It is now well established that Reactive Oxygen Species (ROS) represent a significant source of endogenous DNA damage (Srinivas *et al.*, 2019). The accumulation of DNA damage leads to the blockage of the elongation step, which could increase the possibility to disrupt the progression of replication forks. Otherwise, a recent study has demonstrated that redox signaling mediates a link between the biosynthesis of dNTPs and the replisome activity (Somyajit *et al.*, 2017). They showed that a mild perturbation of the Ribonucleotide reductase (RNR) enzyme results in an increased level of ROS that is accompanied by the dissociation of the fork accelerator TIMELESS from the replisome, resulting in a slowing down of replication forks. The elevated ROS level modifies the oligomerization status of Peroxiredoxin 2 (PRDX2), which promotes the dissociation of TIMELESS. This evidence suggests that the redox signaling can directly influence the regulation of the dNTP biosynthesis, whose balance is a fundamental element of the replication process

*Deregulation of the replication initiation step without any fork slowdown*

In some cases, defects of origin activations lead the cells to genomic instability rather by accelerating the progression of replication forks than by inducing forks stalling. Recently, evidence demonstrating that the number of active origins is inversely correlated to the fork speed have emerged (Zhong *et al.*, 2013). Thus, the depletion of Cdc7 has been shown to concomitantly increase the inter-origin distances and the forks speed (Rodriguez-Acebes, Mourón and Méndez, 2018). This acceleration of the fork progression could be an adaptive mechanism that compensate the longer distance the replisome has to overcome. Despite this compensatory regulation, the paucity of origins can also threaten the completion of DNA replication, by leaving some regions of chromatin under-replicated, hence contributing to a global genomic instability.

## II.C S-phase checkpoint and cellular responses

In order to preserve the genome integrity, cells rely on mechanisms of surveillance referred as to S-phase checkpoints. Ataxia telangiectasia and Rad3-related (ATR) with the serine/threonine kinase/Checkpoint kinase I (CHK1) is the main pathway to face replication stress (Figure 16). Upon replicative stress, the uncoupling between helicase and polymerase generates a larger amount of ssDNA. As a consequence, RPA that has a high affinity for

ssDNA accumulates, protects the ssDNA and recruits sensor proteins such as RAD17-RFC and RAD9-RAD1-HUS1 as well as TopBP1 which in turn activate ATR/Ataxia telangiectasia and Rad3-related interacting protein (ATRIP) kinase activity. ATR then phosphorylates its downstream targets, in particular CHK1 at residues Ser317 and Ser345, ssDNA-bound RPA at Ser33 and Histone H2AX at Ser139.

Checkpoint kinases orchestrate several downstream factors, permitting cells to respond to various threats during replication and to complete DNA replication. Indeed, the ATR/CHK1 pathway leads to the stabilization of stalled replication forks to protect them from collapsing. This may induce the formation of reversed forks called 'chicken foot' that protect stalled forks (Kotsantis, Petermann and Boulton, 2018). Forks restart may thus be achieved through different pathways as homologous recombination, repriming or template switching (Figure 16). In addition to a direct resolution of stalled forks, a regulation of the origin firing also takes place with local activation of adjacent replication origins and inhibition of late origins at a global genome scale. Suppressing late origins allows cells to preserve available replicative factors. Moreover, Chk1 and Chk2 phosphorylate TP53, a pivotal transcription factor of DNA damage response (DDR), which in turn activates genes involved in the cell cycle regulation and DNA repair. Through various pathways including mainly TP53, the cell cycle could be arrested allowing cells to have more time to resolve a perturbed fork progression and to repair DNA damages.

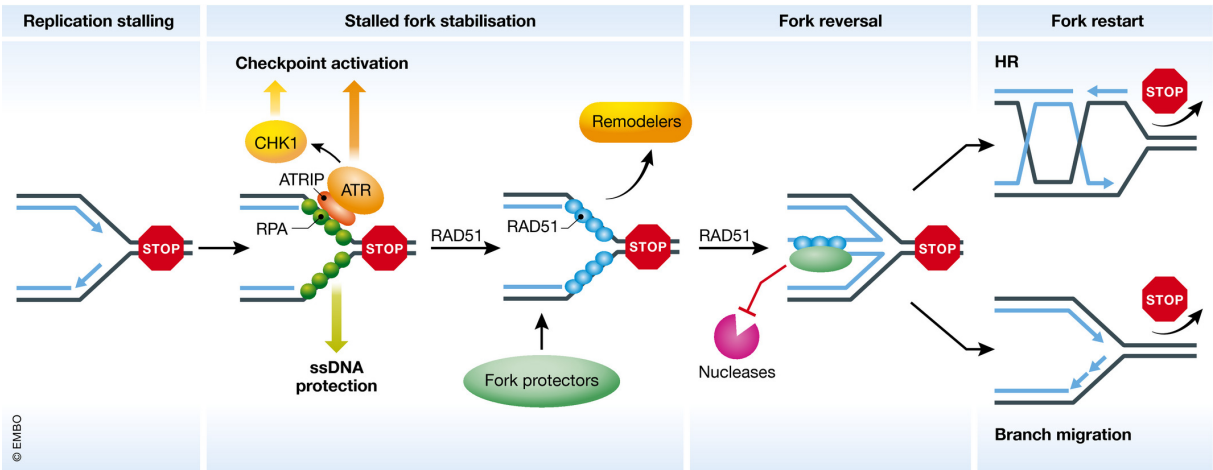


**Figure 16.** A model for the rescue of stalled replication forks (Figure from Liao *et al.*, 2018).

## II.D Consequence of replication stress

Given the importance of the replication process for genome integrity and cell viability, cells have robust cell cycle checkpoints to deal with possible occurrence of replication stress. Despite this surveillance, several consequential defects can result in genomic instability.

Indeed, most cancers represent various characteristics of genomic instability such as increased frequencies of base pair mutation, Chromosome instability (CIN) or microsatellite instability (MIN). CIN consists in a change in the number (aneuploidy) or in the structure of chromosomes such as chromosome breaks or fragmentation (Figure 17; Vargas-Rondón, Villegas and Rondón-Lagos, 2018). During the segregation of chromosomes, remaining under-replicated DNA can induce the appearance of lagging chromosomes and anaphase bridges. This mis-segregation can also generate micronuclei in daughter cells after mitosis (Zeman and Cimprich, 2014). A well-studied model to account for the CIN mechanisms is common fragile sites (CFS) (Debatisse and Rosselli, 2019). CFSs are regions of the genome that are difficult to replicate and prone to breakage. In general, these sites are located in late replicating domains, AT-rich regions and associated with large genes. These features are considered as intrinsic reasons of fragility. Indeed, CFSs are susceptible to molecular conflicts between replication and transcription machineries. Furthermore, due to the poor number of origins and the late replication timing of CFS, these regions are frequently left under-replicated upon replication stress, resulting in chromosome breaks. Hence, additional replication stress can exacerbate the fragility of the regions.

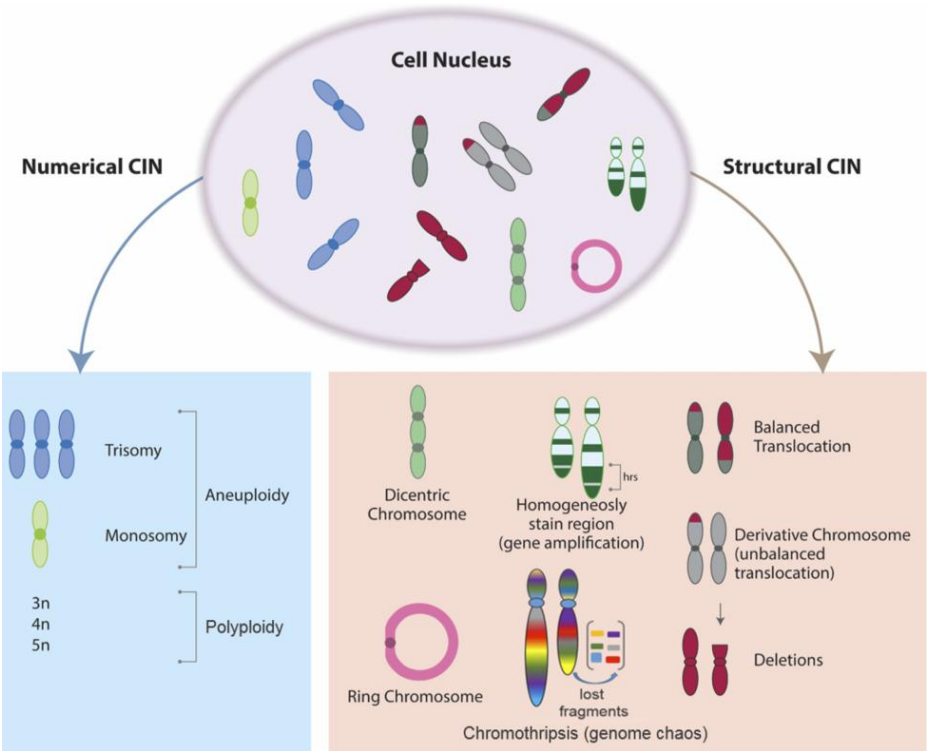


**Figure 17.** Chromosomal instability (CIN) Characteristics (Figure from Vargas-Rondón, Villegas and Rondón-Lagos, 2018).

Targeting replication stress is an attractive idea in the field of cancer therapy. Indeed, replicative stress in cancer has double facets. On one hand, an unstable replication process drives cells toward tumorigenesis, making cells even more proliferative with an aberrant cell cycle and also more flexible to adapt to a changing environment or to bypass tumor suppressor cellular control. Thus, defects in DNA replication constitute the major driving force to genomic instability and cancer. On the other hand, because cancer cells often exhibit chronic replication stress compared to normal cells, they are more sensitive and vulnerable to genotoxic stress. In this point of view, the replication stress and the involved pathways could be exploited as therapeutic targets for cancer (Zhang *et al.*, 2016; Ubhi and Brown, 2019). Therefore, deciphering the mechanisms of replication stress is important for understanding how the latter contributes to genomic instability and cancer development.

## Projects of thesis

During my thesis, I was interested in CDK4/6 inhibitors (palbociclib, ribociclib and abemaciclib) that are promising anticancer drugs. First, analysis of transcriptomic data from "The Cancer Genome Atlas (TCGA)" database had shown that CDK6 overexpression was a marker for a poor prognosis of viability for adrenocortical carcinomas patients. I studied the effects of palbociclib and ribociclib on cell models specific for this cancer, namely SW-13 and NCI-H295R cell lines.

We observed an impact of palbociclib on the viability of pRb deficient NCI-H295R cell line, which was associated with apparent DNA replication defects. Based on these first results, I then focused my work on palbociclib-induced DNA replication stress and genomic instability in two pRb deficient cell lines namely NCI-H295R and MDA-MB-468. For the first time, I demonstrated that palbociclib impairs the activation of DNA replication origins in a pRb independent manner, which in turn triggers replication stress and genomic instability.

The third part of my project is about the action of abemaciclib, a CDK4/6 inhibitor and its synergistic effects with chloroquine, a molecule regulating autophagy. The aim of this study is to achieve more effective cancer treatments using lower doses of drugs through a combination strategy. I demonstrated that the effects of abemaciclib are enforced when cells are co-treated with Chloroquine. This finding could provide a potential combination for the treatment of cancers.

# RESULTS

## I. A hypothesis driven approach identifies CDK4/6 inhibitors as candidate drugs for treatments of adrenocortical carcinomas

### I.A Summary

This study consists of two parts, one of which is the *in silico* analysis of transcriptomic data from The Cancer Genome Atlas (TCGA) database. We focused on 136 genes involved in G1/S transition and DNA replication using RNAseq data from patients suffering from adrenocortical carcinomas (ACC). First, we found that hierarchical clustering based on mRNA levels determined 4 groups of genes. Most of the genes located in clusters 3 and 4 are correlated with the expression of *MKI67*, a classical marker of cell-proliferation rate. 9 genes in the cluster 1 were inversely correlated with this proliferation marker. Then, among the rest of the genes, which showed no significant correlation with the expression of *MKI67*, we identified *CDK6* whose overexpression is highly associated with shorter times to relapse and death.

Based on these results, in the second part, we aimed to assess the effects of CDK4/6 inhibitors (palbociclib and ribociclib) on adrenocortical carcinoma cell lines, a pRb proficient cell line named SW-13 and a pRb deficient cell line named NCI-H295R. CDK4/6 inhibitors efficiently diminish cellular viability with increasing dose and induce the cell cycle arrest in G1-phase at 1μM in SW-13 cells, accompanied with reduced level of phosphorylated pRb. To further distinguish whether the cell cycle arrest is transient or permanent, we characterized several features of senescence including β-galactosidase activity, granularity and cell size shifts, cell flatness, vesicles and irreversibility from cell cycle arrest. Cells treated with either 1 or 5μM of ribociclib showed most of those features, but still a small population of cells entered the cell cycle after the elimination of the treatment. However, palbociclib induces an irreversible arrest referred to as senescence at 5μM, implying the effects of other targets. In contrast to SW-13 cells, NCI-H295R pRb-deficient cells show a resistance to CDK4/6 inhibitors as expected. The cellular viability was not affected up to 5μM of inhibitors. Still, palbociclib but

not ribociclib diminishes the cellular viability at 10μM or more. We further demonstrated that palbociclib used at high dose induces apoptosis in NCI-H295R cells and this is explained by a defect in the Wnt/ β-catenin pathway. This confirms that palbociclib has more pronounced effects on cells as compared to ribociclib.

This paper focuses on ACC by two main approaches: mining transcriptomic data from patients and bringing the result to wet biology in ACC cell lines. These are the first findings that demonstrate molecular mechanisms of action of CDK4/6 inhibitors for ACCs by comparing two cell lines regarding the presence of pRb. It is of note that while we did not mention it in the paper, we remarked one significant observation showing aberrant cell cycle progression in cells treated with palbociclib. This observation has driven us to speculate the effects of palbociclib in the dynamics of DNA replication and leads to the next study (See chapter Result II.A).

This work is published in the journal "Aging" (Hadjadj *et al.*, 2017).

## I.B Article

Research Paper

# A hypothesis-driven approach identifies CDK4 and CDK6 inhibitors as candidate drugs for treatments of adrenocortical carcinomas

**Djihad Hadjadj[1], Su-Jung Kim[1], Thomas Denecker[1], Laura Ben Driss[1], Jean-Charles Cadoret[1], Chrystelle Maric[1], Giuseppe Baldacci[1], Fabien Fauchereau[1,2]**

[1]Pathologies de la Réplication de l'ADN, Université Paris-Diderot – Paris 7, Sorbonne Paris Cité, CNRS UMR7592, Institut Jacques-Monod, 75205 Paris Cedex 13, France
[2]ePôle de Génoinformatique, Université Paris-Diderot – Paris 7, Sorbonne Paris Cité, CNRS UMR7592, Institut Jacques-Monod, 75205 Paris Cedex 13, France

**Correspondence to:** Fabien Fauchereau, Giuseppe Baldacci; **email:** fabien.fauchereau@ijm.fr, giuseppe.baldacci@ijm.fr
**Keywords:** cancer, CDK6, adrenocortical, palbociclib, ribociclib
**Received:** March 31, 2017 **Accepted:** December 17, 2017 **Published:** December 26, 2017

**Copyright:** Hadjadj et al. This is an open-access article distributed under the terms of the Creative Commons Attribution License (CC BY 3.0), which permits unrestricted use, distribution, and reproduction in any medium, provided the original author and source are credited.

## ABSTRACT

**High proliferation rate and high mutation density are both indicators of poor prognosis in adrenocortical carcinomas. We performed a hypothesis-driven association study between clinical features in adrenocortical carcinomas and the expression levels of 136 genes involved in DNA metabolism and G1/S phase transition. In 79 samples downloaded from The Cancer Genome Atlas portal, high *Cyclin Dependent Kinase 6* (*CDK6)* mRNA levels gave the most significant association with shorter time to relapse and poorer survival of patients. A hierarchical clustering approach assembled most tumors with high levels of *CDK6* mRNA into one group. These tumors tend to cumulate mutations activating the Wnt/β-catenin pathway and show reduced *MIR506* expression. Actually, the level of *MIR506* RNA is inversely correlated with the levels of both *CDK6* and *CTNNB1* (encoding β-catenin). Together these results indicate that high *CDK6* expression is found in aggressive tumors with activated Wnt/β-catenin pathway. Thus we tested the impact of Food and Drug Administration-approved CDK4 and CDK6 inhibitors, namely palbociclib and ribociclib, on SW-13 and NCI-H295R cells. While both drugs reduced viability and induced senescence in SW-13 cells, only palbociclib was effective on the retinoblastoma protein (pRB)-negative NCI-H295R cells, by inducing apoptosis. In NCI-H295R cells, palbociclib induced an increase of the active form of Glycogen Synthase Kinase 3β (GSK3β) responsible for the reduced amount of active β-catenin, and altered the amount of *AXIN2* mRNA. Taken together, these data underline the impact of CDK4 and CDK6 inhibitors in treating adrenocortical carcinomas.**

## INTRODUCTION

Adrenocortical carcinomas (ACCs) are rare (annual incidence 0.5 to 2 patients per million individuals) but deadly cancers (the overall five-year survival of patients has been estimated below 35% in most studies) with limited opportunities of treatment [1,2]. In ACCs, indicators of high proliferation rate, such as an abnormal number of mitoses (>5 mitoses per 50 high power fields) and a high Ki-67 labeling index, constitute potent markers of poor prognosis [3–6]. This tendency has been confirmed by transcriptomic approaches that segregated ACCs into two groups. An overall overexpression of genes associated with cell proliferation has been observed in the group of most aggressive ACCs [7–9]. Abnormal expression of genes involved in DNA metabolism may also contribute to a higher mutation rate and thus to the acquisition of new cellular abilities, such as resistance to drugs, and the ability to relapse and to metastasize. In ACCs, mutation

density has recently been associated with clinicopathological parameters such as overall survival time and time to recurrence [10].

Considering the central role of DNA metabolism in the evolution of cancers, we have tested the association of clinical parameters with the expression levels of 136 genes involved in the G1/S phase transition, DNA replication and response to DNA damage. This study was performed on transcriptomic data of 79 ACC patients shared by The Cancer Genome Atlas (TCGA) consortium [10]. The most significant association was obtained with the *Cyclin Dependent Kinase 6* (*CDK6*) gene, whose overexpression is associated with short time before tumor relapse and death of patients. We found that *CDK6* mRNA is overexpressed in a group of aggressive ACCs enriched in mutations in genes of the Wnt/β-catenin pathway.

Based on these results, we considered CDK6 inhibitors as potential candidates for therapy of ACCs. Palbociclib (PD-0332991, IBRANCE®, Pfizer), and ribociclib (LEE011, Kisqali®, Novartis) are both CDK4 and CDK6 (CDK4/6) inhibitors. Palbociclib is efficient in combination with letrozole (Femara®, Novartis) or fulvestrant (FASLODEX®, AstraZeneca) in patients with hormone receptor positive (HR+)-advanced breast cancers. It has recently been approved in the United States of America and the European Union in these combinations [11–14]. Ribociclib, in combination with letrozole, was recently approved by the Food and Drug Administration (FDA) as a frontline treatment for HR+ and human epidermal growth factor receptor 2 negative (HER2-)-advanced or metastatic breast cancers [15,16]. We thus characterized the impacts of these two FDA-approved CDK4/6 inhibitors on the cell cycle and survival of SW-13 and NCI-H295R cell lines as a first step to test their potential therapeutic properties against ACCs.

## RESULTS

### A hierarchical clustering of G1/S transition and DNA replication / repair genes identifies four transcriptional clusters

As a first step of our study on transcriptomic data related to the G1/S transition and DNA replication genes in ACCs, we established a list of 136 genes involved in these processes, based on ontology annotations in the Kyoto Encyclopedia of Genes and Genomes (KEGG) database [17] and bibliographic data (Supplementary Table 1). These genes could be classified into six groups based on their biological functions, namely G1/S transition, DNA polymerases, DNA replication, S phase checkpoint, stalled replication fork restart / double strand break repair, and dNTP synthesis. We added the expression levels of the *Marker of Proliferation Ki-67* (*MKI67*) gene, as its expression is a keystone marker of proliferation widely used in adrenal cancer prognosis. For these 137 genes (including *MKI67*), RNAseq data of ACCs from 79 patients were then downloaded from the TCGA portal.

To identify clusters of co-expressed genes, we first estimated the Pearson correlation coefficient of these 137 genes with each other, based on mRNA levels (Supplementary Figure 1). We then performed a hierarchical clustering of genes, in which the dissimilarity between gene clusters was calculated with the Pearson correlation values. Genes clustered into one group tended to have correlated mRNA levels. Hierarchical clustering produced four clusters of genes. Clusters 3 and 4 contain 56 (including *MKI67*) and 33 genes, respectively. The Pearson correlation test showed that the expression levels of each of the 55 genes of cluster 3 and 28 genes of cluster 4 (out of 33) are significantly correlated with the expression of *MKI67* and are associated with this classical marker of proliferation rate (Supplementary Figure 1 and Supplementary Table 1). These 83 genes are implicated in the six aforementioned functional processes. In particular, they include the genes encoding the replicative DNA polymerases α, δ and ε, with the exception of the *POLD4* gene, which encodes the p12 accessory subunit of polymerase δ. Clusters 1 and 2 contain 23 and 25 genes, respectively. While the expression values in ACCs of 40 genes showed no significant correlation with *MKI67*, 9 genes in cluster 1 were inversely correlated with this proliferation marker. Among these is *POLD4*. The other inversely correlated genes include genes of negative cell cycle regulators (*CDKN1C*, *CCND2* and *RBL2*) and DNA repair genes (*ATM*, *RAD50*, *MCM9*, *RMI1* and *TOP3A*).

### *CDK6* expression shows significant prognostic value in ACCs

We then studied the association of the expression of the 137 genes with the overall survival (OS) and relapse free survival (RFS) of patients (Supplementary Table 1). Association was tested using the Log-rank test, which is routinely used to compare survival distributions of two groups of patients. Among the genes tested, the expression level of 114 genes was significantly correlated with OS, and that of 68 genes with RFS. Since proliferation is widely used in medical oncology, we focused our attention on the 28 genes associated with OS and/or RFS, but unrelated to *MKI67* (Table 1). Higher mRNA levels of genes encoding translesion DNA polymerases, namely *POLB, POLL, REV1* and *REV3L,* and lower expression of *POLK,* indicated poor

prognosis (Table 1). Increased expression associated with poor prognosis was also observed for genes involved in E2F-dependent G1/S transition (*CDK6, CCND1, E2F3-5* and *TFDP2*), in DNA replication initiation (*ORC2L, ORC4L* and *ORC5L*), in S phase checkpoint (*TIPIN, TP53*) and stalled fork restart and double-strand break repair (*SMARCAL1* and *MUS81*). In contrast, associated with poor prognosis, we observed reduced gene expression of inhibitors of the E2F pathway (*CDKN2B, HDAC1, RB1*), of genes involved in DNA replication (*GINS3* and *TOP1*), in S phase checkpoint (*RAD17, NBN* and *TP53BP1*), and in dNTP synthesis (*RRM2B*). The gene with the most significant Log-rank test for RFS is *CDK6* (cutoff value > 10.63, n=25 out of 79 patients, adjusted *p* value = 6,97 x $10^{-6}$). Its expression is also significantly associated with OS (cutoff value > 10.74, n=24 out of 79 patients, adjusted *p* value = 4.05 x $10^{-5}$). *CDK6* and 9 other genes unrelated to proliferation, namely *E2F3, E2F5, ORC2L, ORC4L, ORC5L, CDKN2B, POLG2, REV3L* and *SMARCAL1,* belong to the expression cluster 2 (Supplementary Figure 1) and thus have similar expression profiles in ACC patients. The Kaplan-Meier analyses demonstrate a shorter time of OS and RFS of patients associated with high *CDK6* expression (Figure 1). We confirmed the association between the *CDK6* transcription level and shorter time to relapse and death using the Log-rank test on previously published data from a French cohort [18]. In this sample, patients with levels higher than the cutoff values again showed shorter times to relapse (*p* value = 0.041, cutoff value > 5.067, n=38 out of 44 patients) and death (*p* value = 1.51 x $10^{-6}$, cutoff value > 6.027, n=19 out of 44 patients).

**Table 1. Association between the expression levels of 28 genes with time of RFS and/or OS, but not with the expression of the *MKI67* gene in ACC tumor samples.**

| | | **Correlation with MKI-67** | | **Relapse Free survival** | | | | | **Overall Survival** | | | | |
|---|---|---|---|---|---|---|---|---|---|---|---|---|---|
| Gene | Cellular process | coef. Correl. | P-value | Risk group | Cutoff | Percentile | P-value | Adj. P-val. | Risk group | Cutoff | Percentile | P-value | Adj. P-val. |
| **DNA polymerases** | | | | | | | | | | | | | |
| POLB | Replication / repair | 0.0238 | 0.8268 | - | 7.692 | 9.3 | 0.1461 | 0.1629 | High | 8.705 | 77.2 | 0.0010 | **0.0018** |
| POLG2 | Mitochondrial DNA replication | 0.1385 | 0.201 | High | 7.394 | 88.9 | 0.0058 | **0.0234** | Low | 7.27 | 87.3 | 0.0240 | **0.0303** |
| POLL | Replication / repair | -0.06111 | 0.5738 | High | 9.842 | 81.5 | 0.0128 | **0.0352** | - | 9.327 | 45.6 | 0.1071 | 0.1165 |
| REV3L | Translesion DNA synthesis | 0.149 | 0.1685 | - | 8.224 | 29.6 | 0.1252 | 0.1408 | High | 9.295 | 86.1 | 0.0024 | **0.0039** |
| REV1 | Translesion DNA synthesis | 0.2021 | 0.06062 | High | 9.479 | 44.4 | 0.0122 | **0.0352** | High | 10.22 | 77.2 | 7.64E-06 | **1.89E-05** |
| POLK | Translesion DNA synthesis | -0.1658 | 0.125 | Low | 9.145 | 29.6 | 0.0008 | **0.0075** | Low | 8.899 | 26.6 | 1.26E-05 | **2.90E-05** |
| **G1/S checkpoint** | | | | | | | | | | | | | |
| CDK6 | CDK and their regulators | 0.1239 | 0.2529 | High | 10.63 | 79.6 | 5.12E-08 | **6.97E-06** | High | 10.74 | 69.6 | 1.79E-05 | **4.05E-05** |
| CDKN2B | CDK and their regulators | 0.1209 | 0.2645 | Low | 7.09 | 29.6 | 0.0031 | **0.0169** | High | 8.264 | 75.9 | 0.0025 | **0.0039** |
| CCND1 | CDK and their regulators | 0.02788 | 0.7976 | - | 12.53 | 87.0 | 0.0266 | 0.0510 | High | 12.66 | 81.0 | 0.0038 | **0.0056** |
| HDAC1 | pRB pathway | 0.1997 | 0.06391 | Low | 11.03 | 48.1 | 0.0164 | **0.0399** | Low | 10.31 | 12.7 | 0.0102 | **0.0140** |
| RB1 | pRB pathway | -0.1955 | 0.06975 | Low | 9.334 | 13.0 | 0.0076 | **0.0285** | - | 9.899 | 29.1 | 0.0556 | 0.0652 |
| E2F3 | pRB pathway | 0.1764 | 0.1024 | High | 9.201 | 87.0 | 0.0130 | **0.0352** | - | 7.804 | 11.4 | 0.1264 | 0.1364 |
| E2F4 | pRB pathway | 0.1165 | 0.2827 | Low | 10.96 | 61.1 | 0.0217 | **0.0440** | - | 10.77 | 40.5 | 0.1294 | 0.1375 |
| E2F5 | pRB pathway | 0.08457 | 0.436 | High | 5.532 | 20.4 | 0.0411 | 0.0636 | High | 7.213 | 84.8 | 0.0107 | **0.0146** |
| TFDP2 | pRB pathway | -0.007805 | 0.9428 | High | 8.354 | 72.2 | 0.0049 | **0.0209** | - | 7.35 | 13.9 | 0.1284 | 0.1375 |
| **DNA replication** | | | | | | | | | | | | | |
| ORC2L | Pre-replication complex | 0.137 | 0.2056 | High | 8.245 | 77.8 | 0.0040 | **0.0190** | High | 8.577 | 84.8 | 2.69E-05 | **5.91E-05** |

| | | | | | | | | | | | | | |
|---|---|---|---|---|---|---|---|---|---|---|---|---|---|
| ORC4L | Pre-replication complex | -0.05241 | 0.6296 | High | 8.576 | 29.6 | 0.0104 | **0.0352** | - | 9.099 | 75.9 | 0.0518 | 0.0612 |
| ORC5L | Pre-replication complex | 0.1365 | 0.2076 | - | 8.235 | 16.7 | 0.2891 | 0.2912 | High | 9.51 | 88.6 | 0.0043 | **0.0063** |
| GINS3 | Initiation of DNA replication | 0.01906 | 0.8609 | - | 9.355 | 57.4 | 0.0819 | 0.1032 | Low | 8.902 | 41.8 | 0.0024 | **0.0038** |
| TOP1 | Topoisomerase | -0.03081 | 0.7769 | Low | 10.86 | 25.9 | 0.0090 | **0.0314** | Low | 10.55 | 19.0 | 0.0146 | **0.0195** |
| **S phase checkpoint** | | | | | | | | | | | | | |
| RAD17 | ATR + Rad17-9-1-1 DNA damage sensors | -0.132 | 0.2229 | - | 9.195 | 25.9 | 0.0477 | 0.0684 | Low | 9.471 | 49.4 | 0.0005 | **0.0008** |
| NBN | ATM - MRN DNA damage sensors | -0.04222 | 0.6977 | Low | 9.129 | 9.3 | 0.0034 | **0.0179** | Low | 10.39 | 79.7 | 0.0175 | **0.0225** |
| TIPIN | ATM/ATR pathways mediators | 0.1816 | 0.09256 | - | 5.981 | 40.7 | 0.2053 | 0.2181 | High | 6.53 | 70.9 | 0.0054 | **0.0077** |
| TP53 | ATM and ATR pathways effector | -0.06086 | 0.5754 | High | 10.02 | 79.6 | 0.0002 | **0.0040** | High | 10.13 | 84.8 | 0.0019 | **0.0032** |
| TP53BP1 | ATM and ATR pathways effector | -0.09276 | 0.3927 | - | 9.333 | 11.1 | 0.1691 | 0.1855 | Low | 10.16 | 57.0 | 0.0168 | **0.0217** |
| **Stalled forks restart by remodeling / DSB repair** | | | | | | | | | | | | | |
| SMARCAL1 | Helicase | 0.146 | 0.1773 | High | 8.843 | 35.2 | 0.0205 | **0.0428** | High | 9.37 | 81.0 | 0.0152 | **0.0200** |
| MUS81 | Holliday junction resolution | 0.1526 | 0.1582 | High | 8.886 | 66.7 | 0.0834 | 0.1040 | High | 8.951 | 59.5 | 4.94E-06 | **1.27E-05** |
| **dNTP synthesis** | | | | | | | | | | | | | |
| RRM2B | Ribonucleotide reductase | -0.1183 | 0.2751 | | 10.89 | 70.4 | 0.0296 | 0.0523 | Low | 9.512 | 17.8 | 0.0004 | **0.0007** |

RNAseq and clinical data of n=54 and n=79 ACC samples were downloaded from the TCGA website and used for the Log-rank correlation tests for RFS and OS, respectively. The Log-rank test was used to compare survival distribution of two groups of patients, considering that their gene expression values were higher or lower than a cutoff. For each gene, a succession of Log-rank tests was performed with all possible cutoff values, given gene expression levels in tumors. The cutoff value chosen to segregate the "high" and "low" expression groups of patients was the one that maximized the significance of Log-rank tests. The percentile is the proportion of individuals below the cutoff value. "Adj. P-val." are the *p* values of the Log-rank tests that have been adjusted following the Benjamini Hochberg method (in bold when significant). Coeff. correl. is the Pearson product-moment correlation coefficient estimated between the expression level of each gene with *MKI67*. The risk group is given when the association with RFS and/or OS was significant. High and Low risk groups indicate the group with the worst prognosis, based on their expression level, higher or lower than the cutoff, respectively.

### Molecular and clinical features of patients with high expression of *CDK6*

Since our cell cycle / DNA metabolism approach highlighted the association of high *CDK6* expression with short times to relapse and death, we looked for other clinical and molecular features shared by patients showing *CDK6* overexpression. Hierarchical clustering based on mRNA levels of the 500 most variant genes in ACCs led to the constitution of clusters designated 1, 2 and 3. These clusters as a whole reflect the mRNA-based classification (Clusters of Clusters) recently published by TCGA [10] (Figure 2a). Cluster 2 includes 23 out of the 25 "*CDK6*-high" samples. The average

expression level of *CDK6* is higher in cluster 2 than in cluster 1 or 3 (cluster 2 vs 1, $p$ value = 1.75 x $10^{-20}$, cluster 2 vs 3, $p$ value =4.08 x $10^{-28}$) (Figure 2b). Cluster 2 tumors contain the majority of Cluster 1A (C1A) previously classified samples with a high production of steroids. A clinical feature significantly associated with the *CDK6* mRNA level is the synthesis of hormones, that are known to be an indication of poor prognosis in ACC patients [19] (Table 2). Cluster 2 also includes the majority of mutations and copy number variations that activate the Wnt/β-catenin signaling pathway. The microRNA-based clustering recently published by TCGA has led to a new classification in six groups [10]. Since the data involved *microRNA506* (*MIR506*) in the regulation of both *CDK6* and *CTNNB1* (encoding β-catenin), we analyzed its expression level in the 79 ACC samples. The expression of microRNA 506 was significantly lower in cluster 2 compared to clusters 1 and 3 (cluster 2 vs 1, $p$ value = 6.55 x $10^{-11}$, cluster 2 vs 3, $p$ value = 9.49 x $10^{-18}$) (Figure 2b). Correlation analyses revealed an inversed ratio between the *CDK6* and *MIR506* expression levels (Figure 2c, test for correlation based on Pearson's product moment coefficient, coefficient = -0.442, $p$ value = 4.50 x $10^{-5}$). The anti-correlation between *MIR506* and *CTNNB1* RNAs has been previously described by TCGA [10]. Thus, a low *MIR506* expression level could contribute to higher levels of both *CDK6* and *CTNNB1* mRNAs in ACCs.

**Palbociclib and ribociclib lower cell viability of the SW-13 and NCI-H295R cell lines**

Palbociclib and ribociclib inhibit CDK4/6 and are used for the treatment of breast cancer [11,12,15,16]. We tested the effects on cell viability of CDK4/6 inhibitors either with or without mitotane, a well-known adrenolytic drug that is currently used to treat ACCs. Viability was measured using SW-13 and NCI-H295R cells.

Mitotane was first tested alone. It decreased SW-13 and NCI-H295R viability with an IC50 (concentration needed to reduce viability to 50%) of 68.38 μM and 33.16 μM, respectively (Figure 3a). As previously shown, SW-13 cells are less sensitive to mitotane than NCI-H295R cells [20]. We then combined increasing concentrations of mitotane with either 1 μM of palbociclib or 1 μM of ribociclib on SW-13 and 10 μM of palbociclib or ribociclib on NCI-H295R cells (concentration of ribociclib or palbociclib inducing a 20% reduction of viability when they are used alone). In SW-13 cells, both drugs showed an additive effect with mitotane, with a 50% combination index of 0.997 for mitotane with palbociclib and of 1.043 for mitotane with ribociclib (Figure 3a). However, in NCI-H295R cells, mitotane showed an additive effect only with palbociclib with a combination index of 1.021 (Figure 3a). Mitotane combined with ribociclib showed no difference on cell viability compared to the effect of mitotane alone (Figure 3a).

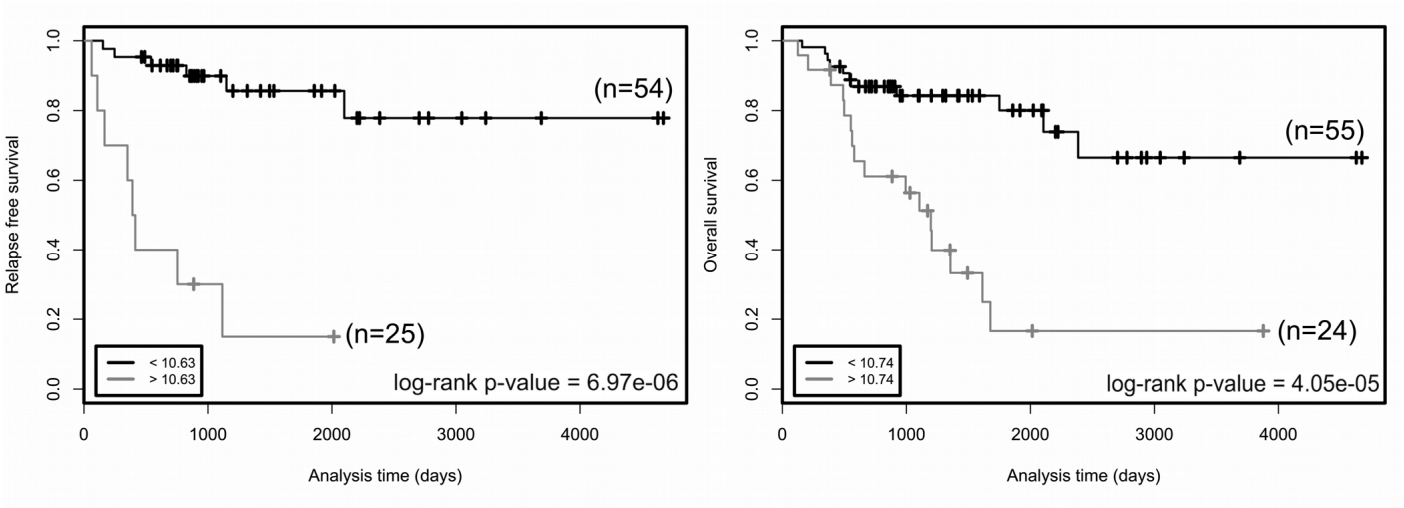


**Figure 1. Relapse free survival (left panel) and overall survival (right panel) rates in groups of patients as a function of *CDK6* expression.** Two groups of patients with *CDK6* expression higher (grey curves) or lower (black curves) than cutoff values (bottom left in the graphs) have been defined for each trait. The number of patients in each group is indicated in parentheses. Cutoffs are expression values that maximized the significance of log-rank tests. $p$ values of log-rank tests are at the bottom right in each box. Cutoff value is a gene-level transcription estimate, in RNA-Seq by Expectation Maximization (RSEM) normalized counts (downloaded from TCGA portal).

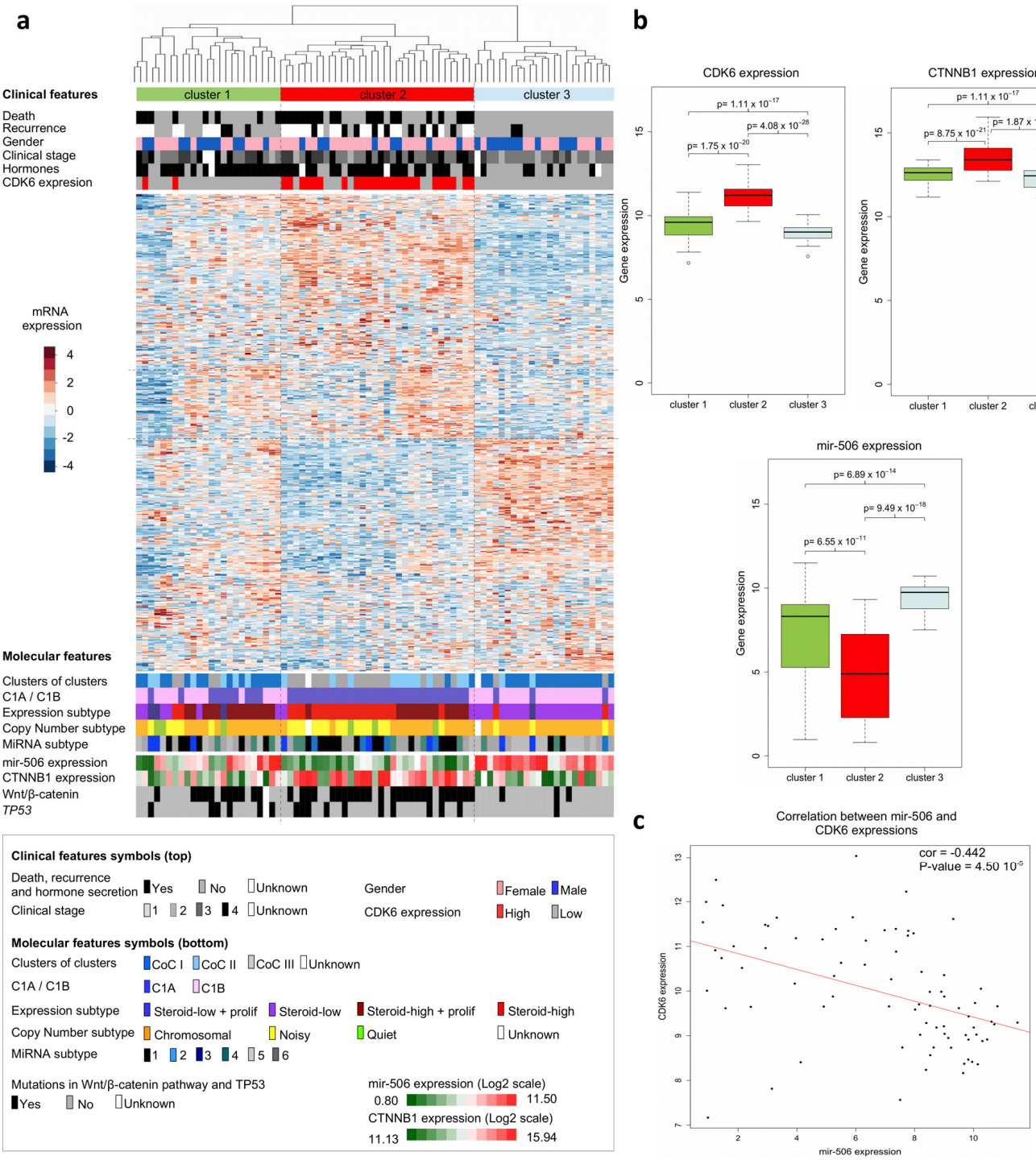


**Figure 2. Clinical and molecular features of adrenocortical carcinomas.** (**a**) Hierarchical clustering of the 79 ACC samples results into clusters 1, 2 and 3, as indicated in color bars at the top of the heatmap. Clustering is based on the expression levels of the top 500 most variant genes from the transcriptomes of the 79 ACCs. Dissimilarities between samples are indicated by the dendrogram at the top of the heatmap. Expression levels are shown by colors. Colors follow the base-2 log color scale at the left of the heatmap. The color symbols for clinical and molecular features are indicated in the frame at the bottom of the heatmap. (**b**) Box-plots showing the distribution of the *CDK6*, *CTNNB1* and *MIR506* gene expression values of tumor samples in the three transcriptome-based clusters. A base-2 log scale is used for the Y-axis showing gene expression. The band at the middle of the box indicates the median value. The bottom and top of the box are the 25$^{th}$ and 75$^{th}$ percentiles. Bottom and top whiskers represent the limits of exclusion of outliers. *p* values show the significance of the unilateral Wilcoxon-Mann-Whitney test. (**c**) Scatter plot showing the expression values of *CDK6* and *MIR506* of ACC samples, for which a base-2 log scale is used. The value of the Pearson coefficient (cor.) and the Pearson test *p* value for correlation are indicated at the top-right of the scatter plot. The red line is the linear regression line illustrating the negative correlation of expression between *CDK6* and *MIR506*. Clinical and molecular features (with the exception of the CDK6 expression group) were previously described [9,11].

**Table 2. Correlation of clinical features with the *CDK6* gene expression level of ACC tumors of n=79 TCGA patients.**

| | High CDK6 | Low CDK6 | *p* value |
|---|---|---|---|
| **Age** | 47.6 [40.2;55.0] | 46.2 [42.2;50.2] | 0.747 |
| **Tumor Size** | 139 [108;169] | 125 [96;154] | 0.531 |
| **Gender** | | | |
| Male | 6 | 25 | 0.132 |
| Female | 18 | 30 | |
| **Hormonal Secretion** | | | |
| Yes | 19 | 29 | **0.038** |
| No | 4 | 22 | |
| **Laterality** | | | |
| Right | 9 | 26 | 0.468 |
| Left | 15 | 29 | |
| **Clinical stage** | | | |
| I | 0 | 9 | |
| II | 10 | 26 | 0.056 |
| III | 7 | 9 | |
| IV | 7 | 8 | |
| **Weiss score** | | | |
| <4 | 4 | 10 | |
| 4-5 | 7 | 9 | 0.491 |
| 6-7 | 3 | 13 | |
| >7 | 5 | 9 | |
| **Recurrence** | | | |
| Yes | 7 | 7 | $6.97 \times 10^{-6}$ |
| No | 2 | 37 | |
| Time to recurrence | 689 [ 297;1080] | 1435 [1117;1753] | |
| **Death** | | | |
| Yes | 16 | 10 | $4.05 \times 10^{-5}$ |
| No | 8 | 42 | |
| Time to death | 1059 [746;1372] | 1495 [1210;1779] | |

The "High" and "Low" CDK6 expression groups are based on the results of the Log-rank test for relapse-free survival. Fisher's exact test was used to test the independence of discrete clinical features (gender, hormonal secretion, laterality and clinical stage) from expression level. Independence was rejected only for hormonal secretion, with an enrichment of hormone secretion among the "High" CDK6 expression group (true odds ratio = 3.5454, 95% confidence interval [0.981;16.385]). *p* values given for Recurrence and Death traits are those of the Log-rank test. Time to recurrence and death are the average values estimated from "High" CDK6 and "Low" CDK6 groups.

The effects of palbociclib and ribociclib alone on both the SW-13 and NCI-H295R cell lines were also tested. Both drugs decreased cell viability in the SW-13 cell line, with an IC50 = 15.50 μM for palbociclib and an IC50 = 19.08 μM for ribociclib (Figure 3b). In NCI-H295R cells only palbociclib had an effect on cell viability with an IC50 = 14.06 μM (Figure 3b). After treatment with 20 μM palbociclib cell viability was estimated to be close to 0%. Hence, palbociclib is the only drug active on both cancer cell lines and it strongly affects cell viability of NCI-H295R cells.

**Palbociclib induces cell cycle arrest and senescence in SW-13 and NCI-H295R cell lines**

To better characterize the effects of the two CDK4/6 inhibitors on the viability of the SW-13 and NCI-H295R cells, the cell cycle of both cell lines upon treatment with either palbociclib or ribociclib was investigated. In SW-13 cells, 1 and 5 μM of both inhibitors induced cell cycle arrest, with a smaller proportion of cells in the S phase and an increased proportion of cells in the G1 and G2 phases, when compared with

mock-treated cells (Figure 4a and Supplementary Figure 2a). The cycle of NCI-H295R cells was also affected by drug treatments (Figure 4a and Supplementary Figure 2a). 10 μM Palbociclib increased the proportion of cells in G2 phase, whereas 10 μM ribociclib increased the proportion of cells in S phase.

We tested whether reduced cell viability was associated with senescence. In SW-13 cells treated with palbociclib or ribociclib, we observed a significant increase in the percentage of cells harboring β-galactosidase activity, an indicator of senescence (Figure 4b and Supplementary Figure 2b). Both treatments also induced higher cell granularity and increased cell size in flow cytometry analyses (Figures 4c and d).

Induction of vesicle formation and increased flatness were also observed with bright-field microscopy (Figure 4g). Reversibility of the cell cycle arrest was tested by clonogenic assay. Ribociclib (1 and 5 μM, $p$ values = 0.001 and 0.011, respectively), and palbociclib (1 and 5 μM, $p$ values = 0.022 and 0.6 x $10^{-3}$, respectively) significantly decreased the ability of SW-13 to form clones, with clonogenic ability close to 0 after treatment with 5 μM palbociclib (Figures 4e and f). Taken together, these observations indicate induction of senescence in SW-13 cells after treatment with either palbociclib or ribociclib. In NCI-H295R cells, only palbociclib induced a significant increase of β-galactosidase activity (Figure 4b) when compared to mock-treated cells. In contrast with our observations using

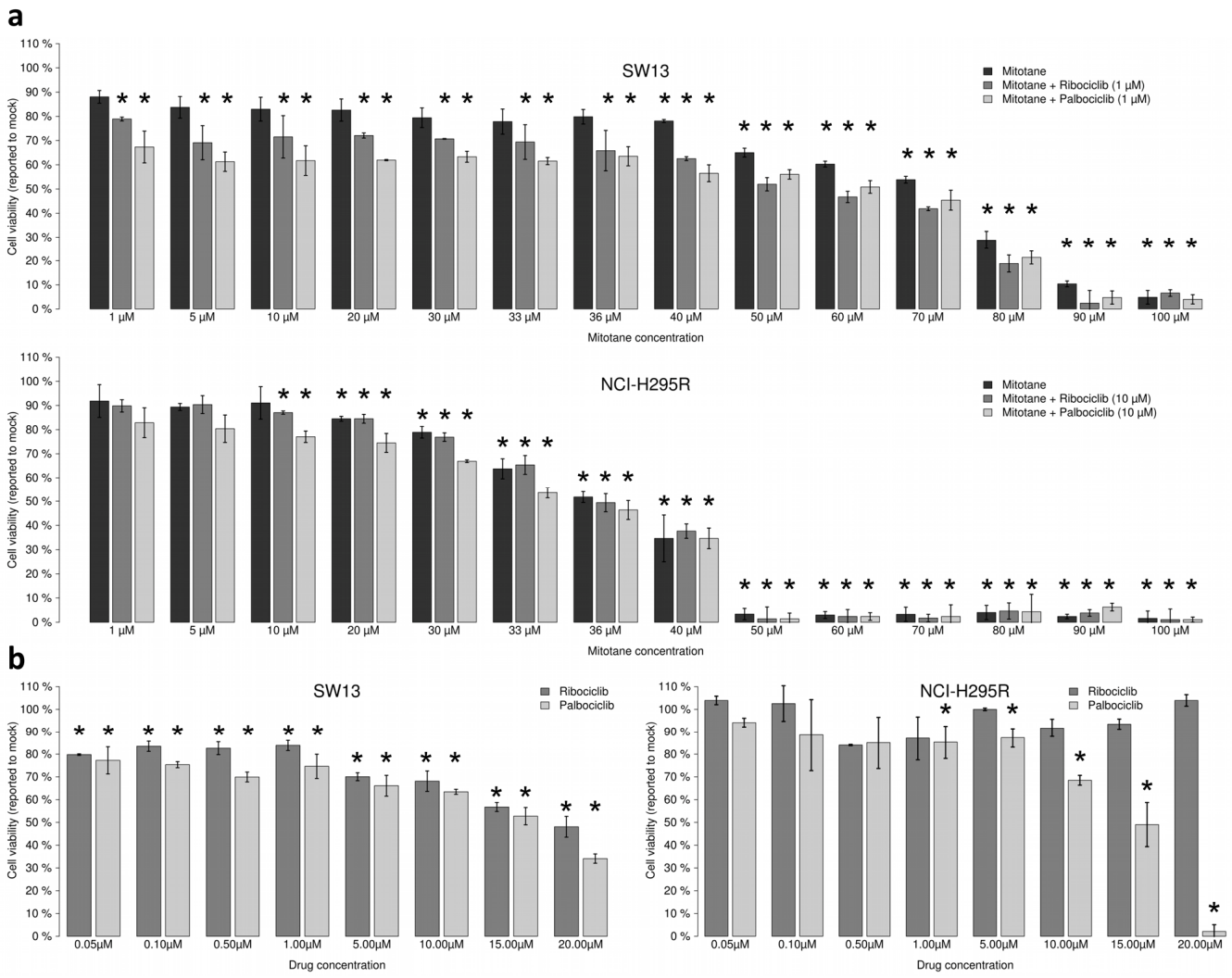


**Figure 3. Ribociclib and palbociclib lower viability of SW-13 and NCIH295R adrenocortical cell lines.** Cells were treated with drugs during 96 h. (**a**) Mitotane alone (from 1 μM to 100 μM) or combined with CDK inhibitors dose-response bar graphs on SW-13 and NCIH295R cells. CI50 = 50% Combination indexes. (**b**) Ribociclib and palbociclib dose-response bar graphs on SW-13 (left panel) and NCI-H295R cells (right panel). Drug concentration ranges from 0.05 μM to 20 μM. For each measurement error bars indicate standard deviation value, estimated from two different experiments. Asterisks show the significant t-tests ($p$ values < 0.05).

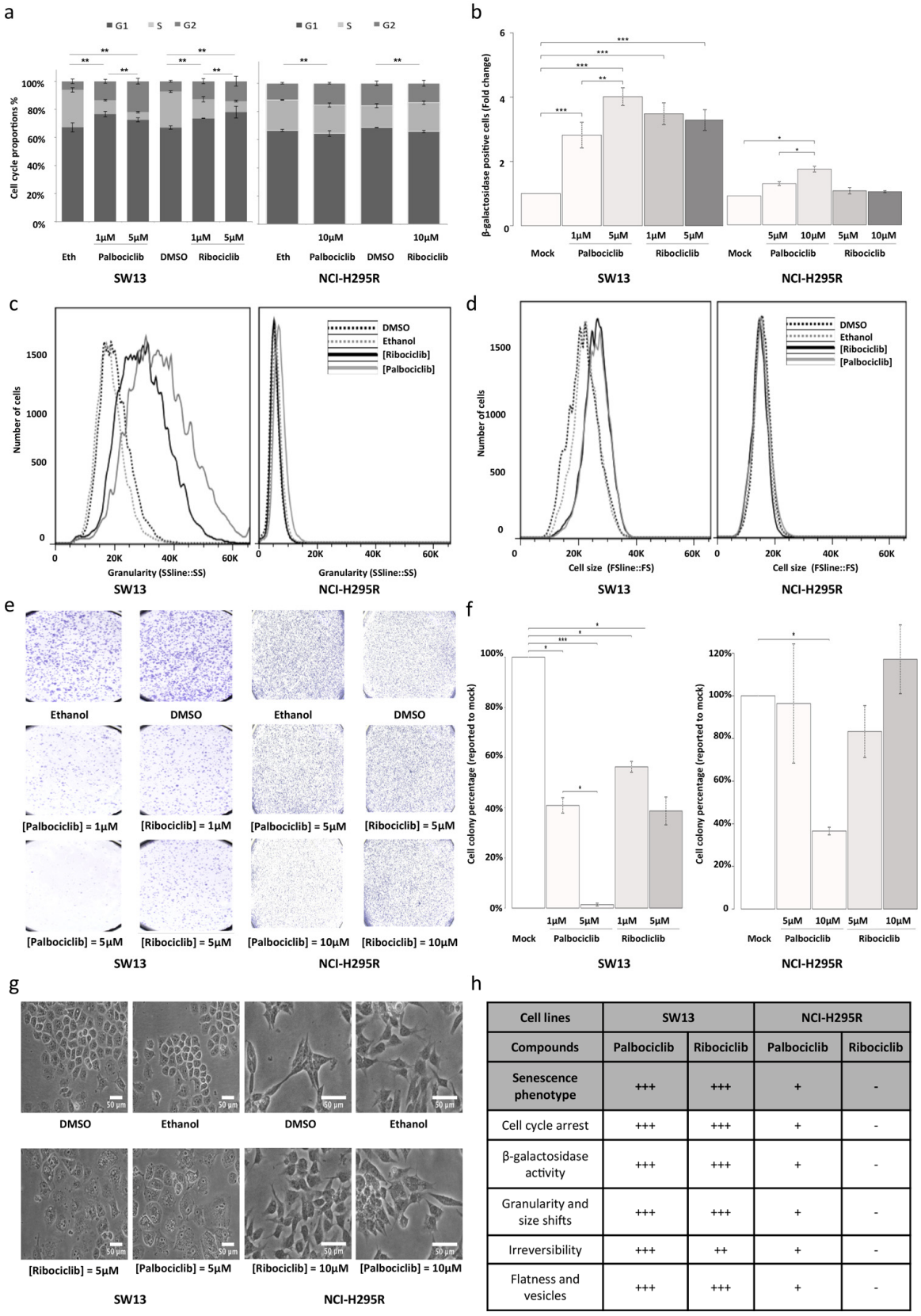


| Cell lines | SW13 | | NCI-H295R | |
|---|---|---|---|---|
| Compounds | Palbociclib | Ribociclib | Palbociclib | Ribociclib |
| Senescence phenotype | +++ | +++ | + | - |
| Cell cycle arrest | +++ | +++ | + | - |
| β-galactosidase activity | +++ | +++ | + | - |
| Granularity and size shifts | +++ | +++ | + | - |
| Irreversibility | +++ | ++ | + | - |
| Flatness and vesicles | +++ | +++ | + | - |

**Figure 4. Senescence features induced by ribociclib and palbociclib.** (**a**) Cumulative bar chart showing the proportion of SW-13 and NCI-H295R treated cells in G1, S and G2/M cell cycle phases. (**b**) β-galactosidase activity is used as marker of senescence. The number of cells with β-galactosidase activity after treatment with ribociclib or palbociclib was counted and related to the number of cells

with β–galactosidase activity after treatment with the vehicle only (DMSO or ethanol, respectively). Mean ratio and standard deviation were estimated from three independent experiments. (**c**) Flow cytometry analyses showing granularity of SW-13 and NCI-H295R cells treated with either palbociclib or ribociclib. Granularity is estimated by measuring the Side Scatter values (on the X-axis). (**d**) Flow cytometry analyses showing cell size of SW-13 and NCI-H295R treated with either palbociclib or ribociclib. Cell size is estimated by measuring the Side Scatter values (on the X-axis). (**e**) Colonies formed by SW-13 and NCI-H295R cells after coloring with crystal violet during the clonogenic assay. (**f**) The number of cell colonies formed after treatment with ribociclib or palbociclib was counted and related to the number of colonies formed after treatment with the vehicle only (DMSO or ethanol, respectively). The mean and standard deviation of percentage of colonies (compared to mock treatment) were estimated with three independent experiments. (**g**) Images in phase contrast showing the change of cell morphology of SW-13 and NCI-H295R cells upon treatment with either palbociclib or ribociclib. (**h**) Table summarizing the main aspects of senescence in both cell lines when treated with either palbociclib or ribociclib. For (**b**) and (**f**), **P*<0.05, ***P*<0.01, ****P*<0.001.

SW-13 cells, no marked increase of cell size was detected in NCI-H295R cells treated with either palbociclib or ribociclib (Figure 4d). Only a slight shift of cellular granularity was observed when NCI-H295R cells were treated with palbociclib, but not with ribociclib (Figure 4c). Finally, only 10 μM palbociclib induced a significant irreversibility of cell cycle arrest, as tested by clonogenic assay (*p* value = 0.013). Thus, NCI-H295R cells treated with palbociclib show some features of senescence, but less pronounced than SW-13 cells (Figure 4h).

Since ribociclib and palbociclib inhibit CDK4/6, they could impair the phosphorylation of the Retinoblastoma protein pRB, a crucial step in the G1/S transition. Consequently, we evaluated the levels of CDK4, CDK6, pRB and phosphorylated-pRb (Phospho-Rb) in such drug-treated cells (Figure 5a). In SW-13 cells, the amount of both CDK4 and CDK6 proteins increased after treatment with palbociclib or ribociclib. Such treatments also significantly lowered the amounts of both Phospho-Rb and pRB (Figures 5a and b). These experiments thus show that CDK4/6 inhibition following palbociclib or ribociclib treatment reduces the amount of Phospho-RB in SW-13 cells, and is associated with a senescence-like phenotype. pRB was not detected in NCI-H295R protein extracts (Figure 5a), which is consistent with the fact that this cell line carries a homozygous deletion of the *RB transcriptional corepressor 1* (*RB1*) gene (COSMIC mutation ID: 19554, c.862_2787del1926) [21]. This deletion could possibly hamper the action of CDK4/6 inhibitors on this cell line, in which only a slight senescence-like phenotype was observed.

**Palbociclib targets the Wnt/β-catenin pathway and induces apoptosis in NCI-H295R cells**

Since palbociclib induced a significant decrease of viability of pRB negative NCI-H295R cells (Figure 3b), we evaluated its pro-apoptotic activity. SW-13 cells treated with either palbociclib or ribociclib showed no detectable apoptotic activity (Figure 6a). In NCI-H295R cells, an increase of apoptosis was detected after treat-

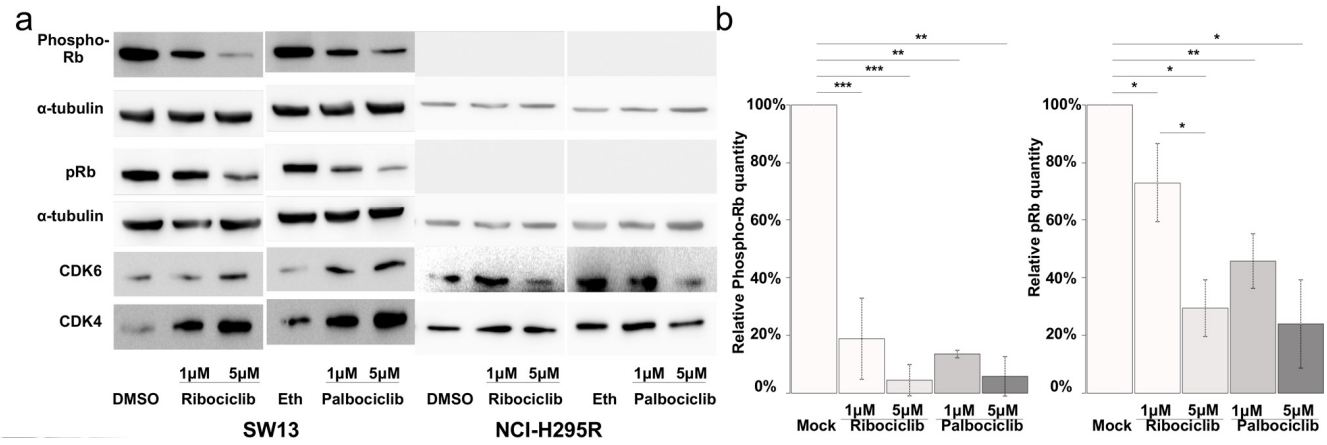


**Figure 5. CDK4/6 inhibitors lower the proportion of Phosphorylated-pRB and the total amount of pRB proteins in SW-13 cells**. (**a** and **b**) total pRB protein, phosphorylated-RB (phospho-RB), CDK6 and CDK4 were detected by western blot. (**a**) The results present the relative amounts of either Phospho-RB or pRB in drug-treated cells, compared to Phospho-RB or pRB in mock-treated cells. Values are the mean and standard deviations of two independent experiments. For the western blot experiments, α-tubulin was used as a loading control. In (**b**), significance was tested with the t-test. **P*<0.05, ***P*<0.01, ****P*<0.001.

ment with 20 μM palbociclib, but not with ribociclib (Figure 6a). This effect, specific of palbociclib, might be explained by the larger spectrum of kinases that it targets, compared with ribociclib. Additional palbociclib targets include GSK3β and its regulator AKT serine/threonine kinase [22]. Thus, the impact of palbociclib and ribociclib on the phosphorylation of GSK3β, in the SW-13 and NCI-H295R cell lines was also tested (Figures 6b and c). In SW-13 cells, only palbociclib reduced the ratio of Serine9-phosphorylat-

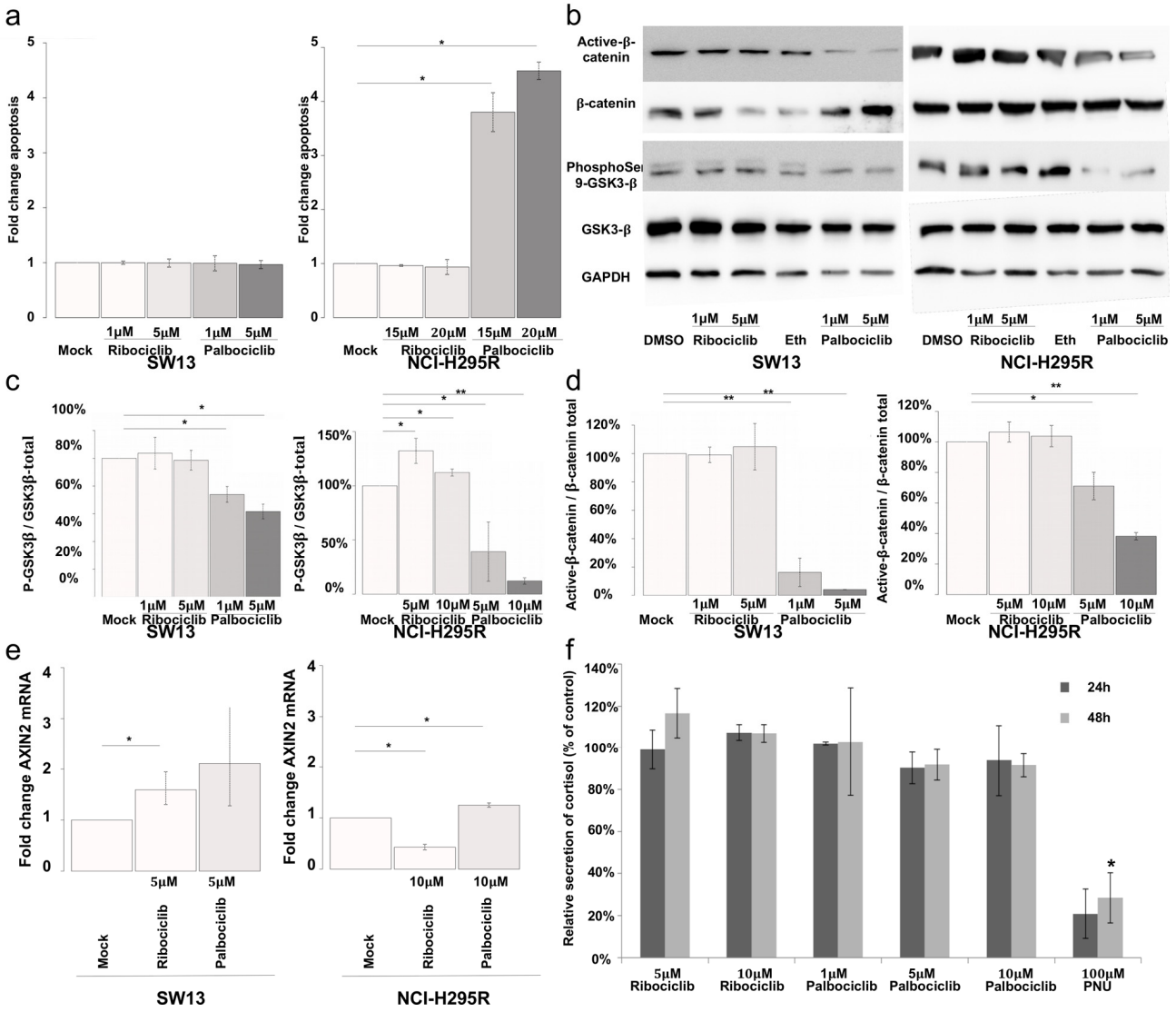


**Figure 6. Palbociclib induces apoptosis in NCI-H295R cells by targeting the Wnt/β-catenin pathway.** (**a**) Bar graphs showing apoptosis fold change in SW-13 or NCI-H295R cells upon treatment with either palbociclib or ribociclib. Caspase 3/7 activity was used as a read out to measure apoptosis. Results are the mean and standard deviations estimated based on three independent experiments. (**b**) Active β-catenin, total β-catenin, phospho-Ser9-GSK3β and total GSK3β were detected by western blot upon treatment with either palbociclib or ribociclib in both cell lines. GAPDH was used as a loading control. (**c** and **d**) Bar graphs showing the relative amount of phospho-Ser9-GSK3β on total GSK3β (c), or active β–catenin over total β-catenin (**d**) in both cell lines. Results are the mean and standard deviations based on two independent experiments. (**e**) Bar graphs showing levels of *AXIN2* mRNA upon treatment with either palbociclib or ribociclib, in both cell lines. The values indicate the fold-change of mRNA levels after treatment with palbociclib or ribociclib, compared to mock-treated cells. *AXIN2* mRNA levels in each condition were normalized to *ACTNB* (β-Actin) mRNA levels. qPCR were performed in triplicate. Mean and standard deviation are based on three different experiments. (**f**) Bar graph showing levels of secreted cortisol in the culture medium of NCI-H295R cells treated with ribociclib or palbociclib for 24 h and 48 h. Values are reported as percentage of concentration assayed with mock-treated cultures. Assay was performed in duplicate on culture media extracted from three different experiments. In (**a**), (**c**) and (**d**) Values are the mean ratio estimated from independent experiments. In (**a**), (**c**) and (**d**) significance was tested with t-test. In (**e**) and (**f**), significance was tested with the paired t-test. *$P<0.05$, **$P<0.01$.

ed-GSK3β (inactive form) to total GSK3β (inactive pGSK3β / total pGSK3β) (Figures 6b and c). In NCI-H295R cells, 5 and 10 μM palbociclib significantly reduced the inactive pGSK3β / total pGSK3β ratio (Figures 6b and c). Ribociclib showed effects opposite to palbociclib, as it increased this ratio. GSK3β was previously shown to phosphorylate β-catenin and consecutively induce its degradation by proteasome. Since loss of β-catenin-dependent transcription was associated with apoptosis in NCI-H295R cells [23], the effects of palbociclib and ribociclib on the amount of β-catenin and on the level of *AXIN2* transcripts (a β-catenin-dependent transcription target) were examined (Figures 6b, 6d and 6e). Ribociclib did not significantly modify the amount of β-catenin in SW-13 and NCI-H295R cells. Nevertheless, the expression of *AXIN2* was significantly altered in both cell lines, through β-catenin-independent regulations. On the con-trary, palbociclib significantly lowered the amount of β-catenin in both cell lines. Palbociclib treatment also increased the level of *AXIN2* transcripts, as expected after inhibition of β-catenin-dependent transcription [23].

A previous analysis showed that apoptosis induced by PNU-74654 (an inhibitor of the T cell factor (Tcf)/β-catenin complex) was preceded by reduction of steroid secretion. We assayed cortisol concentration in the supernatant of NCI-H295R cells (Figure 6f) treated with either ribociclib (5 or 10 μM) or palbociclib (1, 5 or 10 μM). Assays were performed at the times of treatments that precede apoptosis (24 h and 48 h). PNU-74654 (100 μM) was used as a positive control, as this inhibi-tor of Tcf/β-catenin interaction effectively reduced secretion of cortisol and other steroids by NCI-H295R cells [23]. Actually, neither ribociclib nor palbociclib decreased cortisol secretion at concentrations and time-points tested (Figure 6f). Yet, 100 μM PNU-74654 decreased cortisol production by 80% after 24 h treatment ($p$ value = 0.14) and by 72% after 48 h treatment ($p$ value = $6.7 \times 10^{-4}$). These effects of PNU-74654 (Figure 6f) are comparable to those previously observed [23]. Thus, Palbociclib-induced apoptosis of NCI-H295R cells is not preceded by a reduction of cortisol secretion.

Together, these results show that palbociclib-induced apoptosis is associated with a remarkable reduction of the amount of β-catenin and alters β-catenin-dependent transcription. Treatment with palbociclib could have potential benefits for the treatment of ACCs with an activated Wnt/β-catenin pathway.

## DISCUSSION

In this study we first classified 136 genes (Supplementary Table 1) involved in DNA replication/ repair into four groups, according to their mRNA levels. A set of 83 genes overlapping clusters 3 and 4 showed a significant correlation with *MKI67*, a marker commonly used for proliferation in histology-based diagnosis of ACCs. Cluster 3 also includes the *POLQ* gene, encoding the translesional DNA polymerase Polθ (involved in DNA repair and in DNA replication timing program) [24,25], together with homologous recombination repair (HR) genes (namely *BRCA1*, *FANCD2*, *BLM* and *RAD51*). Positive correlations between expression levels of *POLQ* and HR genes have recently been reported in lung, breast and colorectal cancers [26]. The authors suggested that an expression reprogramming involving these genes could prevent genetic instability in a cancer context. Indeed, we observed a similar correlation between *POLQ* and HR genes in ACCs. These genes are also associated with the *MKI67* proliferation marker (Supplementary Figure 1). In ACCs, overexpression of *POLQ* and HR genes could contribute to genomic stability in highly proliferating tumors, possibly through DNA repair processes. mRNA levels of 28 genes in clusters 1 and 2 are associated with shorter time of relapse-free survival and overall survival, and are also independent of the cell proliferation marker *MKI67* cell proliferation. Thus, they may provide additional information in the molecular characterization of ACCs (Table 1). A positive correlation with shorter time to relapse of high mRNA levels of *POLB, POLL, REV1* and *REV3L*, and of low mRNA levels of *POLK* was noted. These genes encode translesion DNA polymerases, which can perform DNA synthesis despite the presence of DNA lesions. Altered gene expression and mutations affecting translesion polymerases have been observed in a variety of tumors and have been suggested to act as biomarkers in response to treatments [27–31]. The ability of translesion polymerases to perform synthesis despite DNA lesions contributes to resistance to DNA damaging treatments, and previous analyses have shown that their inhibition sensitizes tumors to chemotherapeutic agents [31–36]. Translesion poly-merases are also error-prone, and thus can contribute to mutagenesis in tumors and progression of cancers [37]. Our analyses show that abnormal gene expression of translesion DNA polymerases is indeed a marker of poor prognosis independent of proliferation in ACCs. The development of small molecules targeting translesion DNA synthesis could potentially be beneficial for ACC patients with tumors expressing high levels of mRNAs encoding POLβ, POLλ, REV1 and REV3L translesion DNA polymerases.

In the second part of this study, we focused our analyses on the *CDK6* gene. CDK6 shares with CDK4 the ability to phosphorylate pRB and to induce the transition to S-phase of the cell cycle through the E2F-dependent

transcription program. These cell functions are shared by CDK4 and CDK6 but we observed no correlation between the mRNA levels encoding these two kinases. Indeed, a significant correlation with overall survival and time to relapse has only been observed for the *CDK6* mRNA level (Table 1).

Since high expression levels of *CDK6* are associated with poor prognosis in ACCs (Figures 1 and 2), the impact of CDK6 inhibitors on the SW-13 and NCI-H295R cell lines was evaluated (Figure 3). While NCI-H295R cells are classically used as *ex vivo* models of adrenocortical carcinoma, the origin of SW-13 is contested. SW-13 cells were derived from a small cell carcinoma in the adrenal cortex [38]. However, these cells secrete no steroids and it is unclear whether they were derived from a primary tumor in the adrenal cortex or from a metastasis [39]. Keeping in mind the discussions concerning the origin of SW-13 cells, we chose to study the mechanisms reducing cell viability in this cell line in parallel with the pRB negative-NCI-H295R cells. SW-13 cells are highly sensitive to both palbociclib and ribociclib (Figure 3). Both drugs reduced SW-13 cell viability through an irreversible cell cycle arrest with a reduced proportion of cells in S-phase (Figure 4a). We also observed senescence features similar to those previously described in SW-13 cells [40]: β-galactosidase activity, enlarged and flattened cells and high granularity (Figures 4b, 4c, 4d and 4h). Ribociclib being a highly specific inhibitor of CDK4/6, the senescence phenotype is probably induced by deregulation of their effector proteins, such as pRB that plays a pivotal role, as it regulates both G1/S transition and induction of senescence. Such a hypothesis is consistent with the reduction of Phospho-Rb observed in treated cells (Figure 5). However, the senescence phenotype was more pronounced in palbociclib-treated cells and we could not exclude the involvement of other targets. In contrast with SW-13 cells, NCI-H295R cells showed resistance to ribociclib, and a higher IC50 value for palbociclib when compared to SW-13 cells (Figure 3b). A homozygous deletion in the *RB1* gene was previously described [21], and we confirmed the absence of the pRB protein in NCI-H295R extracts (Figure 5). The absence of pRB is probably involved in the NCI-H295R resistance to ribociclib, and also the relative resistance to palbociclib, as was observed in different types of cancers [41–44]. This resistance to CDK4/6 inhibitors caused by pRB loss of function would concern 6.8% and 7% of ACC patients, as estimated with the TCGA and the French cohorts of patients respectively [10,18]. Thus, a majority of ACC patients might benefit from CDK4/6 inhibitors.

While only a slight increase of senescence features was observed at low concentrations of palbociclib (Figure 4b), apoptosis explained the reduction in viability in NCI-H295R cell line detected at >10 μM (Figure 6a). In our effort to determine the cellular mechanism causing apoptosis in these pRB negative cells, we tested the impact of treatments on the activity of GSK3β. This kinase and its regulator AKT are targets of palbociclib and GSK3β phosphorylates β-catenin, leading to β-catenin degradation by the proteasome. Indeed, a higher ratio of active GSK3β and a reduction of the β-catenin active form were observed after treatment with palbociclib (Figures 6b, c and d). Furthermore, the transcriptional activity of β–catenin, was estimated with the level of *AXIN2* mRNA. Actually, increased transcription activity was observed after treatment with palbociclib (Figure 6e). Our results are consistent with the higher *AXIN2* mRNA level observed in NCI-H295R cells after treatment with PNU-74654, an inhibitor of Wnt/β-catenin signaling [23]. Moreover, this Wnt/β-catenin signaling inhibitor increased apoptosis in NCI-H295R cell cultures. Taken together, our observations suggest that palbociclib induces a strong reduction of active β-catenin, leading to aberrant transcription of β-catenin targets and to apoptosis. Besides its impact on β-catenin-dependent transcription, PNU-74654 also decreased steroid hormone secretion by NCI-H295R cells, as early as after 24 h of treatment, at concentrations higher than 50 μM [23]. This reduction preceded the decreased of viability (only after 72 h treatment with 50 μM PNU-74654) and was supposed to result partially from the reduction in gene expression of *SF1* and *CYP21A2* genes. While we confirmed that 100 μM PNU-74654 decreased cortisol secretion, we observed no effect of palbociclib and ribociclib on the concentration of cortisol in the medium, after 24 h and 48 h of treatments (Figure 6f). Actually, PNU-74654 results in direct inhibition of β-catenin-dependent transcription that might cause the reduction of cortisol secretion as soon as after 24 h [23], comparatively to palbociclib that induces β-catenin degradation (Figures 6b and 6d). Thus, the reduction in viability caused by palbociclib on NCI-H295R cells is not a consequence of a long steroid hormone deprivation but probably results from loss of β-catenin-dependent transcription, through pRB-independent processes. Palbociclib concentrations that induced a significant viability reduction of NCI-H295R cells do not fall within a clinically attainable range in the plasma [45]. However, previous assays performed on xenograft mouse tumor tissue showed that higher palbociclib levels could be locally achieved in tumor samples (6h post-dose at 100 mg/kg could be up to 25,163 ng/g), comparatively to plasma levels [46].

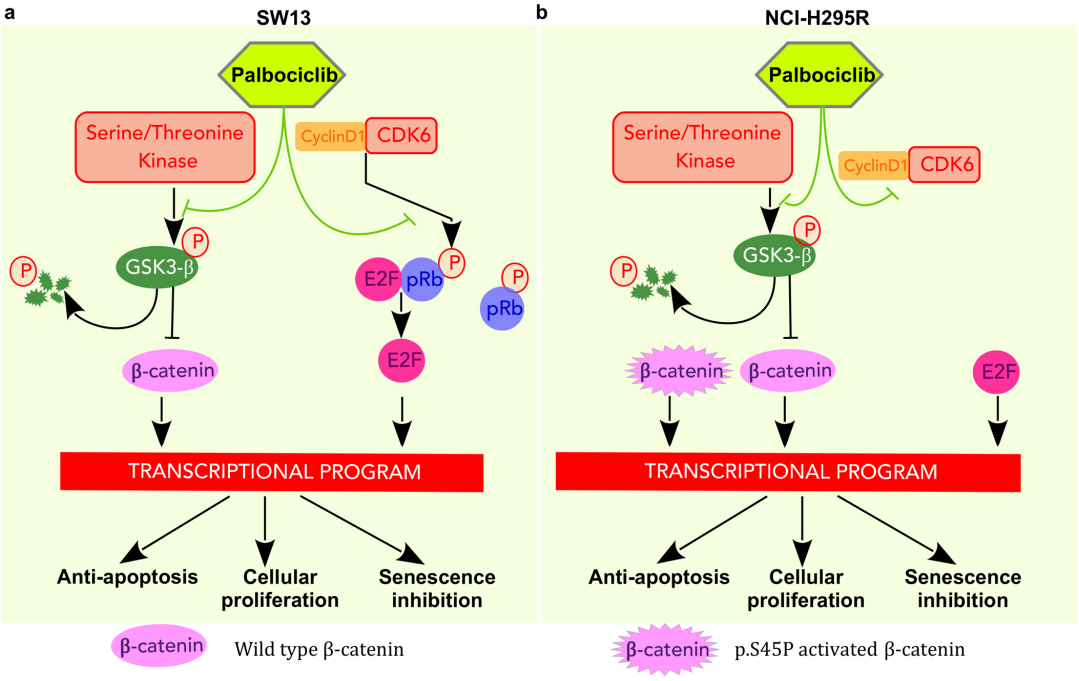


**Figure 7. Pathways targeted by palbociclib in SW-13 and NCI-H295R cells.** (**a**) In SW-13 cells palbociclib acts by inhibiting the kinase activity of CDK6 and leads to a decrease in phosphorylated Rb. E2F is then sequestered and cannot activate the transcription program necessary for the G1/S transition. In addition, palbociclib leads to a decrease of phosphorylated Ser9-GSK3β, resulting in GSK3β stabilization and consecutively to the degradation of β-catenin. Consequently, these events disturb the transcription program involved in inhibition of senescence, in cellular proliferation and in avoidance of apoptosis. (**b**) In NCIH295R cells palbociclib acts by inhibiting the kinase activity of CDK6. Since the cell line is $Rb^{-/-}$, E2F activates the transcription program necessary for G1/S transition. Palbociclib lowers Ser9-GSK3β phosphorylation, increases its stability and ultimately induces β-catenin degradation. However, this cell line carries a heterozygous mutation in the *CTNNB1* gene (p.S45P) that leads to a constitutively active form of β-catenin. Thus, only the non-mutated form of β-catenin is targeted by GSK3β that is stabilized by palbociclib.

Possible models of palbociclib action on the two cell lines used here are shown in Figure 7. In both cases, palbociclib inhibits phosphorylation of Serine9-GSK3β, that in turn induces a decrease of β-catenin signaling and changes the transcription level of its targets. These results indicate that palbociclib and ribocilib constitute potential treatments for ACCs, prompting us to test the impact of combination therapy with mitotane, a drug currently used to treat ACCs. However, only additive effects were observed when tested on the SW-13 and NCI-H295R cell lines. Since SW-13 cells have a normal amount of pRB, palbociclib also directly inhibits pRB phosphorylation, resulting in E2F inactivation and in the consequent arrest of the G1/S transition.

In conclusion, we showed that patients with high CDK6 expression levels present a poor prognosis, and are found in a unique gene expression-based cluster. They share common clinical and molecular features, such as secretion of hormones and the tendency to accumulate mutations in the Wnt/β-catenin pathway. Through its common action on the CDK6 activity and Wnt/β-catenin dependent transcription, palbociclib might be a treatment of choice for patients showing these molecular features. However, clinical assays will be necessary to verify whether ACC patients benefit from this treatment.

## MATERIALS AND METHODS

### Transcriptome and miRNome of adrenocortical carcinomas

Gene expression and miRNA expression in 79 adenocortical carcinomas were initially measured experimentally with Illumina HiSeq 2000 instruments, and treated as previously described [10]. For the present study, TCGA level 3 interpreted gene expression and miRNA expression data were downloaded from the TCGA data portal ( url: https://tcga-data.nci.nih.gov/

docs/publications/tcga/). Level 3 indicates that gene-level expression estimates are given as RSEM (RNA-Seq by Expectation Maximization) normalized counts. Level 3 miRNA expression-interpreted data are the miRNA transcription estimates in log2, as reads per million miRNAs mapped. Expression data from 44 adrenocortical carcinomas of French patients were downloaded from the Gene Expression Omnibus (GEO accession: GSE49278) Database. Gene expression levels were measured using the Affymetrix Human Gene 2.0 ST Array. The downloaded values of gene expression were estimated and normalized as previously described [18]. The 137 gene expression data were selected in transcriptome data files using gene symbols with Unix shell homemade scripts.

**Statistical analyses**

Statistical analyses and figures were obtained using the R 3.2.2 environment [47]. Hierarchical clustering analyses and drawings of heatmaps were performed with homemade scripts using the gplots [48], vegan [49], RColorBrewer and heatmap3 [50] packages, or the ggplot2 [51] R package. Annotations of graphs were drawn using the pBrackets package. Survival analyses were performed with the stats, OIsurv and maxstat R packages. The cutoff value of expression that segregated the patients into two groups was the one that optimized the pValue of the Log-rank test. This optimization was performed using the maxstat R package.

**Reagents**

Palbociclib (PD-0332991, IBRANCE®), Ribociclib (LEE-011, Kiskali®), Mitotane and PNU-74654 were purchased from CliniSciences (A8316, A8641, sc-205754 and sc-258020, respectively). Palbociclib and Ribociclib 1mM stock solutions were prepared in 100% ethanol or DMSO respectively. PNU-74654 stock solution (31.2 mM) was prepared in DMSO. Anti-CDK6 (D4S8S), CDK4 (D9G3E), Phospho-Rb (9308), GSK3-β (D5C5Z), Phospho-GSK3-β (D85E12), non-phospho-β-Catenin (D13A1) were purchased from Cell Signaling Technology. The anti-β-Catenin (MA1-301) and GAPDH (GA1R) were purchased from Thermo Fischer Scientific. The anti-α-Tubulin (T9026) was purchased from Sigma.

**Cell cultures**

The SW-13 (ATCC® CCL-105™) and NCI-H295R (ATCC® CRL-2128™) cell lines from ATCC were from LGC-Standards. SW-13 cells were cultured in DMEM with 4.5 g/L D-glucose, L-glutamine and pyruvate (Thermo Fisher Scientific, Life Technologies, 41966-029), supplemented with 12.5% Nu-Serum™ (Corning, 355500), 1:100 ITS Premix (Corning, 354350), 100 U/mL penicillin and 100 µg/mL streptomycin (Life Technologies, 15140122). SW-13 cells were sub-cultured every three days at a 1:8 ratio. NCI-H295R cells were cultured in Dulbecco's Modified Eagle Medium (DMEM) / Nutrient mixture F-12 Ham (1:1), supplemented with GlutaMAX™-I (Life Technologies, 31331-028), 2.5% Nu-Serum™ (Corning), 1:100 Insulin-Transferrin-Selenium Premix (Corning, 354350), 100 U/mL penicillin and 100 µg/mL streptomycin (Life Technologies, 15140122). The subculture of NCI-H295R was carried out every four days at a 1:4 ratio. SW-13 and NCI-H295R cells were cultured in a humidified incubator with 5% $CO_2$. They were seeded at a density of 5500 cells/cm$^2$ and 50,000 cells/cm$^2$ respectively, in 6-well or 96-well plates (TPP) for viability assays, senescence assays and protein extractions, and Petri dishes before quantitative RT-PCR experiments. Twenty-four hours after plating, palbociclib, ribociclib, 100% ethanol or DMSO was added to the cell culture, and 96 h after the addition of palbociclib or ribociclib, senescence assays, protein extracts and quantitative RT-PCR were performed as described below.

**Cellular proliferation assay**

Cells were plated in 96-well plates (TPP), and incubated for 24 h, before treatment with palbociclib, ribociclib or the corresponding vehicle. After 96 h of treatment, viability was assayed using the CellTiter-Glo® Luminescent Cell Viability kit (Promega), following the manufacturer's instructions. Luminescence was measured with a SpectraMax i3 Multi-Mode Microplate Detection Platform (Molecular Devices, Sunnyvale, CA, USA). Assays were performed in duplicates, in three independent experiments.

**Cell cycle analyses by flow cytometry**

Cells were plated in 6-well plates (TPP), and incubated for 24 h, before treatment with palbociclib, ribociclib or the corresponding vehicle. After 94 h of treatment, 10 µM EdU was added to the cell culture media for 2 h. The cells were then collected and washed twice with PBS. Click-it reactions were performed using the Click-iT Plus EdU Alexa Fluor 647 Flow Cytometry Kit (ThermoFischer Scientific) according to the manufacturer's recommendations. The cells were then counterstained with propidium iodide for 30 min. The cell cycle profile was generated using a CyAn ADP 9C analyser (Beckman Coulter). The analysis was performed with the Flowjo software (LLC). Cell cycle was studied on technical duplicates, in three independent experiments.

**Cortisol assay**

200,000 NCI-H295R cells were plated in 24-well plates (TPP) in a volume of 500 µL of culture medium. After 24 hours, cells were treated with palbociclib, ribociclib, PNU-74654 or the corresponding vehicle. Drugs or vehicle were added in 500 µL of culture medium, to a total volume of 1 mL. After 48h of treatment, cortisol concentration was measured in the supernatant of NCI-H295R cells, using the Cortisol ELISA kit of Cayman chemical (ref: 500360), as described by the manufacturer. Before the assay, all the supernatants (except that with PNU-74654) were diluted 1:10 in fresh culture medium. Assays were performed in technical duplicates on cell media from three independent experiments.

**Measurement of apoptosis**

To measure apoptosis, the cells were seeded at the previously mentioned concentration used in 96-well plates. They were drugged 24 h later and images were obtained using the Essen IncuCyte® ZOOM Live-Cell Analysis system. For the apoptosis experiments, caspase and cytotoxicity reagents (Essen Bioscience, Ltd, Welwyn, Garden City, Hertfordshire, UK) were added to the medium, resulting in a 1:1000 dilution of each reagent. Cell apoptosis and cytotoxicity of the drug were monitored for 96 h after treatment with 4 acquisitions per well every hour. Each condition was performed in triplicate. Analysis was performed using the software for the IncuCyte® ZOOM Live-Cell Analysis system. Assays were performed in duplicates, in three independent experiments.

**Senescence-associated β-galactosidase assay**

After 96 h of cell treatment in 6-well plates (ATCC) with palbociclib, ribociclb or the vehicle, the senescence assay was performed using the Senescence β-Galactosidase Staining Kit (Cell Signaling, #9860), as described by the manufacturer. The cells were rinsed with Dulbecco's phosphate-Buffered Saline (Invitrogen), and fixed as described by the manufacturer. They were then incubated in 500 µL per well of X-Gal staining solution mix overnight at 37°C. Pictures of four fields (200X total magnification) of each well were taken with a Nikon Digital Sight DS-Fi1 mounted on a Nikon Eclipse TS100 microscope (Nikon France, Champigny-sur-Marne, France). Senescent cells were then counted using the ImageJ program. Assays were performed in experimental duplicates (2 wells), in three independent experiments.

**Clonogenic assay**

SW-13 (5,500 cells/cm$^2$) or 50,000 NCI-H295R cells/cm$^2$ were plated in 6-well plates (TPP). Drugs were added to the cell-culture media 24 h later at appropriate concentrations. The cells were incubated with the drugs for 96 h, before new counting and plating at 400 cells/cm$^2$ (SW-13 cells) or 5,000 cells/cm$^2$ (NCI-H295R) in 6-well plates. Seven days (SW-13 cells) or 10 days (NCI-H295R) later, the cells were fixed with 4% paraformaldehyde for 5 min at room temperature and colored with 0.05% crystal violet (Sigma, C3886) diluted in water for 30 min. The clones from three independent experiments were counted.

**Western blot analysis**

Cells were grown on 35 mm plates (ATCC) and protein extracted with lysis buffer containing 25 mM Tris-HCl pH 7.5, 100 mM NaCl, 1 mM EDTA, 1 mM EGTA, 0.5% NP40 (#492016) (Merck Millipore), 1% Triton™ X-100 (9002-93-1, Sigma Aldrich), cOmplete™ EDTA-free Protease Inhibitor Cocktail (Sigma Aldrich), and Phosphatase Inhibitor Cocktail Set II (524625, Merck Millipore). Proteins were separated on NuPAGE™ 4-12% Bis-Tris gels (Thermo Fischer Scientific) and transferred onto nitrocellulose membranes (GE Healthcare). Primary antibodies were diluted at a final concentration of 1:1000 in Tris-buffered saline solution with 0.05% TWEEN® 20. Secondary antibodies were used as recommended in the manufacturer's instructions. Relative quantifications were performed on three different western blot experiments.

**Gene expression**

RNAs were extracted with the Nucleospin® RNA extraction kit (Macherey-Nagel), following the manufacturer's instructions. RNA extracts (2 µg) were treated with 0.1 U/µL of DNAse I (Thermo Fischer Scientific), in a total volume of 20 µL at 37°C for 30 min. DNase I was then inactivated by heating at 65°C for 10 min after addition of 2 µL of 50 mM EDTA (Thermo Fischer Scientific). Reverse transcription of 1 µg of DNase I-treated RNA was performed using 15 ng/µL random primers (Invitrogen), 1 U/µL Ribolock RNase inhibitor, 1 mM of each dNTP and 10 U/µL RevertAid reverse transcriptase (Thermo Fisher Scientific), in a final volume of 20 µL. The reaction was performed in an Eppendorf Mastercycler thermocycler machine (Eppendorf France, Montesson, France), for 5 min at 25°C and then 60 min at 42°C. Reaction was stopped by heating at 70°C for 5 min. Quantitative PCRs were performed with 1 µL of 1/5 diluted first strands of cDNA in a total volume of 15 µL of 1X ABsolute SYBR Capillary Mix (Thermo Fisher Scientific, AB-1285), with 73 nM of each PCR primer. Reactions were performed in 20 µL LightCycler capil-

laries (Roche). Primer sequences were as follows: AXIN2-F 5'-GCTGACGGATGATTCCATGT-3', AXIN2-R 5'-ACTGCCCACACGATAAGGAG-3'[52], ACTB-F 5'-GAGCTACGAGCTGCCTGAC-3' and ACTB-R 5'-GCACTGTGTTGGCGTACAG-3'. PCR amplification was performed with a LightCycler 1.5 thermocycler and analyzed with LightCycler Software 3.5 (Roche, Boulogne-Billancourt, France). Cycling conditions were as follows: initial denaturation of enzyme 95°C for 15 minutes, and 50 amplification cycles (95°C for 15 sec, 60°C for 30 sec and 72°C for 20 sec) before annealing of all samples and gradual temperature increase to 95°C to trace the melting curve. Assays were performed in technical triplicates on RNAs extracted from three independent experiments.

### Abbreviations

ACC, Adrenocortical carcinoma; COSMIC, Catalogue of Somatic Mutations In Cancers; EdU, 5-ethynyl-2'-deoxyuridine; FDA, Food and Drug Administration; GEO, Gene Expression Omnibus; HR, Homologous Recombination; IC50, half maximal inhibitory concentration; OS, Overall Survival; RFS, Relapse Free Survival; TCGA, The Cancer Genome Atlas; KEGG, Kyoto Encyclopedia of Genes and Genomes; RSEM, RNA-Seq by Expectation-Maximization.

## AUTHOR CONTRIBUTIONS

Conceived and designed the experiments: DH, JCC, CM, GB, FF. Performed the experiments: DH, SK, TD, LBD, FF. Analyzed the data: DH, SK, TD, FF, GB. Contributed to analysis tools: DH, TD, SK, FF. Wrote the paper: DH, GB and FF.

## ACKNOWLEDGEMENTS

We thank Anne-Lise Haenni (CNRS-UMR 7592, Institut Jacques-Monod, Paris, France) for attentive reading and correction of the manuscript. We acknowledge Tamara Advedissian and Frédérique Deshayes (CNRS-UMR 7592, Institut Jacques-Monod) for helpful discussions and suggestions, and also Griselda Wentzinger of the ImagoSeine core facility of the Institut Jacques Monod, member of IBiSA and France-BioImaging (ANR-10-INBS-04) insfrastructures, for her technical help. We are grateful to all the patients and families who contributed to The Consortium Genome Atlas study.

## CONFLICTS OF INTEREST

The authors of this manuscript declare no conflicts of interest.

## FUNDING

The project was supported by La Ligue Nationale Contre le Cancer (RS16/75-108 and RS17/75-135), the Groupement des Entreprises Françaises contre le Cancer (GEFLUC), and by the generous legacy from Mrs Suzanne Larzat to the group.

## REFERENCES

1. Kebebew E, Reiff E, Duh QY, Clark OH, McMillan A. Extent of disease at presentation and outcome for adrenocortical carcinoma: have we made progress? World J Surg. 2006; 30:872–78. https://doi.org/10.1007/s00268-005-0329-x
2. Else T, Kim AC, Sabolch A, Raymond VM, Kandathil A, Caoili EM, Jolly S, Miller BS, Giordano TJ, Hammer GD. Adrenocortical carcinoma. Endocr Rev. 2014; 35:282–326. https://doi.org/10.1210/er.2013-1029
3. Ip JC, Pang TC, Glover AR, Soon P, Zhao JT, Clarke S, Robinson BG, Gill AJ, Sidhu SB. Immunohistochemical validation of overexpressed genes identified by global expression microarrays in adrenocortical carcinoma reveals potential predictive and prognostic biomarkers. Oncologist. 2015; 20:247–56. https://doi.org/10.1634/theoncologist.2014-0392
4. Beuschlein F, Weigel J, Saeger W, Kroiss M, Wild V, Daffara F, Libé R, Ardito A, Al Ghuzlan A, Quinkler M, Oßwald A, Ronchi CL, de Krijger R, et al. Major prognostic role of Ki67 in localized adrenocortical carcinoma after complete resection. J Clin Endocrinol Metab. 2015; 100:841–49. https://doi.org/10.1210/jc.2014-3182
5. Morimoto R, Satoh F, Murakami O, Suzuki T, Abe T, Tanemoto M, Abe M, Uruno A, Ishidoya S, Arai Y, Takahashi K, Sasano H, Ito S. Immunohistochemistry of a proliferation marker Ki67/MIB1 in adrenocortical carcinomas: Ki67/MIB1 labeling index is a predictor for recurrence of adrenocortical carcinomas. Endocr J. 2008; 55:49–55. https://doi.org/10.1507/endocrj.K07-079
6. Allolio B, Fassnacht M. Clinical review: Adrenocortical carcinoma: clinical update. J Clin Endocrinol Metab. 2006; 91:2027–37. https://doi.org/10.1210/jc.2005-2639
7. Giordano TJ, Kuick R, Else T, Gauger PG, Vinco M, Bauersfeld J, Sanders D, Thomas DG, Doherty G, Hammer G. Molecular classification and prognostication of adrenocortical tumors by transcriptome profiling. Clin Cancer Res. 2009; 15:668–76. https://doi.org/10.1158/1078-0432.CCR-08-1067
8. de Reyniès A, Assié G, Rickman DS, Tissier F, Groussin L, René-Corail F, Dousset B, Bertagna X, Clauser E,

Bertherat J. Gene expression profiling reveals a new classification of adrenocortical tumors and identifies molecular predictors of malignancy and survival. J Clin Oncol. 2009; 27:1108–15.

https://doi.org/10.1200/JCO.2008.18.5678

9. Assié G, Guillaud-Bataille M, Ragazzon B, Bertagna X, Bertherat J, Clauser E. The pathophysiology, diagnosis and prognosis of adrenocortical tumors revisited by transcriptome analyses. Trends Endocrinol Metab. 2010; 21:325–34. https://doi.org/10.1016/j.tem.2009.12.009

10. Zheng S, Cherniack AD, Dewal N, Moffitt RA, Danilova L, Murray BA, Lerario AM, Else T, Knijnenburg TA, Ciriello G, Kim S, Assie G, Morozova O, et al, and Cancer Genome Atlas Research Network. Comprehensive Pan-Genomic Characterization of Adrenocortical Carcinoma. Cancer Cell. 2016; 29:723–36. https://doi.org/10.1016/j.ccell.2016.04.002

11. Beaver JA, Amiri-Kordestani L, Charlab R, Chen W, Palmby T, Tilley A, Zirkelbach JF, Yu J, Liu Q, Zhao L, Crich J, Chen XH, Hughes M, et al. FDA approval: palbociclib for the treatment of postmenopausal patients with estrogen receptor-positive, HER2-negative metastatic breast cancer. Clin Cancer Res. 2015; 21:4760–66. https://doi.org/10.1158/1078-0432.CCR-15-1185

12. Walker A, Wedam S, Amiri-Kordestani L, Bloomquist E, Tang S, Sridhara R, Chen W, Palmby T, Fourie Zirkelbach J, Fu W, Liu Q, Tilley A, Kim G, et al. FDA Approval of Palbociclib in Combination with Fulvestrant for the Treatment of Hormone Receptor–Positive, HER2-Negative Metastatic Breast Cancer. Clin Cancer Res. 2015; 1:1–14. 10.1017/CBO9781107415324.004

13. Finn RS, Crown JP, Lang I, Boer K, Bondarenko IM, Kulyk SO, Ettl J, Patel R, Pinter T, Schmidt M, Shparyk Y, Thummala AR, Voytko NL, et al. The cyclin-dependent kinase 4/6 inhibitor palbociclib in combination with letrozole versus letrozole alone as first-line treatment of oestrogen receptor-positive, HER2-negative, advanced breast cancer (PALOMA-1/TRIO-18): a randomised phase 2 study. Lancet Oncol. 2015; 16:25–35. https://doi.org/10.1016/S1470-2045(14)71159-3

14. Finn RS, Martin M, Rugo HS, Jones S, Im SA, Gelmon K, Harbeck N, Lipatov ON, Walshe JM, Moulder S, Gauthier E, Lu DR, Randolph S, et al. Palbociclib and Letrozole in Advanced Breast Cancer. N Engl J Med. 2016; 375:1925–36. https://doi.org/10.1056/NEJMoa1607303

15. Infante JR, Cassier PA, Gerecitano JF, Witteveen PO, Chugh R, Ribrag V, Chakraborty A, Matano A, Dobson JR, Crystal AS, Parasuraman S, Shapiro GI. A Phase I Study of the Cyclin-Dependent Kinase 4/6 Inhibitor Ribociclib (LEE011) in Patients with Advanced Solid Tumors and Lymphomas. Clin Cancer Res. 2016; 22:5696–705. https://doi.org/10.1158/1078-0432.CCR-16-1248

16. Hortobagyi GN, Stemmer SM, Burris HA, Yap YS, Sonke GS, Paluch-Shimon S, Campone M, Blackwell KL, André F, Winer EP, Janni W, Verma S, Conte P, et al. Ribociclib as First-Line Therapy for HR-Positive, Advanced Breast Cancer. N Engl J Med. 2016; 375:1738–48. https://doi.org/10.1056/NEJMoa1609709

17. Hiroyuki O, Susumu G, Kazushige S, Wataru F, Hidemasa B, Minoru K. KEGG: Kyoto Encyclopedia of Genes and Genomes. Nucleic Acids Res. 1999; 27: 29–34.

18. Assié G, Letouzé E, Fassnacht M, Jouinot A, Luscap W, Barreau O, Omeiri H, Rodriguez S, Perlemoine K, René-Corail F, Elarouci N, Sbiera S, Kroiss M, et al. Integrated genomic characterization of adrenocortical carcinoma. Nat Genet. 2014; 46:607–12. https://doi.org/10.1038/ng.2953

19. Abiven G, Coste J, Groussin L, Anract P, Tissier F, Legmann P, Dousset B, Bertagna X, Bertherat J. Clinical and biological features in the prognosis of adrenocortical cancer: poor outcome of cortisol-secreting tumors in a series of 202 consecutive patients. J Clin Endocrinol Metab. 2006; 91:2650–55. https://doi.org/10.1210/jc.2005-2730

20. Germano A, Rapa I, Volante M, De Francia S, Migliore C, Berruti A, Papotti M, Terzolo M. RRM1 modulates mitotane activity in adrenal cancer cells interfering with its metabolization. Mol Cell Endocrinol. 2015; 401:105–10. https://doi.org/10.1016/j.mce.2014.11.027

21. Ragazzon B, Libé R, Assié G, Tissier F, Barreau O, Houdayer C, Perlemoine K, Audebourg A, Clauser E, René-Corail F, Bertagna X, Dousset B, Bertherat J, Groussin L. Mass-array screening of frequent mutations in cancers reveals RB1 alterations in aggressive adrenocortical carcinomas. Eur J Endocrinol. 2014; 170:385–91. https://doi.org/10.1530/EJE-13-0778

22. Sumi NJ, Kuenzi BM, Knezevic CE, Remsing Rix LL, Rix U. Chemoproteomics Reveals Novel Protein and Lipid Kinase Targets of Clinical CDK4/6 Inhibitors in Lung Cancer. ACS Chem Biol. 2015; 10:2680–86. https://doi.org/10.1021/acschembio.5b00368

23. Leal LF, Bueno AC, Gomes DC, Abduch R, de Castro M, Antonini SR. Inhibition of the Tcf/beta-catenin complex increases apoptosis and impairs adreno-

cortical tumor cell proliferation and adrenal steroidogenesis. Oncotarget. 2015; 6:43016–32. https://doi.org/10.18632/oncotarget.5513

24. Fernandez-Vidal A, Guitton-Sert L, Cadoret JC, Drac M, Schwob E, Baldacci G, Cazaux C, Hoffmann JS. A role for DNA polymerase θ in the timing of DNA replication. Nat Commun. 2014; 5:4285. https://doi.org/10.1038/ncomms5285

25. Baldacci G, Hoffmann JS, Cadoret JC. Impact of the DNA polymerase Theta on the DNA replication program. Genom Data. 2014; 3:90–93. https://doi.org/10.1016/j.gdata.2014.11.014

26. Goullet de Rugy T, Bashkurov M, Datti A, Betous R, Guitton-Sert L, Cazaux C, Durocher D, Hoffmann JS. Excess Polθ functions in response to replicative stress in homologous recombination-proficient cancer cells. Biol Open. 2016; 5:1485–92. https://doi.org/10.1242/bio.018028

27. Ceppi P, Novello S, Cambieri A, Longo M, Monica V, Lo Iacono M, Giaj-Levra M, Saviozzi S, Volante M, Papotti M, Scagliotti G. Polymerase eta mRNA expression predicts survival of non-small cell lung cancer patients treated with platinum-based chemotherapy. Clin Cancer Res. 2009; 15:1039–45. https://doi.org/10.1158/1078-0432.CCR-08-1227

28. Wang J, Cazzato E, Ladewig E, Frattini V, Rosenbloom DI, Zairis S, Abate F, Liu Z, Elliott O, Shin YJ, Lee JK, Lee IH, Park WY, et al. Clonal evolution of glioblastoma under therapy. Nat Genet. 2016; 48:768–76. https://doi.org/10.1038/ng.3590

29. Zhou W, Chen YW, Liu X, Chu P, Loria S, Wang Y, Yen Y, Chou KM. Expression of DNA translesion synthesis polymerase η in head and neck squamous cell cancer predicts resistance to gemcitabine and cisplatin-based chemotherapy. PLoS One. 2013; 8:e83978. https://doi.org/10.1371/journal.pone.0083978

30. Zhang X, Chen Q, Chen J, He C, Mao J, Dai Y, Yang X, Hu W, Zhu C, Chen B. Association of polymorphisms in translesion synthesis genes with prognosis of advanced non-small-cell lung cancer patients treated with platinum-based chemotherapy. J Surg Oncol. 2016; 113:17–23. https://doi.org/10.1002/jso.24103

31. Peng C, Chen Z, Wang S, Wang HW, Qiu W, Zhao L, Xu R, Luo H, Chen Y, Chen D, You Y, Liu N, Wang H. The error-prone DNA polymerase k promotes temozolomide resistance in glioblastoma through Rad17-dependent activation of ATR-Chk1 signaling. Cancer Res. 2016; 76:2340–53. https://doi.org/10.1158/0008-5472.CAN-15-1884

32. Dai CH, Chen P, Li J, Lan T, Chen YC, Qian H, Chen K, Li MY. Co-inhibition of pol θ and HR genes efficiently synergize with cisplatin to suppress cisplatin-resistant lung cancer cells survival. Oncotarget. 2016; 7:65157–70. https://doi.org/10.18632/oncotarget.11214

33. Srivastava AK, Han C, Zhao R, Cui T, Dai Y, Mao C, Zhao W, Zhang X, Yu J, Wang QE. Enhanced expression of DNA polymerase eta contributes to cisplatin resistance of ovarian cancer stem cells. Proc Natl Acad Sci USA. 2015; 112:4411–16. https://doi.org/10.1073/pnas.1421365112

34. Huang KK, Jang KW, Kim S, Kim HS, Kim SM, Kwon HJ, Kim HR, Yun HJ, Ahn MJ, Park KU, Ramnarayanan K, McPherson JR, Zhang S, et al. Exome sequencing reveals recurrent REV3L mutations in cisplatin-resistant squamous cell carcinoma of head and neck. Sci Rep. 2016; 6:19552. https://doi.org/10.1038/srep19552

35. Wang W, Sheng W, Yu C, Cao J, Zhou J, Wu J, Zhang H, Zhang S. REV3L modulates cisplatin sensitivity of non-small cell lung cancer H1299 cells. Oncol Rep. 2015; 34:1460–68. https://doi.org/10.3892/or.2015.4121

36. Yang L, Shi T, Liu F, Ren C, Wang Z, Li Y, Tu X, Yang G, Cheng X. REV3L, a promising target in regulating the chemosensitivity of cervical cancer cells. PLoS One. 2015; 10:e0120334. https://doi.org/10.1371/journal.pone.0120334

37. Xie K, Doles J, Hemann MT, Walker GC. Error-prone translesion synthesis mediates acquired chemo-resistance. Proc Natl Acad Sci USA. 2010; 107:20792–97. https://doi.org/10.1073/pnas.1011412107

38. Wang T, Rainey WE. Human adrenocortical carcinoma cell lines. Mol Cell Endocrinol. 2012; 351:58–65. https://doi.org/10.1016/j.mce.2011.08.041

39. Leibovitz A, McCombs WM 3rd, Johnston D, McCoy CE, Stinson JC. New human cancer cell culture lines. I. SW-13, small-cell carcinoma of the adrenal cortex. J Natl Cancer Inst. 1973; 51:691–97.

40. Shanahan F, Seghezzi W, Parry D, Mahony D, Lees E. Cyclin E associates with BAF155 and BRG1, components of the mammalian SWI-SNF complex, and alters the ability of BRG1 to induce growth arrest. Mol Cell Biol. 1999; 19:1460–69. https://doi.org/10.1128/MCB.19.2.1460

41. Dean JL, Thangavel C, McClendon AK, Reed CA, Knudsen ES. Therapeutic CDK4/6 inhibition in breast cancer: key mechanisms of response and failure. Oncogene. 2010; 29:4018–32. https://doi.org/10.1038/onc.2010.154

42. Konecny GE, Winterhoff B, Kolarova T, Qi J, Manivong K, Dering J, Yang G, Chalukya M, Wang HJ, Anderson L, Kalli KR, Finn RS, Ginther C, et al. Expression of p16 and retinoblastoma determines response to CDK4/6 inhibition in ovarian cancer. Clin Cancer Res. 2011;

17:1591–602. https://doi.org/10.1158/1078-0432.CCR-10-2307

43. Logan JE, Mostofizadeh N, Desai AJ, VON Euw E, Conklin D, Konkankit V, Hamidi H, Eckardt M, Anderson L, Chen HW, Ginther C, Taschereau E, Bui PH, et al. PD-0332991, a potent and selective inhibitor of cyclin-dependent kinase 4/6, demonstrates inhibition of proliferation in renal cell carcinoma at nanomolar concentrations and molecular markers predict for sensitivity. Anticancer Res. 2013; 33:2997–3004.

44. Michaud K, Solomon DA, Oermann E, Kim JS, Zhong WZ, Prados MD, Ozawa T, James CD, Waldman T. Pharmacologic inhibition of cyclin-dependent kinases 4 and 6 arrests the growth of glioblastoma multiforme intracranial xenografts. Cancer Res. 2010; 70:3228–38. https://doi.org/10.1158/0008-5472.CAN-09-4559

45. Schwartz GK, LoRusso PM, Dickson MA, Randolph SS, Shaik MN, Wilner KD, Courtney R, O'Dwyer PJ. Phase I study of PD 0332991, a cyclin-dependent kinase inhibitor, administered in 3-week cycles (Schedule 2/1). Br J Cancer. 2011; 104:1862–68. https://doi.org/10.1038/bjc.2011.177

46. Nguyen L, Zhong WZ, Painter CL, Zhang C, Rahavendran SV, Shen Z. Quantitative analysis of PD 0332991 in xenograft mouse tumor tissue by a 96-well supported liquid extraction format and liquid chromatography/mass spectrometry. J Pharm Biomed Anal. 2010; 53:228–34. https://doi.org/10.1016/j.jpba.2010.02.031

47. Team RR. A Language and Environment for Statistical Computing. Vienna, Austria; 2015. Available from https://www.r-project.org/

48. Warnes G, Bolker B, Bonebakker L, Gentleman R, Huber W, Liaw A, Lumley T, Maechler M, Magnusson A, Moeller S, Schwartz M, Venables B. gplots: Various R Programming Tools for Plotting Data. 2015.

49. Oksanen J, Blanchet G, Kindt R, Legendre P, Minchin P, O'Hara RB, Simpson G, Solymos P, Stevens H, Wagner H. vegan: Community Ecology Package. 2016. Available from http://cran.r-project.org/package=vegan

50. Shilin Z, Guo Y, Sheng Q, Shyr Y. heatmap3: An Improved Heatmap PackageNo Title. 2015. Available from http://cran.r-project.org/package=heatmap3

51. Wickham H. ggplot2: Elegant Graphics for Data Analysis. Springer-Verlag New York; 2009. Available from http://ggplot2.org

52. Okabe H, Kinoshita H, Imai K, Nakagawa S, Higashi T, Arima K, Uchiyama H, Ikegami T, Harimoto N, Itoh S, Ishiko T, Yoshizumi T, Beppu T, et al. Diverse basis of β-catenin activation in human hepatocellular carcinoma: implications in biology and prognosis. PLoS One. 2016; 11:e0152695. https://doi.org/10.1371/journal.pone.0152695

## SUPPLEMENTARY MATERIAL

Please browse the link in Full text version to see

**Supplementary Table 1. Association of 136 genes involved in G1/S phase transition, DNA replication and DNA damage response with overall survival and relapse free survival) in ACC patients of the TCGA consortium.**

Data from n=54 and n=79 ACC samples were used for the log-rank correlation test for RFS and OS, respectively. Log-Rank tests the difference of RFS or OS time between "High" and "Low" expression groups of patients. The cutoff is the value of gene expression maximizing the significance of the difference between those two groups. The percentile is the proportion of individuals below the cutoff value. Adjusted *p* (Adj *p*) values have been obtained following the Benjamini Hochberg method. Significant Adj *p* values are written in bold characters. The correlation with *MKI67* gene expression value was tested with Pearson test. Correl. coef. is the Pearson product-moment correlation coefficient that estimates the correlation of the expression level of each gene and of *MKI67*.

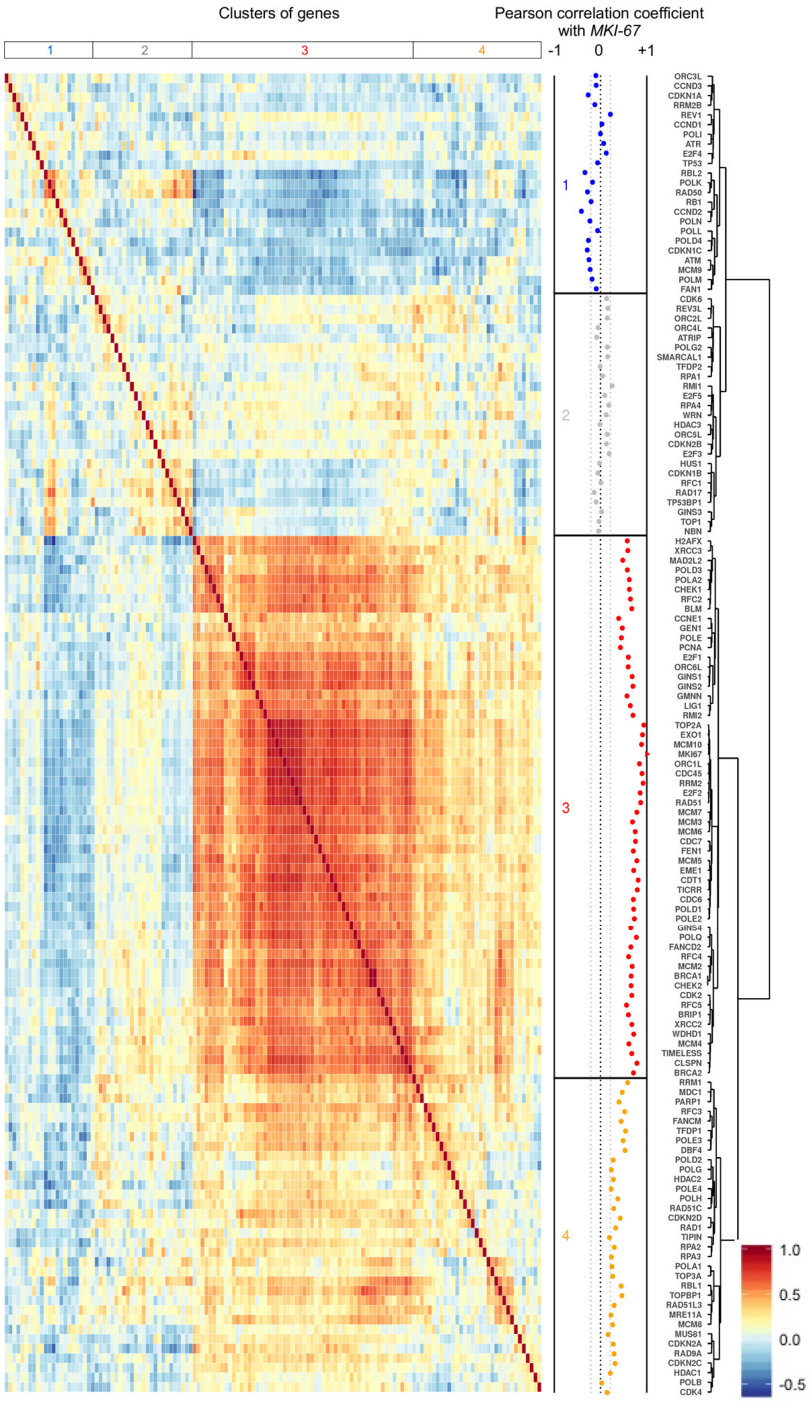


**Supplementary Figure 1 Pearson correlation coefficient-based heatmap representing the similarity of 137 gene expression values in 79 ACCs.** The 137 genes (right side) are involved in G1/S transition, and in DNA replication and repair. Colors indicate the Pearson correlation coefficient values between genes, as indicated by the color scale at the bottom-right. Dissimilarities between clusters are indicated by the dendrogram (right side). Hierarchical clustering of genes based on Pearson correlation coefficient values resulted in four clusters of genes, as indicated in the dot plot at the right side, and at the top of the heatmap. In the dot plot, dots indicate the Pearson correlation coefficient values between each gene and *MKI67*. Grey colored dashed lines indicate the threshold correlation coefficient values for a significant Pearson correlation test (+/- 0.21).

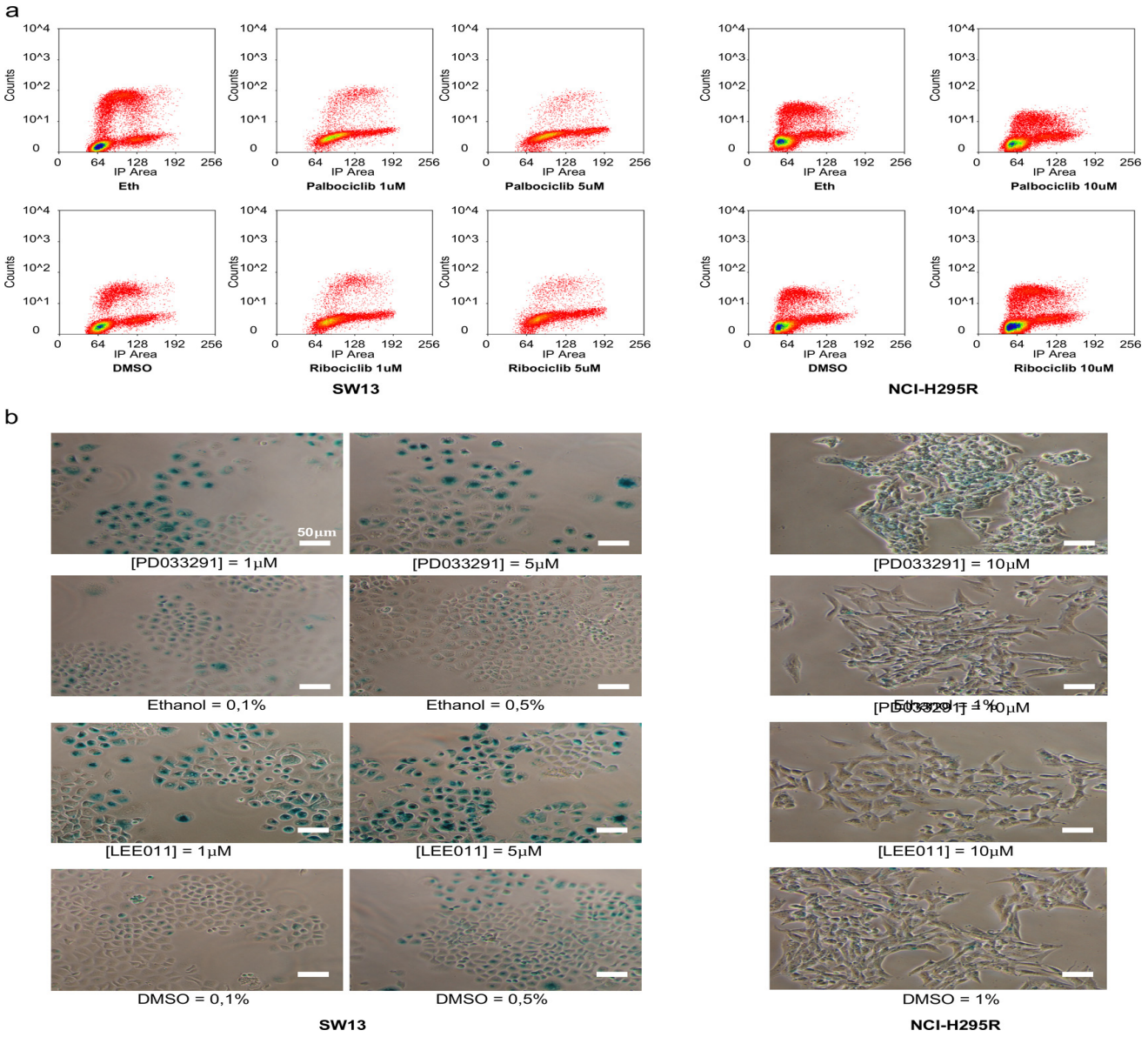


**Supplementary Figure 2. Palbociclib and ribociclib impacts on cell cycle and senescence in NCI-H295R and SW-13 cells.** (**a**) Bivariate plots showing DNA content (propidium iodide staining, x axis) and EdU incorporation (Alexa Fluor® 647 Staining, y axis) for SW-13 cells (left panels) and NCI-H295R cells (right panels) upon treatment with palbociclib, ribociclib or mock-treated cells. (**b**) Images showing β-galactosidase activity staining (senescence marker) in SW-13 cells (left panels) and in NCIH-295R cells (right panels) upon treatments with palbociclib, ribociclib or in mock-treated cells. Magnification scale bars indicate 50 µm.

# II. Palbociclib and DNA replication

## II.A Palbociclib interferes with origin firing in a pRb independent manner

### II.A.1 Summary

During my thesis, I was interested in the molecular mechanisms of the CDK4/6 inhibitor named palbociclib in the dynamics of DNA replication. The originality of this study is that we studied palbociclib in a pRb negative context. As pRb is a major substrate for CDK4/6 in the G1/S transition of the cell cycle, its absence is widely considered as a marker of resistance. However, we surprisingly observed an aberrant progression of the cell cycle accompanied with less DNA synthesis in pRb-deficient cell lines (MDA-MB-468 and NCI-H295R) without any cell cycle arrest when cells are treated with palbociclib. This finding indicates that palbociclib may have impacts on DNA replication even in the absence of pRb.

To decipher the palbociclib mechanisms of action, I performed two powerful methods dedicated to the analysis of the DNA replication process namely the analysis of the replication timing (See chapter Result II.B) and the DNA fiber. The DNA fiber assay provides a genome wide vision of the dynamics of DNA replication at a single molecule scale. This technique relies on the ability of cells to incorporate thymidine during replication. Using thymidine analogs (IdU followed by CldU) that will be detected by specific antibodies, we can visualize tracks of neosynthesized DNA in each pulse. First, the speed of replicative forks can be measured with the length of the track divided by the pulse time. This measurement allows us to understand how the replication forks move and whether replication forks slowdown under a given condition inducing replicative stress. Second, successive pulse-labeling of cells with two analogs can reveal the direction of the progressing forks that provides more information about initiation or termination events. Indeed, initiation events are characterized by specific patterns. For instance, a single CldU track represents an initiation event that occurred during the second pulse (Figure 18.a and b). Inter origin distance (IOD) depicts the distance between two origins, indicating the efficiency of origin activation. In order to precisely estimate the IOD, single stranded DNA should be labeled to ensure that two origins are on the same DNA fiber (Figure 18.c). Thus, the length of the fibers is a critical factor that might bias IOD

measurement. An alternative descriptive statistic for the DNA replication process is the forks density that indirectly indicates the efficiency of origin activation. This value is calculated as an average of the number of forks present per kilobase. Finally, the asymmetry of the two pulses can be measured by calculating the ratio between the length of the two pulses. This represents a perturbation of ongoing forks due to stalling or collapse. Through these measurements, the DNA fiber assay allows to assess the impacts of a given source of replicative stress on replication dynamics.

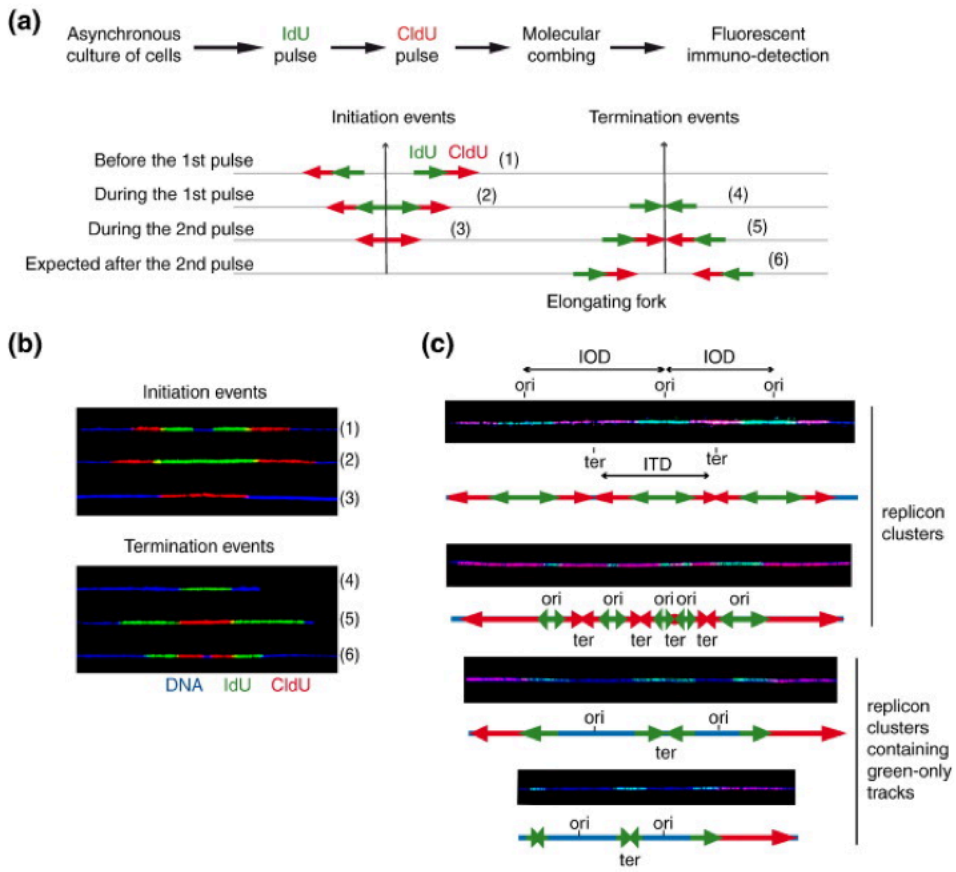


**Figure 18.** Principles of replication dynamics analyses.
a. Scheme of the protocol used for a double pulse labeling of replication forks in asynchronous cell cultures. b. Examples of DNA fibers harboring initiation and termination events. Blue, DNA; green, IdU; red, CldU. c. Examples of replicon clusters. DNA is shown in blue. (Figure from Técher *et al.*, 2013).

Using the aforementioned two methods, we demonstrated how palbociclib disrupts DNA replication and particularly impairs the initiation step in two pRb-deficient cell lines. In addition, by analyzing proteins bound onto chromatin we showed that palbociclib decreases the amount of Dbf4 dependent kinase (DDK), inducing defects in the activation of origins.

These effects must have been ignored in pRb-proficient cells because they are masked by cell cycle arrests at the G1/S transition.

In conclusion, this paper shows novel mechanisms of action of the palbociclib in DNA replication in a pRb independent manner. These findings could provide new possibilities for using palbociclib as a cancer treatment to target Rb loss cancers characterized by their genome instability. The palbociclib could exacerbate this instability by rendering the cells more vulnerable to replicative stress. In this context, palbociclib has the potential to be combined with other therapeutic molecules that target DNA replication.

### II.A.2 Article (In preparation)

**Abstract**

Over the last decade, CDK4/6 inhibitors (palbociclib, ribociclib and abemaciclib) have emerged as promising anticancer drugs. Numerous studies have demonstrated that CDK4/6 inhibitors efficiently block the pRb-E2F pathway and induce cell cycle arrest in pRb-proficient cells. Based on these studies, the inhibitors have been approved by the FDA for treatment of advanced hormonal receptor (HR) positive breast cancers in combination with hormonal therapy. However, some evidence has recently shown unexpected effects of the inhibitors, promoting needs to understand more about the mechanism of inhibitors beyond pRb.

Our study demonstrates here for the first time how palbociclib impairs the origin firing in the DNA replication process in pRb-deficient cell lines. Strikingly, despite the absence of pRb, cells treated with palbociclib synthesize less DNA without any induced cell cycle arrest. Furthermore, palbociclib treatment disturbs the temporal program of DNA replication and reduces the density of replication forks. Cells treated with palbociclib show a defect in the loading of proteins of the Pre-initiation complex (Pre-IC) on chromatin, indicating a reduced initiation of DNA replication. Our findings highlight hidden effects of palbociclib on the dynamics of DNA replication and on its cytotoxic consequences on cell viability in the absence of pRb. This study provides a potential therapeutic application of palbociclib to target genomic instability towards pRb deficient patients.

**Introduction**

Palbociclib is a small molecule inhibitor of cyclin-dependent kinase (CDK) 4 and 6, part of the third generation of CDK inhibitors along with ribociclib and abemaciclib. They are highly selective and specific CDK4/6 inhibitors showing IC50 values in the nanomolar range *in vitro* (Ping Chen *et al.*, 2016). These inhibitors showed their efficacy and safety in many clinical trials (Spring *et al.*, 2019). Based on successful outcome, the United States Food and Drug Administration (FDA) approved palbociclib as a treatment for advanced breast cancer in 2015 (https://www.fda.gov/drugs/resources-information-approved-drugs/palbociclib-ibrance)(Loibl *et al.*, 2017). Today, more than 200 clinical trials are ongoing for different types of cancer, reflecting palbociclib as a promising cancer treatment (Chen *et al.*, 2019).

In an attempt to understand the antiproliferative molecular mechanism of palbociclib, numerous preclinical studies have investigated how palbociclib impacts downstream pathways of CDK4/6 in various cancer cell lines (Bollard *et al.*, 2016)(Hadjadj *et al.*, 2017). The most studied pathway is mediated by the pRb (retinoblastoma protein) that is the major substrate of CDK4/6. Indeed, pRb plays pivotal roles in the G1/S transition of the cell cycle releasing E2F family of transcription factors which in turn regulate the expression of genes involved in the progression of the cell cycle and in DNA replication (Dyson, 1998)(Jingwen, Yaochen and Guojun, 2017). CDK4/6 participate in this cascade as kinases phosphorylating the serine 780/795 and Serine 807/811 of pRb. Upon the treatment with palbociclib in clinical doses (around 1μM), pRb remains underphosphorylated and sequesters E2F factors, which finally induces efficient cell cycle arrest in G1(Marzec *et al.*, 2006). However, emerging evidence have shown that palbociclib has additional effects at high concentrations in a CDK4/6 or pRb independent manner (Miettinen *et al*., 2018)(Wells *et al*., 2020)(Hafner *et al*., 2019)(Hsieh *et al*., 2017). To emphasize these findings, we reveal here the pRb independent actions of palbociclib on the dynamics of DNA replication at high dose.

DNA replication is a highly regulated process that ensures the duplication of genetic materials to transmit the entire genome to daughter cells. In human cells, thousands of origins are licensed through late M and early G1 phase, requiring the loading of the pre-replication complex (pre-RC) onto chromatin. Then, only a subset of licensed origins fires during S phase (Leonard and Me, 2013)(Limas and Cook, 2019). Increasing activity of S-phase related CDKs and DDK (Dbf4 dependent kinase) ensures the activation of origins by the transition from the pre-RC to the pre-initiation complex (pre-IC). Indeed, DDK, a complex of Cdc7 with Dbf4 catalytic subunit, is essential for the initiation of DNA replication (Jiang *et al.*, 1999) (Im *et al.*, 2009). In collaboration with S-phase CDK, DDK recruit helicase activators Cdc45 (Cell division cycle 45) and GINS (Go-Ichi-Ni-San) on chromatin leading to the formation of the active replicative helicase CMG (Cdc45-Mcm-GINS) complex (Tanaka and Araki, 2013). Defects in origins efficiency could induce replicative stress and DNA damage and threaten the accuracy and the completion of DNA replication, which may lead to genomic instability (Ozeri-Galai *et al.*, 2011)(Bonte *et al.*, 2008).

In this study, we focused on two pRb deficient cancer cell lines MDA-MB-468 and NCI-H295R which are derived from either breast cancer or adrenocortical carcinoma, respectively. We demonstrate novel actions of palbociclib impairing the initiation of DNA replication.

Surprisingly, we show that a high dose of palbociclib induces apoptosis in the pRb deficient cell lines associated with the impairment of DNA synthesis during the S-phase of the cell cycle. By using different molecular approaches, we precisely decipher how and at which level palbociclib perturbs DNA replication and the stability of the genome in a pRb negative context. Thus, this study brings palbociclib into focus as a potential treatment targeting replicative stress for patients suffering from pRb deficient cancers.

## Materials and methods

*Cell cultures*

The NCI-H295R (ATCC® CRL-2128TM) cell line from ATCC was cultured in Dulbecco's Modified Eagle Medium (DMEM) / Nutrient mixture F-12 Ham (1 :1) supplemented with GlutaMAX -I (Thermo Fisher Scientific, 31331-028), 2.5% Nu-SerumTM (Corning), 1:100 Insulin-Transferrin-Selenium Premix (Corning, 354350), 100 U/mL penicillin and 100 µg/mL streptomycin (Life Technologies, 15140122). They were seeded at a density of 50,000 cells/cm$^2$ for all experiments.

MDA-MB-468 cell line was cultured in Dulbecco's Modified Eagles Medium (DMEM) with 4.5 g/L D-glucose, L-glutamine and pyruvate (Thermo Fisher Scientific, 41966-029) supplemented with 10% Fetal Bovine Serum, 100 U/mL penicillin and 100 µg/mL streptomycin (Thermo Fisher Scientific, 15140122). They are plated at a density of 20,000 cells/cm$^2$ for all experiments.

Cells were cultured in a humidified incubator with 5% $CO_2$. 24 hours after plating, cells were treated with palbociclib, ribociclib or Dimethyl sulfoxide (DMSO) during 96 hours or 48 hours for NCI-H295R and MDA-MB-468 cell lines, respectively. Palbociclib (PD-0332991, A8316) and Ribociclib (LEE-011, A8641), were purchased from CliniSciences. Palbociclib and Ribociclib 2mM stock solutions were prepared in DMSO.

*Analysis of cellular viability*

After treatment, viability was measured using the CellTiter-Glo® Luminescent Cell Viability kit (Promega), following the manufacturer's instructions. Luminescence was measured with a

SpectraMax i3 Multi-Mode Microplate Detection Platform (Molecular Devices, Sunnyvale, CA, USA). Assays were performed in duplicates, in three independent experiments.

*Apoptosis analysis*

Apoptosis was measured using the Caspase-Glo 3/7 Assay system (#G8090, Promega) as recommended by the manufacturer. Luminescence was measured with a SpectraMax i3 Multi-Mode Microplate Detection Platform (Molecular Devices, Sunnyvale, CA, USA). Assays were performed in duplicates, in two independent experiments.

*Cell cycle analyses by flow cytometry*

Cells were incubated with 10µM EdU (5-ethynyl-2'-deoxyuridine) in culture media for 90 minutes before the end of the drug treatment. Click-it reactions were performed using the Click-iT Plus EdU Alexa Fluor 647 Flow CytometryKit (Invitrogen, C10419) according to the manufacturer's recommendations. The cells were then counterstained with propidium iodide (Invitrogen, P3566) and treated with RNase A (Roche #10109169001) for 30 min. The cell cycle profile was generated using a CyAn ADP 9C analyser (Beckman-Coulter). The analysis was performed with the Kaluza software. Cell cycle was studied on technical duplicates, in more than three independent experiments.

*Total protein extraction*

Total protein extraction was performed with the same number of cells for each condition. The pellets were incubated in Blue Loading Buffer (NEB, B7703S) with 0.1 unit/mL Benzonase (Merck, 70664-3) for 1hour at room temperature. The extracted proteins are denatured at 95°C during 5 minutes.

*Western blot*

Proteins were separated on NuPAGE 4- 12% Bis-Tris gels (Invitrogen, NP0341BOX) and transferred onto nitrocellulose membranes (Invitrogen, IB301031). Primary antibodies were diluted at an adequate concentration in Tris-buffered saline solution with 0.05% TWEEN® 20. Secondary antibodies were used as recommended in the manufacturer’s instructions. Relative quantifications were performed on three different western blot experiments.

Table1. Primary antibodies used in this study.

| *Primary Antibody* | *Concentration* | *Reference* | *Manufacturer* |
|---|---|---|---|
| Mouse-anti-Chk1 | 1/1000 | #2360 | Cell signaling |
| Rabbit-anti-Chk1 pS345 | 1/500 | #2348 | Cell signaling |
| Rabbit-anti-γH2AX | 1/1000 | #9718 | Cell signaling |
| Mouse-anti-αTubulin | 1/2000 | T9026 | Sigma |
| Rabbit-anti-Orc1 | 1/500 | Ab88530 | Abcam |
| Rabbit-anti-Cdt1 | 1/250 | D10F11 | Cell signaling |
| Rabbit-anti-Mcm2 | 1/1000 | 4461 | Abcam |
| Rabbit-anti-Mcm2 phosphoS53 | 1/2000 | Ab109133 | Abcam |
| Mouse-anti-Cdc7 | 1/1000 | Sc 56275 | Santa Cruz |
| Rabbit-anti-Dbf4 | 1/20000 | Ab 124707 | Abcam |
| Mouse-anti-Cdc45 | 1/1000 | Sc 55569 | Santa Cruz |
| Rabbit-anti-Histone H4 | 1/2000 | 07-108 | Millipore |

*Analysis of the replication timing program*

Cells were incubated with 50µM BrdU during 2 hours before the ending point of treatments, harvested and fixed with cold 70% ethanol. Fixed cells were treated with RNaseA (0,5mg/ml) and propidium iodide (50µg/ml) during 30 minutes at room temperature before cell sorting. 100,000 cells were sorted in two fractions using INFLUX 500 (Cytopeia by BD Bioscience). Cells were incubated in lysis buffer (50mM Tris pH=8; 10mM EDTA, 300mM NaCl) and proteinase K (Thermo-Scientific #EO-0491) (0,2 mg/ml) during 2 hours at 65°C. DNA is extracted using phenol-chloroform and precipitated with ethanol and sodium acetate (3M, pH=5.5; Invitrogen #AM9740). After sonication, DNA is denatured at 95°C during 5 minutes and kept on ice for 10 minutes. Immunoprecipitation of nascent DNA was performed as described in our previous study (Hadjadj *et al.*, 2020). Briefly, nascent DNA was immunoprecipitated using the IP-STAR apparatus (Diagenode) with BrdU antibody (10µg, Anti-BrdU Pure, BD Bioscience, #347580). Immunoprecipitated nascent DNA was purified and precipitated as mentioned above.

DNA is amplified using Seq-plex as mentioned by the manufacturer (Sigma, #SEQXE). Each fraction of sorted cells is labeled either Cy3 or Cy5 ULS molecules, respectively (KREATECH #EA-005) and as recommended by the manufacturer. The hybridization was performed according to the manufacturer instructions on 4× 180K human microarrays (SurePrint G3 Human CGH Microarray Kit, 4x180K, AGILENT Technologies, genome reference Hg18, G4449A) that cover the whole genome with one probe every 13 kb. Microarrays were scanned with an Agilent's High-resolution C scanner using a resolution of 3µm and the autofocus option. Software "START-R" was used for analysis of replication timing (Hadjadj *et al.*, 2020). Two independent experiments are performed for each condition.

*Molecular combing and immunodetection*

Cells were pulse-labeled with 50µM IdU and 50µM CldU during 30min consecutively. Then, cells were embedded in agarose plugs (1% low melting agarose, 2-Hydroxyethylagarose, A4018-Sigma) and treated with Proteinase K (1mg/mL, ROCHE, 3115879001) for 48 hours. After melting and digestion with β-Agarase (6.25 units/mL, New England Biolabs, M0392L), DNA fibers were stretched at a rate of 300µm/s on silanized coverslips. DNA was denatured with 1N NaOH solution and immunodetections were performed with the following antibodies: (1) mouse anti-bromodeoxyuridine (BrdU) (BD Biosciences, #347583) and rat anti-BrdU (Abcam, ab6326), (2) A488-conjugated goat anti-mouse (Invitrogen, A11029) and A555-conjugated goat anti-rat (Abcam, A21434), (3) mouse anti-single-stranded DNA (Millipore, MAB 3034), (4) cy5.5-conjugated goat anti-mouse (Abcam, ab6947) and (5) cy5.5-conjugated donkey anti-goat (Abcam, ab6951).

Epifluorescence microscope (Axio Imager Z2; Carl Zeiss) equipped with a 63 × or 40 x objective lens (PL APO, NA 1.4 Oil DIC M27) and a motorized stage (M- 689 XY Microscope Stage with PILine Motor; Physik Instrumente), and connected to a charge-coupled device camera (Cool-SNAP HQ2; Roper Scientific) was used. MetaMorph software (Roper Scientific) allowed image acquisition and the study of replication dynamics. Statistical analysis was performed as described in the article (Técher *et al.*, 2017).

*Fractionation of Chromatin-bound proteins*

The same number of cells was used for each condition to extract chromatin bound proteins. The extraction was performed by following steps. Harvested cells were lysed in Buffer A (10mM

Hepes pH 7.9, 10 mM KCl, 1.5 mM MgCl2, 0.34 M sucrose, 10% glycerol, 1 mM DTT, 10 mM NaF, 1X complete EDTA-free Protease Inhibitor Cocktail (Sigma Aldrich) and 0,1% Triton X-100) during 5 minutes on ice and centrifuged at 1300g for 4 minutes. The pellet was washed in buffer B (3 mM EDTA, 0.2 mM EGTA, 1mM DTT, 10 mM NaF, 1X Protease inhibitors) for 10 minutes on ice and centrifuged at 1700g for 4 minutes. The pellet was resuspended in buffer C (3mM EDTA, 0,2 mM EGTA) and centrifuged at 10000g for 1 minute. The pellet, corresponding to the chromatin fraction, was incubated in 1X Blue Loading Buffer (NEB, B7703S), 5 mM MgCl2 and 0.1 unit/mL Benzonase (Merck, 70664-3) for 30 minutes at room temperature. The extracted proteins are then denatured at 95°C during 5 minutes.

*RT-qPCR*

RNAs were extracted with the Nucleospin® RNA extraction kit (Macherey-Nagel), following the manufacturer's instructions. Reverse transcription of RNA was performed with the Transcriptase inverse SuperScript II (Invitrogen, 18064022), following the manufacturer's instructions. Quantitative PCRs were performed with 1 µL of 1/10 diluted first strands of cDNA in a total volume of 15 µL of 1X KAPA SYBR FAST qPCR Master Mix (Kapa Biosystem, KK4610), containing 10nM of each PCR primer. Reactions were performed in 20 µL LightCycler capillaries (Roche). PCR amplifications were performed with a LightCycler 1.5 thermocycler and analyzed with the LightCycler Software 3.5 (Roche). Assays were performed in technical duplicates on RNAs extracted from two or three independent experiments.

Table2. Primers' list

| Genes | Sequence (3'->5') |
|---|---|
| Tbp | Forward:cacgaaccacggcactgatt<br>Reverse:ttttcttgctgccagtctggac |
| Cdc7 | Forward:caaagtgccccaatcaaact<br>Reverse:tgggccaaagcagttaaatc |
| Dbf4 | Forward:aaaccacttcacctcatccc<br>Reverse:tttactccccatgacaaggc |
| Cdc45 | Forward:gcaaacacctgctcaagtcc<br>Reverse:tcccaaaaaagttcttcctgtc |
| Orc1 | Forward:gccaaagaagagtctcaagcc<br>Reverse:acagcagaaacatgcagcc |
| Mcm2 | Forward:cgtatccgaatccaggagag<br>Reverse:gtgttgagggagccatcatag |

## Results

*Cell viability, apoptosis and cell cycle analysis of pRb deficient cell lines.*

To study the effect of CDK4/6 inhibitors on cellular viability, two pRb deficient cell lines, namely MDA-MB-468 and NCI-H295R, were treated with increasing doses of either palbociclib or ribociclib. Palbociclib reduced the cellular viability in a dose dependent manner while ribociclib had minimal effect on viability in both cell lines, indicating that palbociclib has cytotoxic effects in a pRb negative context **(Fig1.A and B)**. In order to explore the nature of the impact on cellular viability, we first performed apoptosis analysis based on the activity of caspase3/7. MDA-MB-468 cells treated with 15 or 20µM of palbociclib showed a high activity of caspase3/7 whereas ribociclib had modest effect below 20µM **(Fig1.C)**. NCI-H295R cells went to apoptosis at 15µM of palbociclib and the caspase activity could not be observed at 20µM due to massive cell death **(Fig1.D)**. This finding suggests that palbociclib might have other effects in cells at relatively high doses, that do not require the presence of pRb. For all further experiments, we treated cells with 10µM of palbociclib or ribociclib since at this concentration palbociclib reduced significantly cell viability without inducing cell death by apoptosis. Of note, cells were treated for approximately one doubling time (48h for MDA-MB-468 cells and 96h for NCI-H295R)

Then, the effects of these drugs on the cell cycle were investigated. Treatment of palbociclib modestly affected the distribution of the cell cycle, with only a slight increase of the proportion of cells in G2/M phase in MDA-MB-468 and NCI-H295R cells **(Figure supplementary 1.A and B)**. These findings suggest that there may be an extension of the G2 with no cell cycle arrest in both cell lines.

*Palbociclib treatment impairs DNA synthesis during the S-phase of pRb deficient cells*

We further analyzed more precisely the cell cycle through the assay of EdU incorporation to characterize how cells behave during the S phase of the cell cycle. This analysis allowed us to visualize the amount of newly synthesized DNA for every single cell **(Fig2.A and B)**. Comparing medians of EdU incorporation in both cell lines, we noticed that MDA-MB-468 cells incorporate more EdU than NCI-H295R cells consistently with the length of their respective doubling time **(Supplementary Figure 1.C)**. Strikingly, cells treated with palbociclib showed a lower intensity of EdU compared to mock treatment whereas ribociclib

had minor effect on EdU incorporation **(Fig2.C)**. Palbociclib significantly reduced by 40% or 50% the level of EdU incorporation in MDA-MB-468 cells and NCI-H295R cells, respectively. Furthermore, the decrease of EdU incorporation in NCI-H295R cells treated with palbociclib was similar to the level in cells treated with 50µM or 100µM of hydroxyurea (HU) which is considered as a mild replicative stress **(Supplementary Figure 2.A and B)**. These results suggest that palbociclib efficiently impairs the capacity of cells to synthesize DNA during S phase, thus implying that palbociclib may interfere with DNA replication.

Since we observed that palbociclib affects DNA synthesis, we investigated the presence of replicative stress and DNA damage in these cells. The activation of S-phase checkpoint was measured by the status of checkpoint Serine/threonine kinase 1 (Chk1) phosphorylation on Serine 345. We observed with the palbociclib treatment a two-fold increase in the level of phosphorylated Chk1 protein (2.41-fold in MDA-MB-468 and by 2.13-fold in NCI-H295R cells) while the total amount of Chk1 remained constant in both cell lines **(Fig 2.D and E)**. However, ribociclib showed moderate effects on the phosphorylation status of Chk1 in MDA-MB-468 cells and no effects in NCI-H295R cells. The phosphorylation level of Chk1 was similar to mild-replicative stress, according to the treatment with 50µM HU.

Then, we checked the induction level of DNA damage measured by γH2AX levels. We demonstrated that palbociclib triggered the accumulation of γH2AX protein whereas ribociclib had minimal effect in both cell lines. Massive DNA damages were observed in cells treated with 1mM of HU in NCI-H295R cell line. We concluded that the treatment with palbociclib drove cells to accumulate more double strand breaks in DNA. This could partially explain the modest increase of the number of cells in G2-phase that was previously observed (Figure supplementary 1.A and B). Cells may require a longer duration of the G2-phase to manage a complete DNA repair. Hence, cells treated with palbociclib exhibit the activation of the S-phase checkpoint and a sign of genomic instability along with interferences in DNA synthesis.

*Analysis of the temporal program of DNA replication of pRb deficient cells.*

In order to determine how palbociclib affects the DNA replication process at a genome wide scale, we performed the analysis of the temporal program of DNA replication as previously described (Hadjadj *et al*., 2020). Cells organize DNA replication in space and time through the S-phase. This spatial and temporal program of replication orchestrates faithful duplication of

the genetic materials during the S-phase of cell cycle. Analysis of the temporal program allows to characterize the effects of replicative stress and to visualize regions of the genome that are altered in terms of replication timing. To perform this technique, cells are labeled with a short pulse of BrdU and separated into two fractions corresponding to early and late S-phase. The ratio between these two fractions is calculated and visualized for the entire genome. Comparing the profile of control cells and cells treated with palbociclib allowed us to observe that palbociclib induced perturbations of the replication timing in several part of the genome **(Fig3.A and C)**, while the ribociclib treatment induced minimal effect **(Fig3.B and D)**. **(Supplementary Figure 3)**.

In the MDA-MB-468 cell line, 16.82% of the genome showed an altered replication timing program after the palbociclib treatment when compared to the mock-treated control cells **(Fig3.E)**. Among the regions harboring an altered replication timing, 71.3 % displayed a delayed replication timing whereas 28.7% showed an advanced one **(Fig3.F)**. In the NCI-H295R cell line, only 4.12% of the replication timing program is altered after the same treatment with 77.1% and 22.9% of delayed and advanced replicating regions, respectively. These results strengthen that palbociclib perturbs the timing of DNA replication at the genome scale. Three hypotheses could explain these results: i) a slowdown of the replication fork rate, ii) an increased presence of obstacles on the genome that prevent the progression of the replicating forks; iii) an impediment in the firing of some replication origins.

*Palbociclib reduces the number of active origins without altering replication fork progression*

To decipher how palbociclib impacts on DNA replication dynamics, we performed DNA fiber analysis to measure the speed of replication forks and the activation of replication origins (Técher *et al.*, 2013). We first examined the fork speed after a treatment with palbociclib in MDA-MB-468 cells. In control cells, the median fork speed was 2.01 kb/min **(Fig4.A and B)** and showed a slight increase (2.16kb/min), after the palbociclib treatment (although not significant, p-value=0.068). NCI-H295R cells presented a relatively low fork speed (1.18kb/min) in control conditions but a statistically significant increase to 1.47kb/min after the treatment (p-value=0.028). Besides, we did not observe any difference in the replication fork asymmetry, indicating that the elongation step is not disrupted in both cell lines **(Supplementary Figure 4)**. Next, we investigated if palbociclib could impair the activation of replication origins by measuring the density of forks. After the treatment with palbociclib, the density of forks was reduced by 35% and 40% in MDA-MB-468 and NCI-H295R cells,

respectively **(Fig4.C).** It has been observed that replicative stress can induce concomitant effects on origin activation and fork speed which both influence each other (Rodriguez-Acebes, Mourón and Méndez, 2018). With regard to our data, reduced origin firing could trigger a slight acceleration of fork speed that compensate this lack of origins. Our results finally showed that palbociclib reduces the number of active origins but does not interfere with replication fork progression, which provides a mechanistic basis for the reduced EdU incorporation observed in S-phase cells by flow cytometry **(Fig. 2A and 2B)**.

*Palbociclib acts on the pre-initiation complex loading onto chromatin.*

In order to better understand the molecular process, we investigated which step of the initiation of DNA replication is affected by the palbociclib treatment. We first looked at the chromatin loading of proteins constituting the Pre-Replication Complex (PreRC) such as Orc1, Cdt1 and Mcm2. In both MDA-MB-468 and NCI-H295R cell lines, the level of those proteins remains constant **(Fig 5.A and C)** in the different experimental conditions. We further checked the phosphorylation level of Mcm2 and the loading on chromatin of Cdc7, Dbf4 and Cdc45 that are elements of the pre-initiation complex (Pre-IC) **(Fig5.B)**. We found that the loaded amount of Cdc7 and Cdc45 and the level of phosphorylation of Mcm2 were decreased in the MDA-MB-468 cells after the palbociclib treatment **(Fig5.D)**. In the NCI-H295R cells as well, the same treatment efficiently decreased the loaded amount of Cdc7, Dbf4 and Cdc45 **(Fig5.E)**. These results indicate that palbociclib does not interfere with the Pre-RC loading but impairs the assembly of the pre-IC onto chromatin, resulting in reduced origins firing.

We further studied whether the decrease of chromatin bound proteins was due to a variation of the total quantity of proteins or to a defect in the pre-IC loading process. We observed that the total amounts of pre-IC proteins Cdc7 and Cdc45 proteins decreased in MDA-MB-468 cells treated with palbociclib **(Fig6.A and B)**, which is consistent with the result obtained with chromatin extracts **(Fig5.D)**. At the same time, less amount of Cdc7, Dbf4 and Cdc45 proteins were detected in palbociclib-treated NCI-H295R cells **(Fig6.A and C)**. Then, we performed RT-qPCR to check whether palbociclib affects the mRNA level of these genes. We detected significantly reduced levels of *Cdc7* and *Cdc45* in MDA-MB-468 cells after 24 hours and of Dbf4 and Cdc45 after 48 hours of treatment **(Fig6.D and E)**. In NCI-H295R cells, we observed that the expression levels of *Cdc7* and *Cdc45* were reduced after both 48 and 96 hours of treatment with palbociclib **(Fig6.F and G)**. By the way, we did not detect any significant

variations in the level of *Orc1* and *Mcm2* in both cell lines after the treatment. Our results suggest that palbociclib regulates the expression level of specific genes particularly involved in the formation of the pre-IC in pRb-deficient cell lines. This work explains how palbociclib impairs DNA synthesis by reducing the number of activated origins without altering the replication fork progression in a pRb negative context. We revealed that the actions are mediated by transcriptional regulation of genes for the pre-IC.

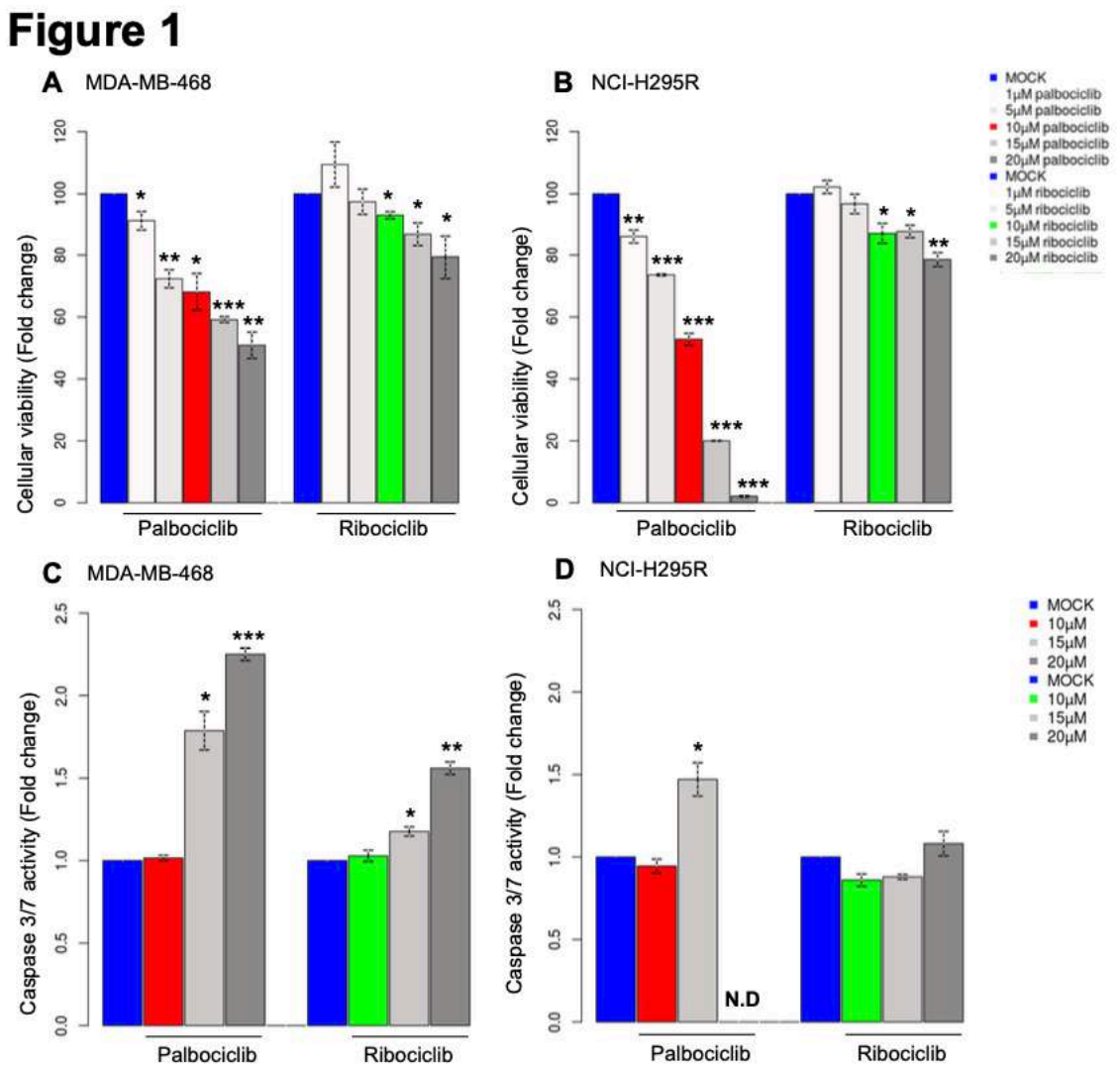


**Figure 1. Analysis of cellular viability, apoptosis in pRb deficient cell lines.**
**A.** The viability of cells is measured after 48 hours of treatment with increasing doses of palbociclib or ribociclib in MDA-MB-468 cells **B**. and in NCI-H295R cells. **C.** Histograms representing the activity of caspase3/7 after treatment with palbociclib or ribociclib in MDA-MB-469 cells **D.** and in NCI-H295R cells. N.D=Non determined. The statistical significance was tested with t-test; *P<0.05, **P<0.01, ***P<0.001.

# Figure 2

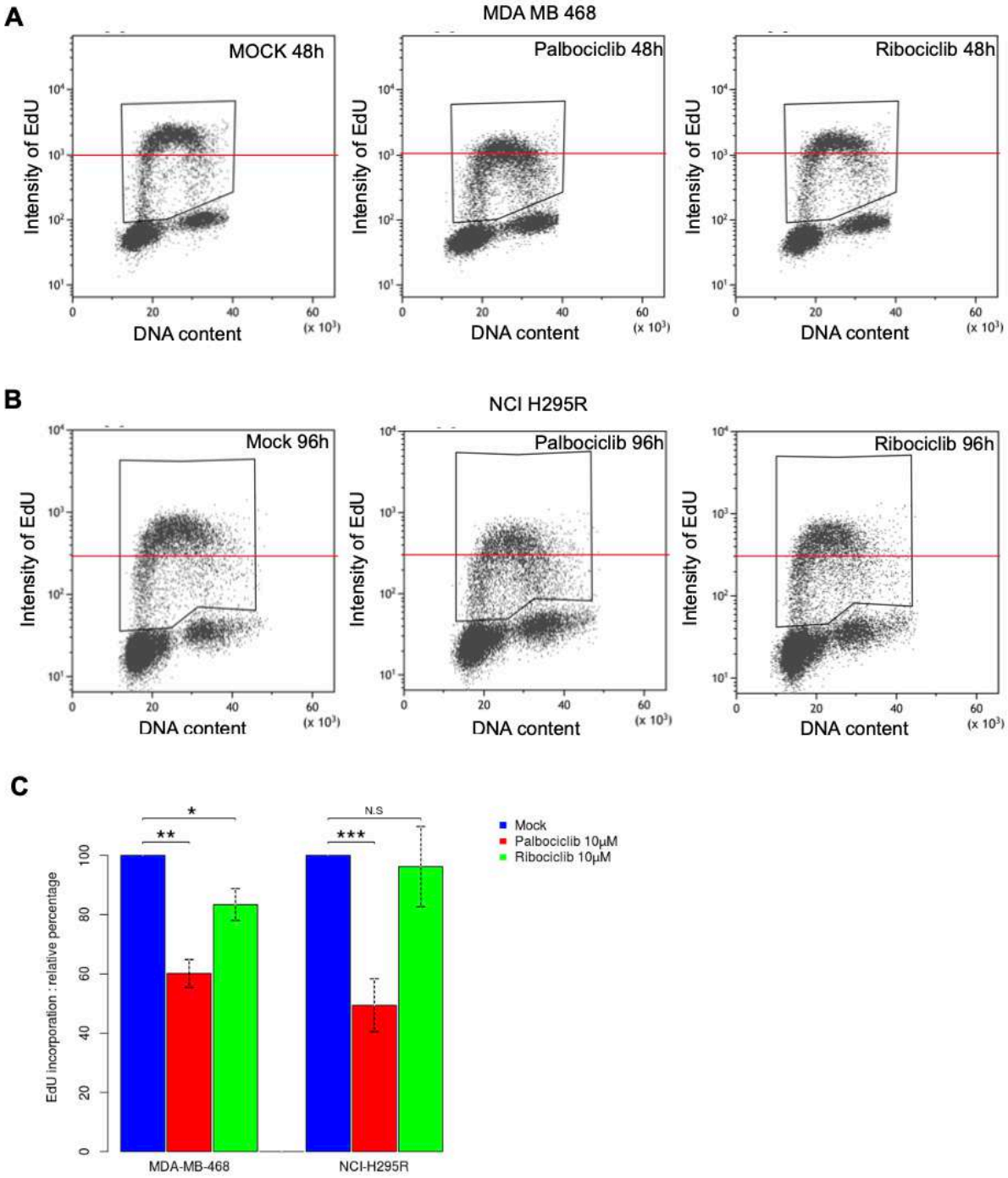
A
MDA MB 468
MOCK 48h
Palbociclib 48h
Ribociclib 48h
Intensity of EdU
DNA content
(x 10³)
B
NCI H295R
Mock 96h
Palbociclib 96h
Ribociclib 96h
C
EdU incorporation : relative percentage
Mock
Palbociclib 10μM
Ribociclib 10μM
MDA-MB-468
NCI-H295R
N.S

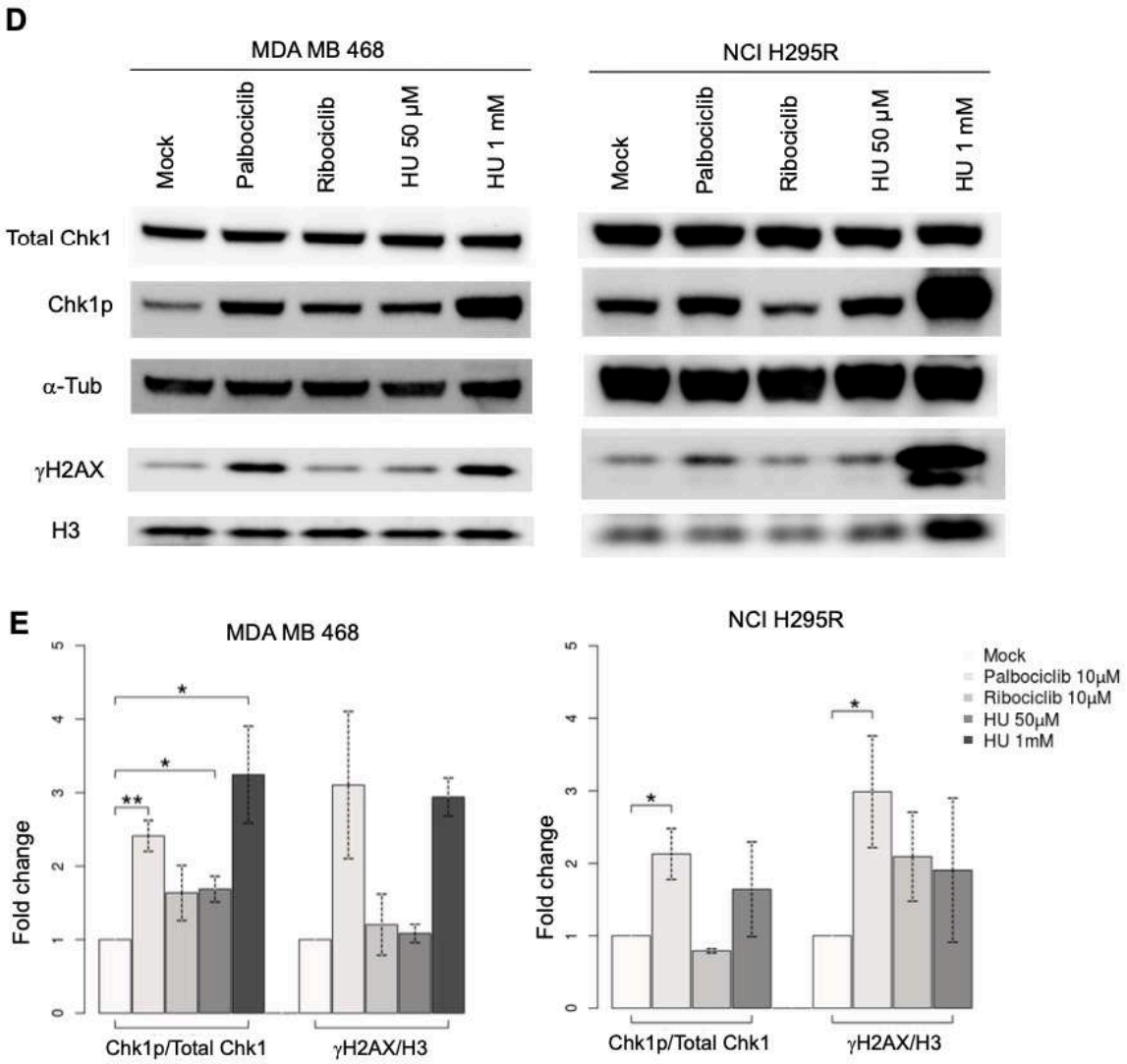


**Figure 2. Effects of palbociclib and ribociclib on DNA synthesis during S-phase.**
**A.** Cell cycle profiles after EdU incorporation and drug treatment in MDA-MB-468 cells **B.** and in NCI-H295R. The red lines represent the same level of incorporated EdU for each condition. **C.** Histogram representing the relative percentage of EdU incorporated in S-phase in MDA-MB-468 and NCI-H295R cell lines. (The statistical significance was tested with t-test; *P<0.05, **P<0.01, ***P<0.001). **D.** Total protein levels of Chk1, Chk1 phosphorylated on Serine 345 residues and γH2AX were measured by Western blot after 48 hours or 96 hours of the treatments in MDA-MB-468 and NCI-H295R cells, respectively. α-Tub and histone H3 were used as loading controls. **E.** Histograms representing the relative quantity of each protein normalized to the controls. (The statistical significance was tested with t-test; *P<0.05, **P<0.01, ***P<0.001). Two or more independent experiments were performed for each analysis (C and E)

# Figure 3

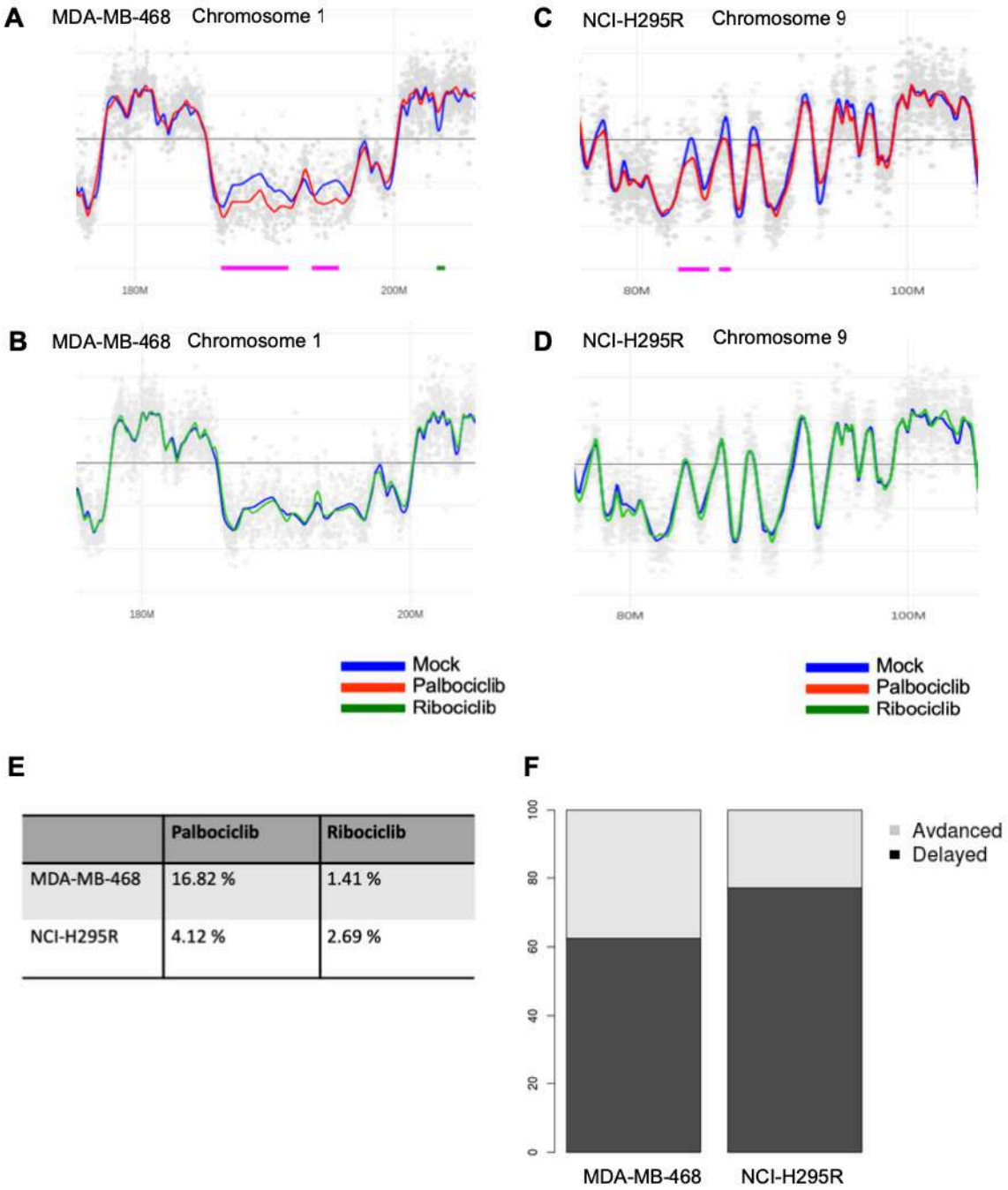


| | Palbociclib | Ribociclib |
|---|---|---|
| MDA-MB-468 | 16.82 % | 1.41 % |
| NCI-H295R | 4.12 % | 2.69 % |

**Figure 3. Analysis of the temporal program of DNA replication in MDA-MB-468 and NCI-H295R cells treated with palbociclib.**

**A and B.** Part of chromosome 1 replication timing profiles in MDA-MB-468 cells. The blue line represents control cells treated with mock, the red one for cells treated with palbociclib and the green one with ribociclib. Chromosome coordinates are indicated below each profile. **C and D.** Profile of replication timing for a part of chromosome 9 in NCI-H295R cells. **E.** Percentages of the whole genome altered after the treatment with either palbociclib or ribociclib. **F.** Stacked histograms representing the proportion of advanced or delayed replicating regions considering their length after the palbociclib treatment.

# Figure 4

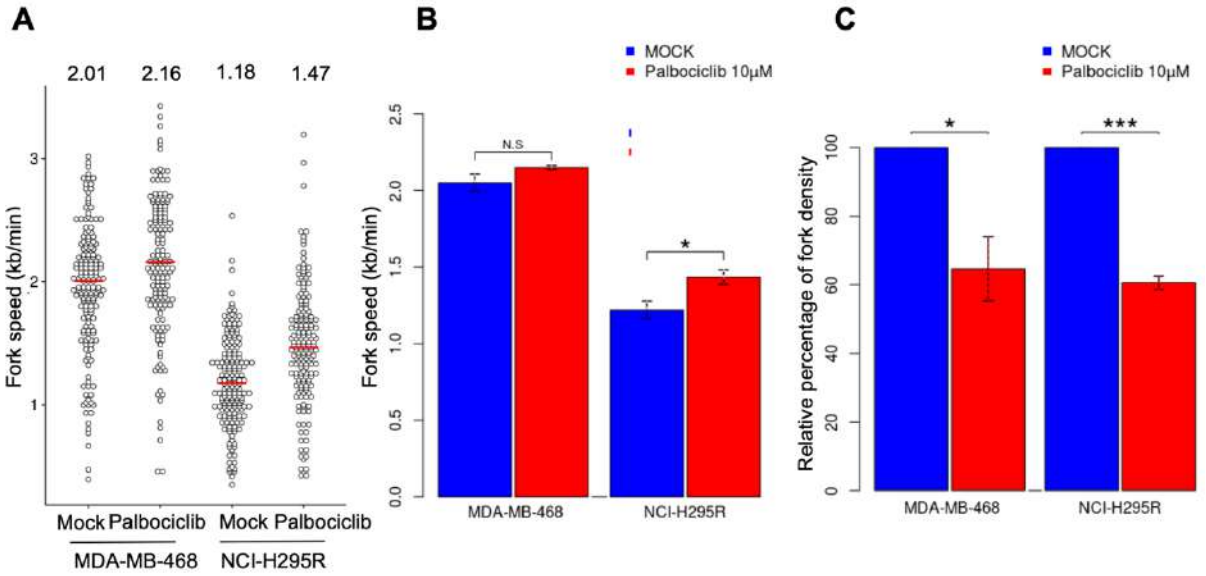


**Figure 4. Analysis of fork speed, fork asymmetry and fork density in MDA-MB-468 and NCI-H295R cells treated with palbociclib.**

**A.** Dotplot indicating the fork speed of both cell lines with or without palbociclib treatment. The red lines show the median for each condition. Minimum 150 forks were scored for each condition. **B.** Histogram representing the fork speed mean in kb/min for each cell line. The statistical significance was tested with t-test; *P<0.05, **P<0.01, ***P<0.001) **C.** Histogram representing relative percentage of fork density in cells treated with palbociclib compared to control cells treated with mock. The density of forks is calculated as the number of forks divided by the sum of the total length of the fibers. A minimum of 250kb of fibers length is counted for each condition. The statistical significance was tested as aforementioned. Two independent experiments were performed for each condition.

# Figure 5

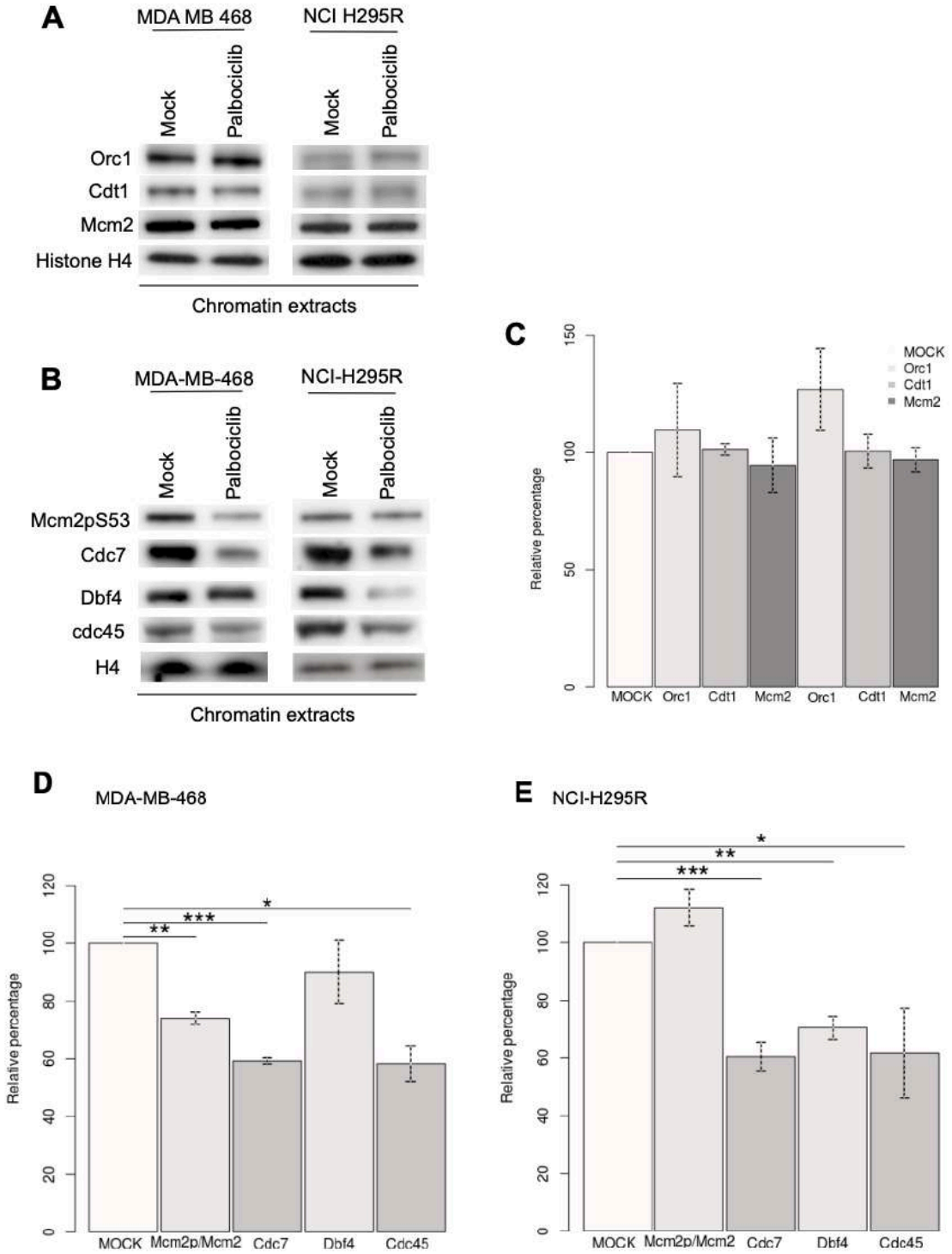


**Figure 5. Chromatin loading of pre-ICs proteins in MDA-MB-468 and NCI-H295R cells treated with palbociclib.**

**A.** The fraction of proteins of the pre-RC bound to chromatin was analyzed by Western blotting. The same number of cells are used for fractionation for each condition. Histone H4 is a loading control. **B.** Same experiment as in A. for the proteins of the pre-IC. **C.** Histogram representing the relative level of

proteins loaded on chromatin of the pre-RC. **D**. Histogram representing the relative level of proteins loaded on chromatin of the pre-IC in MDA-MB-468 cells. **E**. and in NCI-H295R cells Two independent experiments were performed for each condition. (statistical significance; *P<0.05, **P<0.01, ***P<0.001).

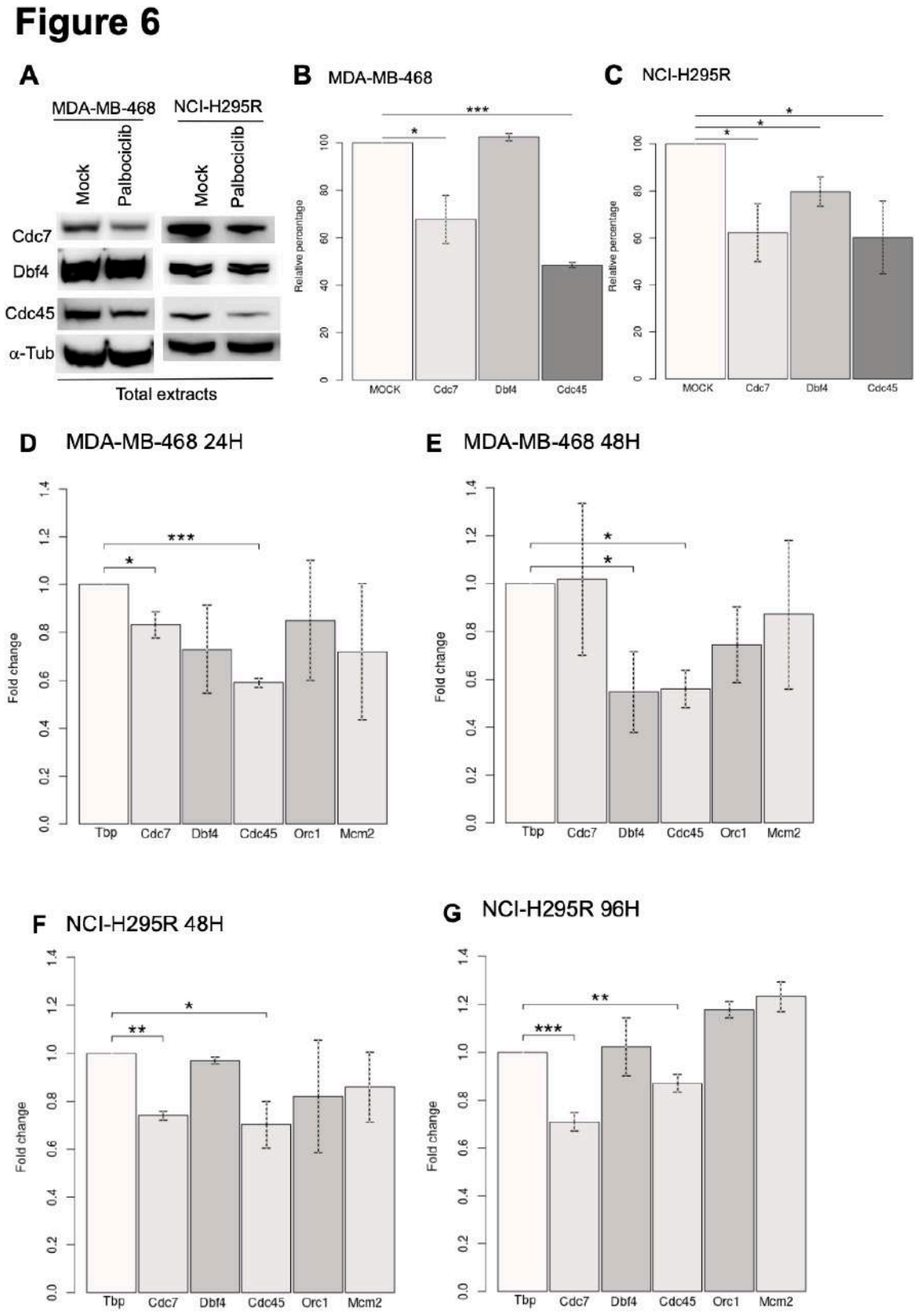

**Figure 6. Analysis of the total amount of proteins and expression levels of messenger RNA.**

**A.** The total level of pre-initiation complex proteins was analyzed by Western blotting. The same number of cells was loaded for each condition. α-Tubulin is a loading control. **B.** Histograms representing the relative total amount of proteins in MDA-MB-468 cells. **C.** in NCI-H295R cells. **D.** Histograms representing fold change of gene expression level for MDA-MB-468 cells treated with palbociclib for 24 hours. **E.** for 48h. **F.** and for NCI-H295R cells treated with palbociclib for 48 hours **G.** and for 96 hours. The level of the Tatabox binding protein (Tbp) was considered as a control and assess at 1, from which the other genes were normalized.

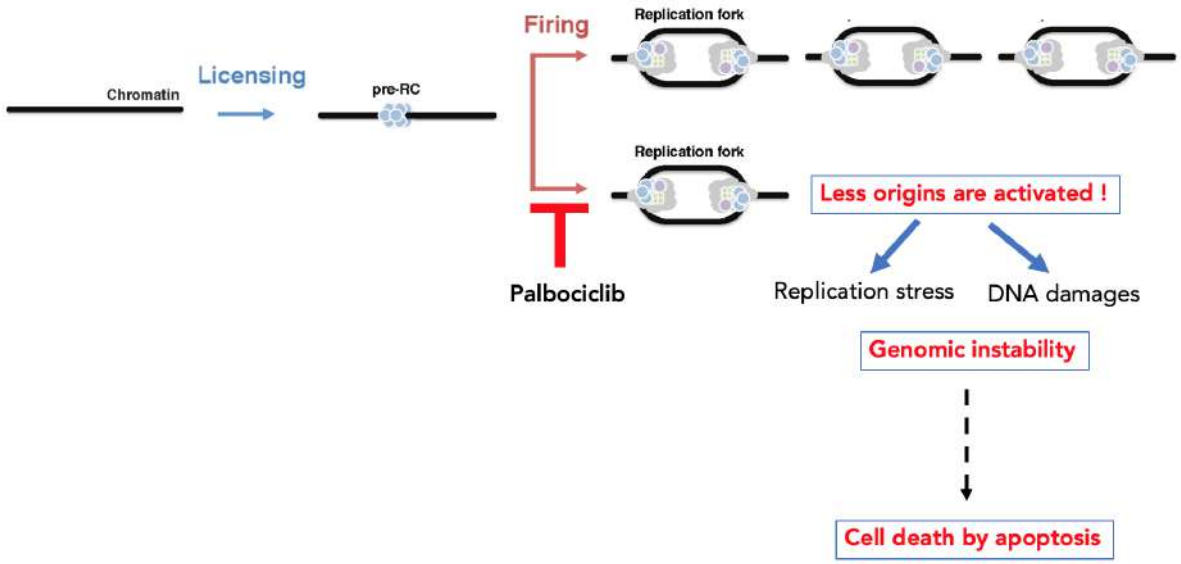


**Figure 7. A model explaining the effects of palbociclib on origin firing and its consequences in pRb deficient cells**.

## Discussion

Our findings highlight the hidden effects of palbociclib using two pRb deficient cancer cell lines. Since pRb is the major phosphorylation substrate of CDK4/6, pRb loss is largely considered as a biomarker for the resistance to CDK4/6 inhibitors (Chen *et al.*, 2019)(Spring *et al.*, 2019). In agreement with other studies, we did not detect any significant impacts of palbociclib or ribociclib around 1 μM that is considered as specific inhibitory doses **(Fig1)**(Bollard *et al.*, 2016)(Dean *et al.*, 2010). Nonetheless, palbociclib significantly reduced the cell viability at 10μM, indicating that this drug has cytotoxic effects in a pRb negative context. In this study, palbociclib is used at a relatively high concentration of 10 μM. Since the effects on cellular viability are barely observed with this same concentration of ribociclib **(Fig1)**, we then suppose the actions of palbociclib are mediated by their off-targets. Recent multi-omic studies have demonstrated the different specificity of three inhibitors (ribociclib, palbociclib and abemaciclib) focusing on a large spectrum of targets for abemaciclib and also revealed that palbociclib targets other kinases than CDK4 and CDK6 at high doses (P. Chen *et al.*, 2016)(Hsieh *et al.*, 2017). Indeed, a group demonstrated that in live cells palbociclib shows more than 60% of occupancy to CDK2, a pivotal kinase involved in the progression of S-phase (Wells *et al.*, 2020). Another work demonstrated that *in vitro* palbociclib also inhibits CDK2/CyclinE complex with an IC50 about 10μM (Hafner *et al.*, 2019).

In this study, we concentrated on elucidating how palbociclib impairs DNA replication, a main process in the S-phase of the cell cycle. To our knowledge, those effects in S-phase have not been described yet in pRb proficient cells. As CDK4/6 inhibitors efficiently induce cell cycle arrest in the G1-phase in pRb proficient cells, it simply could not be observed how cells behave in S-phase. Thus, deficiency of pRb is associated with common features that are absent in pRb proficient cells. Indeed, pRb acts not exclusively in the E2F pathway but also in chromatin remodeling by interacting with histone deacetylases (HDACs) and the ATP-dependent SWI/SNF complex (Dick and Rubin, 2013)(Harbour and Dean, 2000), implying that pRb deficient cells exhibit a higher intrinsic instability of the genome (van Deursen, 2007)(Van Harn *et al.*, 2010). Furthermore, mutations in TP53 are often coupled with pRb losses (Xing *et al.*, 1999). Two cell lines that we have studied here harbor mutation in the *Tp53* gene. On one hand, MDA-MB-468 cells possess only one copy of the *TP53* gene with a missense mutation (R273C) (Rasti and Azimi, 2015). This mutated TP53 is not able to bind to RAD51 and contributes to a

genomic instability of these cells. On the other hand, NCI-H295R cells have homozygous deletion in exons 8 and 9 in the *Tp53* gene, inducing a nonfunctional form of this protein (Sampaoli *et al.*, 2012). Mutations in *TP53* induce defects in the DNA repair response, which contributes to cancer cell survival despite the intrinsic instability of the genome (Mantovani, Collavin and Del Sal, 2019).

Our study demonstrated the unexpected observation of a decreased level in DNA synthesis after a treatment with palbociclib in pRb-deficient cell lines **(Fig2)**. The treatment in pRb deficient cells does trigger neither any cell cycle arrest nor any variation in the proportion of S-phase cells **(Fig supp1.A et B)**. But, we noticed reduced DNA replication efficiency during the S-phase of the cell cycle **(Fig2)**. We demonstrated the effects of palbociclib on DNA replication at the whole genome scale by studying the temporal program of DNA replication. We observed that the palbociclib disturbs the DNA replication timing, inducing significant delays in certain regions **(Fig3)**. To decipher the mechanism of action of palbociclib on the dynamics of DNA replication, we have proposed 3 hypotheses. The first possibility is that palbociclib may disturb the elongation step by slowing down replicative forks and even leading to fork collapse. Secondly, palbociclib may impair the initiation of replication, leading mostly to delayed replicating regions **(Fig3)**. Third, palbociclib may also impact in both initiation and elongation steps. In order to respond to these questions, we performed replication dynamic studies by the DNA fiber assay **(Fig4)**. Our findings allowed us to eliminate the first and third hypothesis that palbociclib affects the elongation of replication since no evidence has been found for fork slowing or neither fork collapse. However, palbociclib reduced the density of replicative forks by 35-40%, implying a defect in the initiation of origins **(Fig4)**.

Finally, to decipher the molecular mechanism of palbociclib in DNA replication, we studied pre-RC and pre-IC in cells treated with palbociclib. We detected that both total amounts of proteins constituting pre-IC, such as Cdc7, Dbf4 and Cdc45 and their loading level on chromatin are reduced after treatment with palbociclib **(Figs5 and 6)**. We also evidenced by quantitative PCR that palbociclib down regulates the expression of genes being part of the pre-IC such as Cdc7, Dbf4 and Cdc45, resulting in less amount of proteins loaded on chromatin. This result shows how palbociclib impacts on origin firing by inducing defects in the pre-IC **(Fig5 and 6)**. It is well studied that a defect of origin firing could provoke an incomplete replication of the genome referred to as under replication and generate genomic instability (Ozeri-Galai *et al.*, 2011) (Petropoulos *et al.*, 2019). Indeed, the proteins in pre-ICs are limiting

factors involved in the initiation of replication and their deregulation is tightly linked to the instability of the genome and cancer development. For instance, deregulation of Cdc7 and Dbf4 has been observed in several cancers. The depletion of Cdc7 with RNAi reduced the activation of origins in the initiation step, inducing replicative stress in the cells (Rodriguez-Acebes *et al.*, 2010) (Montagnoli *et al.*, 2004). Based on these strong evidences, Cdc7 inhibitors have been proposed as a cancer treatment (Montagnoli *et al.*, 2008)(Rainey *et al.*, 2017).

Thus, we propose a model for the actions of palbociclib in inducing replication stress and DNA damages in a pRb negative context **(Fig7)**. Since the loss of pRb is associated with a higher vulnerability to replicative stress, palbociclib may potentially be used in cancer treatment with the aim of exacerbating the instability of the genome and of cancer cells becoming more vulnerable to replicative stress. From this point of view, we can consider that palbociclib may be used for pRb deficient patients combined with other therapeutic molecules that will target the replicative response pathway.

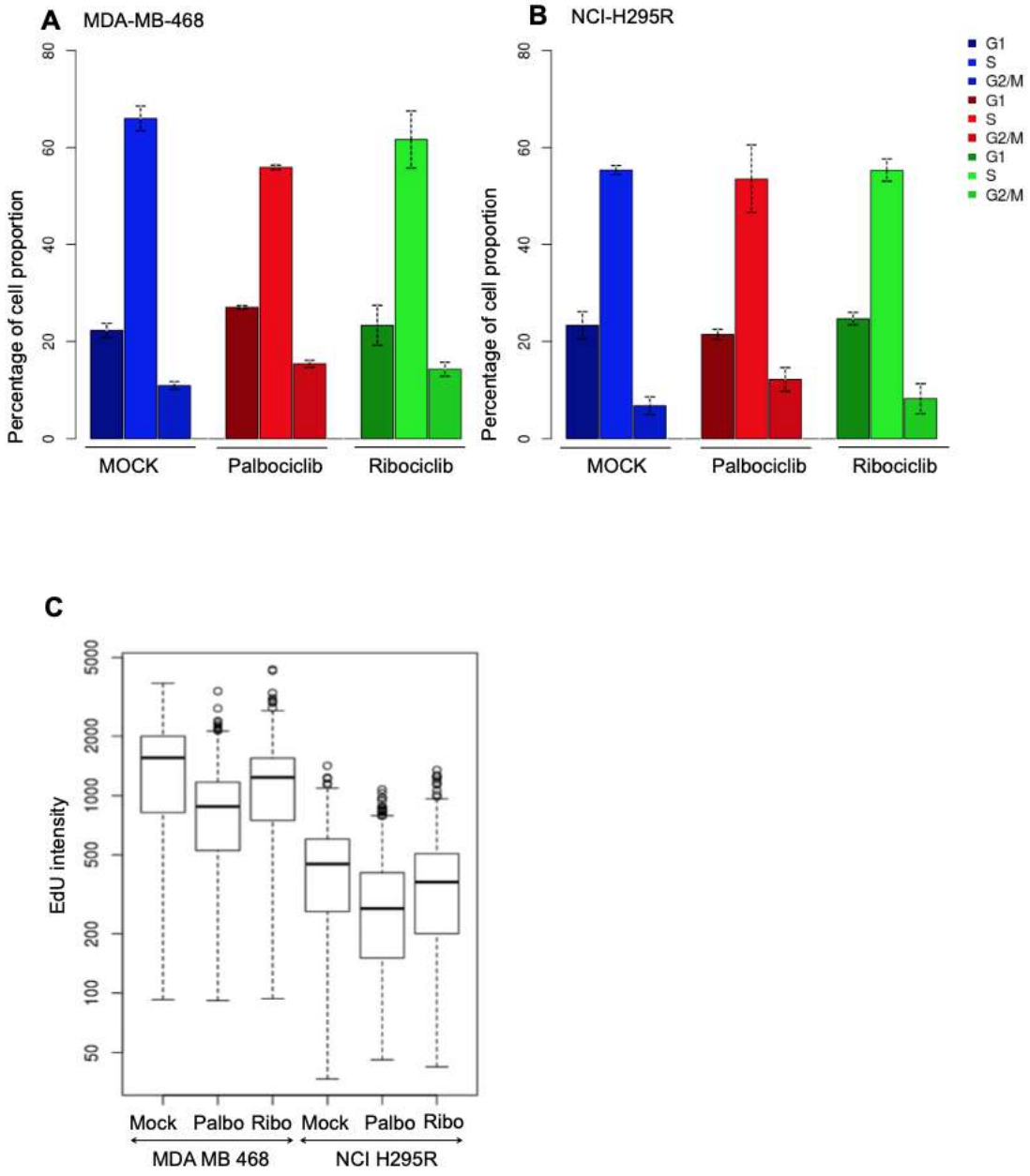


**Figure supplementary 1.**
**A**. The proportion of each phase of the cell cycle is represented by percentage in MDA-MB-468 cells. **B**. and in NCI-H295R cells **C.** Boxplot representing the level of EdU incorporation in S phase in both cell lines. (Palbo=palbociclib treatment, Ribo=ribociclib treatment)

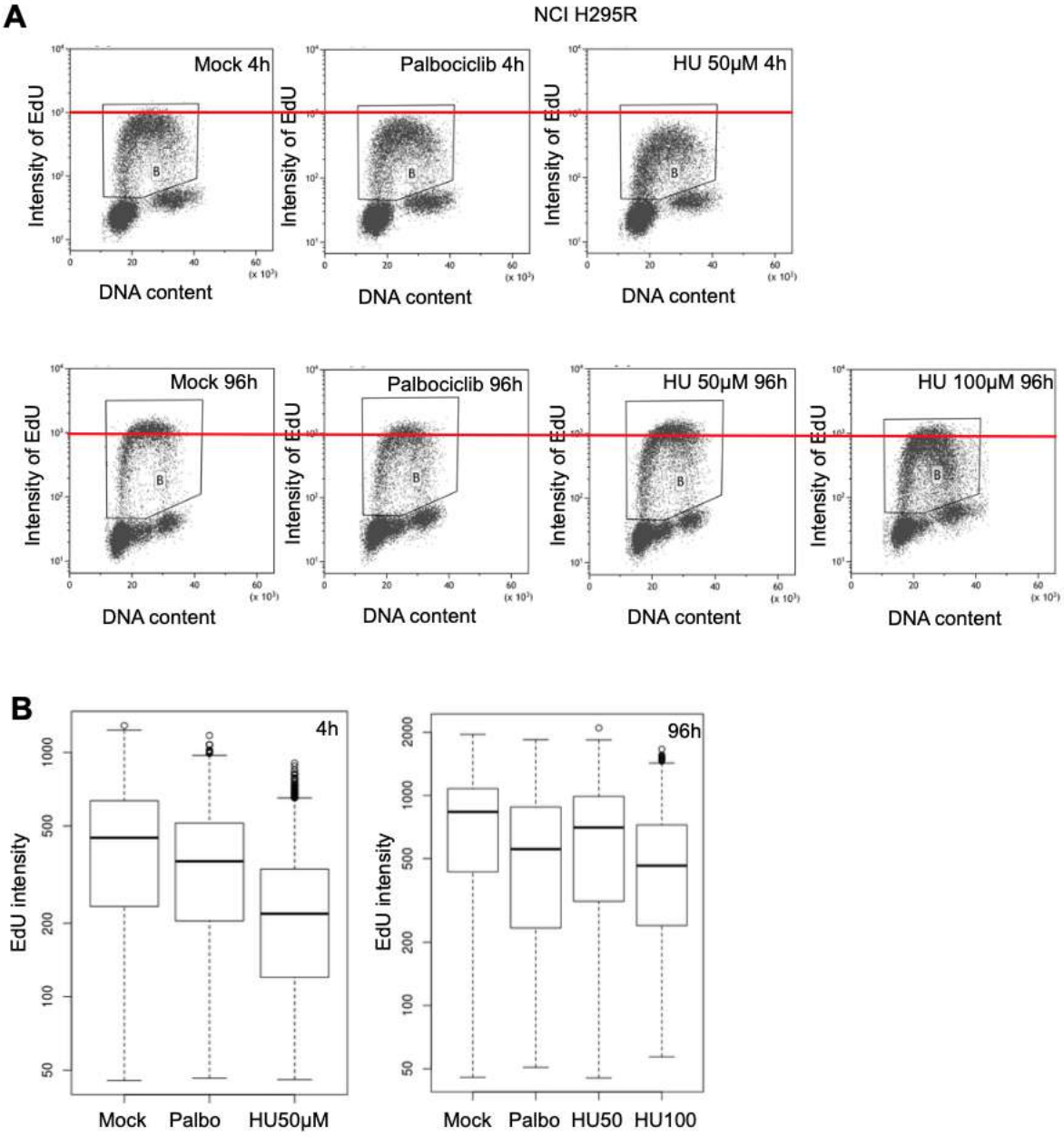


**Figure supplementary 2.**

**A.** Cell cycle profiles of NCI-H295R cells after EdU incorporation and mock, palbociclib or hydroxyurea treatment for 4 or 96 hours. **B.** Boxplots representing the intensity of EdU incorporation in NCI-H295R cells in S-phase for 4 or 96 hours of treatment. (Palbo=palbociclib treatment, Ribo=ribociclib treatment, HU=Hydroxyurea)

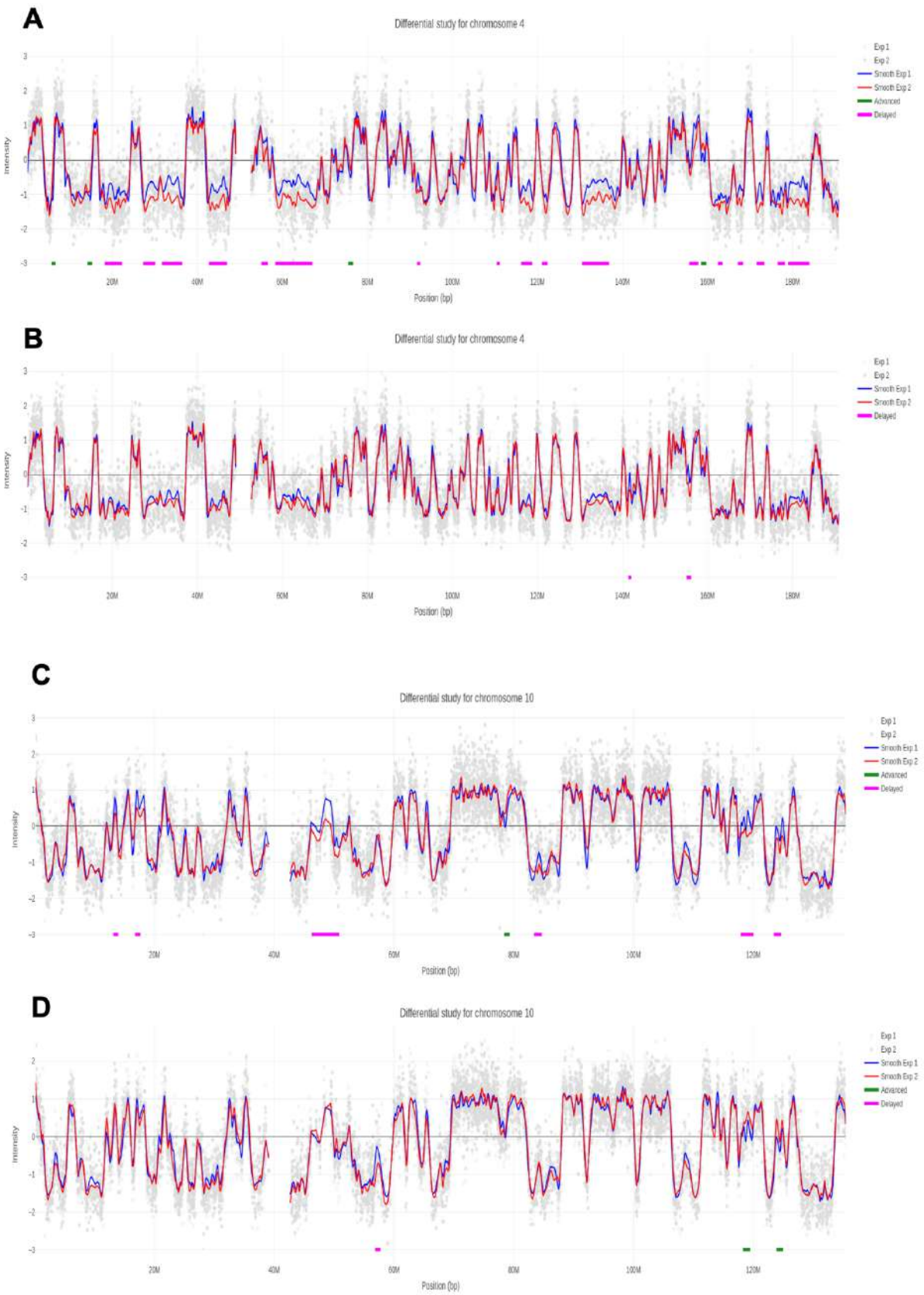


**Figure supplementary 3.**
Analysis of the temporal program of DNA replication in MDA-MB-468 and NCI-H295R cells treated with either palbociclib or ribociclib.

**A and B.** Chromosome 4 replication timing profiles in MDA-MB-468 cells. The blue line represents control cells treated with mock, the red one for cells treated with palbociclib in A and with ribociclib in B. Chromosome coordinates are indicated below each profile. **C and D.** Chromosome 10 replication timing profiles in NCI-H295R cells. The blue line represents control cells treated with mock, the red one for cells treated with palbociclib in A and with ribociclib in B.

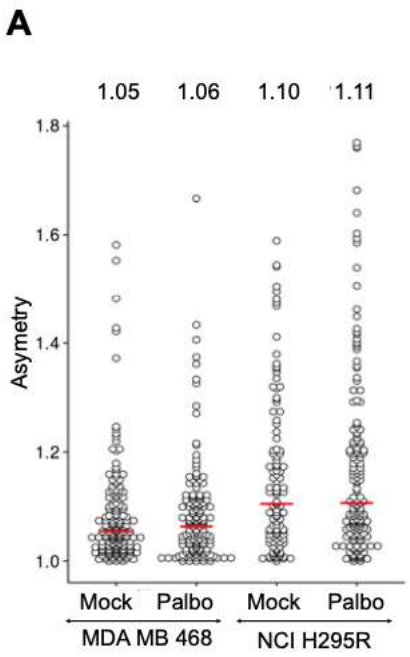


**Figure supplementary 4.**
**A.** Fork asymmetry is measured by CldU/IdU or IdU/CldU ratios higher than 1. The red lines indicate the median of fork asymmetry. (Palbo=palbociclib treatment, Ribo=ribociclib treatment)

Bollard, J. *et al.* (2016) 'Palbociclib (PD-0332991), a selective CDK4/6 inhibitor, restricts tumour growth in preclinical models of hepatocellular carcinoma', *Gut*, p. gutjnl-2016-312268. doi: 10.1136/gutjnl-2016-312268.

Bonte, D. *et al.* (2008) 'Cdc7-Dbf4 kinase overexpression in multiple cancers and tumor cell lines is correlated with p53 inactivation', *Neoplasia*, 10(9), pp. 920–931. doi: 10.1593/neo.08216.

Chen, Ping *et al.* (2016) 'Spectrum and degree of CDK drug interactions predicts clinical performance', *Molecular Cancer Therapeutics*, 15(10), pp. 2273–2281. doi: 10.1158/1535-7163.MCT-16-0300.

Chen, P. *et al.* (2016) 'Spectrum and Degree of CDK Drug Interactions Predicts Clinical Performance', *Molecular Cancer Therapeutics*, 15(10), pp. 2273–2281. doi: 10.1158/1535-7163.MCT-16-0300.

Chen, X. *et al.* (2019) 'Latest overview of the cyclin-dependent kinases 4/6 inhibitors in breast cancer: The past, the present and the future', *Journal of Cancer*, 10(26), pp. 6608–6617. doi: 10.7150/jca.33079.

Dean, J. L. *et al.* (2010) 'Therapeutic CDK4/6 inhibition in breast cancer: Key mechanisms of response and failure', *Oncogene*. Nature Publishing Group, 29(28), pp. 4018–4032. doi: 10.1038/onc.2010.154.

van Deursen, J. M. (2007) 'Rb Loss Causes Cancer by Driving Mitosis Mad', *Cancer Cell*, 11(1), pp. 1–3. doi: 10.1016/j.ccr.2006.12.006.

Dick, F. A. and Rubin, S. M. (2013) 'Molecular mechanisms underlying RB protein function', *Nature Reviews Molecular Cell Biology*, 14(5), pp. 297–306. doi: 10.1038/nrm3567.

Dyson, N. (1998) 'The regulation of E2F by pRB-family proteins', *Genes and Development*, 12(15), pp. 2245–2262. doi: 10.1101/gad.12.15.2245.

Hadjadj, D. *et al.* (2017) 'A hypothesis-driven approach identifies CDK4 and CDK6 inhibitors as candidate drugs for treatments of adrenocortical carcinomas', *Aging*, 9(12), pp. 2695–2716. doi: 10.18632/aging.101356.

Hadjadj, D. *et al.* (2020) 'Efficient, quick and easy-to-use DNA replication timing analysis with START-R suite', *NAR Genomics and Bioinformatics*, 2(2), pp. 1–7. doi: 10.1093/nargab/lqaa045.

Hafner, M. *et al.* (2019) 'Clinical Activity', 26(8), pp. 1067–1080. doi: 10.1016/j.chembiol.2019.05.005.Multi-omics.

Harbour, J. W. and Dean, D. C. (2000) ‘Chromatin remodeling and Rb activity’, *Current Opinion in Cell Biology*, 12(6), pp. 685–689. doi: 10.1016/S0955-0674(00)00152-6.
Van Harn, T. *et al.* (2010) ‘Loss of Rb proteins causes genomic instability in the absence of mitogenic signaling’, *Genes and Development*, 24(13), pp. 1377–1388. doi: 10.1101/gad.580710.
Hsieh, F. S. *et al.* (2017) ‘Palbociclib induces activation of AMPK and inhibits hepatocellular carcinoma in a CDK4/6-independent manner’, *Molecular Oncology*, 11(8), pp. 1035–1049. doi: 10.1002/1878-0261.12072.
Im, J. S. *et al.* (2009) ‘Assembly of the Cdc45-Mcm2-7-GINS complex in human cells requires the Ctf4/And-1, RecQL4, and Mcm10 proteins’, *Proceedings of the National Academy of Sciences of the United States of America*, 106(37), pp. 15628–15632. doi: 10.1073/pnas.0908039106.
Jiang, W. *et al.* (1999) ‘Mammalian Cdc7-Dbf4 protein kinase complex is essential for initiation of DNA replication’, *EMBO Journal*, 18(20), pp. 5703–5713. doi: 10.1093/emboj/18.20.5703.
Jingwen, B., Yaochen, L. and Guojun, Z. (2017) ‘Cell cycle regulation and anticancer drug discovery’, *Cancer Biology & Medicine*, 14(4), p. 348. doi: 10.20892/j.issn.2095-3941.2017.0033.
Leonard, A. C. and Me, M. (2013) ‘cshperspect-REP-a010116’, pp. 1–17.
Limas, J. C. and Cook, J. G. (2019) ‘Preparation for DNA replication: the key to a successful S phase’, *FEBS Letters*, 593(20), pp. 2853–2867. doi: 10.1002/1873-3468.13619.
Loibl, S. *et al.* (2017) ‘Palbociclib Combined with Fulvestrant in Premenopausal Women with Advanced Breast Cancer and Prior Progression on Endocrine Therapy: PALOMA-3 Results’, *The Oncologist*, 22(9), pp. 1028–1038. doi: 10.1634/theoncologist.2017-0072.
Mantovani, F., Collavin, L. and Del Sal, G. (2019) ‘Mutant p53 as a guardian of the cancer cell’, *Cell Death and Differentiation*. Springer US, 26(2), pp. 199–212. doi: 10.1038/s41418-018-0246-9.
Marzec, M. *et al.* (2006) ‘Mantle cell lymphoma cells express predominantly cyclin D1a isoform and are highly sensitive to selective inhibition of CDK4 kinase activity’, *Blood*. American Society of Hematology, 108(5), pp. 1744–1750. doi: 10.1182/blood-2006-04-016634.
Miettinen, T. P. *et al.* (2018) ‘ Thermal proteome profiling of breast cancer cells reveals proteasomal activation by CDK 4/6 inhibitor palbociclib ’, *The EMBO Journal*, 37(10), pp. 1–19. doi: 10.15252/embj.201798359.

Montagnoli, A. *et al.* (2004) 'Cdc7 inhibition reveals a p53-dependent replication checkpoint that is defective in cancer cells', *Cancer Research*, 64(19), pp. 7110–7116. doi: 10.1158/0008-5472.CAN-04-1547.

Montagnoli, A. *et al.* (2008) 'A Cdc7 kinase inhibitor restricts initiation of DNA replication and has antitumor activity', *Nature Chemical Biology*, 4(6), pp. 357–365. doi: 10.1038/nchembio.90.

Ozeri-Galai, E. *et al.* (2011) 'Failure of Origin Activation in Response to Fork Stalling Leads to Chromosomal Instability at Fragile Sites', *Molecular Cell*. Elsevier Inc., 43(1), pp. 122–131. doi: 10.1016/j.molcel.2011.05.019.

Petropoulos, M. *et al.* (2019) 'Replication Licensing Aberrations, Replication Stress, and Genomic Instability', *Trends in Biochemical Sciences*. Elsevier Ltd, 44(9), pp. 752–764. doi: 10.1016/j.tibs.2019.03.011.

Rainey, M. D. *et al.* (2017) 'DNA Replication Dynamics and Cellular Responses to ATP Competitive CDC7 Kinase Inhibitors', *ACS Chemical Biology*, 12(7), pp. 1893–1902. doi: 10.1021/acschembio.7b00117.

Rasti, M. and Azimi, T. (2015) 'TP53 binding to BRCA1 and RAD51 in MCF7 and MDA-MB-468 breast cancer cell lines in vivo and in vitro', *Avicenna Journal of Medical Biotechnology*, 7(2), pp. 76–79.

Rodriguez-Acebes, S. *et al.* (2010) 'Targeting DNA replication before it starts: Cdc7 as a therapeutic target in p53-mutant breast cancers', *American Journal of Pathology*, 177(4), pp. 2034–2045. doi: 10.2353/ajpath.2010.100421.

Rodriguez-Acebes, S., Mourón, S. and Méndez, J. (2018) 'Uncoupling fork speed and origin activity to identify the primary cause of replicative stress phenotypes', *Journal of Biological Chemistry*, 293(33), pp. 12855–12861. doi: 10.1074/jbc.RA118.003740.

Sampaoli, C. *et al.* (2012) 'p53 Stabilization Induces Cell Growth Inhibition and Affects IGF2 Pathway in Response to Radiotherapy in Adrenocortical Cancer Cells', *PLoS ONE*, 7(9). doi: 10.1371/journal.pone.0045129.

Spring, L. M. *et al.* (2019) 'CDK 4/6 Inhibitors in Breast Cancer: Current Controversies and Future Directions', *Current Oncology Reports*, 21(3), pp. 1–14. doi: 10.1007/s11912-019-0769-3.

Tanaka, S. and Araki, H. (2013) 'Helicase activation and establishment of replication forks at chromosomal origins of replication', *Cold Spring Harbor Perspectives in Biology*, 5(12), pp. 1–14. doi: 10.1101/cshperspect.a010371.

Técher, H. *et al.* (2013) 'Replication dynamics: Biases and robustness of DNA fiber analysis',

*Journal of Molecular Biology*. Elsevier Ltd, 425(23), pp. 4845–4855. doi: 10.1016/j.jmb.2013.03.040.

Técher, H. *et al.* (2017) 'The impact of replication stress on replication dynamics and DNA damage in vertebrate cells', *Nature Reviews Genetics*. Nature Publishing Group, 18(9), pp. 535–550. doi: 10.1038/nrg.2017.46.

Wells, C. I. *et al.* (2020) 'Quantifying CDK inhibitor selectivity in live cells', *Nature Communications*. Springer US, 11(1), pp. 1–11. doi: 10.1038/s41467-020-16559-0.

Xing, E. P. *et al.* (1999) 'Loss of heterozygosity of the Rb gene correlates with pRb protein expression and associates with p53 alteration in human esophageal cancer', *Clinical Cancer Research*, 5(5), pp. 1231–1240.

### II.A.3 Annexes

In order to assess the impact of palbociclib in temporal program of DNA replication, I compared two conditions (DMSO vs palbociclib or ribociclib) in each cell line and demonstrated the percentage of genome regions in which the replication timing is altered. It was figured out that the treatment of palbociclib mainly results in delayed regions in both studied cell lines.

Then, I performed further analysis to characterize molecular features of these regions (Figure 19). The coverage of advanced or delayed regions with early, mid, late or TTR regions is calculated. We remark that the delayed regions in MDA-MB-468 cells after the treatment with palbociclib are mainly detected in late replicated regions, indicating that palbociclib disturbs the origin firing in the late S-phase of the cell cycle. Then, the coverage for G4 and origins is calculated for each fraction of genome (early, mid, late, TTR) and each altered region after the palbociclib treatment (advanced or delayed). The delayed regions in late replicated domains display a poor G4 and origin coverage probably because of their enrichment in late S-phase in which constitutive origins are poorly determined. Compared to MDA-MB-468, we observed that delayed regions after the treatment with palbociclib are mainly positioned in early replicated regions and in TTR regions in NCI-H295R cells.

In order to explain this different response relative to each cell type, we compared these two cell lines in normal condition and detected 52.8% of difference in their temporal program (Figure 20). The total number of detected regions is similar in both cell lines (1674 in MDA-MB-468 cells and 1609 in NCI-H295R cells) but, we observed that the repartition in each fraction (early, mid, late replicated regions) is variable for each cell line. For instance, MDA-MB-468 cell line represents a greater number of late replicating regions than NCI-H295R cell line and inversely we found that NCI-H295R cells are more enriched in early replicating regions than MDA-MB-468 cells. The findings indicate that both cell lines have their own replication timing program, which could explain why palbociclib induces a delay in different regions of the genome in each cell line.

In line with this observation, we only found 20 common regions between both cell lines (10 advanced and 10 delayed domains) after the treatment with palbociclib (Table 4). We then

compared if these commonly altered regions position in the same fraction of the genome. The advanced regions are distributed in late and TTR regions (Table 5). Among the 10 common delayed regions, 7 regions are found in common late replicated regions with high values of coverage (Table 6). It could be interesting now to investigate if these regions are positioned near common fragile sites to study the effects of palbociclib on the induction of chromosomal instability.

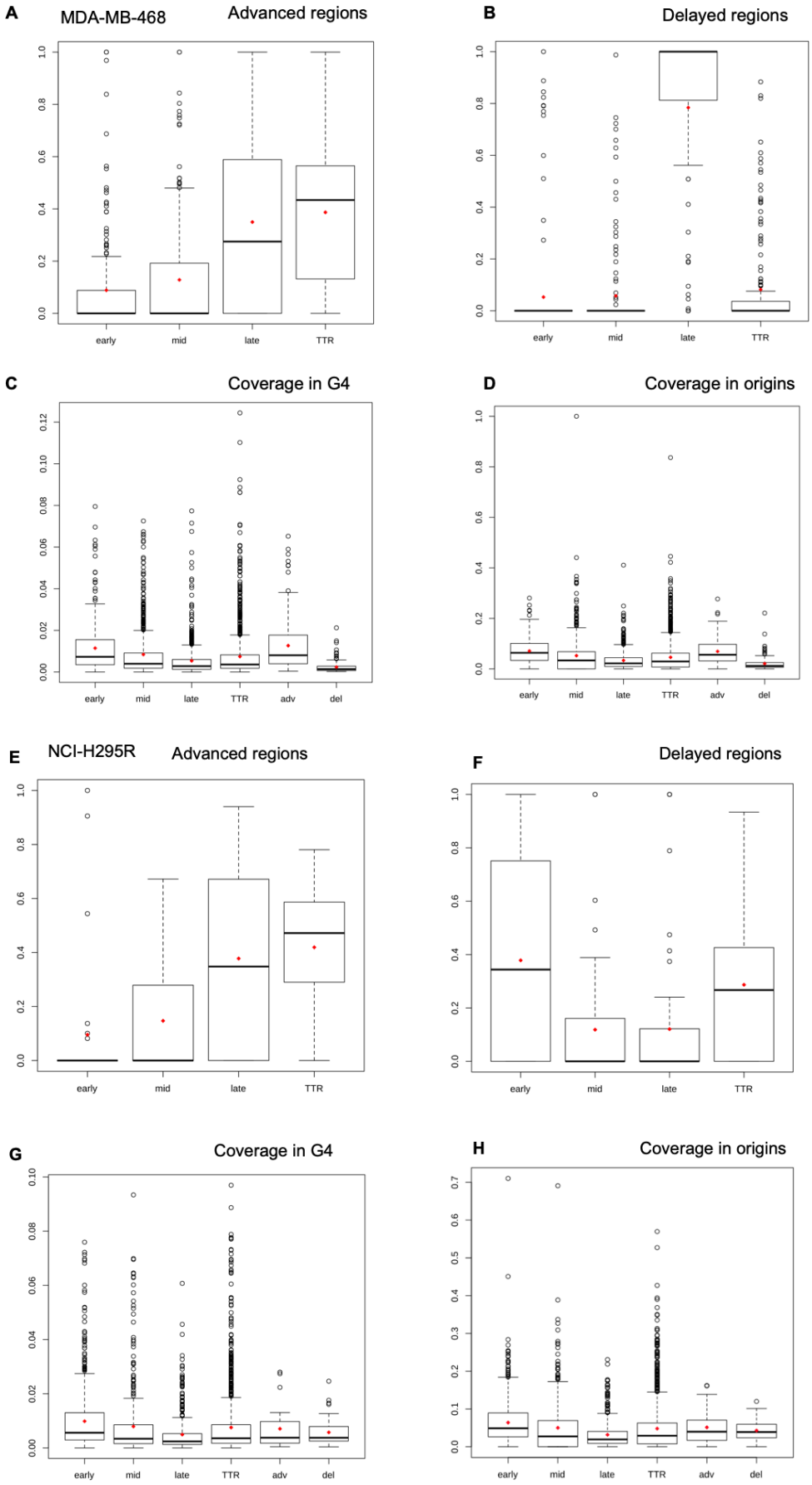
A
MDA-MB-468
Advanced regions
B
Delayed regions
C
Coverage in G4
D
Coverage in origins
E
NCI-H295R
Advanced regions
F
Delayed regions
G
Coverage in G4
H
Coverage in origins
early
mid
late
TTR
adv
del

**Figure 19.** Analysis of molecular features for advanced and delayed regions after treatment with palbociclib. A.B.C.D in MDA-MB-468 cells and E.F.G.F in NCI-H295R cells.
Boxplots depicting the coverage for each fraction of the genome (early, mid, late or TTR) are shown in A and E for advanced regions, and in B and F for delayed regions. G4 (C and G) and origins (D and H) coverage are shown in boxplots for each fraction of the genome (early, mid, late, TTR, advanced and delayed regions)

B

| | Total | Early | Mid | Late |
|---|---|---|---|---|
| MDA-MB-468 | 1674 | 381 (23%) | 662 (40%) | 631 (38%) |
| NCI-H295R | 1609 | 692 (43%) | 432 (27%) | 485 (30%) |

**Figure 20.** Comparing replication timing profiles of both cell lines.
A. Profiles showing replication timing for three different chromosomes in MDA-MB-468 (blue) and in NCI-H295R (red) cell lines. Advanced and Delayed regions are highlighted by green and pink lines, respectively.
B. Table showing the number of regions representing timing discrepancies for the total genome, early, mid or late replicating regions for each cell line.

| Common advanced regions in MDA-MB-468 and NCI-H295R | | | | Common delayed regions in MDA-MB-468 and NCI-H295R | | | |
|---|---|---|---|---|---|---|---|
| Chromosome | Start | End | Name | Chromosome | Start | End | Name |
| chr1 | 210402871 | 211202347 | ADVANCED | chr10 | 83372442 | 84668602 | DELAYED |
| chr10 | 78423336 | 79280001 | ADVANCED | chr10 | 123442842 | 124269144 | DELAYED |
| chr11 | 59596008 | 60295837 | ADVANCED | chr15 | 25787291 | 26216850 | DELAYED |
| chr11 | 84730619 | 84982894 | ADVANCED | chr2 | 145426168 | 145791717 | DELAYED |
| chr14 | 22303636 | 22907120 | ADVANCED | chr3 | 179854491 | 179861540 | DELAYED |
| chr15 | 60848498 | 61660815 | ADVANCED | chr5 | 5292052 | 5317015 | DELAYED |
| chr20 | 41366872 | 42034104 | ADVANCED | chr8 | 93020721 | 93604572 | DELAYED |
| chr21 | 42045270 | 42495615 | ADVANCED | chr8 | 136329400 | 136398312 | DELAYED |
| chr6 | 26014376 | 26941958 | ADVANCED | chr9 | 119988570 | 120008936 | DELAYED |
| chr6 | 29371396 | 29409803 | ADVANCED | chrX | 83669939 | 85152345 | DELAYED |

**Table 4.** List of regions commonly advanced or delayed after treatment with palbociclib in both cell lines.

| Advanced | | | | Early | Mid | Late | TTR |
|---|---|---|---|---|---|---|---|
| Chromosome | Start | End | Name | | | | |
| chr1 | 210402871 | 211202347 | ADVANCED | 0.0 | 0.0 | 0.61 | 0.013 |
| chr10 | 78423336 | 79280001 | ADVANCED | 0.0 | 0.0 | 0.0 | 0.0 |
| chr11 | 59596008 | 60295837 | ADVANCED | 0.0 | 0.0 | 0.0 | 0.181 |
| chr11 | 84730619 | 84982894 | ADVANCED | 0.0 | 0.0 | 0.0 | 0.0 |
| chr14 | 22303636 | 22907120 | ADVANCED | 0.054 | 0.0 | 0.252 | 0.546 |
| chr15 | 60848498 | 61660815 | ADVANCED | 0.0 | 0.0 | 0.0 | 0.096 |
| chr20 | 41366872 | 42034104 | ADVANCED | 0.0 | 0.0 | 0.569 | 0.297 |
| chr21 | 42045270 | 42495615 | ADVANCED | 0.0 | 0.0 | 0.115 | 0.0 |
| chr6 | 26014376 | 26941958 | ADVANCED | 0.0 | 0.0 | 0.279 | 0.0 |
| chr6 | 29371396 | 29409803 | ADVANCED | 0.0 | 0.0 | 0.582 | 0.0 |

**Table 5.** List of regions commonly advanced after treatment with palbociclib in both cell lines and their coverage for each fraction of the genome. The coverage value is written in red except 0.

| Delayed | | | | Early | Mid | Late | TTR |
|---|---|---|---|---|---|---|---|
| Chromosome | Start | End | Name | | | | |
| chr10 | 83372442 | 84668602 | DELAYED | 0.0 | 0.0 | 1.0 | 0.0 |
| chr10 | 123442842 | 124269144 | DELAYED | 0.0 | 0.0 | 0.0 | 0.183 |
| chr15 | 25787291 | 26216850 | DELAYED | 0.0 | 0.0 | 1.0 | 0.0 |
| chr2 | 145426168 | 145791717 | DELAYED | 0.0 | 0.0 | 0.89 | 0.0 |
| chr3 | 179854491 | 179861540 | DELAYED | 0.0 | 0.0 | 1.0 | 0.0 |
| chr5 | 5292052 | 5317015 | DELAYED | 0.0 | 0.0 | 0.601 | 0.0 |
| chr8 | 93020721 | 93604572 | DELAYED | 0.0 | 0.0 | 0.0 | 0.0 |
| chr8 | 136329400 | 136398312 | DELAYED | 0.0 | 0.0 | 0.0 | 0.0 |
| chr9 | 119988570 | 120008936 | DELAYED | 0.0 | 0.0 | 1.0 | 0.0 |
| chrX | 83669939 | 85152345 | DELAYED | 0.0 | 0.0 | 0.79 | 0.0 |

**Table 6.** List of regions commonly delayed after treatment with palbociclib in both cell lines and their coverage for each fraction of the genome. The coverage value is written in red except 0.

## II.B Efficient, quick and easy-to-use DNA replication timing analysis with START-R suite

### II.B.1 Summary

Replication Timing is a well-preserved cellular program that ensures accurate DNA replication along with spatial origin activations. Monitoring this program allows us to understand how cells organize replication timing for each region of the genome throughout the S-phase of the cell cycle. Analysis of the temporal program of DNA replication provides an insight into the efficiency of activation of origins and the fork movements at the genome scale from early to late S-phase. In addition, by comparing two conditions, this allows to evaluate the impacts of a drug or of a gene modification as sources of replicative stress. Furthermore, combining replication timing results with other available data such as replication origins map, transcriptome, secondary structures prediction allows us to characterize the molecular features of altered regions upon replication stress.

In this paper, we show quick and easy-to-use methods for analyzing the replication timing (Figure 21). First, the immunoprecipitation step was automated using the IP-Star® robot making experimental steps more rapid and precise. By enlarging the windows to sort cells, we found that the replication timing profiles from Repli-Chip are similar to those from Repli-Seq data. Second, we developed the START-R suite, which is dedicated to the analysis of DNA replication timing results. This software provides robust tools that any biologist can use. START-R analyzer proposes different parameters and statistical tools easy to use. START-R viewer allows the visualization of replication timing profiles at the whole genome scale and distinguishes regions that are altered in terms of replication timing by comparing two different conditions. Our method has been validated with both microarray and Repli-Seq data and is suitable for data from different species such as drosophila, zebrafish, mouse and human cells.

This paper proposes an entire pipeline to study efficiently and easily replication timing. We confirm that Repli-Chip method is as precise as Repli-Seq while consuming less time and cost. Finally, the user-friendly START-R suite makes the manipulation of huge amounts of data more accessible to biologists.

This study is published in the journal 'NAR Genomics and Bioinformatics' (Hadjadj *et al.*, 2020).

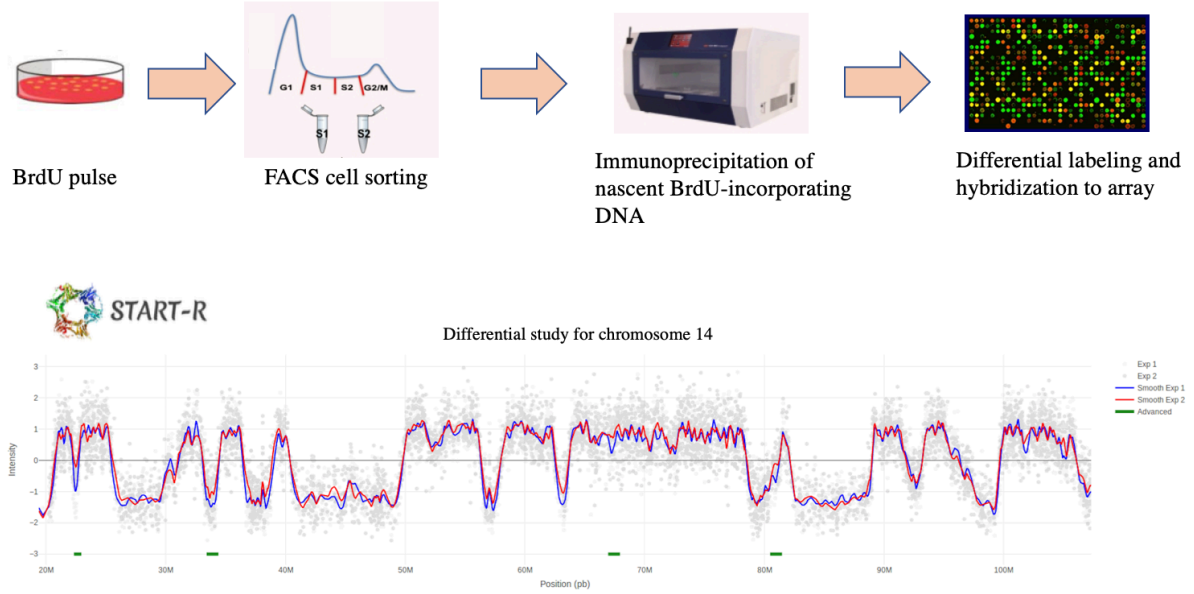


**Figure 21.** A brief description of the DNA replication timing analysis. Asynchronous cells are incubated with BrdU (Bromodesoxyuridine), a thymidine analog during 1.5 hours, then cells that have incorporated BrdU are sorted into two fractions of S-phase corresponding to early and late S-phase. Then, the neosynthesized BrdU labeled DNA is precipitated using an antibody against BrdU. Each fraction is labeled differently with fluorochromes, then both fractions are hybridized on a Comparative Genomic Hybridization (CGH) array containing a reference genome with respect to species. The signal ratios of each fraction is calculated for each region of the genome. START-R is a software developed in our laboratory to visualize replication timing profiles and compare two conditions with statistical tools.

## II.B.2 Article

*Published online 19 June 2020*

*NAR Genomics and Bioinformatics, 2020, Vol. 2, No. 2* **1**
*doi: 10.1093/nargab/lqaa045*

# Efficient, quick and easy-to-use DNA replication timing analysis with START-R suite

**Djihad Hadjadj[1,†], Thomas Denecker[2,†], Eva Guérin[1], Su-Jung Kim[1], Fabien Fauchereau[1], Giuseppe Baldacci[1], Chrystelle Maric[1,‡] and Jean-Charles Cadoret[1,*,‡]**

[1]Pathologies de la Réplication de l'ADN, Université de Paris; Institut Jacques-Monod, UMR7592, CNRS, F-75006 Paris, France and [2]Institut de Biologie Intégrative de la Cellule, UMR9198, CNRS, Université Paris-Saclay, Université Paris-Sud, F-91405 Orsay, France

Received February 20, 2020; Revised May 19, 2020; Editorial Decision May 28, 2020; Accepted June 15, 2020

## ABSTRACT

**DNA replication must be faithful and follow a well-defined spatiotemporal program closely linked to transcriptional activity, epigenomic marks, intranuclear structures, mutation rate and cell fate determination. Among the readouts of the spatiotemporal program of DNA replication, replication timing analyses require not only complex and time-consuming experimental procedures, but also skills in bioinformatics. We developed a dedicated Shiny interactive web application, the START-R (Simple Tool for the Analysis of the Replication Timing based on R) suite, which analyzes DNA replication timing in a given organism with high-throughput data. It reduces the time required for generating and analyzing simultaneously data from several samples. It automatically detects different types of timing regions and identifies significant differences between two experimental conditions in ∼15 min. In conclusion, START-R suite allows quick, efficient and easier analyses of DNA replication timing for all organisms. This novel approach can be used by every biologist. It is now simpler to use this method in order to understand, for example, whether 'a favorite gene or protein' has an impact on replication process or, indirectly, on genomic organization (as Hi-C experiments), by comparing the replication timing profiles between wild-type and mutant cell lines.**

## INTRODUCTION

DNA replication is a highly regulated process involved in the maintenance of genome stability (1–3). Its accuracy relies partly on a spatio-temporal program that regulates timing and location of origin firing (4,5). Based on this program, replication is organized into large-scale domains that replicate at different times in S phase (6–8). Protocols developed to study the replication timing (RT) in specific cell lines have been established in different laboratories (9–13). A script dedicated to RT analysis was previously developed by David Gilbert's laboratory (10,12), but it required skills in bioinformatics and R language. In order to make the analysis of experimental results easier for biologists, we implemented an interactive suite, START-R (Simple Tool for the Analysis of the Replication Timing based on R) Analyzer and START-R Viewer, showing user-friendly interfaces. This START-R suite is dealing with RT experiments made with microarrays or with Repli-seq data (either Early/Late or S/G1 ratios) from different organisms. These web applications would make easier differential analyses of RT, by comparing conditions such as treated/untreated cells or mutated/normal cells. They are free and may be improved by developers, according to specific needs. In addition, RT profiles correlate with A/B compartment profiles predicted by chromosome conformation methods. Regions of the genome defined by Hi-C profiles as A compartments are also identified as Early replicated domains, whereas regions defined as B compartments are Late replicating domains (14). Furthermore, some replicating domains coincide with a subset of topologically associating domains and more closely with the ones located at compartment boundaries (15). Studies of RT programs with START-R suite take shorter time to perform and therefore open new research perspectives for many laboratories working in DNA replication, in chromosome conformation and in other closely related molecular processes.

## MATERIALS AND METHODS

### START-R suite

START-R Analyzer and START-R Viewer (doi:10.5281/zenodo.3251905) were developed using the Shiny R package (W. Chang, J. Cheng, J. Allaire,

*To whom correspondence should be addressed. Tel: +33 1 57 27 80 74; Email: jean-charles.cadoret@ijm.fr
†The authors wish it to be known that, in their opinion, the first two authors should be regarded as Joint First Authors.
‡The authors wish it to be known that, in their opinion, the last two authors should be regarded as Joint Last Authors.

© The Author(s) 2020. Published by Oxford University Press on behalf of NAR Genomics and Bioinformatics.
This is an Open Access article distributed under the terms of the Creative Commons Attribution Non-Commercial License (http://creativecommons.org/licenses/by-nc/4.0/), which permits non-commercial re-use, distribution, and reproduction in any medium, provided the original work is properly cited. For commercial re-use, please contact journals.permissions@oup.com

Y. Xie and J. McPherson, Shiny: web application framework for R, R package version 1.2.0, 2018, https://CRANR-project.org/package=shiny). The source code and the installation procedure are available on GitHub (https://github.com/thomasdenecker/START-R). All R packages used in the START-R suite are listed in the Readme file on GitHub. Users should install Docker and then follow installation procedures described for each operating system (Windows, Linux and Mac OS) in the Readme file (Figure 1). Although the installation of these web-based applications has been simplified as much as possible, it may even so require some computer knowledge (especially on Linux). Once installed, the START-R suite is an easy-to-use tool requiring no computer skills (see Supplementary Figure S1 and the Wiki section on GitHub for more details).

### Validation of START-R suite using microarray data from other laboratories

We analyzed with the START-R suite the microarray data obtained by Hiratani *et al.* (16) of D3esc and D3npc9 cell lines during mouse cells' differentiation (GEO accession numbers: GSM450273 and GSM450285, respectively). As data extracted from the Nimblegen platform are in PAIR format, we used a script to convert data into a valid format for START-R Analyzer (convertPair.R, available on GitHub in 'supplement script' file, https://github.com/thomasdenecker/START-R).

### Early/Late-seq data and conversion

In order to validate our software, we used data corresponding to Repli-seq 46C mouse cells—Early S fraction or Late S fraction, respectively (GSM2496038 and GSM2496039). Read mapping was obtained using Bowtie2 (2.3.4.2 version) with the very sensitive end-to-end option. Then, PCR duplicates were removed by RmDUP from SAMTools (2.0.1 version). BamCoverage parameters were fixed (3.1.2.0.0 version with default parameters) to a bin size of 10 kb (corresponding to the genomic distance between microarray probes) and reads per kilobase million (RPKM) normalization to generate a bedGraph file. A headline was added to the file to name the four columns (chr, start, end and gProcessedSignal for Early file or rProcessedSignal for Late file, respectively). Then, a script to convert and merge the bedGraph files from Early and Late samples to a format compatible with START-R Analyzer was developed. This script is available on GitHub in 'supplement script' file as convert_bamcoverage_file.R.

### Validation of START-R suite using S/G1 data from multiple species

Different laboratories analyze variations of DNA copy number between G1 and S phase cells (S/G1 ratio) to study the RT program with Repli-seq. We used data obtained from different organisms such as *Drosophila*, zebrafish and humans (17–19), to validate the START-R suite (GSM3154888, GSM3154890, GSM2282090, SRX3413939-40). As previously, BAM coverage files from G1 and S fractions are converted to a format compatible with START-R Analyzer with the aforementioned 'convert_bamcoverage_file.R.' script.

## RESULTS

### RT analysis with START-R suite allows robust statistical analysis

We developed a software allowing an automatic detection of RT regions and a differential analysis between two conditions. The START-R suite is implemented into an HTML interface for more efficient use and sharing by biologists. START-R is built-in and packaged into a virtual environment with Docker (Figure 1). Thus, START-R can be easily deployed on a personal computer or on a server, and can run independently of any library updating. START-R provides as many parameters as possible for a comprehensive analysis of the RT program (Supplementary Figure S1A–K). Furthermore, we added new scaling, normalization and smoothing methods (Supplementary Figure S2) and also novel statistical approaches to detect differences between two samples. A classical differential analysis performed with START-R takes ∼15 min with a standard laptop computer. START-R Analyzer can run data from all organisms with different genome assemblies. This flexibility is one of the new aspects of the START-R suite that allows to analyze RT program in every organism (Supplementary Figure S1B). In addition, START-R generates RT profiles in PDF and all the files necessary for a better and customized visualization with START-R Viewer. START-R Analyzer also produces specific files that could be visualized with START-R Viewer, a specific genome browser tool dedicated to START-R suite.

### A large panel of new settings and tools for RT analysis

We based our method on four major steps: *normalization* (between Early and Late fractions, between two replicates and between two independent experiments; Supplementary Figure S2A), *smoothing* (different options are available; Supplementary Figure S2B), *identification* of transition timing regions (TTRs; Supplementary Figure S3) and *segmentation*. The originality of our approach is to first detect TTRs in order to better identify constant timing regions (CTRs; Supplementary Figure S3). The identification of TTRs is based on their intrinsic properties: regions that include more than three consecutive probes with significantly different Early/Late intensity log ratios are considered as TTRs (Supplementary Figure S3). The statistical significance of differences between intensity log ratios is calculated by the outlier box plot method (Supplementary Figure S4) (20). Following TTR detection, START-R Analyzer localizes CTRs: TTRs are subtracted from the genome (Supplementary Figure S3) and the remaining regions are considered as CTRs. At the end of these steps, START-R Analyzer automatically generates a BED file for CTRs and TTRs making easier further bioinformatic analyses and the display of the RT domains via a genome browser (Supplementary Figure S1F). A codebook is also generated to ensure the traceability of options chosen for each analysis.

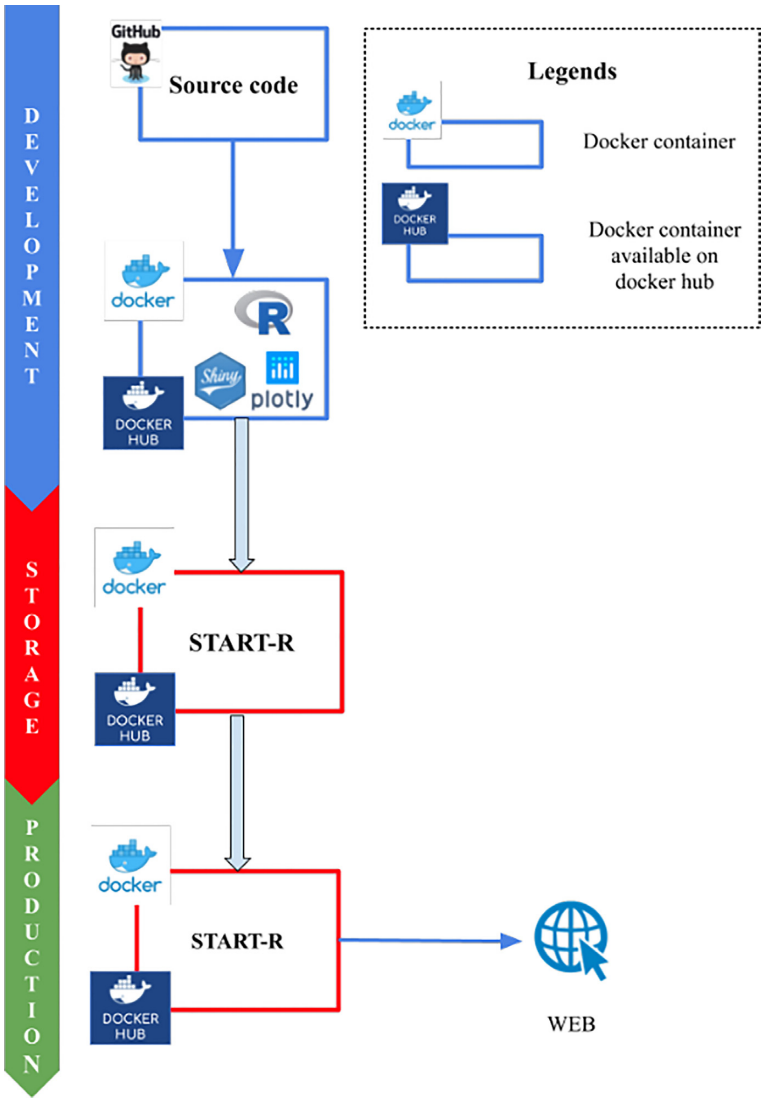


**Figure 1.** Stack overview of the START-R suite. The START-R suite is able to analyze all types of genome-wide RT data formats like microarray data, Repli-seq data with Early/Late and S/G1 ratios, and RT data from multiple organisms. The START-R suite was developed using the Shiny R package (W. Chang, J. Cheng, J. Allaire, Y. Xie and J. McPherson, Shiny: web application framework for R, R package version 1.2.0, 2018, https://CRANR-project.org/package=shiny) and Plotly visualization tools (C. Sievert, C. Parmer, T. Hocking, S. Chamberlain, K. Ram, M. Corvellec and P. Despouy, plotly: create interactive web graphics via 'plotly.js', R package version 4.7.1, 2017, https://CRANR-project.org/package=plotly). The START-R software (START-R Analyzer and START-R Viewer) are open-source web-based applications (doi:10.5281/zenodo.3251905). For the storage and production steps, the START-R suite was concatenated using Docker in order to install, use and share it easily. These software can be used with different operating systems: Windows, Mac OS and Linux. The source code and the installation procedure are available on GitHub (https://github.com/thomasdenecker/START-R). To install the START-R suite, users should install Docker and follow the Readme file containing the installation procedure (https://github.com/thomasdenecker/START-R/blob/master/README.md). Finally, in order to run the START-R suite, users should double-click on the START-R file (Windows) or launch the command line (Mac OS X, Linux), followed by opening an internet browser at the following URLs: http://localhost:3838/ for START-R Analyzer and http://localhost:3839/ for START-R Viewer.

We added a step allowing the differential analysis of RT programs from two experiments. Thus, we can now compare RT profiles obtained in different conditions and/or with different cell lines to identify genomic elements that can modify the RT program. Our differential analysis includes three different methods of comparison: the Mean method, the Euclidean method and the Segment comparison method. When the goal is to identify most regions with strong RT changes, we recommend using the most stringent Mean method. The less stringent Segment and Euclidean methods allow the detection of a larger set of RT changes, while increasing the risk of obtaining false positives.

The last major implementation is START-R Viewer (Supplementary Figure S1K). This web-based interface allows the visualization of the RT profile generated by START-R Analyzer in dynamic charts obtained with the Plotly library (C. Sievert, C. Parmer, T. Hocking, S. Chamberlain, K. Ram, M. Corvellec and P. Despouy, plotly: create interactive web graphics via 'plotly.js', R package version 4.7.1, 2017, https://CRANR-project.org/package=plotly).

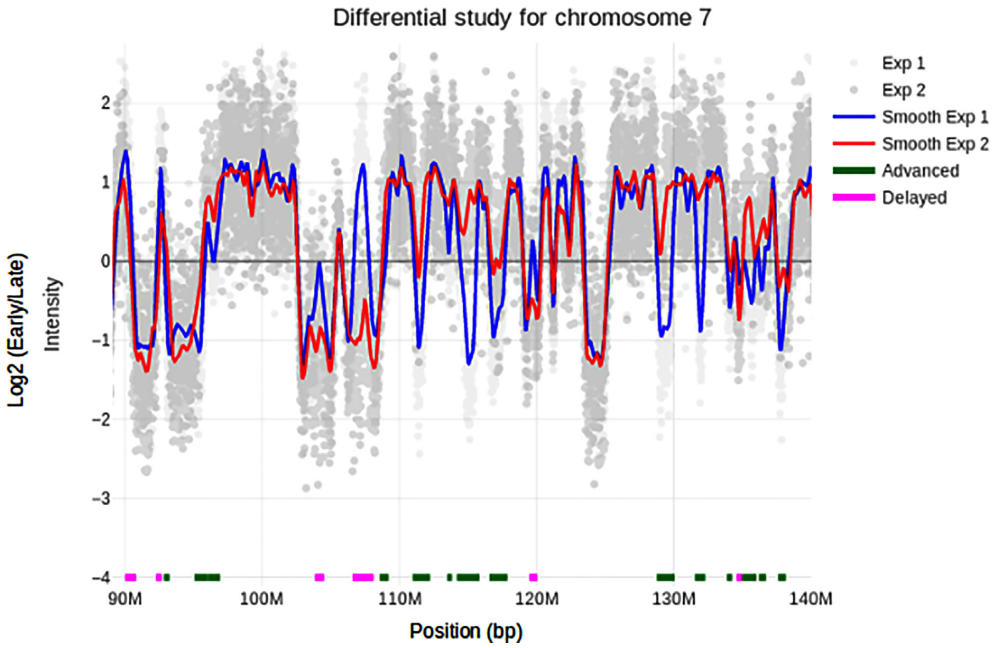


**Figure 2.** Genomic characteristics of regions harboring different RT programs. START-R Viewer allows the visualization of RT data with many features. The START-R differential analysis of RT profiles is shown here for a portion of chromosome 7 in mouse D3esc (blue) and D3npc9 (red) cells. We used START-R Analyzer with the standard options: Loess Early/Late normalization, scale inter-replica normalization, inter-experiment standardization, Loess method for smoothing (span = 300 kb), 2.5 for SD difference between two segments and mean comparison analysis with a Holm's method *P*-value of 0.05 for the differential analysis. The advanced (green) and delayed (pink) regions identified with START-R Analyzer are indicated underneath the RT profiles. Light gray and gray spots indicate data from both RT experiments. With these parameters, 2066 CTRs were detected in the genome and 910 regions showed different RT between D3esc and D3npc9 cells. Box plots illustrating genomic characteristics (GC content, LINE-1 content and gene coverage) of regions harboring different RT programs are shown in Supplementary Figure S6.

One can easily identify CTRs, TTRs (Supplementary Figure S5A) and significantly advanced or delayed regions (Supplementary Figure S5B). We therefore developed a genome browser to optimally display the maximum of data generated by START-R Analyzer. The START-R suite also automatically generates files with different output formats essential for further molecular characterizations and compatible for classical bioinformatic tools and/or for GALAXY genomic tools (21).

### START-R analysis of RT programs during differentiation in mouse: a new analysis of previous data

To validate our START-R based-approach without *a priori* consideration, we decided to re-analyze the data generated by the Gilbert's group concerning the changes of RT program during cell differentiation in mouse D3esc and D3npc9 cell lines (16). We converted these raw data with the convertPair.R script available in our GitHub project into the correct format for START-R Analyzer. RT profiles generated with START-R Analyzer (Figure 2) and molecular signatures (Supplementary Figure S6) are identical to the ones previously described by Gilbert's group. Each modified timing region had a particular molecular signature: Late-to-Early or advanced regions show a GC/LINE-1 density and gene coverage similar to constant Early regions, while Early-to-Late or delayed regions showed GC/LINE-1 density and gene coverage similar to constant Late regions.

### Validation of START-R with Early–Late Repli-seq data from mouse

Nowadays, many data of RT program are generated with Repli-seq experiments, but their analysis is time-consuming and often requires bioinformatics skills. We analyzed the Early/Late Repli-seq data from Marchal *et al.* (12). We specifically developed a supplemental script to convert the BAM coverage file to a log Early/Late file (convert_bamcoverage_file.R) to be sure that the integration into the START-R pipeline was correct. Then, we compared the RT smooth profiles generated from Early/Late Repli-seq data with those generated by the same group using microarrays (Figure 3A). Profiles are almost identical to the ones described by Marchal *et al.* (12). Thus, START-R Analyzer and START-R Viewer can be easily used to analyze Early/LateIDEX Repli-seq data, showing their versatility and their simplicity of use.

### Validation of START-R with S–G1 Repli-seq data from *Drosophila*, zebrafish and humans

Other laboratories use the ratio of DNA content between G1 and S phases to analyze the RT program. We wanted to know whether START-R suite can run the correct analyses with this type of data and also with other organisms than mice and humans. We performed exactly the same pipeline used for Early/Late Repli-seq data described above with *Drosophila*, zebrafish and human S/G1 data (17–19). Then and as expected, START-R can be run with S/G1 log ratio

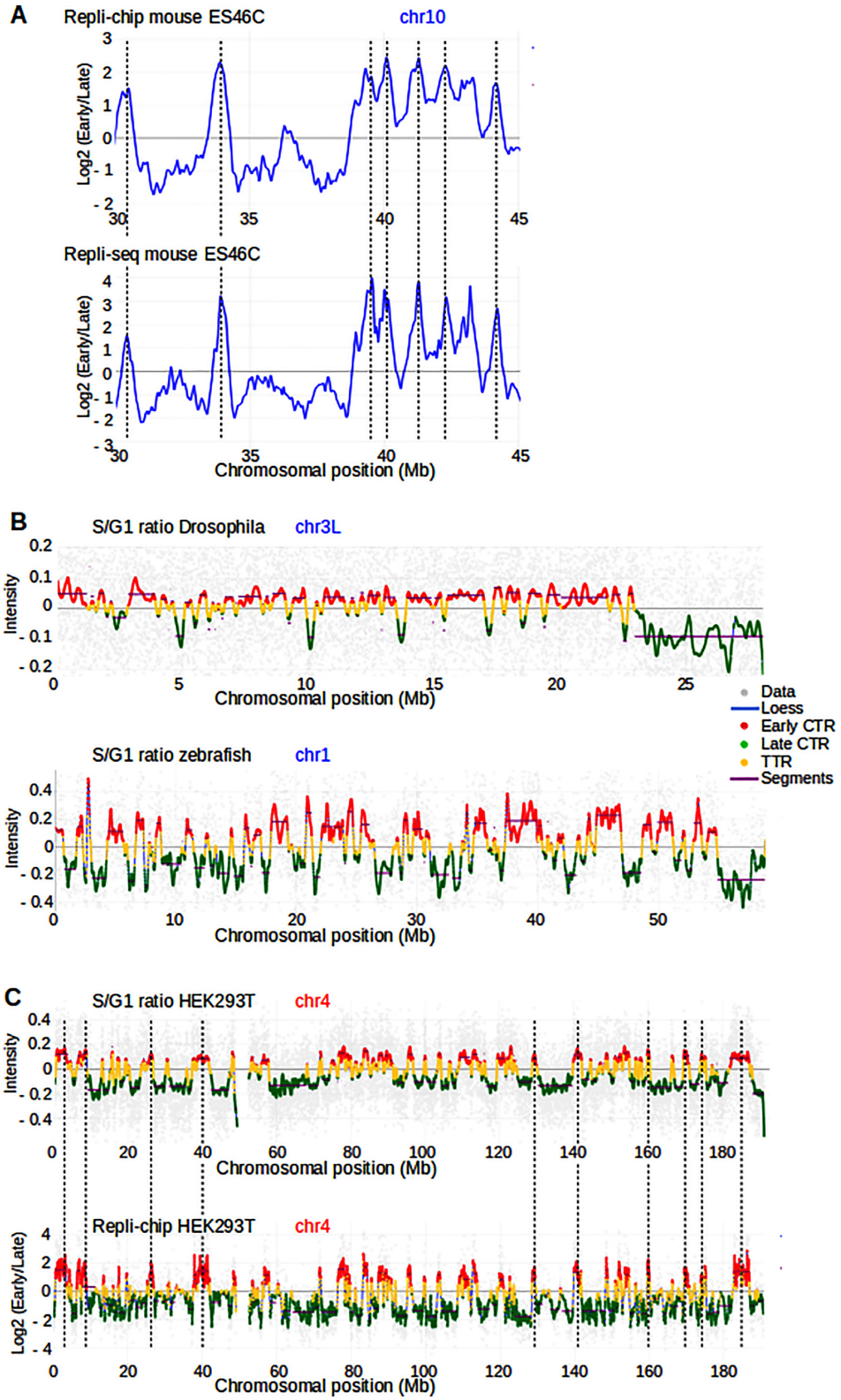


**Figure 3.** The START-R suite allows analysis and visualization of both Repli-chip and Repli-seq data from different model systems. (**A**) RT profiles of a portion of mouse chromosome 10 from ES46C cell line are generated using Repli-chip (top panel) and Repli-seq data (bottom panel) with START-R web applications. Dashed vertical lines show common RT regions between both profiles. (**B**) RT profiles obtained by S/G1 ratios are shown for the left part of *Drosophila* chromosome 3 (3L) and for zebrafish chromosome 1 (blue lines). The profiles display distribution of Early and Late CTRs, in red and green, respectively, and of TTRs, in yellow. Segments corresponding to regions of constant timing are shown in purple. Gray spots indicate data from RT experiments. (**C**) RT profiles of human HEK293T chromosome 4 are generated using S/G1 ratio and Repli-chip data. The empty space inside the RT profiles represents the centromere region.

data (Figure 3B and C). We observed similar profiles as the ones already observed for these different organisms.

## DISCUSSION

In this study, we show a new automated protocol for analyzing RT profiles (Figure 1), obtained with different methods, in all organisms. As a proof of concept, we succeed in generating RT analyses for human, mouse, *Drosophila* and zebrafish genomes (Figures 2 and 3). START-R suite's user-friendly interface allows choices between different parameters at all steps used to generate RT profiles (Supplementary Figure S1). Compared to the previous methods (10,12), START-R Analyzer first detects TTRs and thus better refines and improves the CTR detection (Supplementary Figures S3 and S5A). In addition, START-R Analyzer contains new calculation methods for differential analyses between two conditions or cell lines (Supplementary Figure S5B).

This flexibility gives the users the opportunity to choose the differential analysis method and different parameters according to their questions. It also automatically generates files with different output formats essential for further molecular characterizations and compatible for classical bioinformatic tools and/or for GALAXY genomic tools (21). Then, START-R Viewer produces a nice interface to visualize all the data generated by START-R Analyzer. Furthermore, START-R suite freeware are available on GitHub and their source codes are open to anyone who wants to improve them, as, for example, for studies of allelic changes of RT.

In conclusion, it is now possible for any biologist or laboratory to readily explore new or previous RT data simply and quickly. Thus, a large number of laboratories can today use our software to find out whether their experimental conditions are affecting the RT process or are correlated with other molecular mechanisms. START-R also allows to determine what parts of the genome are impacted and in which proportion and to characterize further those loci. Thanks to the accessibility of our approaches and software, their speed and efficiency, new research perspectives can be efficiently envisaged.

## SUPPLEMENTARY DATA

Supplementary Data are available at NARGAB Online.

## ACKNOWLEDGEMENTS

We thank Gaëlle Lelandais for helpful discussions. We also acknowledge the ImagoSeine core facility of the Institut Jacques-Monod, member of the France BioImaging (ANR-10-INBS-04) supported by the Region Île-de-France (E539). This project was supported by the generous legacy from Ms Suzanne Larzat to our group.

## FUNDING

La Ligue Nationale Contre le Cancer RS16/75-108, RS17/75-135; GEFLUC; Institut National du Cancer INCa-10493; IDEX Université de Paris ANR-18-IDEX-0001.

*Conflict of interest statement.* None declared.

## REFERENCES

1. Hanahan,D. and Weinberg,R.A. (2011) Hallmarks of cancer: the next generation. *Cell*, **144**, 646–674.
2. Macheret,M. and Halazonetis,T.D. (2015) DNA replication stress as a hallmark of cancer. *Annu. Rev. Pathol. Mech. Dis.*, **10**, 425–448.
3. Técher,H., Koundrioukoff,S., Nicolas,A. and Debatisse,M. (2017) The impact of replication stress on replication dynamics and DNA damage in vertebrate cells. *Nat. Rev. Genet.*, **18**, 535–550.
4. Dileep,V., Rivera-Mulia,J.C., Sima,J. and Gilbert,D.M. (2015) Large-scale chromatin structure–function relationships during the cell cycle and development: insights from replication timing. *Cold Spring Harb. Symp. Quant. Biol.*, **80**, 53–63.
5. Rivera-Mulia,J.C. and Gilbert,D.M. (2016) Replicating large genomes: divide and conquer. *Mol. Cell*, **62**, 756–765.
6. Ryba,T., Hiratani,I., Lu,J., Itoh,M., Kulik,M., Zhang,J., Schulz,T.C., Robins,A.J., Dalton,S. and Gilbert,D.M. (2010) Evolutionarily conserved replication timing profiles predict long-range chromatin interactions and distinguish closely related cell types. *Genome Res.*, **20**, 761–770.
7. Cornacchia,D., Dileep,V., Quivy,J.P., Foti,R., Tili,F., Santarella-Mellwig,R., Antony,C., Almouzni,G., Gilbert,D.M. and Buonomo,S.B.C. (2012) Mouse Rif1 is a key regulator of the replication-timing programme in mammalian cells. *EMBO J.*, **31**, 3678–3690.
8. Desprat,R., Thierry-Mieg,D., Lailler,N., Lajugie,J., Schildkraut,C., Thierry-Mieg,J. and Bouhassira,E.E. (2009) Predictable dynamic program of timing of DNA replication in human cells. *Genome Res.*, **19**, 2288–2299.
9. Hansen,R.S., Thomas,S., Sandstrom,R., Canfield,T.K., Thurman,R.E., Weaver,M., Dorschner,M.O., Gartler,S.M. and Stamatoyannopoulos,J.A. (2010) Sequencing newly replicated DNA reveals widespread plasticity in human replication timing. *Proc. Natl Acad. Sci. U.S.A.*, **107**, 139–144.
10. Ryba,T., Battaglia,D., Pope,B.D., Hiratani,I. and Gilbert,D.M. (2011) Genome-scale analysis of replication timing: from bench to bioinformatics. *Nat. Protoc.*, **6**, 870–895.
11. Dileep,V., Didier,R. and Gilbert,D.M. (2012) Genome-wide analysis of replication timing in mammalian cells: troubleshooting problems encountered when comparing different cell types. *Methods*, **57**, 165–169.
12. Marchal,C., Sasaki,T., Vera,D., Wilson,K., Sima,J., Rivera-Mulia,J.C., Trevilla-García,C., Nogues,C., Nafie,E. and Gilbert,D.M. (2018) Genome-wide analysis of replication timing by next-generation sequencing with E/L Repli-seq. *Nat. Protoc.*, **13**, 819–839.
13. Petryk,N., Kahli,M., d'Aubenton-Carafa,Y., Jaszczyszyn,Y., Shen,Y., Silvain,M., Thermes,C., Chen,C.L. and Hyrien,O. (2016) Replication landscape of the human genome. *Nat. Commun.*, **7**, 10208–10220.
14. Miura,H., Takahashi,S., Poonperm,R., Tanigawa,A., Takebayashi,S.I. and Hiratani,I. (2019) Single-cell DNA replication profiling identifies spatiotemporal developmental dynamics of chromosome organization. *Nat. Genet.*, **51**, 1356–1368.
15. Marchal,C., Sima,J. and Gilbert,D.M. (2019) Control of DNA replication timing in the 3D genome. *Nat. Rev. Mol. Cell Biol.*, **20**, 721–737.
16. Hiratani,I., Ryba,T., Itoh,M., Yokochi,T., Schwaiger,M., Chang,C.W., Lyou,Y., Townes,T.M., Schübeler,D. and Gilbert,D.M. (2008) Global reorganization of replication domains during embryonic stem cell differentiation. *PLoS Biol.*, **6**, 2220–2236.
17. Armstrong,R.L., Penke,T.J.R., Strahl,B.D., Matera,A.G., McKay,D.J., MacAlpine,D.M. and Duronio,R.J. (2018) Chromatin conformation and transcriptional activity are permissive regulators of DNA replication initiation in *Drosophila*. *Genome Res.*, **11**, 1688–1700.
18. Siefert,J.C., Georgescu,C., Wren,J.D., Koren,A. and Sansam,C.L. (2017) DNA replication timing during development anticipates

transcriptional programs and parallels enhancer activation. *Genome Res.*, **8**, 1406–1416.
19. Massey,D.J., Kim,D., Brooks,K.E., Smolka,M.B. and Koren,A. (2019) Next-generation sequencing enables spatiotemporal resolution of human centromere replication timing. *Genes (Basel)*, **10**, E269.
20. Krzywinski,M. and Altman,N. (2013) Error bars. *Nat Methods*, **10**, 921–922.
21. Afgan,E., Baker,D., Batut,B., Van Den Beek,M., Bouvier,D., Ech,M., Chilton,J., Clements,D., Coraor,N., Grüning,B.A. *et al.* (2018) The Galaxy platform for accessible, reproducible and collaborative biomedical analyses: 2018 update. *Nucleic Acids Res.*, **46**, W537–W544.

**A**

START-R

Workflow

# Welcome

DNA replication is a highly regulated process involved in maintaining of genome stability. It relies on a spatio-temporal program determining where and when replication starts along the genome. The replication timing (RT) program is finely tuned and reflects the high order organization of the metazoan genome. It is clear that this program evolves with cell differentiation and cell fate. Moreover aberrant DNA RT has been reported in many diseases including cancer.

The protocol developed to study the RT of a given cell type is well established. We have improved the method permitting analysis of RT of the entire genome in mammalian cells. We implemented two bioinformatic tools, START-R (Simple Tool for Analysis of Replication Timing with R) and START-R viewer. START-R written in R language, makes it possible to analyse the data from microarrays with five steps: normalization, smoothing, TTR (Timing Transition Region) and CTR (Constant Timing Region) detection and finally differential analysis. For each step, several options are available and selectable by the user. At the end, with a classical computer configuration, the analysis takes few minutes. START-R viewer is a tool that allows to visualize the data generated by START-R as does a genome browser. These softwares have a user-friendly interface requiring only a “simple click” and can be run under Windows, Mac OS X and Linux systems without virtual machine. The script will remain open to the scientific community so that the software can always be improved or developed.

Visit website !

This web application will allow you to enter the necessary informations for the analysis to run correctly. All the steps are organized in workflow. Each input is checked to avoid incorrect analyses.

Next

**B**

START-R

Workflow Initialisation

# Initialisation

## Organism

Two types of organisms can be studied in START-R

Human (hg18) No centromere Others (Human > hg19 or other species)

## Differential

Detect differences between 2 experiments

Yes No

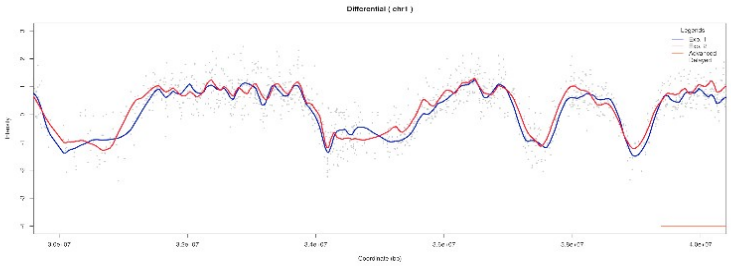

Prev. Next

**C**

START-R

Workflow | Initialisation | Import data

# Import data

In this step, you set up and select the files to import

## General parameters

**Column name of green signal :** gProcessedSignal

**Column name of red signal :** rProcessedSignal

**Early fraction**
- Cy3
- Cy5

**Late fraction**
- Cy3
- Cy5

## Select file

### Experiment 1

#### Replica 1

Browse... US92003687_252206079783_

Upload complete

**Header**
Yes No

**Separator**
Comma Semicolon Tab

**Quote**
None Double Quote Single Quote

**Number of microarray information lines to skip**
9

**Display**
Head More (100 lines) No

Preview

Show 25 entries

Search:

| FEATURES | FeatureNum | Row | Col | SubTypeMask | SubTypeName | Start | Sequence | ProbeUID | ControlType | ProbeName | GeneName | SystematicN |
|---|---|---|---|---|---|---|---|---|---|---|---|---|
| DATA | 1 | 1 | 1 | 0 | | 0 | | 0 | 1 | HsCGHBrightCorner | HsCGHBrightCorner | HsCGHBrightC |
| DATA | 2 | 1 | 2 | 0 | | 0 | | 1 | 1 | DarkCorner2 | DarkCorner2 | DarkCorner2 |
| DATA | 3 | 1 | 3 | 0 | | 0 | | 1 | 1 | DarkCorner2 | DarkCorner2 | DarkCorner2 |
| DATA | 4 | 1 | 4 | 0 | | 0 | | 1 | 1 | DarkCorner2 | DarkCorner2 | DarkCorner2 |
| DATA | 5 | 1 | 5 | 0 | | 0 | | 1 | 1 | DarkCorner2 | DarkCorner2 | DarkCorner2 |
| DATA | 6 | 1 | 6 | 0 | | 0 | | 1 | 1 | DarkCorner2 | DarkCorner2 | DarkCorner2 |

FEATURES | FeatureNum | Row | Col | SubTypeMask | SubTypeName | Start | Sequence | ProbeUID | ControlType | ProbeName | GeneName | SystematicN

Showing 1 to 6 of 6 entries

Previous 1 Next

#### Replica 2

Browse... No file selected

Preview

**Display**
Head More (100 lines) No

**Header**
Yes No

**Separator**
Comma Semicolon Tab

**Quote**
None Double Quote Single Quote

**Number of microarray information lines to skip**
9

D

START-R

Workflow | Initialisation | Import data | Normalisation

# Normalisation

In this step, you can choose the types of normalizations you want to apply to your data.

## Intra array

Correction of global intensities in a microarray.

### Methods

- (●) loess
- ( ) control
- ( ) composite
- ( ) printtiploess
- ( ) median
- ( ) none
- ( ) robustspline

### Description

The loess normalization methods ("loess", "printtiploess" and "composite") were proposed by Yang et al (2001, 2002). Smyth and Speed (2003) review these methods and describe how the methods are implemented in the limma package, including choices of tuning parameters. More information on the loess control parameters span and iterations can be found under loessFit.

## Inter replica

Standardization of replicates to make them comparable.

### Methods

- (●) scale
- ( ) quantile
- ( ) none
- ( ) cyclicloess

### Description

Scale (method='scale') scales the columns to have the same median.

## Inter experience

With START-R, it is possible to compare two experiences. However, from one microarray to another, the quantity of material deposited or the quality of marking may differ. In order to make the most accurate comparisons possible, a standardization between the data from the two experiments is proposed in order to limit this type of experimental bias.

### Methods

- (●) standardization
- ( ) without normalization
- ( ) unitization

### Description

(x-mean)/sd

Prev. Next

**E**

START-R

Workflow | Initialisation | Import data | Normalisation | Analysis

# Analysis Parameters

In this step, you can set up the different steps of the analysis.

| Steps | Objective | Method | Method description | Additional options |
|---|---|---|---|---|
| **Smooth** | The smoothing step will generate a curve that will try, depending on the algorithm used, to be the most representative of this cloud of points. Once again, START-R allows the user to choose several smoothing functions. | Loess | Fit a polynomial surface determined by one or more numerical predictors, using local fitting. | **Span :** The parameter alpha which controls the degree of smoothing.Fitting is done locally. That is, for the fit at point x, the fit is made using points in a neighbourhood of x, weighted by their distance from x (with differences in 'parametric' variables being ignored when computing the distance). The size of the neighbourhood is controlled by alpha (set by span or enp.target). For alpha < 1, the neighbourhood includes proportion alpha of the points, and these have tricubic weighting (proportional to (1 - (dist/maxdist)^3)^3). For alpha > 1, all points are used, with the 'maximum distance' assumed to be alpha^(1/p) times the actual maximum distance for p explanatory variables. 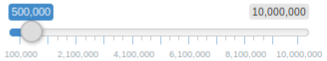  |
| **TTR** | The curves obtained, after smoothing from DNA chip data, show 'flat' areas that replicate either early or late, called CTRs for Constant Timing Regions. Between an early and a late zone, there is a transition zone called TTR for Timing Transition Region. | | | |
| **Segmentation** | Detection of Constant Timing Regions with TTR information | | | **Standard deviation:** The number of SDs between means to keep a split 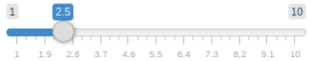  |
| **Fusion** | Combine result of TTR and CTR | | | |

Prev. Next

F

START-R

Workflow | Initialisation | Import data | Normalisation | Analysis | Outputs

# Outputs

## File Outputs (positions,intensity,...)

- .bed
- .txt
- both

## Graphical outputs

- Yes
- No

Prev. Next

G

START-R

Workflow | Initialisation | Import data | Normalisation | Analysis | Outputs | Summary

# Summary

## General informations

Organism : Human
Differential : No

## Selected Files

### Experience 1

Replica 1

File name : US92003687_252206079783_S01_CGH_1105_Oct12_1_1.txt

Replica 2

File name :

### Experience 2

Replica 1

File name :

Replica 2

File name :

## Normalisation

Intra array : loess
Inter replica : scale
Inter experience : n1

## Analysis

### Smooth

Realiazed? : TRUE
Method : Loess
Span : 500000

### TTR

Realiazed? : TRUE

### Segmentation

Realiazed? : TRUE
SD : 2.5

### Differential

Realiazed? : FALSE
Method : Mean method
PVT : 0.05
Method adjustment PV : holm
Empirical threshold: 0.45
Overlap: 30
Windows size: 60

## Outputs

File format : both
Graphical : Yes

Prev. | Validate

**H**

START-R

Workflow Initialisation Import data Normalisation Analysis Outputs Summary Job

Click to run analysis

Run !

**I**

START-R

Workflow Initialisation Import data Normalisation Analysis Outputs Summary Job

Processing

**J**

START-R

Workflow Initialisation Import data Normalisation Analysis Outputs Summary Job

The analysis was successful!

**K**

START-R
<Viewer/>

**Choose CSV File**

Browse... chr9.SRV

Upload complete

Load data

## Data informations

Organism : Human
Chromosome : chromosome 9
Method differential : Mean method
# of advanced : 0
# of delayed : 0

Smooth method : Loess
Normalisation intra : loess
Normalisation inter replicas : scale
Normalisation inter experiences : standardization

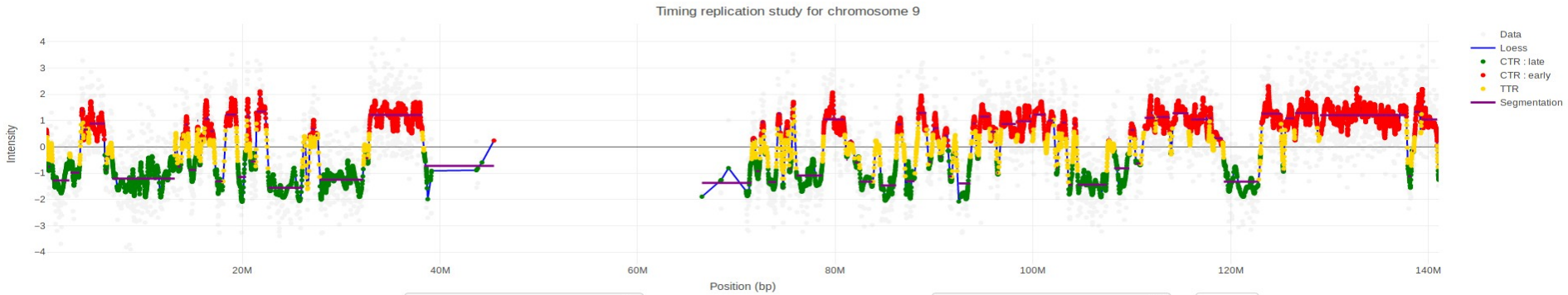


Start of the viewing window 204193 End of the viewing window 141018925 Change

## Customization

| Data | Smooth | CTR : late | CTR : early | TTR | Segmentation |
|---|---|---|---|---|---|
| #CCCCCC | #0000FF | #00FF00 | #FF0000 | #FFD700 | #8B008B |

Change

## General informations about chromosome 9

General informations about chromosome 9

**Select general information to plot:**

- None
- Data intensity
- CTR/TTR boxplots

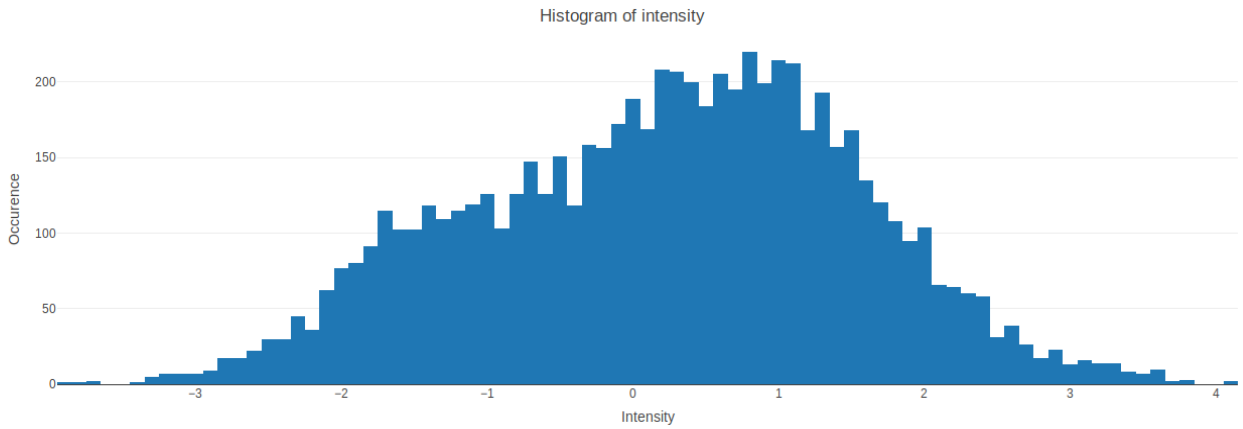

**Supplementary Figure S1: Screenshots showing the web-based user-friendly interface of START-R Analyzer and START-R Viewer.**

A) START-R Analyzer homepage.

START-R Analyzer is designed to analyze RT data with 5 steps: normalisation, smoothing, TTR and CTR detections and differential analysis. Several options are available and can be selected by the user for each step. All the steps are organized in workflow with a "Next" button allowing the user to access the next page. Each input is checked to avoid incorrect analyses. A link to the website containing precisions on the START-R Analyzer protocol and START-R Viewer use is available in this homepage (https://thomasdenecker.github.io/START-R/).

B) Organism and differential analysis selection.

The initialisation step consists in choosing the analyzed organism which can be either Human (for microarray data obtained with the hg18 genome assembly), or No centromere (for example for Drosophila genomic data) or Others (for human data obtained with a genome assembly higher than hg19 or for other species). We have to note that it's also possible to upload a file containing the centromeres coordinates for non mammalian organisms. The user has then to choose to perform a differential analysis or not. "Prev" and "Next" buttons allow the user to move forward or backward within START-R Analyzer.

C) Upload of intensity files.

The user has first to set up the general parameters for the Early and Late replicating fractions, by choosing the column names of the files for the green and red signals and attributing the Cy3 or Cy5 dye to the Early or Late fractions. The selected files for the analyses are imported and should be in txt format. A format compatible with START-R Analyzer can be obtained for NGS data by using a script available on GitHub in the "supplement script" file (convert_bamcoverage_file.R). The user can choose several options concerning the imported files as the presence of a header, the kind of separator, the presence of a quote in the file, the number of information lines to skip before launching the analysis and the display of a part of the loaded files.

D) Selection of intra-array, inter-replicate and inter-experiment normalisation algorithms.

The next step is the choice of the normalisation's algorithms that the user wants to apply to the data. For each method available for each step of the normalisation (intra array, inter replica and inter experience), a short explanation of the method will be displayed on the screen when checked by the user.

E and F) Selection of differential analysis settings and output files.

The set up of the analysis parameters is next chosen by the user. For each step, the objective of the analysis is described beside. The smoothing method is chosen with a drop-down menu and a short description of the method is displayed on a dialog box. An additional option allows to fix the span to control the degree of smoothing. The second step is the TTR detection which is followed by the segmentation step to detect the CTR. The user can then adjust the standard deviation if wanted. The last step is the fusion that will combine the results of the TTR and CTR detections.

The file and graphical outputs are then selected by the user.

G) Validation of the analysis summary.

The user can click to the “Validate” button after checking the summary of the START-R analysis. The “Prev” button allows to get backward inside the software if needed.

H, I and J) The analysis running sections. The user just has to click on the “Run” button to launch the analysis, which will be processed in around 15 minutes. A green check mark will appear on the screen when the analysis is performed. When an analysis is done with START-R analyzer, all results for this analysis are available in the folder START-R_analyzer/Outputs. The folder name begins with the date of analysis and successive numbers (the first analysis will be named 20200511_1, the second analysis 20200511_2 …). A summary of the analysis can be found in the codebook.txt file. This software offers several types of outputs to evaluate the results. Text outputs are in bed format. The BED format consists of one line per feature, each containing 3-12 columns of data, plus optional track definition lines. The first three fields in each feature line are required: chrom (name of the chromosome or scaffold), chromStart and chromEnd (start and end position of the feature in standard chromosomal coordinates). With bed files outputs, START-R results can be integrated in Galaxy workflow to perform further analyses. Galaxy is an open source web-based platform for data intensive biomedical research.

K) START-R Viewer interface allowing the START-R Analyzer files to be uploaded and the RT profile to be visualized for each chromosome with general information about each chromosome.

START-R Viewer allows the visualization of the analyzed data for each chromosome as a genome browser. After the analysis, the user can find different informations in the Differential file or in the Experience 1 file from the output folder, depending of the type of analysis performed by START-R (differential analysis or not). Files showing the analysis for each chromosome are available in pdf format. The user can also find a file containing differential percentage for each chromosome and a file named differential_position in txt format showing for each RT changing region its location on a specific chromosome with its associated chromosome coordinates chromStart, chromEnd and its Status (advanced or delayed). A viewer folder containing the results for each chromosome allows to upload files in Javascript and SRV format for a visualization on START-R viewer. A summary of the analyses done with START-R Analyzer is displayed nearby the load data button. The RT profile of the selected chromosome is displayed in a dynamic chart showing the distribution of RT intensities along the chromosome, with positives intensities displaying early replicating regions and negative ones displaying late replicating regions. Early and late CTRs appear in red and green, respectively and TTRs in yellow. Segments corresponding to regions of constant timing are shown in purple. Grey spots indicate data from the RT experiment and the blue line depicts the smooth method used for the analysis. START-R viewer offers a dynamic exploration for each chromosome with the Plotly library. This dynamic chart gives the user the possibility to zoom in the chart by selecting a shorter window on the chart as in a genome browser or by indicating the chromosome coordinates in the viewing windows and clicking on the “Change” button. The user can also select the curves displayed in the chart directly by clicking on the chart or by selecting the curves in the Customization dialog box and eventually take pictures of the chart.

General information about the chromosome can be chosen in the “Select general information to plot” dialog box, like the histogram of intensity, showing the occurrence versus the intensity of the RT signal. We can note that the intensity of the signal is mostly distributed between -2 and +2, corresponding to late and early replicating regions, respectively. The user can also display the box plot of CTR/TTR intensity.

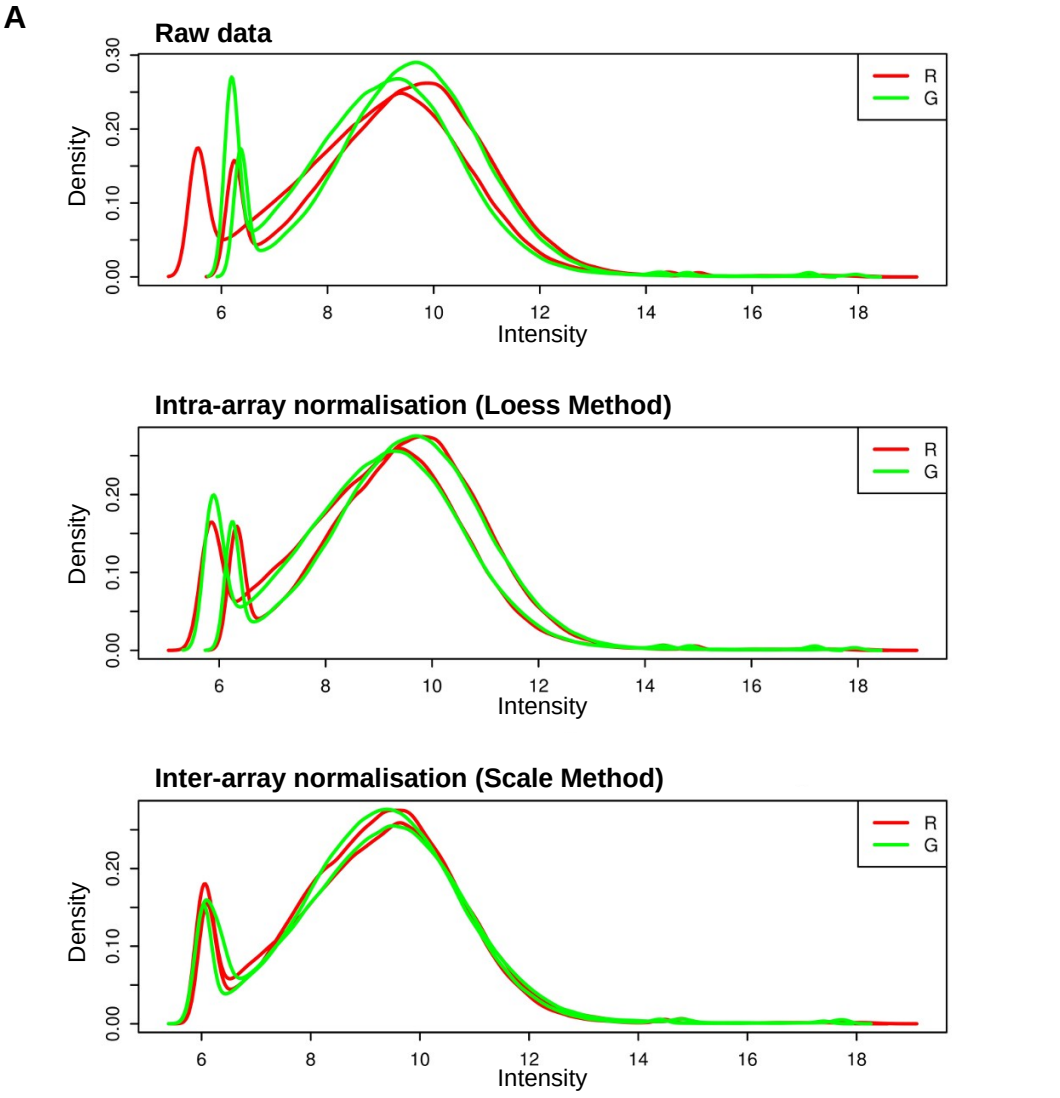


**Supplementary Figure S2: Normalisation and smoothing of the chip data.**
A) Normalisation of the chip data. Graphs depicting the distribution of log ratio intensities of Cy3 and Cy5 shown in red (R) and green (G), for 2 replicas before (raw data) and after intra-array normalisation with the Loess method, and inter-array normalisation with the scale method. B) Smoothing of the normalized data obtained by chip. Smoothing was applied on the normalised data to generate the most representative curve of the distribution of dots using either the Loess method based on linear regression or the Triangular method using a moving mean with overlapping windows.

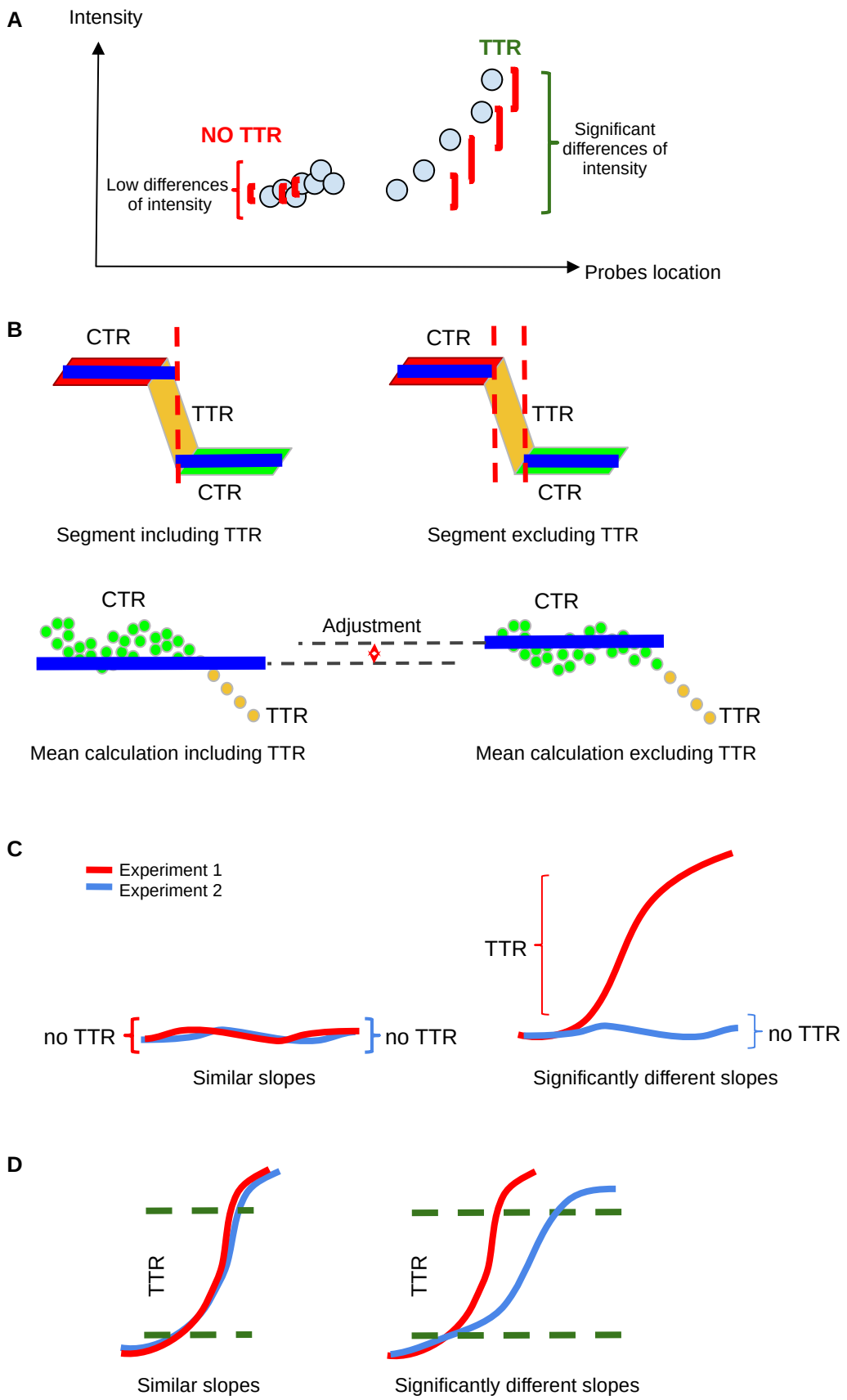


**Supplementary Figure S3: TTR detection.**
A) Diagram showing that a TTR is defined by significant differences of intensity of at least 3 consecutive adjacent probes. B) Schemes representing how CTRs are precisely defined by subtraction of the TTR. The calculation of the mean for the CTR region, excluding the TTR, allows an adjustment for the segment value and a more precise characterization of this domain. C) Drawings illustrating the comparison of the slopes for two experiments (red and blue lines) to detect the presence of TTR D) Diagrams illustrating differences between the slopes of two TTRs for two experiments.

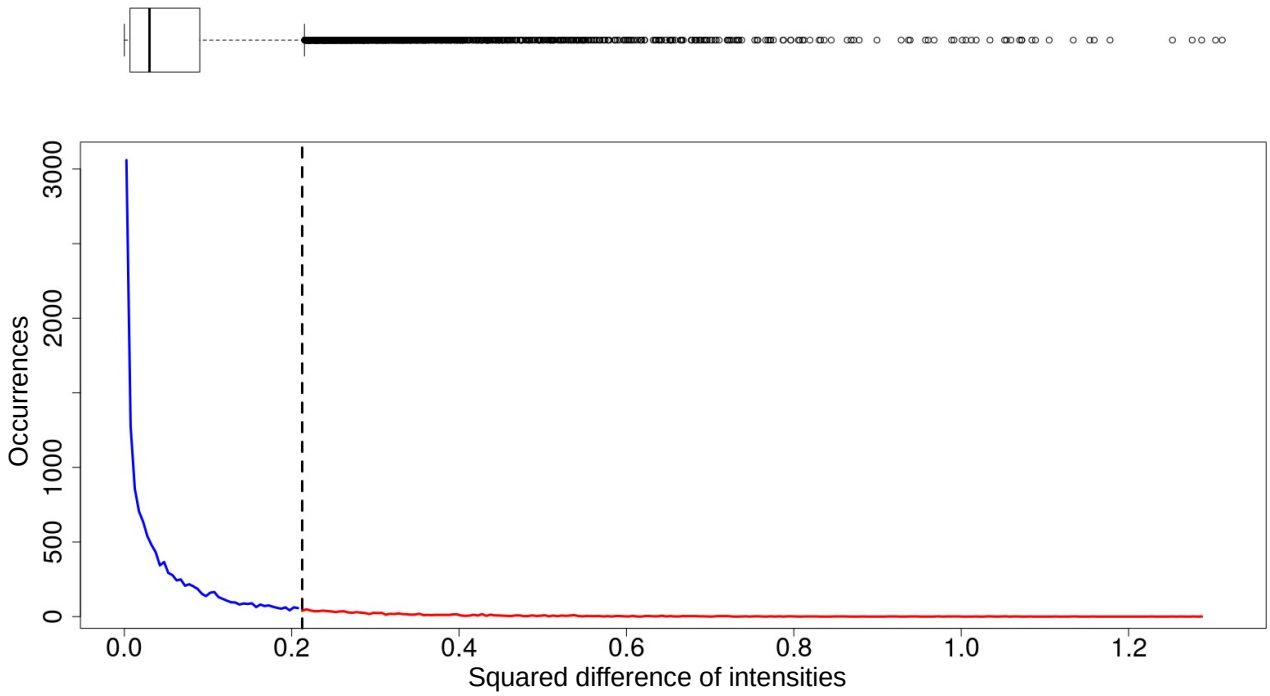


**Supplementary Figure S4: Boxplot of squared difference of intensities computed by the Euclidean method.**
Squared differences of the log2(Early/Late) for the same probes for two different experiments are plotted in a boxplot. The outliers (open circles) are significantly different and correspond to the red line in the graph depicting the squared difference of intensities versus their occurrences in the boxplot.

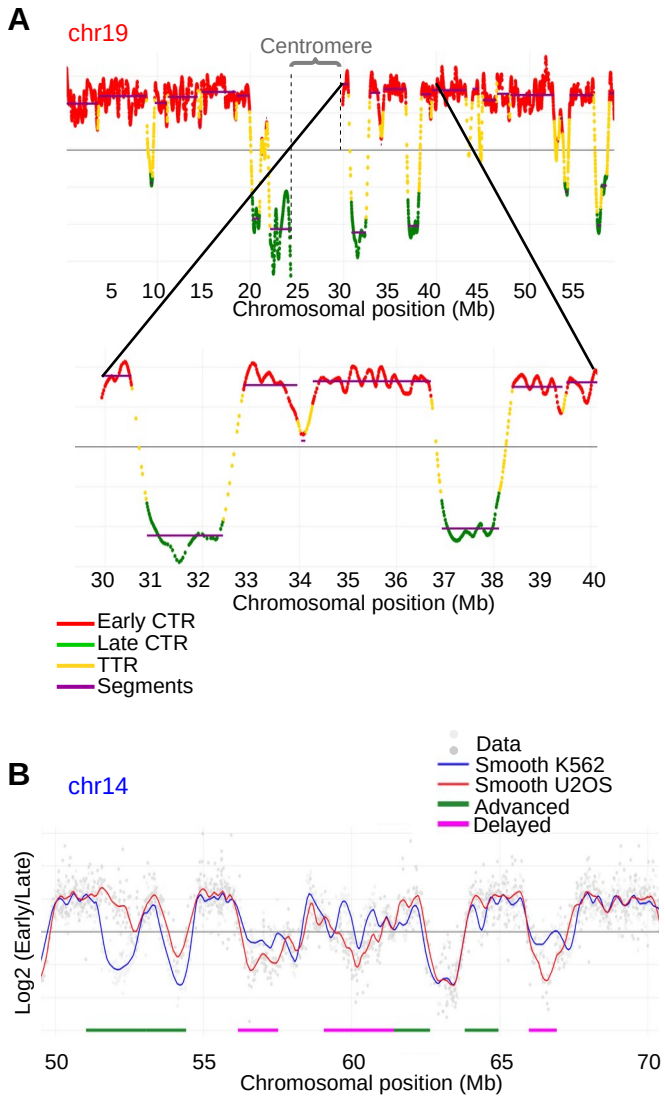


**Supplementary Figure S5 : Examples of data generated with our RT protocol visualized by START-R-Viewer.**

A) START-R Viewer allows visualizing RT data with many features. The top panel displays the distribution of early and late constant timing regions (CTR, in red and green, respectively) and of transition timing regions (TTR, in yellow) on a portion of human chromosome 19. Segments corresponding to regions of constant timing are shown in purple. Chromosome 19 centromere is indicated by grey dashed lines and a curly bracket. The bottom panel displays a zoom of a smaller region of chromosome 19 where timing profile can be seen through the zoom option of START-R-Viewer. B) Differential analyses are done on a portion of human chromosome 14 comparing RT profiles of two cell lines: K562 in blue and U2OS in red. Advanced (green) and Delayed (pink) regions are identified with START-R Analyzer using the mean comparison analysis with the Holm's p-value correction and a limit corrected p-value of 0.05. Light grey and grey spots indicate data from both RT experiments.

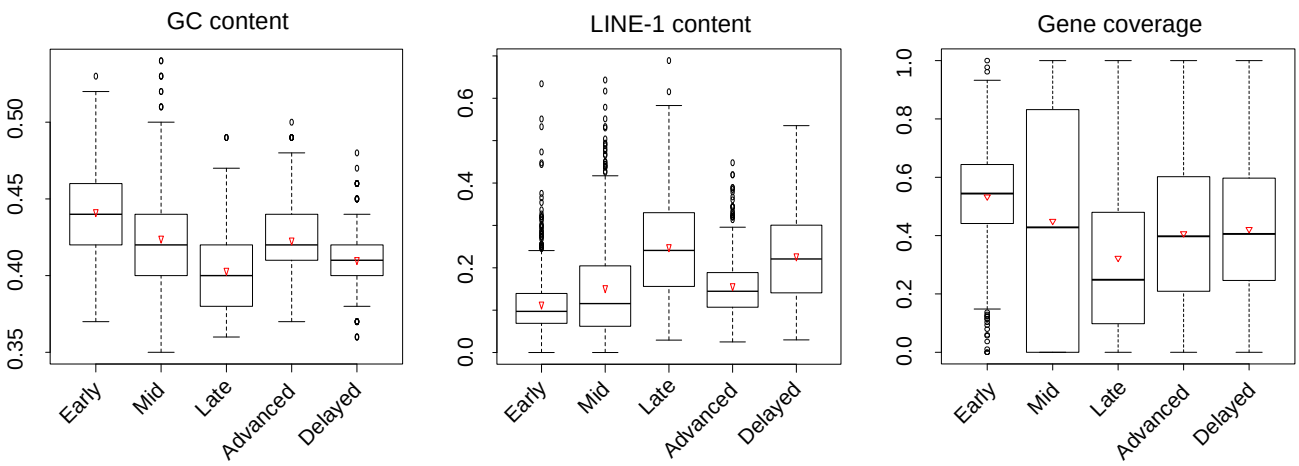


**Supplementary Figure S6: Genomic characteristics of regions harboring different replication timing programs.**

Using START-R Analyzer with the standard options, 2,066 CTRs were detected in the genome and 910 regions showed a different replication timing between D3esc and D3npc9 cells. A portion of chromosome 7 is depicted in Figure 2. START-R Analyzer automatically generates BED files that can be imported into a GALAXY session in order to generate complementary results by using the "Coverage of a set of intervals on second set of intervals" software. Boxplots illustrating differences in GC content, LINE-1 content and gene coverage between Early, Mid and Late replicating regions are shown. The two other categories show the characteristics of Advanced and Delayed regions. For each category, the mean value is indicated by an open red triangle. The band at the middle of the box indicates the median value. The bottom and top of the box are the 25$^{th}$ and 75$^{th}$ percentiles. Bottom and top whiskers represent the limits with exclusion of outliers (open circles). Advanced regions showed a GC/LINE-1 density and gene coverage similar to constant early regions, while Delayed regions showed GC/LINE-1 density and gene coverage similar to constant late regions. The genomic regions detected with the START-R suite showed the same specific molecular signatures as the ones previously described in Gilbert's laboratory. Unfortunately, we cannot compare the regions that we have identified with START-R with those previously discovered, since the article of Hiratani *et al* does not mention the genome coordinates.

# III. Improvement of abemaciclib effects in combination with autophagy inhibitors

## III.A Article (On-going)

### Introduction

The pRB pathway controls cellular progression during the G1-phase of the cell cycle, following growth factors stimulation of Cyclin D synthesis and its association with cyclin-dependent kinases CDK4/6 that phosphorylate Retinoblastoma-associated protein (pRB). Later on, CDK2 associated with Cyclin E completes the phosphorylation of pRB thus dissociating it from transcription factor E2F. Free E2F can activate its targets and allow entry into the S-phase of cell cycle (Bracken *et al.*, 2004). Recently, the inhibitors of CDK4/6 palbociclib, ribociclib and abemaciclib have been introduced in the treatment of HR+ HER2- metastatic breast cancers, usually in association with endocrine therapy (Goel *et al.*, 2018). However, loss of *RB1* gene in triple negative breast cancer cells is a relatively frequent mechanism of resistance to inhibitors of CDK4/6 (Knudsen and Zacksenhaus, 2018). Recently, it has been shown that only abemaciclib shows a cytotoxic effect on different Rb negative cancer cell lines at relatively high concentration and induces an atypical cell death through lysosomal dysfunction (Hino *et al.*, 2020). Chloroquine, a well-known drug used as an antimalarial and anti-inflammatory agent, is able to inhibit autophagosome-lysosome fusion, thus impairing cellular autophagy (Mauthe *et al.*, 2018). Thus, we reasoned that affecting the lysosomal function with two drugs that have different mechanisms of action.

In this paper we studied the combined effects of Chloroquine and Abemaciclib on pRb-deficient cancer cell lines, in which abemaciclib activity is unrelated to inhibition of RB/E2F regulated genes. We observe that the low-dose combination of these two drugs induces classical cell death through apoptosis in pRb-deficient cancer cells. Taken together, these results open the possibility of a novel therapeutic treatment for Rb-deficient tumors.

### Materials and methods

*Cell cultures*

The NCI-H295R (ATCC® CRL-2128TM) cell line from ATCC was cultured in Dulbecco's Modified Eagle Medium (DMEM) / Nutrient mixture F-12 Ham (1 :1) supplemented with GlutaMAX -I (LifeTechnologies, 31331-028), 2.5% Nu-Serum™ (Corning), 1:100 Insulin-Transferrin-Selenium Premix (Corning, 354350), 100 U/mL penicillin and 100 µg/mL streptomycin (Life Technologies, 15140122). They were seeded at a density of 50,000 cells/cm$^2$ for all experiments.

MDA-MB-468 cell line was cultured in Dulbecco's Modified Eagles Medium (DMEM) with 4.5 g/L D-glucose, L-glutamine and pyruvate (Thermo Fisher Scientific, Life Technologies, 41966-029) supplemented with 10% Fetal Bovine Serum, 100 U/mL penicillin and 100 µg/mL streptomycin (Life Technologies, 15140122). They are plated at a density of 20,000 cells/cm$^2$ for all experiments.

Cells were cultured in a humidified incubator with 5% $CO_2$. 24 hours after plating, cells were treated with palbociclib, ribociclib or Dimethyl sulfoxide (DMSO) during 96 hours or 48 hours for NCI-H295R and MDA-MB-468 cell lines, respectively. Palbociclib (PD-0332991, A8316) and Ribociclib (LEE-011, A8641), were purchased from CliniSciences. Palbociclib and Ribociclib 2mM stock solutions were prepared in DMSO. Chloroquine (C6628, Sigma) was prepared in water.

*Analysis of cellular viability*

After treatment, viability was measured using the CellTiter-Glo® Luminescent Cell Viability kit (Promega), following the manufacturer's instructions. Luminescence was measured with a SpectraMax i3 Multi-Mode Microplate Detection Platform (Molecular Devices, Sunnyvale, CA, USA). Assays were performed in duplicates, in three independent experiments.

*Apoptosis analysis*

Apoptosis was measured using the Caspase-Glo 3/7 Assay system (#G8090, Promega) as recommended by the manufacturer. Luminescence was measured with a SpectraMax i3 Multi-Mode Microplate Detection Platform (Molecular Devices, Sunnyvale, CA, USA). Assays were performed in duplicates, in two independent experiments.

## Results

Chloroquin potentiates the effects of abemaciclib on the viability of pRB-negative cells

In order to assess the impact of sole drug on the viability of cells, we treated cells either abemaciclib or chloroquine in two cell lines (MDA-MB-468 and NCI-H295R). We then determined the curves of cellular viability by increasing doses. As expected, these two pRb deficient cell lines show resistance up to 1µM of abemaciclib which is generally considered as an inhibitory dose. However, abemaciclib impacts on the viability at higher concentrations in both cell lines. Of note, MDA-MB-468 cells are more sensitive to Abemaciclib than NCI-H295R cells (IC50 MDA-MB-468 2.64 µM; IC50 NCI-H295R 12.61 µM) (Figure 1). Similarly, sensitivity to the autophagy inhibitor Chloroquine (CQ) was also higher in MDA-MB-468 cells than in NCI-H295R ones (IC50 MDA-MB-468 14.06 µM, IC50 NCI-H295R 42.49 µM).

With the aim to find combinations having synergistic effects on the viability of cells, we then tested several combinations of co-treatments with two drugs in different concentrations. When MDA-MB-468 cells are treated with 1µM of abemaciclib showing no impact on the viability of cells, in combination with 14µM of chloroquine, we detected that the cell viability is close to 0% (Figure2). Also, 5µM Abemaciclib resulted in a reduction of viability close to 0 % when combined to 25 µM CQ in NCI-H295R cells. Altogether, these experiments show that CQ potentiates Abemaciclib impact on cell viability of the pRB-negative MDA-MB-468 and NCI-H295R cells.

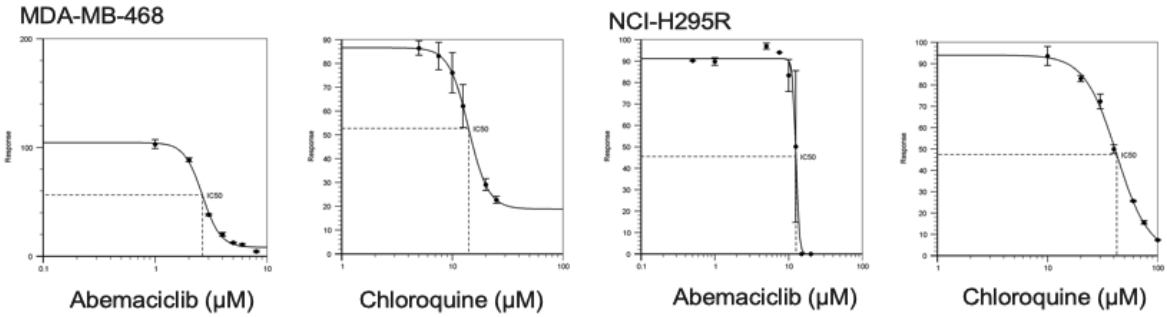


| MDA-MB-468 | IC30 | IC50 | IC70 |
|---|---|---|---|
| Abemaciclib (µM) | 2.34 | 2.64 | 3.31 |
| Chloroquine (µM) | 11.16 | 14.06 | 19.6 |

| NCI-H295R | IC30 | IC50 | IC70 |
|---|---|---|---|
| Abemaciclib (µM) | 11.86 | 12.61 | 13.08 |
| Chloroquine (µM) | 31.84 | 42.49 | 47.86 |

**Figure 1.** Impact of Abemaciclib and Chloroquine on MDA-MB-468 and NCI-H295R cellular outgrowth. Upper panels: dose-response curves; viability was estimated after 48h treatments with either Abemaciclib or Chloroquine. Lower panels: half maximal Inhibitory Concentration (IC50), IC30 and IC70 that were estimated from viability assays.

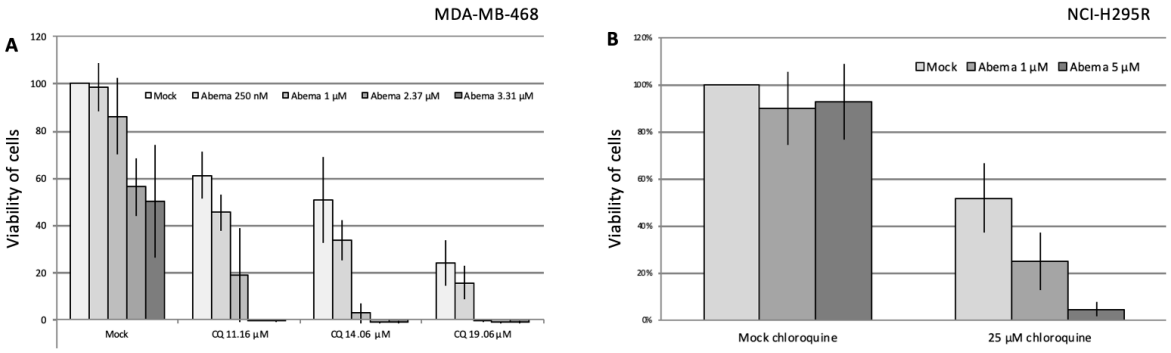


**Figure 2**. Impact of co-treatments of Abemaciclib and Chloroquine on MDA-MB-468 (A) and NCI-H295R (B) cellular viability. Viability assay was performed after 48h treatment with drugs.

<u>Combination of Abemaciclib and Chloroquin induces apoptotic cell death</u>

To explain the reduced viability in co-treated cells, caspase3/7 activity was assessed after the treatment with Abemaciclib, alone or in combination with CQ. When MDA-MB-468 cells were treated with 1 µM Abemaciclib or 14.06 µM CQ alone, Caspase 3/7 activity remained unchanged. However, combination of 1 µM Abemaciclib with 14.06 µM CQ significantly increased this activity (Fig3). In the same way, the sole treatment with 5 µM Abemaciclib or 25 µM CQ shows no effect in activity of caspase3/7 whereas the co-treatment increases 5 times of caspase activity. These results suggest that potentiated effects of abemaciclib combined with CQ are mediated by apoptosis, resulting in cell death.

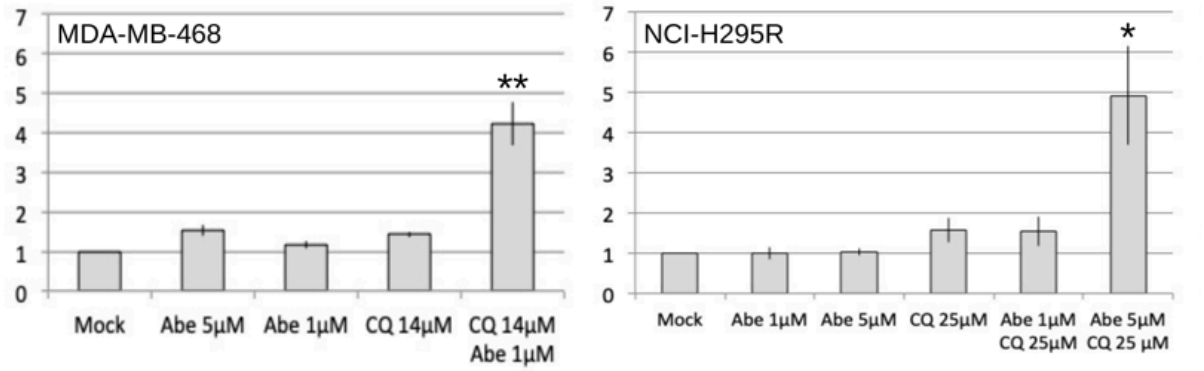


**Figure 3**. Impact of Abemaciclib and Chloroquine on MDA-MB-468 and NCI-H295R cellular apoptosis. Apoptosis assay was performed after 48h treatment with drugs. Apoptosis assay is based on the detection of caspase-3/7 activity through the measure of a luminescent product. Y-Axes: mean of measured luminescence within each condition, reported to the respective mock. Asterisks indicate the significance of Student's *t*-test: * *p*-value<0.05, ** *p*-value<0.01.

## Discussion

We demonstrated that abemaciclib in combination with chloroquine reduces more efficiently the viability of pRB deficient cells by apoptosis. This on-going project envisage to demonstrate if these synergetic effects are mediated by autophagy. Many evidences illustrated that abemaciclib has other targets than CDK4/6, which will impact cellular metabolism in a pRb independent manner. For instance, it has been reported that CDK4/6 inhibitors induce autophagy in several cancer cell lines. In this context, autophagy inhibitors such as chloroquine and Spautin-1 have been combined with CDK4/6 inhibitors and have been shown to have synergistic effects in breast and gastric cancer cell lines (Valenzuela *et al.*, 2017; Vijayaraghavan *et al.*, 2017). Following this point of view, we will study the induction of autophagy by measuring indicative markers such as monodansylcadaverine (MDC) or LC3A/B and p62 level in cells treated with abemaciclib alone or in combination with autophagy inhibitors. In this work, we have shown that autophagy inhibitors potentiate the actions of abemaciclib. The next step is to propose this combination of drugs to enhance the efficacy and to reduce the eventual toxicity of abemaciclib to treat cancer patients.

# Conclusion

My study comprises 3 projects with the aims of understanding actions of CDK4/6 inhibitors.

The first chapter describes anti-proliferative effects of CDK4/6 relative to the presence of pRb in ACC. Analysis of transcriptomic data allowed us to identify different sub-groups of ACC with one group in which CDK6 is revealed as a biomarker. Then we validated that CDK4/6 inhibitors efficiently induce cellular senescence in a pRb proficient ACC cell line (SW-13) but not in a pRb deficient cell line (NCI-H295R). Our findings propose CDK4/6 inhibitors as a new treatment of ACCs that are considered as aggressive cancers and have for now limited options of treatments. During this project, we highlighted some evidence showing that palbociclib induced a reduction in the viability of pRb deficient cells coupled with aberrant cell cycles. These observations drive us to characterize the actions of palbociclib in a pRb negative context.

In the second chapter, we particularly studied the effects of palbociclib on the dynamics of DNA replication using two pRb deficient cell lines (MDA-MB-468 and NCI-H295R). The analysis of the temporal program allows us to visualize how palbociclib disrupts DNA replication at the whole genome scale. The DNA fibers assay brings us a profound comprehension of the progression of replicating forks and the efficacy of origins at a molecular level. We found that palbociclib impairs the origin firing step of replication initiation by down regulating the expression of genes encoding proteins of the pre-IC.

Finally, the third chapter about an ongoing project shows the effects of abemaciclib in combination with other drugs that inhibit autophagy on pRb deficient cell lines. The co-treatment with abemaciclib and chloroquine shows synergistic effects on cellular viability of the two pRb deficient cell lines that we particularly studied (MDA-MB-468 and NCI-H295R). This indicates that the action of abemaciclib is not mediated by the presence of pRb. We also demonstrated that this combination induces cell death by apoptosis at low doses of each drug. The findings could further encourage abemaciclib in combination with chloroquine for the treatment of cancer.

# Discussion and perspectives

*Characteristics of pRb loss cancer*

In the "palbociclib and DNA replication" chapter, I highlighted the effects of palbociclib beyond the presence of pRb using two pRb deficient cell lines, MDA-MB-468 and NCI-H295R, which are respectively derived from Triple negative breast cancer and Adrenocortical carcinoma. Both harbor a large deletion in *RB1* gene (Bookstein *et al.*, 1989; Ragazzon *et al.*, 2014), resulting in the loss of function of pRb. pRb loss is frequently observed in several cancers. It was reported that about 75 % of Small Cell Lung Cancer harbor mutations in *RB1* gene (Bhateja *et al.*, 2019). In hepatocellular carcinoma, a loss of chromosome 13 is observed in about 30% of the patients and this deleted region commonly includes *RB1* locus at 13q14 (Laurent-Puig and Zucman-Rossi, 2006). In particular, Triple negative breast cancer exhibits about 40% of incidence for pRb loss compared to other subtypes of breast cancer only showing 2-3% of loss (Treré *et al.*, 2009).

On one hand, cells exhibiting loss of pRb have common features: deregulated E2F activity, overexpression of *CDKN2A* encoding p16 and diminished amount of Cyclin D (Witkiewicz and Knudsen, 2014). These characteristics could provide advantages for cancer cells to proliferate in an uncontrolled manner, which contribute to the development of tumors. Thus, the resistance to anti-proliferative effects of CDK4/6 inhibitors is associated with the absence of pRb, the overexpression of p16 and small amounts of CyclinD, which makes cells independent toward the CDK4/6 pathway. (Lin and Scott, 2012). Thus, another study showed that the palbociclib treatment could neither reduce the phosphorylation of p107 nor of p130 in pRb deficient Hep3B cells (Lin and Scott, 2012). A recent study also demonstrated that CDK4 is not activated in pRb deficient cells due to its absence of phosphorylation at the T172 amino acid in T-loop (Raspé *et al.*, 2017). Finally, all these findings suggest the absence of functional CDK4/6 in pRb deficient cells.

On the other hand, cells with pRb loss exhibit intrinsic genome instability. Interestingly, the two pRb deficient cell lines we studied harbor mutation in the *TP53* gene. MDA-MB-468 cells possess only one copy of *TP53* gene (hemizygous) with a missense mutation (R273C).

NCI-H295R cells have a homozygous deletion of exons 8 and 9 in the *TP53* gene, which makes the protein nonfunctional (Sampaoli *et al.*, 2012). The mutation of Tp53 provides cancer cells to survive by escaping from the DNA damage response control despite the instability of the genome. Using a RNA interference approach, a study demonstrated the pro-survival effects of TP53 mutants (Lim *et al.*, 2009; Casey G et al., 1991). Moreover, this mutated TP53 is not able to bind to RAD51, which contributes to the instability of the cells (Rasti and Azimi, 2015).

In this perspective, palbociclib can be proposed as a potential treatment for cancer with the aim of exacerbating the instability of the genome and of rendering cancer cells more vulnerable to replicative stress. We can consider that palbociclib might be used for patients with pRb deficient cancer combined with other therapeutic molecules that target the replicative response pathway even though the concentration of palbociclib used is high relative to the specific inhibitory dose. These effects could be potentialized in combination with other drugs targeting the vulnerability of pRb loss in cancers that already exhibit some instabilities of their genome. The findings are significant for a potential use of palbociclib in pRb deficient cancers. This study provides for the first time an extensive understanding of additional effects of palbociclib in a pRb negative context and proposes palbociclib as a new drug targeting the vulnerability of the genome in cancer deficient for pRb.

*Effects of CDK4/6 inhibitors outside of the pRb pathway.*

My work reveals here an unexpected result demonstrating that palbociclib has cytotoxic effects and impairs DNA replication in pRb deficient cells. Indeed, these effects may not be observed in pRb proficient cells because CDK4/6 inhibitors efficiently target the canonical pRb-E2F pathway, inducing cellular senescence. Indeed, considering that pRb plays a central role in the cell cycle progression as a major downstream target of CDK4/6, many studies including ours have focused on the anticancer effects of CDK4/6 inhibitors in pRb proficient cells. However, no more cells are observed in S-phase in this context. Furthermore, pRb proficient cells do not exhibit the intrinsic instability of the genome present in pRb loss context, implying that the effects could be only observable in pRb deficient cells. Finally, we applied a relatively high dose of palbociclib that exceeded the required concentration for canonical inhibitory actions. Actually, due to their narrow specificity for CDK4 and CDK6, these inhibitors are highly dependent on the presence of pRb if they are used at low

concentrations around 1μM which is defined as the specific inhibitory dose. Hence, it could be worthy to evaluate the effects of inhibitors in pRb independent manner.

*How can I explain the results mechanistically?*

Keeping in mind these particularities of our study, I would speculate on two scenarios which could explain our findings either by indirect effects of palbociclib by a change in the conformation of the CDK4/6-cyclinD complex or by effects of palbociclib on off-target at high dose.

First, some studies showed that CDK4/6 inhibitors may have "non-canonical" mechanisms of actions on CDKs. A study has shown that palbociclib efficiently inhibits the activity of CDK4/6 but paradoxically stabilizes CyclinD3 bound to CDK4/6 (Paternot *et al.*, 2014). Strikingly, this complex has been found to be devoid of p21 and p27 kinase inhibitors. Moreover, a recent study revealed the crystal structures of trimeric p21/p27-CDK4-CylinD complexes and discovered different mechanisms of action of palbociclib in relation to different allosteric forms of the enzymes (Figure 22; Guiley *et al.*, 2019). Indeed, phosphorylated p27 associated with CDK4/Cyclin D1 complexes promote their kinase activity. This trimeric complex has been shown to be insensitive to palbociclib. Surprisingly, palbociclib preferentially binds to monomeric CDK4/6 in breast cancer cell lines, which prevents the binding of p21 to CDK4/6-CyclinD complexes. As a consequence, this free p21 was shown to inhibit CDK2 instead. This reveals that CDK4/6 inhibitors have indirect effects on CDK2 through the non-canonical pathway of p21.

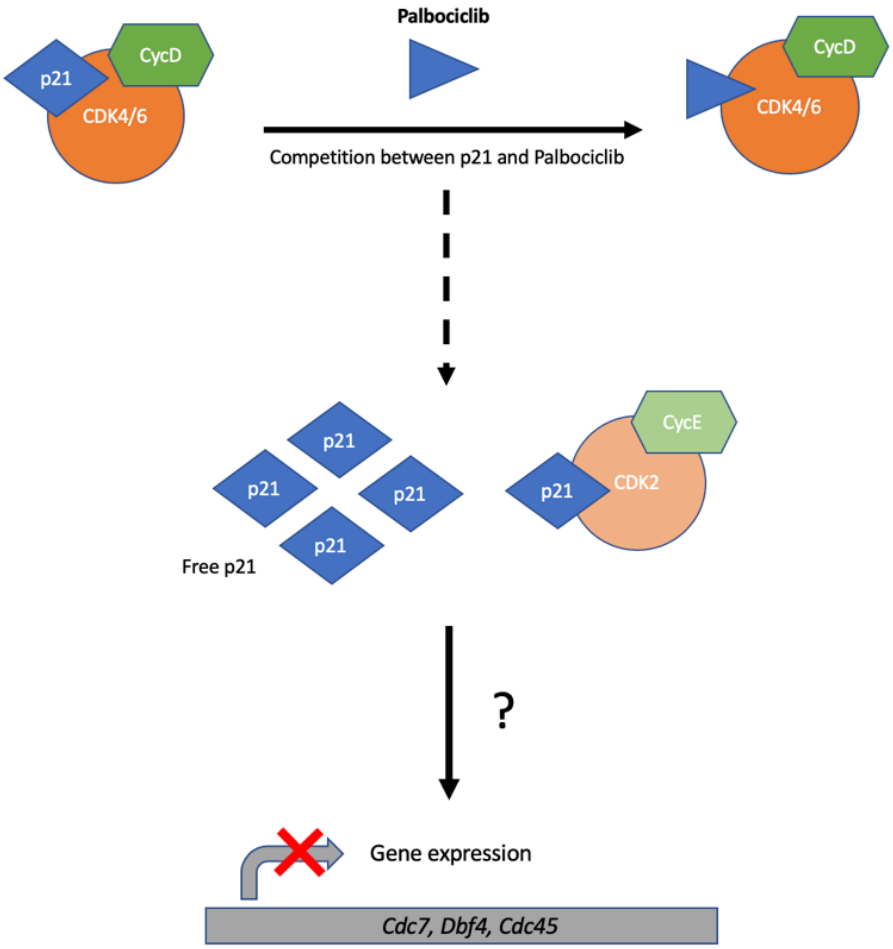


**Figure 22.** Model for understanding how p27 mediates cyclin-dependent kinase 4 (CDK4) assembly, activity, and sensitivity to the kinase inhibitor palbociclib.

*Off-targets of palbociclib at 10µM*

CDK4/6 inhibitors of third generation (palbociclib, ribociclib and abemaciclib) are specific small molecules acting within a nanomolar range of affinity for CDK4 and CDK6. Nonetheless, these inhibitors have their own targets other than CDK4 and CDK6, as referred to off-target. In general, ribociclib is considered as the most selective inhibitor to CDK4 and CDK6 and abemaciclib has the largest spectrum of off-targets. Palbociclib is regularly placed at an intermediate position and often underrated relative to abemaciclib for the study of off-target. Still, some evidence shows that palbociclib has potential off-targets at 10µM. Peter Karl Sorger's group described differences in CDK4/6 inhibitors activities by multi-omic analysis. They performed kinase activity assays *in vitro* and showed that palbociclib inhibits

CDK2/cyclinA1 and CDK2/cylinE1 in the μM range (Hafner *et al.*, 2019). A recent study quantifying CDK inhibitor selectivity in live cells revealed that 10 μM of palbociclib has a target occupancy of 65% for CDK2 (Wells *et al.*, 2020) compared to nearly 0% for ribociclib. Overall, it is probable that the concentration of palbociclib that we used in pRb deficient cells is sufficient to target CDK2 but it is not the case for ribociclib. Thus, this concentration is considered as too high but possibly attainable to treat patients (Nguyen *et al.*, 2010).

*What are the consequences of these effects? Comparison with Cdc7i?*

I determined that palbociclib impairs the origin firing process of DNA replication by down regulating the expression of genes forming the Pre-IC as CDC7, DBF4 and CDC45. The transition from the Pre-RC to the Pre-IC is a critical step for the efficacy of origins activation. The defects in these elements elicit either the activation of sur-numerous origins or a paucity of activated origins that may be sources of genome instability.
Consistent with our results, Santocanale Corrado's group has demonstrated that small interference RNA of *Cdc7* impairs the progression of S-phase and that the Cdc7 inhibitor PHA-767491 decreases origin firing without changes in fork speed, thus leading to cell death by apoptosis (Montagnoli *et al.*, 2004; Montagnoli *et al.*, 2008). On the opposite, overexpression of CDC45 is associated with more fired origins coupled with a slowdown of fork rate and thus triggering the cell death by apoptosis. Taken together, rate limiting replicative factors are essential for the organized activation of origins. Activation of an insufficient number of origins could then generate under-replicated DNA regions and lead to chromosomal instability. We can further investigate if palbociclib could also induce chromosome abnormalities by measuring the formation of micronuclei, chromosome breaks in metaphase and anaphase bridges or aneuploidy.

*Potentiality of abemaciclib in combination with chloroquine*

Finally, in the third chapter, I demonstrated that abemaciclib in combination with chloroquine reduces more efficiently the viability of pRB deficient cells by apoptosis. This study could demonstrate that autophagy inhibitors potentiate the actions of abemaciclib, suggesting autophagy as a process that will protect cells from the cytotoxic effects of abemaciclib. Furthermore, autophagy is known as a cellular self-degradation process that allows cells to eliminate proteins and non-functional organelles. Under physiological condition, autophagy

maintains homeostasis through fusion with the lysosome. Along with its physiological role, autophagy plays a crucial role in the development of cancers. Autophagy can give cells the ability to tolerate stress, which makes it possible to maintain the level of energy production in the cancer cells, enhance the tumor growth, and induce resistance to the cancer treatment. On the contrary, autophagy may increase the sensitivity to the treatment by facilitating senescence or apoptosis (Zhineng J. Yang, Cheng E. Chee *et al.*, 2012; Glick, Barth and Macleod, 2010). We revealed here that inhibition of autophagy enhances the cytotoxic effects of abemaciclib, suggesting the cells protect by autophagy process in response to abemaciclib. This finding implies that the combination of two drugs could diminish the resistance in use of cancer treatment.

Taken together, the studies during my PhD thesis provide more precise information about the mechanism of CDK4/6 inhibitors. On one hand, I demonstrated the clinical potential of CDK4/6 inhibitors for ACCs. On the other hand, I showed that the effects of palbociclib or abemaciclib/chloroquine targeting pRb loss cancers, which contribute to enlarge the possibilities of drugs. These findings may also improve precise medicine for patients of cancer.

## Abbreviations in the alphabetical order

Anaphase promoting complex/cyclosome (APC/C)

Ataxia telangiectasia mutated (ATM)

Ataxia telangiectasia and rad3 related (ATR)

Ataxia telangiectasia and Rad3-related interacting protein (ATRIP)

Bromo-desoxy-uridine (BrdU)

CDK activating kinase (CAK)

Cdc10-dependent transcipt1 (Cdt1)

Cell division cycle 7 (Cdc7)

Cell division cycle (Cdc45)

CDK inhibitors (CKI)

Cell division cycle 6 (Cdc6)

Common fragile site (CFS)

Check point kinase 1 (CHK1)

Chlorodeoxyuridine (CldU)

CIN (Chromosome instability)

CMG complex (Cdc45/Mcm/GINS)

Cyclin-Dependent Kinases (CDKs)

Dbf4 dependent kinase (DDK)

DNA damage response (DDR)

Double-strand breaks (DSBs)

Dimerization partners, Rb-like, E2F and Multi-vulval class B (DREAM)

Epidermal growth factor (EGF)

Food and Drug Administration (FDA)

Flap Endonuclease 1 (FEN1

Go-Ichi-Ni-San (GINS)

G-quadruplex DNA (G4)

Hepatocellular carcinoma (HCC)

Hormone receptor-positive (HR+)

Insulin-like growth factor (IGF)

Inter origin distance (IOD)

Iododeoxyuridine (IdU)

Mini chromosome maintenance protein (MCM)

Microsatellite instability (MIN)

Monodansylcadaverine (MDC)

Origin decision point (ODP)

Origin recognition complex (ORC)

Progression free survival (PFS)

Peroxiredoxin 2 (PRDX2)

Pre-initiation complex (Pre-IC)

Pre-replication complex (pre-RC)

Proliferating cell nuclear antigen (PCNA)

Protein RB family (pRb)

Polo like kinase 1 (Plk1)

Replication factor C (RFC)

Replication protein A (RPA)

Ribonucleotide reductase (RNR)

Reactive oxygen species (ROS)

Replication stress (RS)

Single-stranded DNA (ssDNA)

Timing decision point (TDP)

Werner syndrome ATP-dependent helicase (WRN)

# References

Ahuja, A. K. *et al.* (2016) 'A short G1 phase imposes constitutive replication stress and fork remodelling in mouse embryonic stem cells', *Nature Communications*. Nature Publishing Group, 7(May 2015). doi: 10.1038/ncomms10660.

Asghar, U. *et al.* (2015) 'The history and future of targeting cyclin-dependent kinases in cancer therapy', *Nature Reviews Drug Discovery*, 14(2), pp. 130–146. doi: 10.1038/nrd4504.

De Azevedo, W. F. *et al.* (1996) 'Structural basis for specificity and potency of a flavonoid inhibitor of human CDK2, a cell cycle kinase', *Proceedings of the National Academy of Sciences of the United States of America*, 93(7), pp. 2735–2740. doi: 10.1073/pnas.93.7.2735.

Ballabeni, A. *et al.* (2013) 'Geminin deploys multiple mechanisms to regulate Cdt1 before cell division thus ensuring the proper execution of DNA replication', *Proceedings of the National Academy of Sciences of the United States of America*, 110(30), pp. 8–13. doi: 10.1073/pnas.1310677110.

Bártová, I. *et al.* (2004) 'Activation and inhibition of cyclin-dependent kinase-2 by phosphorylation; a molecular dynamics study reveals the functional importance of the glycine-rich loop', *Protein Science*, 13(6), pp. 1449–1457. doi: 10.1110/ps.03578504.

Bertoli, C., Skotheim, J. M. and Bruin, R. A. M. De (2015) 'Control of cell cycle transcription during G1 and S phases Cosetta', *Nature Reviews Molecular Cell Biology*, 14(8), pp. 518–528. doi: 10.1038/nrm3629.Control.

Bhateja, P. *et al.* (2019) 'Retinoblastoma mutation predicts poor outcomes in advanced non small cell lung cancer', *Cancer Medicine*, pp. 1459–1466. doi: 10.1002/cam4.2023.

Bollard, J. *et al.* (2016) 'Palbociclib (PD-0332991), a selective CDK4/6 inhibitor, restricts tumour growth in preclinical models of hepatocellular carcinoma', *Gut*, p. gutjnl-2016-312268. doi: 10.1136/gutjnl-2016-312268.

Bookstein, R. *et al.* (1989) 'Human retinoblastoma gene: long-range mapping and analysis of its deletion in a breast cancer cell line.', *Molecular and Cellular Biology*, 9(4), pp. 1628–1634. doi: 10.1128/mcb.9.4.1628.

Bracken, A. P. *et al.* (2004) 'E2F target genes: Unraveling the biology', *Trends in Biochemical Sciences*, 29(8), pp. 409–417. doi: 10.1016/j.tibs.2004.06.006.

Chen, P. *et al.* (2016) 'Spectrum and Degree of CDK Drug Interactions Predicts Clinical Performance', *Molecular Cancer Therapeutics*, 15(10), pp. 2273–2281. doi: 10.1158/1535-

7163.MCT-16-0300.
Chen, X. *et al.* (2019) 'Latest overview of the cyclin-dependent kinases 4/6 inhibitors in breast cancer: The past, the present and the future', *Journal of Cancer*, 10(26), pp. 6608–6617. doi: 10.7150/jca.33079.
Cheng, M. (1999) 'The p21Cip1 and p27Kip1 CDK `inhibitors' are essential activators of cyclin D-dependent kinases in murine fibroblasts', *The EMBO Journal*, 18(6), pp. 1571–1583. doi: 10.1093/emboj/18.6.1571.
Courtot, L., Hoffmann, J. S. and Bergoglio, V. (2018) 'The protective role of dormant origins in response to replicative stress', *International Journal of Molecular Sciences*, 19(11). doi: 10.3390/ijms19113569.
Coverley, D., Laman, H. and Laskey, R. A. (2002) 'Distinct roles for cyclins E and A during DNA replication complex assembly and activation', *Nature Cell Biology*, 4(7), pp. 523–528. doi: 10.1038/ncb813.
Debatisse, M. and Rosselli, F. (2019) 'A journey with common fragile sites: From S phase to telophase', *Genes Chromosomes and Cancer*, 58(5), pp. 305–316. doi: 10.1002/gcc.22704.
Dewar, J. M. *et al.* (2017) 'CRL2Lrr1 promotes unloading of the vertebrate replisome from chromatin during replication termination', *Genes and Development*, 31(3), pp. 275–290. doi: 10.1101/gad.291799.116.
Dewar, J. M. and Walter, J. C. (2017) 'Mechanisms of DNA replication termination', *Nature Reviews Molecular Cell Biology*, 18(8), pp. 507–516. doi: 10.1038/nrm.2017.42.
Dyson, N. (1998) 'The regulation of E2F by pRB-family proteins', *Genes and Development*, 12(15), pp. 2245–2262. doi: 10.1101/gad.12.15.2245.
Ekholm-Reed, S. *et al.* (2004) 'Deregulation of cyclin E in human cells interferes with prereplication complex assembly', *Journal of Cell Biology*, 165(6), pp. 789–800. doi: 10.1083/jcb.200404092.
Engeland, K. (2018) 'Cell cycle arrest through indirect transcriptional repression by p53: I have a DREAM', *Cell Death and Differentiation*. Nature Publishing Group, 25(1), pp. 114–132. doi: 10.1038/cdd.2017.172.
Enserink, J. M. and Kolodner, R. D. (2010) 'An overview of Cdk1-controlled targets and processes', *Cell Division*, 5, pp. 1–41. doi: 10.1186/1747-1028-5-11.
Evrin, C. *et al.* (2009) 'A double-hexameric MCM2-7 complex is loaded onto origin DNA during licensing of eukaryotic DNA replication', *Proceedings of the National Academy of Sciences of the United States of America*, 106(48), pp. 20240–20245. doi: 10.1073/pnas.0911500106.

Fragkos, M. *et al.* (2015) 'DNA replication origin activation in space and time', *Nature Reviews Molecular Cell Biology*. Nature Publishing Group, 16(6), pp. 360–374. doi: 10.1038/nrm4002.
Fujita, M. (2006) 'Cdt1 revisited: Complex and tight regulation during the cell cycle and consequences of deregulation in mammalian cells', *Cell Division*, 1, pp. 1–9. doi: 10.1186/1747-1028-1-22.
Gaillard, H., García-Muse, T. and Aguilera, A. (2015) 'Replication stress and cancer', *Nature Reviews Cancer*. Nature Publishing Group, 15(5), pp. 276–280. doi: 10.1038/nrc3916.
Garcia-murillas, I. *et al.* (2017) 'Early Adaptation and Acquired Resistance to CDK4/6 Inhibition in Estrogen Receptor–Positive Breast Cancer', *Cancer Research*, 76(8), pp. 2301–2313. doi: 10.1158/0008-5472.CAN-15-0728.Early.
Gheghiani, L. *et al.* (2017) 'PLK1 Activation in Late G2 Sets Up Commitment to Mitosis', *Cell Reports*, 19(10), pp. 2060–2073. doi: 10.1016/j.celrep.2017.05.031.
Gilbert, D. M. (2009) '[Establishment of spatial and temporal program for mammalian chromosome replication].', *Tanpakushitsu kakusan koso. Protein, nucleic acid, enzyme*, 54(4 Suppl), pp. 320–326.
Gilbert, D. M. (2010) 'Cell fate transitions and the replication timing decision point', *Journal of Cell Biology*, 191(5), pp. 899–903. doi: 10.1083/jcb.201007125.
Glick, D., Barth, S. and Macleod, K. F. (2010) 'Autophagy : cellular and molecular mechanisms', *Journal of Pathology The*, 221(1), pp. 3–12. doi: 10.1002/path.2697.Autophagy.
Goel, S. *et al.* (2018) 'CDK4/6 Inhibition in Cancer: Beyond Cell Cycle Arrest', *Trends in Cell Biology*, 28(11), pp. 911–925. doi: 10.1016/j.tcb.2018.07.002.
Gong, Y. *et al.* (2017) 'PHF11 promotes DSB resection, ATR signaling, and HR', *Genes and Development*, 31(1), pp. 46–58. doi: 10.1101/gad.291807.116.
Gu, Y., Rosenblatt, J. and Morgan, D. O. (1992) 'Cell cycle regulation of CDK2 activity by phosphorylation of Thr160 and Tyr15.', *The EMBO Journal*, 11(11), pp. 3995–4005. doi: 10.1002/j.1460-2075.1992.tb05493.x.
Guiley, K. Z. *et al.* (2019) 'P27 allosterically activates cyclin-dependent kinase 4 and antagonizes palbociclib inhibition', *Science*, 366(6471). doi: 10.1126/science.aaw2106.
Hadjadj, D. *et al.* (2017) 'A hypothesis-driven approach identifies CDK4 and CDK6 inhibitors as candidate drugs for treatments of adrenocortical carcinomas', *Aging*, 9(12), pp. 2695–2716. doi: 10.18632/aging.101356.
Hadjadj, D. *et al.* (2020) 'Efficient, quick and easy-to-use DNA replication timing analysis with START-R suite', *NAR Genomics and Bioinformatics*, 2(2), pp. 1–7. doi:

10.1093/nargab/lqaa045.
Hafner, M. *et al.* (2019) 'Clinical Activity', 26(8), pp. 1067–1080. doi: 10.1016/j.chembiol.2019.05.005.Multi-omics.
Hall, J. R. *et al.* (2008) 'Cdt1 and Cdc6 are destabilized by rereplication-induced DNA damage', *Journal of Biological Chemistry*, 283(37), pp. 25356–25363. doi: 10.1074/jbc.M802667200.
Hino, H. *et al.* (2020) 'Abemaciclib induces atypical cell death in cancer cells characterized by formation of cytoplasmic vacuoles derived from lysosomes', *Cancer Science*, 111(6), pp. 2132–2145. doi: 10.1111/cas.14419.
Hoffmann, I., Draetta, G. and Karsenti, E. (1994) 'Activation of the phosphatase activity of human cdc25A by a cdk2-cyclin E dependent phosphorylation at the G1/S transition.', *The EMBO Journal*, 13(18), pp. 4302–4310. doi: 10.1002/j.1460-2075.1994.tb06750.x.
Im, J. S. *et al.* (2009) 'Assembly of the Cdc45-Mcm2-7-GINS complex in human cells requires the Ctf4/And-1, RecQL4, and Mcm10 proteins', *Proceedings of the National Academy of Sciences of the United States of America*, 106(37), pp. 15628–15632. doi: 10.1073/pnas.0908039106.
Jeffrey, P. D., Tong, L. and Pavletich, N. P. (2000) 'Structural basis of inhibition of CDK-cyclin complexes by INK4 inhibitors', *Genes and Development*, 14(24), pp. 3115–3125. doi: 10.1101/gad.851100.
Jiang, W. *et al.* (1999) 'Mammalian Cdc7-Dbf4 protein kinase complex is essential for initiation of DNA replication', *EMBO Journal*, 18(20), pp. 5703–5713. doi: 10.1093/emboj/18.20.5703.
Jingwen, B., Yaochen, L. and Guojun, Z. (2017) 'Cell cycle regulation and anticancer drug discovery', *Cancer Biology & Medicine*, 14(4), p. 348. doi: 10.20892/j.issn.2095-3941.2017.0033.
Kara, N. *et al.* (2015) 'Orc1 binding to mitotic chromosomes precedes spatial patterning during G1 phase and assembly of the origin recognition complex in human cells', *Journal of Biological Chemistry*, 290(19), pp. 12355–12369. doi: 10.1074/jbc.M114.625012.
Knudsen, E. S. *et al.* (2017) 'Biological specificity of CDK4/6 inhibitors: Dose response relationship, in vivo signaling, and composite response signaturez', *Oncotarget*, 8(27), pp. 43678–43691. doi: 10.18632/oncotarget.18435.
Knudsen, E. S. and Zacksenhaus, E. (2018) 'The vulnerability of RB loss in breast cancer: Targeting a void in cell cycle control', *Oncotarget*, 9(57), pp. 30940–30941. doi: 10.18632/oncotarget.25797.

Kotsantis, P., Petermann, E. and Boulton, S. J. (2018) ‘Mechanisms of oncogene-induced replication stress: Jigsaw falling into place’, *Cancer Discovery*, 8(5), pp. 537–555. doi: 10.1158/2159-8290.CD-17-1461.
Laurent-Puig, P. and Zucman-Rossi, J. (2006) ‘Genetics of hepatocellular tumors’, *Oncogene*, 25(27), pp. 3778–3786. doi: 10.1038/sj.onc.1209547.
Lengronne, A. and Schwob, E. (2002) ‘The yeast CDK inhibitor Sic1 prevents genomic instability by promoting replication origin licensing in late G1’, *Molecular Cell*, 9(5), pp. 1067–1078. doi: 10.1016/S1097-2765(02)00513-0.
Liao, H. *et al.* (2018) ‘Mechanisms for stalled replication fork stabilization: new targets for synthetic lethality strategies in cancer treatments’, *EMBO reports*, 19(9), pp. 1–18. doi: 10.15252/embr.201846263.
Lim, L. Y. *et al.* (2009) ‘Mutant p53 mediates survival of breast cancer cells’, *British Journal of Cancer*. Nature Publishing Group, 101(9), pp. 1606–1612. doi: 10.1038/sj.bjc.6605335.
Lin, G. G. and Scott, J. G. (2012) ‘NIH Public Access’, 100(2), pp. 130–134. doi: 10.1016/j.pestbp.2011.02.012.Investigations.
Löbrich, M. and Jeggo, P. a (2007) ‘and Cancer Induction’, *Group*, 7(November), pp. 861–870. doi: 10.1038/nrc2248.
Macheret, M. and Halazonetis, T. D. (2018) ‘Intragenic origins due to short G1 phases underlie oncogene-induced DNA replication stress’, *Nature*, 555(7694), pp. 112–116. doi: 10.1038/nature25507.
Machida, Y. J., Hamlin, J. L. and Dutta, A. (2005) ‘Right place, right time, and only once: Replication initiation in metazoans’, *Cell*, 123(1), pp. 13–24. doi: 10.1016/j.cell.2005.09.019.
Marchal, C., Sima, J. and Gilbert, D. M. (2019) ‘Control of DNA replication timing in the 3D genome’, *Nature Reviews Molecular Cell Biology*. Springer US, 20(12), pp. 721–737. doi: 10.1038/s41580-019-0162-y.
Mauthe, M. *et al.* (2018) ‘Chloroquine inhibits autophagic flux by decreasing autophagosome-lysosome fusion’, *Autophagy*. Taylor & Francis, 14(8), pp. 1435–1455. doi: 10.1080/15548627.2018.1474314.
Mcintosh, D. *et al.* (2012) ‘and the Response to Replicative Stresses’, pp. 1–10.
Merrick, K. A. and Fisher, R. P. (2010) ‘Putting one step before the other: Distinct activation pathways for Cdk1 and Cdk2 bring order to the mammalian cell cycle’, *Cell Cycle*, 9(4), pp. 706–714. doi: 10.4161/cc.9.4.10732.
Mohaghegh, P. (2001) ‘The Bloom’s and Werner’s syndrome proteins are DNA structure-specific helicases’, *Nucleic Acids Research*, 29(13), pp. 2843–2849. doi:

10.1093/nar/29.13.2843.
Montagnoli, A. *et al.* (2004) 'Cdc7 inhibition reveals a p53-dependent replication checkpoint that is defective in cancer cells', *Cancer Research*, 64(19), pp. 7110–7116. doi: 10.1158/0008-5472.CAN-04-1547.
Montagnoli, A. *et al.* (2008) 'A Cdc7 kinase inhibitor restricts initiation of DNA replication and has antitumor activity', *Nature Chemical Biology*, 4(6), pp. 357–365. doi: 10.1038/nchembio.90.
Mukherjee, S. *et al.* (2018) 'Werner syndrome protein and dna replication', *International Journal of Molecular Sciences*, 19(11). doi: 10.3390/ijms19113442.
Neelsen, K. J. *et al.* (2013) 'Deregulated origin licensing leads to chromosomal breaks by rereplication of a gapped DNA template', *Genes and Development*, 27(23), pp. 2537–2542. doi: 10.1101/gad.226373.113.
Nguyen, L. *et al.* (2010) 'Quantitative analysis of PD 0332991 in xenograft mouse tumor tissue by a 96-well supported liquid extraction format and liquid chromatography/mass spectrometry', *Journal of Pharmaceutical and Biomedical Analysis*. Elsevier B.V., 53(3), pp. 228–234. doi: 10.1016/j.jpba.2010.02.031.
Ohtani, K. *et al.* (1996) 'Expression of the HsOrc1 gene, a human ORC1 homolog, is regulated by cell proliferation via the E2F transcription factor.', *Molecular and Cellular Biology*, 16(12), pp. 6977–6984. doi: 10.1128/mcb.16.12.6977.
Paternot, S. *et al.* (2014) 'The CDK4/CDK6 inhibitor PD0332991 paradoxically stabilizes activated cyclin D3-CDK4/6 complexes', *Cell Cycle*, 13(18), pp. 2879–2888. doi: 10.4161/15384101.2014.946841.
Petropoulos, M. *et al.* (2019) 'Replication Licensing Aberrations, Replication Stress, and Genomic Instability', *Trends in Biochemical Sciences*. Elsevier Ltd, 44(9), pp. 752–764. doi: 10.1016/j.tibs.2019.03.011.
Ragazzon, B. *et al.* (2014) 'Mass-array screening of frequent mutations in cancers reveals RB1 alterations in aggressive adrenocortical carcinomas', *European Journal of Endocrinology*, 170(3), pp. 385–391. doi: 10.1530/EJE-13-0778.
Randell, J. C. W. *et al.* (2006) 'Sequential ATP hydrolysis by Cdc6 and ORC directs loading of the Mcm2-7 helicase', *Molecular Cell*, 21(1), pp. 29–39. doi: 10.1016/j.molcel.2005.11.023.
Raspé, E. *et al.* (2017) ' CDK 4 phosphorylation status and a linked gene expression profile predict sensitivity to palbociclib ', *EMBO Molecular Medicine*, 9(8), pp. 1052–1066. doi: 10.15252/emmm.201607084.

Rasti, M. and Azimi, T. (2015) 'TP53 binding to BRCA1 and RAD51 in MCF7 and MDA-MB-468 breast cancer cell lines in vivo and in vitro', *Avicenna Journal of Medical Biotechnology*, 7(2), pp. 76–79.
Rivera-Mulia, J. C. and Gilbert, D. M. (2016) 'Replicating Large Genomes: Divide and Conquer', *Molecular Cell*, 62(5), pp. 756–765. doi: 10.1016/j.molcel.2016.05.007.
Rodriguez-Acebes, S., Mourón, S. and Méndez, J. (2018) 'Uncoupling fork speed and origin activity to identify the primary cause of replicative stress phenotypes', *Journal of Biological Chemistry*, 293(33), pp. 12855–12861. doi: 10.1074/jbc.RA118.003740.
Sampaoli, C. *et al.* (2012) 'p53 Stabilization Induces Cell Growth Inhibition and Affects IGF2 Pathway in Response to Radiotherapy in Adrenocortical Cancer Cells', *PLoS ONE*, 7(9). doi: 10.1371/journal.pone.0045129.
Sánchez-Martínez, C. *et al.* (2015) 'Cyclin dependent kinase (CDK) inhibitors as anticancer drugs', *Bioorganic and Medicinal Chemistry Letters*, 25(17), pp. 3420–3435. doi: 10.1016/j.bmcl.2015.05.100.
Sheu, Y. and Stillman, B. (2010) 'mediated mechanism to promote S phase progression', *Molecular Cell*, 24(1), pp. 101–113. doi: 10.1016/j.molcel.2006.07.033.Cdc7-Dbf4.
Sobhani, N. *et al.* (2019) 'Combinations in Breast Cancer', *Cells*, 8(4), pp. 1–24.
Somyajit, K. *et al.* (2017) 'Genome Integrity', 802(November), pp. 797–802. doi: 10.1126/science.aao3172 Metabolic.
Spring, L. M. *et al.* (2019) 'CDK 4/6 Inhibitors in Breast Cancer: Current Controversies and Future Directions', *Current Oncology Reports*, 21(3), pp. 1–14. doi: 10.1007/s11912-019-0769-3.
Srinivas, U. S. *et al.* (2019) 'ROS and the DNA damage response in cancer', *Redox Biology*, 25(December). doi: 10.1016/j.redox.2018.101084.
Stodola, J. L. and Burgers, P. M. (2016) 'Resolving individual steps of Okazaku Fragment maturation at a msec time-scale', *Natural Structural Molecular Biology*, 23(5), pp. 402–408. doi: 10.1038/nsmb.3207.Resolving.
Tanaka, S. and Araki, H. (2013) 'Helicase activation and establishment of replication forks at chromosomal origins of replication', *Cold Spring Harbor Perspectives in Biology*, 5(12), pp. 1–14. doi: 10.1101/cshperspect.a010371.
Técher, H. *et al.* (2013) 'Replication dynamics: Biases and robustness of DNA fiber analysis', *Journal of Molecular Biology*. Elsevier Ltd, 425(23), pp. 4845–4855. doi: 10.1016/j.jmb.2013.03.040.
Timofeev, O. *et al.* (2010) 'Cdc25 phosphatases are required for timely assembly of CDK1-

cyclin B at the G2/M transition', *Journal of Biological Chemistry*, 285(22), pp. 16978–16990. doi: 10.1074/jbc.M109.096552.
Treré, D. *et al.* (2009) 'High prevalence of retinoblastoma protein loss in triple-negative breast cancers and its association with a good prognosis in patients treated with adjuvant chemotherapy', *Annals of Oncology*, 20(11), pp. 1818–1823. doi: 10.1093/annonc/mdp209.
Ubhi, T. and Brown, G. W. (2019) 'Exploiting DNA replication stress for cancer treatment', *Cancer Research*, 79(8), pp. 1730–1739. doi: 10.1158/0008-5472.CAN-18-3631.
Valenzuela, C. A. *et al.* (2017) 'Palbociclib-induced autophagy and senescence in gastric cancer cells', *Experimental Cell Research*. Elsevier Inc., 360(2), pp. 390–396. doi: 10.1016/j.yexcr.2017.09.031.
Vargas-Rondón, N., Villegas, V. E. and Rondón-Lagos, M. (2018) 'The role of chromosomal instability in cancer and therapeutic responses', *Cancers*, 10(1), pp. 1–21. doi: 10.3390/cancers10010004.
Vermeulen, K., Van Bockstaele, D. R. and Berneman, Z. N. (2003) 'The cell cycle: A review of regulation, deregulation and therapeutic targets in cancer', *Cell Proliferation*, 36(3), pp. 131–149. doi: 10.1046/j.1365-2184.2003.00266.x.
Vigneron, S. *et al.* (2018) 'Cyclin A-cdk1-Dependent Phosphorylation of Bora Is the Triggering Factor Promoting Mitotic Entry', *Developmental Cell*, 45(5), pp. 637-650.e7. doi: 10.1016/j.devcel.2018.05.005.
Vijayaraghavan, S. *et al.* (2017) 'CDK4/6 and autophagy inhibitors synergistically induce senescence in Rb positive cytoplasmic cyclin e negative cancers', *Nature Communications*. Nature Publishing Group, 8(May), pp. 1–17. doi: 10.1038/ncomms15916.
Wells, C. I. *et al.* (2020) 'Quantifying CDK inhibitor selectivity in live cells', *Nature Communications*. Springer US, 11(1), pp. 1–11. doi: 10.1038/s41467-020-16559-0.
Witkiewicz, A. K. and Knudsen, E. S. (2014) 'Retinoblastoma tumor suppressor pathway in breast cancer: Prognosis, precision medicine, and therapeutic interventions', *Breast Cancer Research*, 16(2), pp. 1–12. doi: 10.1186/bcr3652.
Wu, J. R. and Gilbert, D. M. (1996) 'A distinct G1 step required to specify the Chinese hamster DHFR replication origin', *Science*, 271(5253), pp. 1270–1272. doi: 10.1126/science.271.5253.1270.
Zeman, M. K. and Cimprich, K. A. (2014) 'Causes and consequences of replication stress', *Nature Cell Biology*, 16(1), pp. 2–9. doi: 10.1038/ncb2897.
Zhang, J. *et al.* (2016) 'Targeting DNA replication stress for cancer therapy', *Genes*, 7(8). doi: 10.3390/genes7080051.

Zhineng J. Yang, Cheng E. Chee, S. H. *et al.* (2012) 'The role of autophagy in cancer: therapeutic implications.', *Molecular cancer therapeutics*, 10(9), pp. 1533–1541. doi: 10.1158/1535-7163.MCT-11-0047.The.

Zhong, Y. *et al.* (2013) 'The level of origin firing inversely affects the rate of replication fork progression', *Journal of Cell Biology*, 201(3), pp. 373–383. doi: 10.1083/jcb.201208060.